Newcastle University

In Vitro properties and *in vivo* responses of CoaR, ZiaR & Zur (trans-family metal-sensing)

Carl John Patterson
BSc (Hons) Biochemistry, MRes
Newcastle University

Thesis submitted in partial fulfilment of the requirements
of the regulations for the degree of Doctor of Philosophy
Newcastle University
Faculty of Medical Sciences
Institute for Cell and Molecular Biosciences
September 2010

Memorandum

Part of this work has been published as:

Dainty S.J., Patterson C.J., Waldron K.J. & Robinson N.J. (2010) Interaction between cyanobacterial copper chaperone Atx1 and zinc homeostasis. *J. Biol. Inorg. Chem.* 15: 77-85.

Additional manuscripts in preparation.

Declaration

No portion of the work referred to in this thesis has been submitted in support of an application for another degree or qualification of this or any other University, or institution of learning.

Acknowledgements

I would like to thank Prof. Nigel Robinson for supervision throughout this project as well as other members, past and present, of the Robinson group for insight, advice and expertise. In particular, I thank Dr. Kevin Waldron, Dr. Samantha Dainty and Dr. Steve Tottey for allowing their data to be included as part of this thesis. I also thank Natasha Cant, an undergraduate project student, for assistance in the purification and characterisation of CoaR.

Outside the lab. I would like to thank the innumerable characters who have all helped in their own little ways in making this a great three years. I thank Fran, Miranda, Tom and many others for fun Friday nights in the Terrace. Thanks to all of my housemates and friends over the past three years for putting up with me-you know who you are! In particular, thanks to Kate Sharples, Tash, Andy, Ruth, Adam, Emily, Teresa, James and Wayne (for much needed adventures here and abroad!) and last, but by no means least, Laura Brocklehurst, for countless fun evenings in and out and constant kind words of support and encouragement.

Finally, I would like to thank my parents for standing by me during this, through thick and thin and during the times when I thought that I was beaten. This is for you.

"Coming home from very lonely places, all of us go a little mad: whether from great personal success, or just an all-night drive, we are the sole survivors of a world no one else has ever seen."

John le Carré

Abstract

In prokaryotic organisms metal-sensing transcriptional regulators must respond selectively to metal ions. The factors which govern selectivity across different sensor families from *Synechocystis* sp. PCC 6803 have been investigated using three sensor proteins; ZiaR, an ArsR-SmtB Zn^{2+}-de-repressor; Zur, a Fur-like Zn^{2+} co-repressor and CoaR, a MerR-like Co^{2+}-dependent activator. Zn^{2+} bound and allosterically regulated recombinant ZiaR and Zur *in vitro*. Cu^{+} failed to allosterically regulate recombinant Zur and inhibited Zn^{2+}-mediated allostery *in vitro*. In Δ*atx1*Δ*gshB Synechocystis* cells, proposed to be defective in normal cytosolic Cu^{+} trafficking, copper toxicity and inhibition of Zn^{2+}-mediated repression of Zur-regulated gene expression was detected, consistent with inhibition of Zn^{2+}-sensing *in vivo* by Cu^{+} normally bound to Atx1. Cu^{+} bound in preference to Zn^{2+} at the α3N sites of recombinant ZiaR and was allosterically ineffective; however, divalent metal binding and allostery were retained at the α5 sites *in vitro*. In Δ*atx1 Synechocystis* cells, enhanced ZiaR-dependent expression was observed with no copper-dependency suggesting Atx1 also sequestered Zn^{2+}. Hence, Atx1 is proposed to restrict access to Zn^{2+} and Cu^{+} ions *in vivo*. Co^{2+} bound to recombinant Zur and ZiaR, impaired ZiaR binding to DNA *in vitro* but ZiaR does not respond to Co^{2+} *in vivo*. Unexpectedly, the Co^{2+} affinity of recombinant CoaR was weaker than ZiaR and Zur, and Zur acquired Co^{2+} in preference to CoaR following direct competition. ZiaR and Zur are soluble however CoaR is membrane associated with predicted hydrophobic regions and requires a non-ionic detergent for preparation *in vitro*. Membrane-localised CoaR is proposed to exist in an intracellular niche in which $[Co^{2+}] >> \text{CoaR } K_{Co}$ and is thus sufficient to activate the protein. Zn^{2+} binds to CoaR more tightly than Co^{2+} but ZiaR and Zur out-compete CoaR for Zn^{2+} Thus, *in vivo* responses to Zn^{2+} correlate with relative affinities for this group of sensors.

Contents

Abbreviations

Arg	arginine
ATP	adenosine triphosphate
AU	arbitrary units
bp	base-pair
BCS	bathocuproine disulfonate
BSA	bovine serum albumin
CMC	critical micelle concentration
Cys	cysteine
DAS	dense alignment surface method
dATP	deoxyadenosine triphosphate
dCTP	deoxycytosine triphosphate
DDM	n-Dodecyl β-D-maltoside
dGTP	deoxyguanosine triphosphate
dNTP	deoxynucleotide triphosphate
DNA	deoxyribonucleic acid
ds	double stranded
DTNB	5,5'-dithiobis-(2-nitrobenzoic) acid
DTT	dithiothreitol
dTTP	deoxythymidine triphosphate
EC	enzyme commission
EDTA	ethylenediaminetetraacetic acid
EMSA	electrophoretic mobility shift assay
FA	fluorescence anisotropy
Fur_{EC}	*Escherichia coli* Fur
Fur_{PA}	*Pseudomonas aeruginosa* Fur
Fur_{VC}	*Vibrio cholerae* Fur
GSH	glutathione
GST	glutathione S-transferase
HEX	hexachlorofluorescein
His	histidine
HPLC	high performance liquid chromatography

ICP-MS	Inductively Coupled Plasma Mass Spectrometry
IPTG	isopropyl β-D-1-thiogalactopyranoside
LB	luria broth
LMCT	ligand-to-metal charge transfer
MCO	metal catalysed oxidation
NAD(H)	nicotinamide adenine dinucleotide
NMR	nuclear Magnetic Resonance
NS	non-specific DNA fragment
OD	optical density
O/P	operator-promoter
ORF	open reading frame
PAGE	polyacrylamide gel electrophoresis
PAR	4-(2-pyridylazo)-resorcinol
PMSF	phenylmethanesulfonylfluoride
rQRT-PCR	real time quantitative reverse transcriptase polymerase chain reaction
r.p.m	revolutions per minute
RCF	relative centrifugal force
RNA	ribonucleic acid
r_{obs}	observed anisotropy
ROS	reactive oxygen species
RT-PCR	reverse transcriptase polymerase chain reaction
SDM	site directed mutagenesis
SDS	sodium dodecyl sulphate
Ser	serine
ss	single stranded
UV	ultraviolet
v/v	volume per volume
w/v	weight per volume
Zur_{BS}	*Bacillus subtilis* Zur
Zur_{EC}	*E.coli* Zur
Zur_{MT}	*Mycobacterium tuberculosis* Zur
Zur_{SS}	*Synechocystis* sp. PCC 6803 Zur
X-Gal	bromo-chloro-indolyl-galactopyranoside

Chapter 1. Introduction

1.1 The biological requirement for metals

Metal cofactors are essential for the function of a large proportion of proteins from all three domains of life. A recent bioinformatics survey of 1371 enzymes for which three-dimensional structures are known estimated that close to half (47 %) required metals and a substantial proportion of these proteins (41 %) contained metals at their active sites (Waldron *et al.* 2009). In most organisms, including prokaryotes, the unique chemical properties of transition metals have led to their extensive recruitment into catalytic metal centres of enzymes. Surveys of metal utilisation in identified protein sequences have shown metalloenzymes to be present in all six Enzyme Commission (EC) classes (Andreini *et al.* 2008).

The functions of metal ions recruited into catalytic centres in each enzyme class are correlated with the chemical conversions catalysed by the enzymes; for example, for oxidoreductases almost 75 % of metal cofactors are utilised as redox centres however in hydrolases a similar proportion of metals are employed as non-redox activators. The types of metal elements found in active centres is also correlated with chemical properties of the metal ions. For example, copper and iron are abundant as redox centres in metalloenzymes and iron is the predominant redox centre in the enzymes surveyed (Andreini *et al.* 2008). The ability of both of these species to readily undergo changes in oxidation states and the ability of protein ligands to modulate their redox potentials makes them well suited for use in redox active systems. Some ions can fulfil multiple, diverse roles; notably, Zn^{2+} can act as a lewis acid and so is utilised as a substrate activator (e.g. in hydrolases) however Zn^{2+} can also fulfil structural roles in proteins (a function that has been greatly expanded in eukaryotic proteomes) (Andreini *et al.* 2008)

In addition to selection of metal ions through evolution based on the chemical properties required of metals by enzymes, the relative distribution of metal ions in enzyme classes is also largely a product of geochemical factors which have influenced metal availability throughout the evolution of life on Earth. The high abundance of iron as a redox centre in proteins is likely due to its early incorporation into proteins prior to the evolution of oxygenic photosynthesis which rendered it poorly bioavailable in the form of precipitated $Fe(OH)_3$. Copper was incorporated into biology later than iron

which partly accounts for its lower abundance in metalloenzyme sites (Andreini *et al.* 2008). Thus, the evolution of metal requirements of proteins have been chemically constrained by metal availability in the environment (Saito *et al.* 2003; Williams & da Silva 2003).

1.2 Regulation of metal cofactor acquisition by proteins

The large number of intracellular proteins containing unique metal cofactors presents a problem-how do the correct metals bind to the correct protein within the complex molecular environment inside the cell? A simple explanation would be for proteins to select the correct metal from the cell solution simply as a consequence of absolute affinity for the requisite metal. In this case, specificity for particular metals would be conferred by structural features at the metal binding site unique to that metal-protein interaction (e.g. primary ligand sphere structure, ligand type and geometry). In reality metal speciation is much more complex. For divalent, transition metal elements an empirical, universal affinity series, known as the Irving-Williams series exists, which ranks metals in order of their relative affinity for proteins (equation 1) (Irving & Williams 1948). This series is independent of the ligand present and arises from the intrinsic features of metal ions. For example, metals higher in the series (with higher nuclear charges) have increased lewis acidity increasing metal-ligand bonding strength.

$$(Mg^{2+} + Ca^{2+}) < Mn^{2+} < Fe^{2+} < Co^{2+} < Ni^{2+} < Cu^{2+} (Cu^{+}) > Zn^{2+} \qquad \text{eq. 1}$$

Copper has the highest relative affinity for proteins out of all the metals of the series; the original series only described the binding properties of Cu^{2+} however Cu^{+} has since been added. The tight affinities exhibited by copper are explained in terms of its high lewis acidity and also through the formation of unusually strong complexes stabilised through Jahn-Teller distortion effects (da Silva & Williams 2002). Zn^{2+} is usually shown second to copper in the series however there is some ambiguity as to whether it is actually below Co^{2+} due to the nephelauxetic effect (Johnson & Nelson 1995). Thus, different proteins within the cytosol must be metallated by highly competitive and weakly competitive metal ions simultaneously. For many proteins, correct metallation is the result of kinetic regulation. Metallochaperones have been identified that bind and deliver metal ions to target proteins. Compartmentalisation of metal ions may be

important in more complex organisms. It has been shown that differential localisation of proteins themselves can facilitate effective metallation. In the cyanobacterium *Synechocystis* sp. PCC 6803 two proteins with the same ligands and similar cupin motifs fold in different locations. MncA folds in the cytosol during which it acquires Mn^{2+} which becomes kinetically trapped inside the protein. Copper-requiring CucA folds and acquires copper in the periplasm. Hence, acquisition by MncA of tightly binding metals such as copper and zinc, which are poorly available as free ions in the cytosol but which are abundant in the periplasm, is avoided (Tottey *et al.* 2008). Control of cytosolic metal ion concentration can be achieved through the presence of selective metal transporter systems in the plasma membrane regulating influx and efflux of metal ions.

1.3 Transcriptional regulation of metal homeostatic systems

Homeostatic mechanisms have evolved to maintain cytosolic metal ion concentrations in ranges optimal for efficient metal cofactoring and also to detoxify metal ions that have accumulated but which serve no biological function. The total quantity of intracellular metal is determined by the activity of metal import and export systems which control the movement of metal ions in and out of the cell. The buffered cytosolic concentration of metal ions is a function of the number of the ligands (e.g. proteins, small molecules) which bind particular metal ions. In prokaryotic organisms regulation of the buffering and transport systems is substantially exerted at the transcriptional level through the action of metal sensing transcriptional regulators. Each regulator detects changes in the cytosolic concentrations of certain metal ions and modulates transcription of genes involved in metal homeostasis (e.g. metal import, export, sequestration).

The set-point metal concentrations for activation of each of these regulator 'switches' are presumed to have evolved in tandem with the intracellular requirements for each metal ion. The responses initiated by each sensor act to buffer the cytosolic concentrations of each metal ion to ranges optimal for protein metallation. However, metal ion concentrations may not be uniform throughout the cytosol; niches of high metal ion abundance have been proposed to exist in close proximity to metal import systems and sites of degradation of metalloproteins (Waldron *et al.* 2009). Metal

sensors are thought to lie at the apex of the metal partitioning processes in bacterial cells (Tottey *et al.* 2007).

1.4 Overview of prokaryotic metal sensor strategies

Seven major classes of soluble, metal-sensing transcriptional regulators have been identified and the key features of each family are summarised in Table 1. In addition to these major groupings, individual, specialised sensors have also evolved and examples include ModE, a molybdenum sensor regulating expression of the *Escherichia coli modABCD* operon which encodes a high affinity molybdate uptake system (Grunden *et al.* 1996; Anderson *et al.* 1997) and IscR which detects Fe-S cluster assembly status in *E.coli* (Schwartz *et al.* 2001). Two-component sensor systems such as CusS/R (copper) (Munson *et al.* 2000) and PhoQ/R (magnesium) (Cromie & Groisman 2010) have also been identified. Although the seven main families often have divergent metal preferences, structural features and mechanisms of action they can be broadly and simply grouped into three classes based on the primary mechanism employed to modulate transcription in response to metal binding. For proteins of the CopY, CsoR and ArsR-SmtB families, metal ions inhibit binding to DNA and promote metal-dependent de-repression of metal regulated genes. Proteins of the Fur, NikR and DtxR families generally exhibit a converse mode of action; metal ions promote binding to DNA and facilitate repression of transcription. The third class of proteins are represented by the MerR-like family of regulators. These proteins bind to DNA with high affinity in both apo and metal bound forms. On binding of metal ions to the DNA bound, apo- repressing form of the protein, conformational changes in the protein lead to promoter reorganisation causing activation of gene transcription.These studies focus on metalloregulators from three families, each defining at least one of the three major functional classes described above- the ArsR-SmtB family, the Fur family and the MerR-like family.

1.5 The ArsR-SmtB family of metal sensing de-repressors

The ArsR-SmtB family represents one of the largest and best characterised of all prokaryotic metalloregulator families. Representatives of this family have been identified in most bacterial genomes with one recent estimation of more than 500

Family	DNA binding motif/regulatory Mechanism	Metals sensed *in vivo*	Examples
ArsR-SmtB	Winged helix Derepression	As, Sb, Zn Bi, Pb, Cd, Cu, Ag, Co, Ni	ArsR, SmtB, CadC, CmtR, BxmR, NmtR
CsoR	α helical bundle Derepression	Cu, Ni	CsoR, RcnR
CopY	Winged helix Derepression	Cu	CopY
Fur	Winged helix Corepression	Fe, Mn, Ni, Zn	Fur, Mur, Nur, Zur
NikR	Ribbon-helix-helix Corepression	Ni	NikR
DtxR	Winged helix Corepression	Fe, Mn	DtxR, IdeR, MntR, AntR, ScaR
MerR	Winged helix Activation	Hg, Cu, Pb, Zn, Au, Ag, Cd	MerR, CueR, PbR, ZntR, GolS, CadR

Table 1. Summary of the major prokaryotic metal sensing transcriptional regulator families. The seven families are organised based on their mechanism of action. The metals sensed *in vivo* only are shown. Example proteins that have been shown to sense each of the metals listed are also shown. The mechanism employed by some members of each family deviate from the mechanism listed. Notably, Fur can derepress gene expression directly and indirectly in the iron-bound form (see section 1.6.1). *H. pylori* NikR can also act as both a repressor and activator of gene expression (Iwig & Chivers 2010). Example structures for members of the ArsR-SmtB, Fur and MerR sensor familes are shown in Appendix E.

candidate proteins in sequenced bacterial genomes (Campbell *et al.* 2007). These proteins appear to be particularly prevalent in Actinobacteria, such as *Mycobacterium tuberculosis*, with multiple representatives often encoded by the same genome. This may reflect selective pressure in some lineages that are particularly exposed to substantial metal stresses to maximise the efficiency of metal homeostasis systems (Osman & Cavet 2010).

Despite extensive diversification through evolution the same basic mechanism has been conserved in many members of this family. In the metal-free apo-state, these proteins bind with high affinity to the promoter elements of regulated genes, which generally encode proteins involved in metal efflux and/or metal sequestration, repressing transcription by sterically hindering RNA Polymerase binding to the promoter. Under conditions of metal surplus, metal ions bind to the protein and inhibit DNA binding, allowing transcription of genes involved in metal detoxification to proceed. More unusual modes of regulation have evolved in ArsR-SmtB homologues; SrnR regulates expression of *sodF* (encoding iron zinc superoxide dismutase (SOD)) in *Streptomyces griseus,* but requires interaction with a Ni^{2+}-binding co-repressor protein, SrnQ, for enhancement of high-affinity binding to DNA (Kim *et al.* 2003). Other ArsR-SmtB homologues have been identified that respond to inputs other than metal (see section 1.5.3).

The promoter binding sites for ArsR-SmtB proteins take the form of highly conserved hyphenated inverted 12-2-12 repeat motifs usually located between the transcriptional start site of the regulated gene and the -10 RNA polymerase recognition hexamer. Genes encoding the ArsR-SmtB regulator are often divergently transcribed from this promoter and their expression is often autoregulated (Busenlehner *et al.* 2003). Binding stoichiometries to these repeat sequences vary between members of the family; quantitative *in vitro* DNA binding assays have shown some proteins to bind as single dimers (e.g. CadC) (Busenlehner *et al.* 2001) however multimeric complexes of up to four or five dimers have also been detected for other members of the family such as CzrA (Pennella *et al.* 2003). The ability to form higher order complexes at the operator-promoter site is supported by the presence of large, protected regions observed in DNA footprinting analyses (Singh *et al.* 1999) and by the presence of multimeric complexes implied by EMSA analyses for multiple members of this family (Erbe *et al.* 1995; Turner *et al.* 1996; Thelwell *et al.* 1998).

The originally characterised founder members of this family were ArsR from *E.coli* and SmtB from *Synechococcus* PCC 7942. ArsR was initially identified as the regulator of the *E.coli ars* resistance operon, which is both chromosomally (Xu *et al.* 1996) and plasmid encoded (Wu & Rosen 1991). This operon confers resistance to arsenite and antimonite (Carlin *et al.* 1995). The R773 plasmid encoded version of this operon encodes five proteins; ArsR, ArsA & B (which form the catalytic and membrane spanning subunits of a metal-translocating ATPase transporter respectively (Rosen *et al.* 1988; Tisa & Rosen 1990), ArsC (a reductase that converts arsenate to arsenite which is then extruded by the transport system) (Gladysheva *et al.* 1994) and ArsD (a metallochaperone that transfers arsenite/antimonite to ArsA for export) (Lin *et al.* 2006). The chromosomal operon encodes only ArsR, B and C and is associated with a lower degree of arsenic resistance (Xu *et al.* 1996). Apo-ArsR binds to and represses transcription from this promoter. This repression is inhibited by As^{3+}, Sb^{3+} and Bi^{3+} (both *in vitro* and *in vivo*) allowing transcription of metal regulated genes to occur (Wu & Rosen 1993). Subsequent studies determined the metal binding motif to be comprised of three α3 helix-derived cysteine residues producing trivalent As^{3+} coordination. Although all three cysteines were utilised in metal binding only a single pair within a CVC motif were found to be essential for metal induced allostery (Shi *et al.* 1996).

Characterisation of the *smt* locus of the cyanobacterium *Synechococcus* PCC 7942 showed that it conferred resistance to Zn^{2+} and Cd^{2+} (Turner *et al.* 1993). The *smtA* gene in this locus encoded a metallothionein (SmtA) which bound Zn^{2+} and Cd^{2+} *in vitro* (as a GST-tagged recombinant protein) (Shi *et al.* 1992) and promoted Zn^{2+} accumulation *in vivo* (Shi *et al.* 1992; Turner *et al.* 1995). The *smtB* gene divergently transcribed from *smtA* encoded a transcriptional regulator (SmtB) which was similar to ArsR and contained a predicted helix-turn-helix motif (Huckle *et al.* 1993). SmtB was shown to repress transcription of the *smtA* gene (Huckle *et al.* 1993) with disassociation of protein-DNA complexes promoted by Zn^{2+} *in vitro* (Morby *et al.* 1993; Erbe *et al.* 1995) with Zn^{2+}-mediated relief of repression of *smtA in vivo* (Huckle *et al*. 1993). Critically, mutation of two histidine residues caused loss of inducer response *in vivo* whereas mutation of cysteine residues conserved in ArsR and shown to be essential for inducer response for ArsR (Shi *et al.* 1996) caused no loss of induction *in vivo* (Turner *et al.* 1996). These data confirmed that SmtB contained a metal binding motif distinct to that found in ArsR (Tuner *et al*. 1996).

Structural and biochemical studies of metal binding to SmtB confirmed metal binding to a tetrahedral site comprised of two histidines, an aspartate and a glutamate residue derived from the α5 helices of both dimer subunits (two from each) at the dimer interface (Cook *et al.* 1998). The chromosomally encoded CzrA protein from *Staphylococcus aureus* was identified as a Zn^{2+}/Co^{2+}sensing regulator controlling expression of a Zn^{2+}/Co^{2+} exporting membrane protein (Kuroda *et al.* 1999; Singh *et al.* 1999). CzrA has a conserved α5 site containing ligands nearly identical to those in SmtB (containing a histidine in place of a glutamate residue) (Eicken *et al*. 2003) which produces similar tetrahedral Zn^{2+} and Co^{2+} binding environments and allosteric responses *in vitro* (Pennella *et al.* 2003).

1.5.1 Diversity within the ArsR-SmtB family of proteins

Since the initial identification of ArsR and SmtB, it has become clear that the diversification in the metals sensed by ArsR-SmtB proteins has in large part arisen through often relatively minor modifications to these simple α3 and α5 sensory motifs within a conserved structural framework. The evolution of novel metal binding properties through changes to these sites has been described as a 'themes and variations' model (Busenlehner *et al.* 2003). The simple trivalent motif of ArsR is optimal for binding small, thiophilic Sb^{3+} and As^{3+} ions. In other proteins additional thiol and non-thiol ligands have been recruited into this binding site from a flexible, N-terminal arm which is not present in ArsR (Busenlehner *et al.* 2003). This site can accommodate a wider range of metal ions with binding preferences further tuned by changes to individual ligand residues.

The α3N sensor CadC provides a demonstration of this evolutionary fine tuning. CadC was identified as a $Cd^{2+}/Pb^{2+}/Bi^{2+}/Zn^{2+}$ responsive sensor (Endo & Silver 1995) regulating expression of the *cadA* gene in the *S.aureus* plasmid pI258 (Yoon *et al.* 1991a,b) which encodes a $Cd^{2+}/Pb^{2+}/Zn^{2+}$ exporting P-type ATPase that confers resistance to toxic concentrations of Cd^{2+} in addition to Zn^{2+} and Pb^{2+} (Nucifora *et al.* 1989). *In vitro* characterisation of CadC demonstrated that the N-terminal tail afforded flexibility in the coordination geometries adopted; Zn^{2+}, Cd^{2+}, Bi^{3+} and Co^{2+} were shown to bind in a tetrathiolate S_4 site utilising two cysteine residues from the α3 helix of one dimer subunit and two cysteine residues from the N-terminal tail of the other subunit (Busenlehner *et al*., 2001 & 2002a,b). This site was subsequently confirmed in

the high resolution crystal structure of the protein (Ye *et al.* 2005). Pb^{2+} was shown to bind in a trithiolate S_3 complex utilising all of the same ligands with the exception of a single cysteine in the N-terminal tail (Busenlehner *et al.* 2002b). Mutational studies demonstrated a primary role for two cysteines (Cys-7 from the N-terminal tail and Cys-60 from the α3 helix) in transducing the allosteric response (Busenlehner *et al.* 2002b). The α3 $Zn^{2+}/Cd^{2+}/Pb^{2+}$ sensing regulator AztR from *Anabaena* PCC 7120 regulates expression of a Zn^{2+}/Pb^{2+} exporting CPx-ATPase efflux pump AztA (Liu *et al.* 2005). The α3N site of AztR has a S_3N structure which accommodates metal ions (Zn^{2+}, Co^{2+} and Cd^{2+}) in a more restricted distorted tetrahedral environment although Pb^{2+} is likely accommodated in a trithiolate S_3 complex (Liu *et al.* 2005).

The α5 sensors have also been subject to extensive diversification. With analogy to the α3 sites, variation in the metals sensed at the α5 sites has been accompanied by recruitment of additional ligands from a C-terminal α5 helix extension. The notable example for this paradigm is the Ni^{2+}/Co^{2+} sensor NmtR from *M. tuberculosis* which represses transcription of *nmtA* that encodes a P-type ATPase (Cavet *et al.* 2002). In contrast to the tetrahedral geometries adopted by Zn^{2+} and Co^{2+} ions in SmtB (VanZile *et al.* 2001a) and CzrA (Pennella *et al.* 2003), NmtR binds to Ni^{2+} and Co^{2+} in a hexadentate octahedral coordination geometry (Pennella *et al.* 2003) likely recruiting two additional, functionally essential histidine residues from the C-terminal tail of the helix to accommodate binding of metals that prefer higher coordination geometries (Cavet *et al.* 2002; Pennella *et al.* 2003). The comparison of the coordination geometries adopted by NmtR and SmtB highlighted the importance of allostery in facilitating selective metalloregulator responses (this is discussed in detail in section 1.5.5).

A remarkable feature of this family of sensors is the conservation of high affinity metal binding to apparently vestigal binding sites without conservation of the allosteric response. High affinity metal binding at opposing metal sites has been shown for both α3 and α5 sensors. The α5 sensor SmtB retains detectable high affinity metal binding at its α3N sites (VanZile *et al.* 2002a) despite these sites not being regulatory (Turner *et al.* 1996). This is because only one of the pair of cysteines in the α3 CVC motif, shown to be absolutely required for induction of ArsR (Shi *et al.* 1996) and which is essential for regulation in all other α3 sensors identified subsequently, is conserved in SmtB. The other cysteine within the triad is also not conserved in SmtB. The α3N site of SmtB is, however, similar to the α3N site of the *bona fide* α3N sensor

AztR. In AztR the α3N site forms an S_3N complex (Liu *et al.* 2005) however in SmtB a single cysteine within the CVC motif (shown to be critical for allostery in CadC (Busenlehner *et al.* 2002b)) is not conserved resulting in an $S_2(NO)$ site (VanZile *et al*. 2002a).

The archetypal α3N sensor CadC is capable of binding both Zn^{2+} and Cd^{2+} (although in contrast to the α3N site Zn^{2+} binds more tightly than Cd^{2+}) at a pair of intact, non-regulatory α5 sites on the dimer (Kandegedara *et al*. 2009). Comparison with SmtB shows both proteins to contain essentially identical α5 site ligand sets. However, an arginine residue in SmtB structurally validated as important for transduction of the α5 allosteric response in SmtB (Eicken *et al.* 2003) is replaced in CadC with a glycine residue which is proposed not to propagate changes induced on metal binding into shifts in the positions of the α5 helix associated with allosteric switching in SmtB (Kandegedara *et al*. 2009). Thus, these comparisons show how a subtle change of only one or two amino acid residues is sufficient to uncouple metal binding from allostery at a given site in an ArsR-SmtB protein and generate a sensor with different metal binding preferences and responses. Some sensors, notably ZiaR (Thelwell *et al.* 1998) and BxmR (Liu *et al.* 2008) retain regulation through variants of both α5 (both conserve the residues (including those corresponding to His-117 and Arg-87 in SmtB) that are proposed to form the hydrogen bond network in α5 sensors) and α3 sites, leading to further functional specialisation within the family (see section 3.1).

Additional diversity has been generated through evolution of other metal sensing motifs on different conserved structural elements within the protein. CmtR from *M.tuberculosis* regulates expression of a P_1-type ATPase in response to Pb^{2+} and Cd^{2+} (Cavet *et al.* 2003b). Cd^{2+} and Pb^{2+} binding utilises two cysteines from the α4-DNA recognition helix from one monomer (Cys-57 and Cys-61) and a cysteine from a C-terminal extension (Cys-102), producing a trigonally coordinated site at the dimer interface of the protein (Cavet *et al.* 2003b; Wang *et al.* 2005; Banci *et al.* 2007). The C-terminal cysteine is not essential for Cd^{2+} binding however is vital for induction of allosteric switching in the dimer (Wang *et al.* 2005). It has also been suggested that the position of this residue distal to the α4 cysteine pair may have evolved to facilitate the selective binding of ions such as Pb^{2+} and Cd^{2+} which have relatively large ionic radii (Cavet *et al.* 2003b).

The recently discovered Pb^{2+}/Cd^{2+} sensing CmtR homologue from *Streptomyces coelicolor* also contains an α4C binding site forming a trigonal coordination complex

with Pb^{2+} and Cd^{2+}. However, the metal binding function is further expanded by the presence of second metal site that can bind an additional equivalent of Pb^{2+} or Cd^{2+} using a C-terminal vicinal pair of cysteine residues (Cys 110 and Cys-111) and at least one additional ligand (potentially Cys-24 from the opposing dimer subunit) to produce a trigonal S_3 or S_3O complex. The precise role for this second site is unclear at present; this site is required for full induction by Cd^{2+} *in vivo* leading to the suggestion that it may enhance the negative allosteric effect of Cd^{2+} producing enhanced de-repression of transcription. A greater response to Cd^{2+} may have evolved to maximise detoxification of Cd^{2+} compounds which are more bioavailable than those of Pb^{2+} in the soil-based habitat of this organism (Wang *et al.* 2010).

KmtR from *M. tuberculosis* is a Ni^{2+}/Co^{2+} sensor which regulates expression of a CDF family metal exporter (Campbell *et al.* 2007). An α5-3 sensory motif utilises ligands derived from the α5 helix which do not align with residues previously identified in other α5 or α5C sites, with a minimal estimate of four histidines, a glutamate and an aspartate residue potentially involved in metal binding (Campbell et. al., 2007). This is consistent with the preference of Ni^{2+} for higher coordination number geometries and the ability of Co^{2+} also to form octahedral complexes.

1.5.2 Classification of ArsR-SmtB proteins

The metal sensing ArsR-SmtB proteins identified to date can be grouped into eight different classes based on their sensory motif and these are shown in Table 2. Analyses of the evolutionary relationships between ArsR-SmtB proteins have shown that sequences can be divided into eight different groups based on global sequence similarities. However, the metal binding motifs representing each of the sensory paradigms in the family are scattered throughout these groups and are not congruent with overall sequence similarity (Campbell *et al.* 2007). Additionally, these sequence groups do not correlate with established organism phyla. This suggests the diversity of sensory motifs has arisen through a process of concerted and convergent evolution and confirms that the metal sensing motif present in the protein sequence represents a much more effective means of predicting metal sensing preferences (Harvie *et al.* 2006; Campbell *et al.* 2007).

Sensory site	Example protein	Metal sensed *in vivo*
α3	ArsR	As, Sb
α3N	CadC AztR	Cd, Pb, Bi, Zn
α5	SmtB, CzrA	Zn
α5C	NmtR	Ni, Co
α4C	CmtR	Cd, Pb
α5-3	KmtR	Ni, Co
α3N and α5	ZiaR	Zn
α3N or α5	BxmR	Zn, Cd, Pb, Cu, Ag

Table 2. The major sensory ArsR-SmtB family sensory paradigms. The structural motifs from which metal ligands are derived are shown (and which denote the major classes of sensory site within the family) together with key example proteins and the metals that are sensed *in vivo* by these proteins. ArsR, CadC, AztR, SmtB, NmtR, CmtR, KmtR, ZiaR and BxmR are all derived from organisms listed in Figure 4. (section 3.1). CzrA is from *S. aureus*. Note: recent characterisation of a CmtR homologue has identified a functional metal site, in addition to the α4C site present in the protein that utilises a C-terminal vicinal pair of cysteine residues which are essential for effective regulation by cadmium (Wang *et al.* 2010).

1.5.3 Non-metal sensing ArsR-SmtB proteins

Like other metalloregulator families, diversification through evolution has produced ArsR-SmtB-like proteins that can regulate genes that are not involved in metal homeostasis. SoxR negatively regulates the *sox* gene cluster involved in oxidation of reduced sulphur compounds in *Pseudaminobacter salicylatoxidans* (Mandal *et al*. 2007) and contains none of the metal binding motifs found in known metal responsive regulators (Bagchi *et al.* 2005). In *Vibrio cholerae* HlyU positively regulates expression of the gene encoding the cytotoxic virulence protein HlyA (Williams & Manning 1991; Williams *et al.* 1993). BigR negatively regulates expression of an operon containing genes implicated in biofilm formation in a metal independent manor (Barbosa & Benedetti 2007). Both HlyU and SoxR contain two cysteine residues in the α2 and α5 helices which are conserved within the subgroup containing these sensors (Campbell *et al. 2007)*. HlyU and another protein within this subgroup, EcaR (from *Erwinia carotovora*), have both been shown to form complexes with their cognate promoter elements that are unaffected by metal ions (Campbell *et al.* 2007) leading to the proposal that this α2-α5 motif may be predictive of non-metal sensing ArsR-SmtB proteins (Campbell *et al.* 2007; Osman & Cavet 2010). The inducers of these proteins await identification.

1.5.4 Allosteric mechanisms utilised by ArsR-SmtB proteins

Structural studies of selected ArsR-SmtB proteins have begun to elucidate the mechanisms underlying the allosteric responses, induced on metal binding, that are required to inhibit promoter binding and de-repress gene transcription. High resolution crystal structures of the α5 site sensors SmtB and CzrA in both apo- and Zn^{2+} bound forms identified an inter-subunit allosteric switch that is activated on metal binding and which links the metal binding site to the DNA binding domain (Eicken *et al.* 2003). On Zn^{2+} binding to SmtB (and CzrA) a hydrogen bond network is formed that extends from the α5 site to the DNA recognition helix; the non-liganding $N^{\varepsilon 2}$ atom of His-117 forms a side-chain-main chain hydrogen bond to the carbonyl oxygen atom of Arg-87 in the opposing dimer subunit. A backbone hydrogen bond then forms within this subunit between the amide group of leu-88 and the carbonyl oxygen atom of leu 83, which is located at the C-terminal of the DNA binding helix. Additionally, Arg-87 also closely

approaches the metal chelate with the guanidino group moving into hydrogen bonding distance of the carbonyl oxygen atom of His-117 and the non-liganding $O^{\varepsilon 2}$ atom of Glu-120 (Eicken *et al.* 2003).

A hydrogen bond network analogous to that of SmtB also underpins the responses of CzrA (Eicken *et al.* 2003); however, the metal stoichiometry required to drive allostery in the two proteins may differ and is still subject to debate. The crystal structures of apo-SmtB and Zn_1SmtB are superimposable implying that both sites may need to be filled to drive allostery (which is also the case for the α3 sensor CadC (Sun *et al.* 2002)). However, occupation of one site has been shown to mediate partial disassociation from DNA (VanZile *et al.* 2002b). In CzrA, Zn^{2+} binding to only one α5 site on the dimer is required to facilitate effectively complete disassociation from DNA and is associated with significant quaternary switching (Lee *et al.* 2006). Negative homotropic cooperativity resulting in occupation of only a single symmetry related site per dimer, which is likely to be sufficient to mediate allosteric switching, has also been observed in BxmR (Liu *et al.* 2008), AztR (Liu *et al.* 2005) and CmtR (Wang *et al.* 2005). There may be variation in the metal stoichiometry needed to drive allosteric switching for members of this family. Recent studies of the CsoR-NikR family Cu^+ sensor CsoR from *M. tuberculosis* have shown that Cu^+ binding and allostery can be 'uncoupled' by alteration of Cu^+ liganding residues, suggesting that allosteric switches similar to those identified in CzrA and SmtB may be used across families to transduce metal binding into changes in DNA binding responses (Ma *et al.* 2009b).

Although the end result of metal binding induced allostery is the stabilisation of low affinity DNA binding conformations in both SmtB and CzrA, the global structural changes underpinning these changes are different. The apo-protein structures of both proteins are characterised by a high degree of global quaternary structural flexibility which likely facilitates high affinity DNA binding. For SmtB, Zn^{2+} binding induces a quaternary change that results in compaction of the dimer and spatial reorientation of the DNA recognition helices. For CzrA, Zn^{2+} binding merely acts to 'freeze-out' the internal dynamics of the dimer such that the high affinity DNA binding conformation is no longer accessible. The Zn^{2+} bound conformer is also associated with much lower mobility in the DNA binding region (Eicken *et al.* 2003). The NMR solution of structure of DNA-bound CzrA showed it to have a conformation dramatically different to that of Zn^{2+}-CzrA and is characterised by a 'closed'conformation in which the dimer subunits are rotated relative to one another (Arunkumar *et al.* 2009). Although the

mobility in the α5 sites is increased and their stability lower than in Zn^{2+}-CzrA, the mobility of the DNA binding regions of the protein is lower in the Zn^{2+}-form and this conformation also experiences much lower structural heterogeneity with a reduced conformational ensemble (Arunkumar *et al.* 2009).

Changes in protein structural dynamics on metal binding have also been observed for *M. tuberculosis* CmtR. Here, the dimeric apo-protein solution structure was characterised by the presence of well defined secondary structural elements but also by a highly dynamic tertiary structure with a high degree of conformational heterogeneity. In this state binding of three protein dimers to DNA was observed (Banci *et al.* 2007). Binding of Cd^{2+} to the dimer interface inhibited binding to DNA and dramatically reduced the conformational flexibility across the dimers, 'locking' the protein into a rigid tertiary and quaternary structure preventing sampling of conformations that were able to bind DNA (Banci *et al.* 2007). Therefore, although there may be some variability across the ArsR-SmtB family in the details of the allosteric switch, the examples above portray a largely conserved overall mechanism of allostery in which metal binding stabilises a conformation of low DNA binding affinity with a much higher degree of conformational flexibility in apo-protein species facilitating selection of a conformers of high DNA binding affinity, optimal for DNA binding. At present it remains unclear whether de-repression *in vivo* is mediated via metal-induced disassociation of protein-DNA complexes or is instead due to metal-mediated inhibition of protein association with DNA.

1.5.5 Selectivity in ArsR-SmtB proteins

In vivo, ArsR-SmtB proteins must respond selectively to the correct metal. Selectivity has been shown to be mediated at the level of allosteric switching. A notable example of this mechanism comes from comparison of the responses of two ArsR-SmtB sensors, NmtR and SmtB, which have different metal responses *in vivo*. Metal dependent regulation of the *nmt* promoter by NmtR was analysed in *Synechococcus* PCC 7942 and it was found that Co^{2+} and not Ni^{2+} was the most potent regulator in this organism and SmtB continued to sense Zn^{2+} only (Cavet *et al.* 2002). It was initially hypothesised that these differences in selectivity may be due to absolute affinity of each protein for metal; SmtB was predicted to have a tighter affinity for Zn^{2+} and a weaker affinity for Co^{2+} and conversely NmtR was thought to have a tighter affinity for Co^{2+} and a weaker affinity

for Zn^{2+}. Instead, NmtR had a Zn^{2+} affinity much tighter than that for Co^{2+} and Ni^{2+} and SmtB had a Co^{2+} affinity much tighter than that of NmtR (Cavet *et al.* 2002).

Analysis of the metal sites in NmtR demonstrated that both Co^{2+} and Ni^{2+} adopted a hexadentate coordination geometry with involvement of six α5 site ligands all of which were obligatory for function *in vivo* (Cavet *et al.* 2002). Ni^{2+} and Co^{2+} both form higher coordination number complexes much more readily than Zn^{2+} which prefers tetrahedral geometries (da Silva & Williams 2002). Thus, it was concluded that the absence of response to Zn^{2+} was due to recruitment of only a subset of ligands instead of the full six that are required for allosteric switching. This was confirmed in subsequent analyses which showed adoption of a four coordinate geometry by Zn^{2+} in NmtR which was less effective at impairing DNA binding than octahedral Co^{2+}/Ni^{2+} complexes (Pennella *et al.* 2003). The Zn^{2+}-sensor CzrA, from *S. aureus* also binds Ni^{2+} in an allosterically ineffective six-coordinate geometry (Pennella *et al.* 2003). Therefore, even though different metal ions may bind to a protein, this mechanism restricts allosteric switching to the correct metal ion (Cavet *et al.* 2002).

A key observation was that NmtR did not respond to Ni^{2+} in *Synechococcus* PCC 7942 despite Ni^{2+} being the most potent inducer ion in *M. tuberculosis* (Cavet *et al.* 2002). It was shown that when cells were exposed to elevated Ni^{2+} concentrations, in mycobacterial cells the Ni^{2+} content increased to between 2 x 10^4 to 7.4 x10^5 atoms $cell^{-1}$ whereas in *Synechococcus* PCC 7942 cells Ni^{2+} contents were lower and ranged between 2 x 10^4 and 7 x 10^4 atoms $cell^{-1}$ (Cavet *et al.* 2002). The implication is that in *Synechococcus* Ni^{2+} never accumulates to levels sufficient to trigger de-repression of the *nmtA* promoter. SmtB had an affinity for Co^{2+} tighter than that of NmtR but did not respond to Co^{2+} *in vivo*. Additionally, Zn^{2+} bound more tightly to NmtR than Co^{2+} or Ni^{2+} but did not disrupt Co^{2+} sensing *in vivo* (Cavet *et al.* 2002). These data implied that access of sensors to metal pools (in this case Co^{2+} and Zn^{2+}) present in the same cytosol are restricted and that this is likely to contribute to the selective metal responses of sensors *in vivo* (Cavet *et al.* 2002).

Comparison of metal sensing preferences of *M. tuberculosis* NmtR and CmtR showed that for this pair of ArsR-SmtB proteins *in vivo* responses were correlated with their relative binding affinities for Ni^{2+} and Cd^{2+} (Cavet *et al.* 2003b). Cd^{2+} bound to CmtR in preference to NmtR following direct competition of the proteins and NmtR had a tighter affinity for Ni^{2+} than CmtR, although both proteins had similar affinities for Co^{2+} and so their different responses to this metal are not correlated with relative

affinity (Cavet *et al.* 2003b). The second Ni^{2+}/Co^{2+} sensor identified in this organism, KmtR, was subsequently shown to have a Co^{2+} affinity tighter than that of NmtR (Campbell *et al*. 2007) (and by inference CmtR) suggesting that the responses of KmtR and CmtR to Co^{2+} *in vivo* are correlated with relative Co^{2+} affinity for these two proteins.

1.6 The Fur-like family of metal sensing repressors

The Fur (Ferric Uptake Regulator) proteins are another large family of metal sensors, with a recent survey identifying over 800 representatives annotated in bacterial genome databases (Lee & Helmann *et al.* 2007). The founding member of the family, *E.coli* derived Fur (Fur_{EC}) was initially characterised as an iron responsive repressor of iron acquisition systems in *E.coli* (Hantke 1981 & 1984; Bagg & Neilands 1987). Many Fur homologues share a conserved metal co-repression mechanism although alternative modes of regulation have evolved (see section 1.6.1). It is thought that in conditions of high intracellular iron, iron binding to Fur triggers binding to so-called 'Fe-boxes', highly conserved 19 bp DNA sequences identified in the promoters of regulated genes (e.g. encoding components of iron uptake systems and iron siderophores), which in low iron are constitutively expressed (de Lorenzo *et al.* 1987; Griggs & Konisky 1989). Binding of Fe-bound Fur sterically inhibits binding of RNA polymerase to the promoter thus impairing open complex formation (Lee & Helmann 2007).

Iron-sensing Fur homologues have been identified in a wide range of organisms and often regulate expression of a multitude of genes in each organism. The presence of conserved Fur-boxes in regulatory regions of genes is correlated with regulation by Fur although Fur-regulated genes may also be associated with regulatory sequences with little similarity to conserved sequences and genes. Conversely, in some instances genes associated with conserved Fur-box sequences may not be Fur-regulated (Baichoo *et al*. 2002). Fur has been described as a global regulator of cellular responses to iron-stress conditions (Lee & Helmann 2007).

1.6.1 Alternative mechanisms of Fur regulation

In addition to Fur being able to repress gene transcription in the iron-bound form, iron binding can also lead to enhanced transcription both directly and indirectly. One

mechanism of indirect activation of gene expression by Fur is exemplified by the Fur repressed RhyB sRNA system of *E.coli*. Under iron depleted conditions, expression of RhyB is derepressed leading to decreased levels of target mRNAs which encode iron-requiring/storage proteins FeSOD, aconitase A, fumarase A, succinate dehydrogenase and ferritin; expression levels are enhanced in iron replete conditions (Massé & Gottesman 2002). Homologues of RhyB (Davis *et al.* 2005) and similar anti-sense RNA dependent mechanisms have been confirmed in other organisms (Wilderman *et al*. 2004; Gaballa *et al.* 2008; Metruccio *et al*. 2009) suggesting this mode of action is widespread. This mechanism underpins a so-called 'iron sparing' response in which the proteome of the organism is remodelled under conditions of iron-starvation to reduce the expression of abundant iron pools thus minimising intracellular iron requirements (Masse & Gottesman 2002; McHugh *et al.* 2003).

Direct iron-dependent activation of gene expression utilising RhyB-independent mechanisms has also been demonstrated. A Fur homologue from *Helicobacter pylori* represses expression of the ferritin gene in its apo-form and iron causes a decrease in the binding affinity of Fur for this promoter resulting in de-repression (Delany *et al.* 2001). Mn^{2+} has also been shown to reduce binding of Fur to the promoter of the Fur-regulated SodB gene implying a similar mode of regulation (Ernst *et al.* 2005). In *Neisseria meningitidis* Fur has been shown to regulate to the promoter regions of the genes *pan1* (encoding a nitrite reductase), *norB* (encoding a nitric oxide reductase) and *nuoABCDE* (encoding subunits of NADH dehydrogenase) and positively regulate their expression *in vivo* and, in the case of *norB*, *in vitro* (Delany *et al.* 2004). In this instance it was proposed that iron-activated Fur bound to sequences upstream of the RNA polymerase binding site and would thus not occlude polymerase binding DNA as would be the case for Fur-binding sites straddling the promoter (Delany *et al.* 2004). Moreover, activation of transcription observed *in vitro* suggested direct interaction with and recruitment of RNA polymerase (Delany *et al.* 2004).

Iron-dependent activation of the Fur_{EC} regulated *ftnA* gene (encoding FtnA, the major iron storage protein in *E.coli*) has been proposed to function via a novel anti-repression mechanism (Nandal *et al.* 2010). Under iron-deplete conditions the *ftnA* promoter is proposed to be transcriptionally silenced through the action of the global repressor of transcription, H-NS, which polymerises on DNA from sites upstream of *ftnA*, sequestering the H-NS promoter. Under iron-replete conditions iron-activated Fur would compete with H-NS for upstream binding sites, preventing H-NS polymerisation,

making the *ftnA* promoter available for interaction with polymerase thus allowing initiation of transcription (Nandal *et al*. 2010).

1.6.2 Metal binding characteristics of Fur proteins

The nature of the metal binding sites in Fur and the molecular basis for iron-induced allostery has been and remains controversial. Fur_{EC} is known to contain two metal binding sites- an exchangeable regulatory site in which iron is bound in a distorted octahedral environment utilising histidine and carboxylate ligands (Adrait *et al.* 1999) and a non-exchangeable (Althaus *et al.* 1999), structural site containing tetrahedrally coordinated Zn^{2+} with an $S_2(N/O)_2$ ligand sphere (Jacquamet *et al.* 1998). The first member of the Fur family to be structurally characterised was the Fur homologue from *Pseudomonas aeruginosa* (Fur_{PA}) complexed with Zn^{2+} in place of iron (Pohl *et al.* 2003). The structure is composed of an N-terminal winged helix DNA binding domain and a C terminal dimerisation domain with two Zn^{2+} binding sites on each monomer. Site one coordinates the bound metal ion in a distorted octahedral geometry, utilising residues exclusively derived from the dimerisation domain, and includes a well ordered water molecule and a bidentate carboxylate group. The second Zn^{2+} site was found to comprise residues derived from the DNA binding and dimerisation domains to form a distorted tetrahedral site.

In the structure of Fur_{PA} the second Zn^{2+} site was initially designated as the structural Zn^{2+} site in the protein as Zn^{2+} routinely co-purified with this site even in the presence of excess Fe^{2+} (Pohl *et al.* 2003). However, subsequent studies demonstrated Zn^{2+} could be readily removed from this site by EDTA (Lewin *et al.* 2002). Additionally, mutation of two histidine residues in the putative regulatory site one of Fur_{PA} showed the protein to retain iron responsiveness however, mutation of a putative structural site histidine ligand in Zn^{2+} site two abolished iron responsiveness *in vivo* (Lewin *et al.* 2002). Another conserved structural site histidine ligand in Fur_{PA} has also been shown to be critical for iron-responsiveness in *Bacillus subtilis* (Bsat & Helmann 1999), *Salmonella typhimurium* (Hall & Foster 1996) and *V. cholerae* (Lam *et al*. 1994). These observations led to the suggestion that Zn^{2+} site two may actually be the physiological iron sensory site instead of Zn^{2+} site one with this protein most likely having no structural Zn^{2+} ion (Lee & Helmann, 2007). This re-assessment is supported by recent *in silico* molecular modelling studies of Fur_{PA} and Fur_{EC} which suggest

hexacoordinate octahedral coordination of Fe^{2+} at a regulatory site two (Ahmad *et al*. 2009). The crystal structure of *V.cholerae* Fur (Fur_{VC}) also supports this site two geometry, supporting a regulatory role *in vivo* (Sheikh & Taylor 2009).

1.6.3 Zur-a Zn^{2+}-sensing Fur homologue

Since the identification of the iron-sensing Fur homologues, new members with a range of metal specificities have been characterised. Probably the best characterised metal sensing homologue is the zinc sensor Zur. Originally, Zur was discovered simultaneously in *B. subtilius* (Zur_{BS}) (Gaballa & Helmann 1998) and *E.coli* (Zur_{EC}) (Patzer & Hantke 1998). Zur binding sites have since been identified in a host of other organisms suggesting Zur regulons are widely dispersed amongst genomes (Panina *et al.* 2003). Zur_{EC} is probably the best characterised of the Zur homologs. Under zinc-replete conditions, Zur_{EC} binds to the operator-promoter region of a gene cluster encoding an ABC-like Zn^{2+} uptake system (ZnuABC) and represses its expression. Under low-zinc conditions, Zur_{EC} is released from the operator-promoter sequence and expression is restored, thus facilitating Zn^{2+} uptake into the cell (Patzer & Hantke 1998). Characterisation of Zur_{EC} confirmed the presence of two distinct zinc binding sites. In one of these sites Zn^{2+} binds extremely tightly in a tetrahedral $S_3(N/O)$ coordination environment (Outten *et al.* 2001). This site is not exchangeable and removal of the bound Zn^{2+} ion can only be achieved via protein denaturation in the presence of a high-affinity chelating agent such as EDTA; hence, this is almost certainly a structural Zn^{2+} ion site (Outten *et al.* 2001). The second site is the primary allosteric site being highly exchangeable and accommodates Zn^{2+} in an $S(N/O)_3$ environment (Outten *et al.* 2001). This tetrahedral coordination sphere is optimised for Zn^{2+} binding and contrasts with the six-coordinate environment in the regulatory site of Fur which is optimal for binding Fe^{2+} (and Mn^{2+}) which prefer higher coordination numbers. The affinity of Zur_{EC} for Zn^{2+} has been determined to be in the order of 10^{-16} M suggesting that Zur_{EC} acts to buffer levels of free intracellular Zn^{2+} to concentrations substantially less than a single atom per cell implying that there is no freely available Zn^{2+} in the cytosol of *E.coli* (Outten & O'Halloran 2001).

Zur proteins await detailed structural comparisons. However, a high resolution structure of the *M. tuberculosis* homologue (Zur_{MT}) (also known as FurB) has been generated and the metal binding sites resolved (Lucarelli *et al.* 2007). This shows the

presence of three Zn^{2+} binding sites. Site one binds Zn^{2+} in a tetrahedral $SO(N)_2$ complex and is present within a hinge region linking the N-terminal DNA binding domain to a C-terminal dimerisation domain. Although ligand residues are poorly conserved between Zur_{EC} and Zur_{BS}, this site can be readily substituted with Co^{2+} and is ideally positioned to induce the substantial conformational changes in the DNA binding domains thought to be required for interaction with DNA. Hence, this is the likely allosteric site. Site two contains a tetrahedrally bound Zn^{2+} ion in an S_4 complex which was designated a structural Zn^{2+} site due to conservation of these cysteine residues in Zur_{Ec} (although Zur_{EC} employs only three of these cysteines as ligands) and because the Zn^{2+} ion was refractory to removal (Lucarelli *et al.* 2007). Tetrahedral cysteine sites are also the most prevalent structural Zn^{2+} motifs (Auld *et al.* 2001) and an S_4 structural Zn^{2+} sites has been identified in the Fur protein from *H.pylori* (albeit this Zn^{2+} being able to be removed following EDTA treatment) (Vitale *et al.* 2009). A third Zn^{2+} site of lower occupancy and unknown function was also identified within the dimerisation domain although this has been suggested to be a crystallisation artefact with no physiological significance (Lucarelli *et al.* 2007 & 2008).

Zur homologues can regulate a variety of genes in addition to those encoding metal transport systems. In *Corynebacterium glutamicum* Zur indirectly regulates expression of 18 genes and directly regulates expression of nine genes which putatively encode two potential ABC-type transporters, a secreted protein, a predicted oxidoreductase enzyme and a P-loop GTPase protein (Schröder *et al.* 2010). A bioinformatics survey of Zur binding sites and regulated genes across multiple species showed suggested Zur-dependent regulation of several paralogs of ribosomal proteins (Panina *et al.* 2003). These paralogs represent duplications of some existing ribosome proteins and lack some or all of the binding motifs predictive of Zn^{2+} binding in the non-Zur regulated genes (Panina *et al.* 2003). Subsequently, Zur mediated repression of these paralogs has been shown in a range of bacterial species (Maciag *et al.* 2007; Shin *et al.* 2007; Li *et al*. 2009). It is thought that this differential expression pattern facilitates a 'Zn^{2+} sparing response'; under low-Zn^{2+} conditions Zur-mediated repression of ribosome paralogs that do not bind Zn^{2+} is de-repressed and they are incorporated into ribosomes in place of Zn^{2+} binding paralogs, freeing Zn^{2+} for utilisation in other proteins (Panina *et al*. 2003).

Recent analyses of gene transcription profiles of *E.coli* cultured in medium selectively depleted in Zn^{2+} have directly confirmed an increase in Zur regulated

paralog expression (Graham *et al.* 2009). It has also been proposed that this response may actively 'mobilise' Zn^{2+} stored in the ribosome for intracellular redistribution (Akanuma *et al.* 2006). Supporting this model, replacement of the Zn^{2+} binding ribosomal protein RpmE by the non-Zn^{2+} binding YtiA protein has been confirmed in Zn^{2+} starved *B. subtilis* cells (Nanamiya *et al.* 2004) and the ribosome has been shown to preferentially incorporate YtiA which liberates RpmE bound to pre-existing ribosomes (Akanuma *et al.* 2006). Additionally, a 'fail-safe' mechanism also appears to operate in which continued ribosome synthesis is allowed during Zn^{2+} starvation by incorporation of Zn^{2+} sparing paralogs into ribosomes in addition to displacement of Zn^{2+} paralogs from existing ribosomes (Natori *et al.* 2007; Gabriel & Helmann 2009). Thus, much like Fur, Zur appears to act as a global regulator of intracellular zinc levels.

1.6.4 Fur homologues that sense Ni^{2+} and Mn^{2+}

Diversification through evolution has produced a range of additional metal selectivities in the Fur family. Nur is a Ni^{2+} sensing Fur homologue from *Streptomyces coelicolor* that negatively regulates expression of the *sodF* gene (encoding the FeSOD) and the *nikABCDE* operon (which encodes a putative Ni^{2+} transport system) in response to nickel (Ahn *et al.* 2006). Loss of Ni-dependent expression of the NiSOD gene in a Nur knockout strain also confirms a role as a positive regulator of Ni-SOD expression although the mechanism through which this occurs is currently unknown (Ahn *et al*. 2006). Nur is extremely selective for Ni^{2+} both *in vivo* and *in vitro* (Ahn *et al.* 2006). Determination of the high resolution crystal structure of Nur showed the presence of two metal binding sites on each dimer subunit with mutation of each causing loss of DNA binding activity (An *et al.* 2009). One of these sites occupies a position similar to the Zn^{2+} site in structure of *P. aeruginosa* Fur and can bind both Zn^{2+} and Ni^{2+}. The second site is also required for regulation however exclusively binds Ni^{2+} in an octahedral coordination geometry and it is thought that occupancy of this site determines the highly selective response of Nur (An *et al.* 2009). A manganese sensitive uptake regulator, Mur, has been identified in *Rhizobium leguminosarum* and has been shown to repress transcription of the *sitABCD* operon (which encodes an ABC-type manganese importer) in manganese replete conditions (Diaz-Mireles *et al.* 2004) by binding to a unique MRS DNA binding sequence (Díaz-Mireles *et al.* 2005).

1.6.5 Non-metal sensing Fur proteins

As is the case for the ArsR-SmtB family of proteins, some members of the Fur family have evolved to detect stimuli other than metal ions. In *Bradyrhizobium japonicum* iron sensing Fur together with the Fur-like protein Irr act together to regulate intracellular iron homeostasis and iron utilisation in heme biosynthesis pathways (Hamza *et al.* 1998). Under iron-deficient conditions Irr represses expression of genes expressing heme biosynthesis proteins thus preventing protoporphyrin production exceeding iron-availability (Qi & O'Brian 2002). Irr interacts directly with Ferrochelatase and has been shown to bind two molecules of heme (Qi & O'Brian 2002; Yang *et al.* 2005). Under iron replete conditions binding of heme to Irr is proposed to trigger degradation of Irr and relief of repression of transcription (Qi *et al.* 1999; Qi & O Brian 2002). Homologues of Irr have been isolated in other organisms, notably in *Rhodobacter capsulatus* where in the absence of a Fur homologue Irr represents the only regulator of the iron responsive network (Zappa *et al.* 2010). It has been proposed that in this and other alpha proteobacteria Irr and RirA have effectively replaced Fur as the global regulators of iron response networks (with Fur switching to Mn^{2+} sensing in these lineages) and by detecting changes in physiological effects of iron utilisation provided a more flexible response to changes in iron abundance (Rodionov *et al.* 2006).

In *B. subtilis,* genes encoding proteins involved in resistance to oxidative stress are regulated by the three transcriptional regulators; OhrR, the general stress regulator ς^B and the Fur-paralog PerR (Helmann *et al.* 2003). The PerR regulon serves to protect cells from peroxide mediated damage and includes katA (the major vegetative catalase), AhpCF (alkyl hydroperoxide reductase), HemAXCDBL (enzymes of heme biosynthesis) and MrgA (a Dps-like DNA binding protein) (Lee & Helmann 2007). The PerR regulon also includes the iron sensing repressor Fur and ZosA, which encodes a P-type ATPase proposed to import Zn^{2+} in response to oxidative stress (Fuangthong *et al.* 2002; Gaballa & Helmann 2002). Like other Fur family proteins PerR contains two metal binding sites- a structural, Zn^{2+} site containing four cysteine residues (Traoré et *al.* 2006; Lee & Helmann 2006b) and a regulatory site that preferentially binds Mn^{2+} and Fe^{2+} although only the Fe^{2+} form is sensitive to peroxides *in vitro* and *in vivo* (Herbig & Helmann, 2001). The protein detects H_2O_2 via a metal catalysed oxidation (MCO) reaction of two metal liganding histidine residues; the bound metal ion is proposed to coordinate H_2O_2 and generate OH radicals which then oxidise nearby

liganding histidine residues. This causes release of the bound metal ion and disassociation from the DNA (Lee & Helmann 2006a). Structural studies have determined the basis for the somewhat complex allosteric mechanism of this protein. The apo-form of dimeric PerR consists of an 'open'conformation in which the N-terminal winged helix DNA binding domains are 'splayed out' from the C-terminal dimerisation domains which contain the tetrathiolate structural Zn^{2+} site that stabilises the dimer structure. It has been proposed that this apo-structure is not inconsistent with a high degree of conformational freedom in the DNA binding domains relative to the dimerisation domain (Traoré *et al.* 2006; Giedroc 2009). In contrast, the Mn^{2+} form of the protein adopts a closed 'caliper' like conformation in which the DNA interacting helices are ideally positioned to interact with DNA (Jacquamet *et al.* 2009).

Structural data characterised a Metal Catalysed Oxidation mechanism (MCO). A histidine oxidised form of the protein (in which a histidine residue required for metal binding and allostery) adopts a conformation identical to that of the apo-protein form which also has a low affinity for DNA (Traoré *et al.* 2009). Thus, activation of the protein by metal is achieved through formation of the DNA binding caliper structure and subsequent relief of DNA binding occurs via oxidation of metal binding histidines and reorganisation of this structure into one suboptimal for DNA binding (Jacquamet *et al.* 2009; Giedroc 2009). The Mn^{2+} ion (and almost certainly the Fe^{2+} ion) adopts a pentacoordinate geometry allowing coordination of H_2O_2. The structure of this site also accounts for the selective activation of the protein by H_2O_2; steric constraints mean that the relatively small H_2O_2 molecule is readily accommodated at the metal binding site however larger species are excluded (Jacquamet *et al.* 2009; Giedroc 2009).

1.6.6 Factors determining the selectivity of metal-sensing Fur proteins

As for ArsR-SmtB proteins, allostery is likely to be important for selective responses of Fur proteins. Mn^{2+}, $Fe^{2+/3+}$, Co^{2+} and Zn^{2+} have been show to activate Fur *in vitro* (Mills & Marletta 2005). Notably, a response to Mn^{2+} is also implied *in vivo* by higher growth levels of *fur* mutants exposed to high levels of Mn^{2+} (Hantke 1987). These ions (except Zn^{2+}) can readily adopt the six-coordinate geometry formed by iron in the sensory site (Jacquamet *et al.* 1998) which is likely to be the structure adopted by the physiologically relevant active complex. Zn^{2+} may activate the protein via a different mechanism. The *in vivo* responses of Fur are relatively restricted, responding only to

Fe^{2+} and Mn^{2+} (Hantke 1987). The equilibrium disassociation constants of Fur for these ions together with the estimated intracellular levels of each metal suggest that only Fe^{2+} and potentially Mn^{2+} accumulate to levels which can facilitate repression *in vivo* (Mills & Marletta 2005; Lee & Helmann 2007). In *E.coli* a range of other sensors may act to maintain cytosolic concentrations of these non-effective ions sufficiently low enough so as to prevent binding to Fur and ensure that Fe^{2+}/Mn^{2+}-Fur complexes are the dominant complexes formed *in vivo*.

Studies of the Mn^{2+}-sensing Fur homologue Mur support the notion that regulation of access to metal ions contributes to selective responses *in vivo*. Mur has been shown to bind Mn^{2+}, Fe^{2+} Zn^{2+} and Co^{2+} with similar micromolar range disassociation constants and all of these ions can also activate the protein for DNA binding (Bellini & Hemmings *et al.* 2006). In *R. leguminosarum* Mur responds to Mn^{2+} but Zn^{2+}, Co^{2+}, Cu^{2+}, Fe^{3+} and Ni^{2+} all have no effect on Mur regulated gene expression in this organism (Díaz-Mireles *et al.* 2005). However, when Mur was expressed in an *E.coli fur* deficient host, iron but not manganese-dependent regulation of expression of a gene (*bfd*) containing a canonical Fur box was observed (Díaz-Mireles *et al.* 2005), which was consistent with earlier studies demonstrating that Mur was able to bind Fur boxes and that overexpression of a *R. leguminosarum mur* gene in an *E.coli fur* mutant partially corrected the constitutive expression of a *bfd-lac* fusion under iron replete conditions (Wexler *et al.* 2003).

Iron readily adopts the six-coordinate coordination geometry favoured by Mn^{2+}; thus the response of Mur to iron in *E.coli* is likely to be due to iron adopting a native (Mn^{2+}-like) geometry that is optimal for allosteric activation. With analogy to the difference in Ni^{2+} responses of NmtR in different organisms (Cavet *et al.* 2002) (section 1.5.5), it is hypothesised that in *R.leguminosarum,* Fe^{2+}, Co^{2+} and Zn^{2+} never accumulate to concentrations that are sufficient to activate the protein for DNA binding (Lee & Helmann 2007). The set-point concentrations for metals in each organism may have evolved divergently to produce selective responses for the ensemble of sensors expressed in each organism.

1.6.7 Allosteric regulation in other metal-dependent co-repressor sensor families

Allostery has also been shown to be important in generating selective metal responses of sensors from other metal dependent co-repressor families. NikR is activated to bind

DNA by binding four Ni^{2+} ions per tetramer with picomolar affinities in square planar geometry sites (Chivers & Sauer 2002). On DNA binding octahedral sites are formed which potentiate binding to DNA (Carrington *et al.* 2003) however, this response was shown to be selective for Ni^{2+} with other divalent metals producing weaker DNA binding affinities (Bloom & Zamble 2004). Analysis of derivatives of NikR bound to Zn^{2+}, Co^{2+}, Ni^{2+}, Cu^{+} and Cu^{2+} showed that only Cu^{2+} formed the four-coordinate planar geometry characteristic of the high affinity Ni^{2+} binding sites in the protein and that this was correlated with Ni^{2+}-like changes in protein structure. Moreover, Cu^{2+} (in addition to Ni^{2+}) was able to organise the low-affinity regulatory sites into an octahedral geometry optimal for Ni^{2+} binding (Leitch *et al.* 2007). Thus, in NikR only metal ions that adopt a square-planar-like geometry at the primary high affinity Ni^{2+}-binding sites are able to organise the protein into a high-affinity DNA binding conformation.

In the Fe^{2+}-sensor DtxR it has been shown that Fe^{2+}, Co^{2+}, Mn^{2+} and Ni^{2+} activate the protein for DNA binding however Zn^{2+} is a much less effective activator of DNA binding (Tao & Murphy 1992; Spiering *et al.* 2003). The DNA bound structure of DtxR showed that Ni^{2+} bound to the primary metal binding site via a six coordinate octahedral geometry (White *et al.* 1998), a geometry that can be readily adopted by Fe^{2+}, Co^{2+} and Mn^{2+} but not Zn^{2+}. Zn^{2+} can bind to the DtxR-like Mn^{2+} sensor MntR *in vitro* (Golynskiy *et al.* 2006) however it is not regulatory *in vivo* (Que & Helmann 2000). Zn^{2+} was shown to be less allosterically effective than Mn^{2+} *in vitro* (Lieser *et al.* 2003) and binds to one of the pair of metal binding sites in a tetrahedral geometry distinct to that of Mn^{2+}; that causes structural perturbations impairing subsequent binding to a second site, occupation of which is necessary for effective co-repressor function (Kliegman *et al.* 2006). However, Cd^{2+} can bind in a binuclear cluster almost identical in structure to the physiological Mn^{2+} cluster (Kliegman *et al.* 2006). Formation of this native-like chelate is associated with Cd^{2+} being a potent regulatory ion *in vitro* (Golynskiy *et al.* 2006; Lieser *et al.* 2003).

1.7 The MerR-like family of metal sensing transcriptional activators

1.7.1 The mercuric ion resistance system

The MerR family comprises metal dependent activator proteins; metals bind to the regulator proteins and activate transcription. The founding and defining member of the

family is the MerR protein which regulates expression of genes in the mercuric ion resistance (*mer*) operon which confers resistance to mercury compounds. Mercury resistance loci are thought to be ubiquitous in prokaryotic species however, the best characterised mercury resistance systems are those derived from the gram negative bacterial transposons Tn*21* and Tn*501* (Summers 1992). The simplest resistance mechanism characterised for the Tn*501* locus is summarised in Figure 1 (adapted from Hobman *et al.* 2005). In this system the apo-MerR protein binds as a homodimer to the mer O/P region, repressing transcription of the *mer* operon which includes the resistance genes (*merTPAD*) as well as the *merR* gene itself. On binding of Hg^{2+} ions to the DNA-bound apo-MerR homodimer, conformational change cause under-winding of the *mer*OP DNA allowing RNA polymerase to proceed with transcription producing a polycistronic mRNA containing the resistance transcripts. Only a four-fold reduction in DNA binding affinity was observed on binding of Hg^{2+} to apo-MerR protein (Parkhill *et al.* 1993). Hence, metal-induced changes in DNA binding are much less significant in facilitating changes in regulation at the promoter and regulation is primarily correlated with reorganisation of promoter DNA structure.

1.7.2 Metal-sensing homologues of MerR

As with the other metal sensor families, adaptive radiation through evolution has produced numerous homologues with a wide range of metal-sensing specificities. Well characterised examples include CueR, a copper sensor from *E.coli* regulating expression of Cu^{+} exporting P-type ATPase CopA (Petersen & Møller 2000; Stoyanov *et al.* 2001) and which also responds to Ag^{+} and Au^{+} (Stoyanov *et al.* 2001; Stoyanov & Brown, 2003), ZntR a zinc sensor which also responds to Pb^{2+} and Cd^{2+} (Brocklehurst *et al.* 1999; Binet *et al.* 2000) which regulates expression of the Zn^{2+}/Cd^{2+}/Pb^{2+} P-Type ATPase ZntA (Rensing *et al.* 1997 & 1998), CadR from *P. aeruginosa* which responds to Cd^{2+} (and also Zn^{2+} and Hg^{2+} but with lower efficacy) (Brocklehurst *et al.* 2003) and PbrR from *Ralstonia Metallidurans,* which regulates the *pbrABCD* operon and confers specific resistance to Pb^{2+} (Borremans *et al.* 2001; Hynninen, 2009). More unusual examples include GolS which has been shown to respond specifically to gold ions and regulates expression of GolT (a predicted plasma membrane efflux protein), GolB (a predicted metallochaperone protein) (Checa *et al.* 2007) as well as the *gesABC* operon

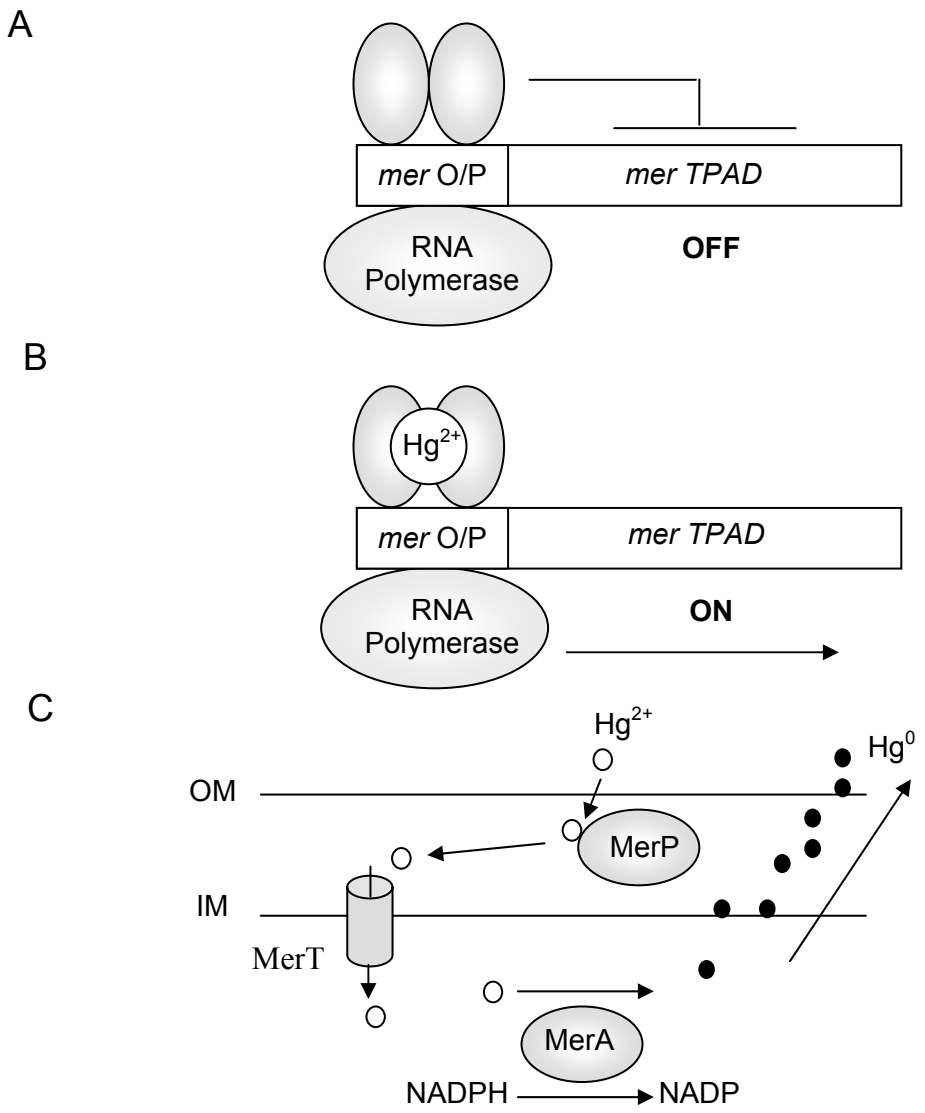

Figure 1. Mechanism of mercury resistance mediated by MerR in an *E.coli* cell containing the Tn*501* resistance operon. (a) *merR* is transcribed to produce MerR protein which then binds as a homodimer to the *mer* O/P region. RNA polymerase is recruited to the *mer* operon where transcription of the resistance genes (*merTPAD*) is repressed by the bound MerR protein. (b) Hg^{2+} diffuses through the bacterial membranes into the cytosol and binds to DNA-bound apo-MerR homodimer. The resulting conformational change causes reorganisation of the promoter allowing RNA Polymerase to proceed with transcription producing a polycistronic mRNA containing the resistance transcripts. The resulting resistance proteins are each localised to their respective sites of action. MerP localises to the periplasm where it binds Hg^{2+} and mediates its transfer to MerT, localised to the inner membrane. Hg^{2+} is then transferred to MerA, a cytosolic NADPH-dependent disulfide oxidoreductase which catalyses the reduction of Hg^{2+} to Hg^0 which then diffuses out of the cell (c). MerD forms a ternary complex with metallated MerR and *merO/P* causing dissociation of MerR from DNA thus allowing the synthesis of new apo-MerR which can then bind to the promoter and restore repression of *mer* transcription when levels of intracellular mercury have returned to normal (Champier *et al.* 2004; Hobman *et al.* 2005). (Figure adapted from Hobman *et al.* 2005).

which encodes a CBA export system conferring resistance to gold salts in *S. typhimurium* (Pontel *et al.* 2007). CoaR from *Synechocystis* is the only known Co^{2+} sensing MerR family member, regulating expression of CoaT, a cobalt exporting P-Type ATPase (discussed in section 1.8.2) (Rutherford *et al.* 1999).

1.7.3 Non-metal sensing homologues of MerR

In addition to metal sensing homologues of MerR, non-metal sensing functions have also apparently evolved on the ancestral MerR scaffold. A principle example is the *E.coli* SoxR protein. This protein is a MerR homologue (Amábile-Cuevas & Demple 1991) which regulates expression of the SoxS protein (Nunoshiba *et al.* 1992) which is itself a transcriptional activator which directly regulates expression of a large number of genes involved in the oxidative stress response (Wu & Weiss 1991; Li & Demple 1994). SoxR contains a 2Fe-2S cluster that allows SoxR to act as a sensitive redox sensor; oxidation of the cluster primarily by superoxide and nitric oxide species (Nunoshiba *et al.* 1993; Storz & Imlay 1999) to form a fully oxidised Fe^{3+}-Fe^{3+} cluster (Gaudu and Weiss 1996) activates the protein enabling transcription of *soxS*. Reduction of the cluster by a single electron causes loss of transcriptional activation (Ding *et al.* 1996). MerR-like proteins have also been identified that detect toxic organic molecules and which regulate expression of multidrug efflux transporter systems to remove these molecules from the cytosol. Examples include BmrR which regulates expression of the multidrug transporter gene *bmr* in response to rhodamine 6G and tetraphenylphosphonium (TPP) (Ahmed *et al.* 1994), BltR, which regulates expression of *blt* which encodes another multidrug transporter (Ahmed *et al.* 1995) and Mta, which regulates expression of *blt, bmr* and *ydfk* (a predicted membrane protein) and acts as a global regulator of multidrug efflux systems in *B. subtilis* (Baranova *et al.* 1999).

1.7.4 The DNA under-winding allosteric mechanism utilised by MerR proteins

Despite the evolution of numerous, specialised functions for each member of this family of sensors, a universal conserved feature that is the hallmark of this family is the unusual underwinding and DNA distortion mechanism by which transcriptional activation is achieved. The unique structure of the *merD* and other MerR-regulated promoters underpins this mechanism. MerR binds to a dyad repeat sequence located

between the -10 and -35 σ^{70} RNA polymerase hexamer elements and these elements are separated by 19 base-pairs (Park *et al.* 1992) instead of the 16-18 base-pairs found in the majority of *E.coli* promoters (Harley and Reynolds 1987). The positioning of these promoter elements is suboptimal for RNA polymerase binding and activation of transcription at the promoter and their positioning is crucial for regulation of the promoter; shortening of the spacing region by mutation causes constitutive up-regulation of transcription at the promoter (Parkhill & Brown 1990). Furthermore, binding of apo-MerR to the promoter induces a dramatic bend in the DNA further impairing RNA polymerase association with the promoter (Ansari *et al.* 1995).

On binding of apo-MerR to the promoter RNA-polymerase is recruited to form a transcriptionally inactive ternary complex in which RNA polymerase and MerR are in direct association (Heltzel *et al.* 1990; Kulkarni & Summers 1999). Binding of Hg^{2+} to MerR causes a conformational change in MerR which results in underwinding of the DNA by approximately 33^{o} (Ansari *et al.* 1992) accompanied by relief of DNA bending induced by promoter bound MerR (Ansari *et al.* 1995). These events realign the -10 and -35 elements into positions which are then optimal for RNA polymerase binding allowing transcriptional activation to proceed. This model is summarised in Figure 2.

1.7.5 Factors determining selective metal binding and responses of MerR proteins

Extensive structural and biochemical characterisation of members of MerR family have revealed the detailed nature of the metal binding sites in different family members and comparisons between these sites emphasise the degree to which subtle changes to the metal ligand spheres in a common structural scaffold have fine-tuned metal selectivity. Although the structure of MerR is yet to be solved it is known that a single Hg^{2+} ion binds to the MerR homodimer (O'Halloran *et al.* 1989; Shewchuk *et al.* 1989a). The Hg^{2+} ion binds to the dimer in a tri-coordinate geometry, bridging both subunits within the dimer. This coordination sphere utilises three conserved cysteine residues; a single cysteine from one subunit (C-82) and two cysteines from the other subunit in the dimer(C-117 and C-126) (Helmann *et al.* 1990). Mutation of a non-conserved cysteine to alanine in Tn*501* MerR protein causes a substantial increase in transcriptional activation *in vivo* (Shewchuk *et al.* 1989b). This cysteine may compete with liganding cysteines for Hg^{2+} in this homologue; perhaps this additional ligand has evolved to attenuate the binding of and/or response to Hg^{2+} in this protein.

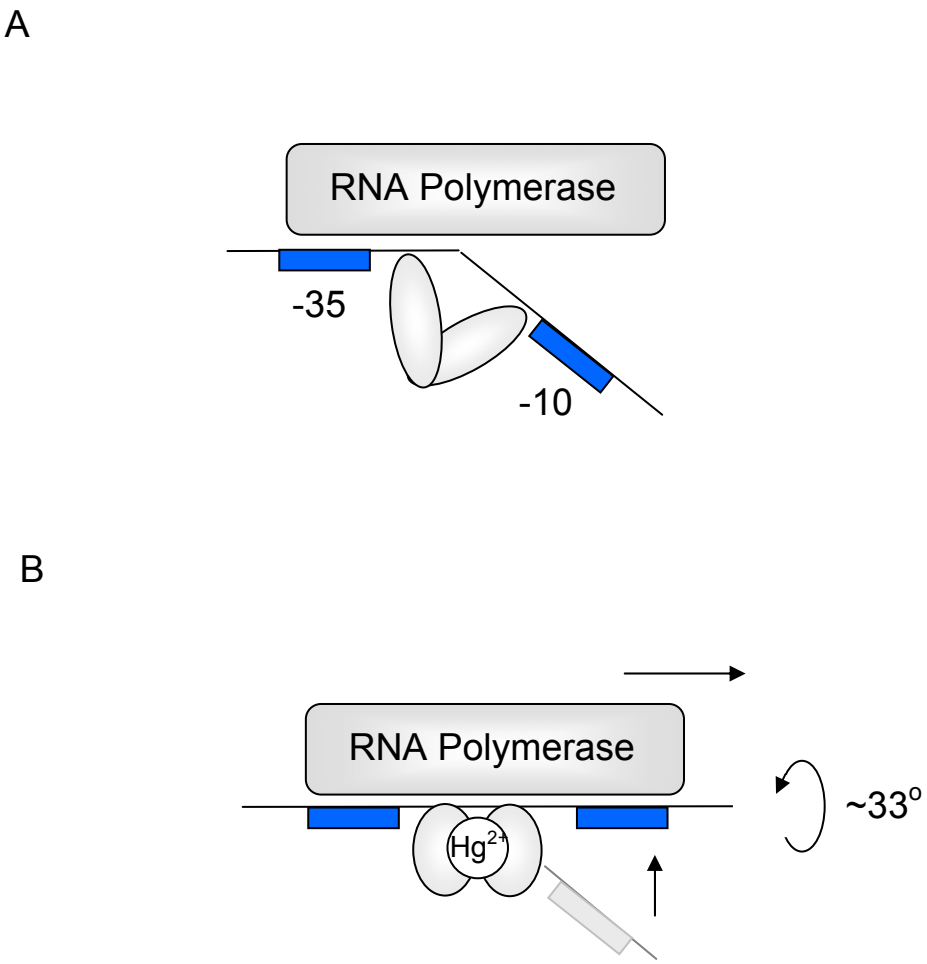

Figure 2. The DNA underwinding mechanism of MerR family proteins exemplified by MerR. A. In the apo-form, MerR binds to specific binding sequences located between the -10 and -35 recognition hexamers (Blue boxes) in the promoter of the regulated gene. These sequences are separated by an unusually large spacer region which results in the -10 and -35 sequences being suboptimally aligned for RNA polymerase binding. Additionally, apo-MerR causes a substantial bend to be introduced into the DNA which further impairs optimal RNA polymerase association. B. On binding Hg^{2+}, a conformational change in MerR is induced causing relief of the DNA distortion and underwinding of the DNA by approximately 33o. These changes in promoter structure facilitate full contact with RNA polymerase allowing open complex formation and transcriptional activation (Figure adapted from Hobman 2007).

As well as the composition of the primary ligand sphere, the structure of the entire metal binding motif may also contribute to selectivity in the metals bound by MerR. It has been shown that MerR and a synthetic polypeptide reconstituting the metal binding domain both bound to Hg^{2+}, Zn^{2+}, Cd^{2+} *in vitro* and *in vivo*. However, the metal binding domain was more effective at binding As^{3+} and less effective at binding Hg^{2+} both *in vitro* and *in vivo*, suggesting that each protein adopted a different conformation, with the ligands not arranged to optimally accommodate As^{3+} binding. This implicated a role for steric hinderance of thiol ligands, imposed by the structural elements of MerR that were not present in the polypeptide, in modulating the metal binding profile of the protein (Song *et al.* 2004).

Structural studies of other MerR family members have elucidated the mechanisms that are used within this family to facilitate selective metal binding. Principal examples are the Cu^{+} and Zn^{2+} sensors CueR and ZntR from *E.coli*. The crystal structures of both proteins showed that they share a similar overall fold with a conserved winged helix DNA binding domain. Additionally, both proteins contain a loop structure near the extended dimerisation helix within which metal ions are ligated by residues derived from both subunits within the dimer (Changela *et al*. 2003) (which also align with residues shown to ligate Hg^{2+} in MerR (Hobman *et al.* 2005). However, the metal binding spheres have diverged substantially during evolution to accommodate different metal ions. In the case of ZntR, Zn^{2+} binding occurs in a binuclear Zn^{2+} site with each Zn^{2+} ion bound a tetrahedral configuration. One Zn^{2+} ion is ligated by Cys-114 and Cys-124 and the other is ligated by Cys-115 and His-119, all from the same metal binding loop. Each Zn^{2+} ion is also bridged by oxygen atoms from a phosphate or sulphate anion and by the sulphur atom of Cys-79 from the other monomer (Changela *et al.* 2003). Mutation of all five protein derived ligands has been shown to reduce or abolish the Zn^{2+} response *in vivo* (Khan *et al.* 2002). Although this binuclear motif is unusual for Zn^{2+} the tetrahedral coordination geometry is optimal for the four coordinate geometries preferred by Zn^{2+}. In CueR the metal binding ligands are optimal for binding monovalent ions and Cu^{+} has been shown to bind cysteines analogous to Cys114 and Cys124 to form a two-coordinate linear S-Cu^{+}-S complex (Changela *et al.* 2003). In ZntR a single residue has a critical role in mediating binding selectivity. In ZntR a cysteine-79 bridges the two bound Zn^{2+} ions in place of a non-liganding serine in CueR, favouring binding of metal ions which prefer higher coordination numbers in ZntR. Thus, the ZntR site is optimal for binding divalent ions such as Zn^{2+}. Structural features

additional to those found in the primary coordination shell are also vital. In CueR the presence of partial positive charge from a nearby helix dipole repels divalent ions. This partial positive charge together with the formation of hydrogen bonds neutralises the net negative charge at the S-Cu-S site on binding of monovalent but not divalent metal ions (Changela *et al.* 2003).

For MerR proteins, selectivity of metal regulated responses appears to be controlled by the metal site ligands and as for the Fur and ArsR-SmtB proteins effective allostery is correlated with native coordination geometries. Replacement of the metal sensing site of GolS with that from CueR has been shown to change the metal sensing characteristics of GolS; normally, GolS preferentially responds to Au^{+} however, replacement of the metal binding loop causes copper sensing *in vivo* (Checa *et al.* 2007). Although GolS and CueR are similar proteins their responses have presumably been fine-tuned through evolution by modification to the metal-binding loop. In CueR the digonal coordination geometry adopted by Cu^{+} is also adopted by Ag^{+} and Au^{+} which are also allosterically effective *in vitro* (Changela *et al.* 2003) and (for Ag^{+}) *in vivo* (Stoynaov *et al.* 2001). Zn^{2+} and Cd^{2+} elicit different conformational changes in DNA-bound MerR compared to those induced by Hg^{2+} (Song *et al.* 2007) which is able to form the compact structure associated with activated protein (Guo *et al.* 2010).

Because of the absence of MerR protein structures crystallised in multiple forms (ideally structures are required of proteins bound to DNA in the presence and absence of a bound metal ion) the detailed molecular bases for how ligand-protein interactions in MerR-like proteins are converted into the allosteric changes necessary for transcriptional activation remain unclear. Structural studies of the N-terminal DNA binding domain from the MerR-like sensor Mta have shown that in the DNA-bound form the DNA binding domains undergo an 11° rotation and a 6 Å inward translation which results in a shortening of the distances between the two DNA reading helices. These changes are mediated by large structural changes in a flexible hinge region linking the dimerisation and DNA binding domains (Changela *et al.* 2003; Newberry & Brennan 2004). In ZntR, it has been suggested that metal binding to Cys-79 could reorient the hinge region of the protein, causing a global allosteric change. Notably, this residue is conserved in MerR. For CueR, it has been suggested that the binding of a Cu^{+} ion to a critical cysteine residue (Cys-112) modifies a hydrogen bond formed with the carbonyl O atom of residue Ser-77 (analogous to the metal binding hinge residue C79 in ZntR), therefore potentially indirectly triggering an allosteric change analogous to that

induced on Zn^{2+} binding to Cys-79 in ZntR (Hobman *et al.* 2007). The conservation of this hinge region in CueR and ZntR and potentially other metal sensing members of the MerR family suggests conservation of this mechanism across the family.

The spacing between the -10 and -35 hexamer repeats also varies and this may be a determinant of specificity for MerR proteins in the same organism. For example, the -10 and -35 promoter elements are separated by 20 base-pairs in the promoter of *zntA* (Brocklehurst *et al.* 1999) however, they are separated by 19 base-pairs in the promoter of *copA* (Stoyanov *et al.* 2001). Longer spacer regions require a greater degree of underwinding to restore optimal spacing and facilitate RNA polymerase binding which may require different degrees of conformational change in the MerR protein on metal binding. Hence, it has been suggested that only the correct metal, recruiting the correct ligands and forming the right chelate structure, may trigger a conformational change that can efficiently reorganise the promoter structure (Hobman *et al.* 2007).

1.8 *Synechocystis* sp. PCC 6803 as a model organism for the study of metal homeostasis

1.8.1 The physiology and metal requirements of *Synechocystis*

Synechocystis is ideally suited as a model organism for the study of metal homeostasis. Rapid evolution of cyanobacteria occurred during a period in which metal availability and therefore the requirements for metal homeostasis were also changing rapidly (Cavet *et al.* 2003a). Cyanobacteria have metal requirements which are not present in many other bacteria (Cavet *et al.* 2003a) and have evolved oxygenic photosynthetic systems with high intracellular metal demands. Cyanobacteria such as the freshwater strain *Synechocystis* sp. PCC 6803 are therefore highly suited for analyses of metal homeostasis. The genome of *Synechocystis* encodes 3168 proteins and is highly enriched in genes encoding metalloproteins and metal-sensor systems due to the presence of metal requiring photosynthetic proteins. For example, four Mn^{2+} ions are found in the water splitting catalytic centre and copper ions are required by plastocyanin and cytochrome oxidase. Iron is required in the form of heam groups and iron-sulfur clusters in both photosystem I and II and it has been shown that *Synechocystis* cells can contain up to one hundred times more iron than *E.coli* cells (Keren *et al.* 2004). *Synechocystis* also has a requirement for Co^{2+} which is inserted into the corrin ring

during vitamin B_{12} synthesis. More generally, cyanobacteria also produce an atypically large number of metal-binding tetrapyrroles, including heme and siroheme (containing iron) and chlorophyll (containing magnesium) (Tottey *et al.* 2007). A requirement also exists for Zn^{2+} and Mg^{2+} in the form of carboxysome-localised carbonic anhydrase and Ribulose-1,5-bisphosphate carboxylase oxygenase (RuBisCO) respectively. Many cyanobacteria can also fix atmospheric dinitrogen (N_2) into ammonia (NH_3) via nitrogenase (Tamagnini *et al.* 2002) and so have a Mo requirement in the form of a FeMo-co-metal cluster present in the MoFe-protein subunit of the enzyme (Schwarz *et al.* 2009).

1.8.2 Transcriptional regulation of metal homeostasis in *Synechocystis*

A range of metal sensing strategies have evolved in *Synechocystis* to remove toxic metal ions and maintain concentrations of essential metal ions in ranges optimal for efficient co-factoring of proteins. The *Synechocystis* genome encodes proteins with homology to five of the seven major classes of prokaryotic metal sensing transcriptional regulator families (Table 1) and these are summarised in Figure 3. Multiple de-repressor families represented are present. The ArsR-SmtB family has two representatives; ArsR has been shown to regulate expression of the arsenic resistance *arsBHC* operon in response to As^{3+} (López-Maury *et al.* 2003). ZiaR has been shown to be a Zn^{2+} sensor *in vivo*, regulating expression of a Zn^{2+}-exporting ATPase, ZiaA (Thelwell *et al.* 1998). Unusually amongst ArsR-SmtB proteins, ZiaR was shown to require both α3N and α5 metal sites for function *in vivo* (Thelwell *et al.* 1998). A protein with similarity to both CsoR and RcnR is present however the metals sensed by this protein are currently unknown. A protein with similarity to the Cu^{+} sensor CopY is also present; the metal sensing properties of this protein also remain to be determined however, recent bioinformatics analyses suggest that this protein may not sense Cu^{+} as it lacks the C-terminal CopY consensus motif (Cys-x-Cys-x_4-Cys-x-Cys) (Magnani & Solioz 2007).

Metal-sensing co-repressor proteins are represented by Fur-like proteins of which three are encoded within the genome. One of these proteins (gene sll1738) is a PerR homologue which regulates changes in gene expression in response to oxidative stress (Kobayashi *et al.* 2004; Li *et al.* 2004). Multiple lines of evidence suggest that the second Fur homologue (gene sll0567) is the iron-sensor in this organism; it has been shown to regulate iron responsive genes (Kunert *et al.* 2003) and has a high degree of

similarity to the iron-sensing Fur protein from *Synechococcus* PCC 7942, which was shown previously to regulate iron stress genes with a reduction in growth evident in a deletion mutant strain in iron-replete medium (Ghassemian & Straus 1996). The third homologue (gene sll1937) is annotated as a zinc-sensor (Zur_{SS}). It is divergently transcribed from a set of genes with homology to the *znuABC* genes, previously shown to encode proteins forming the Zn^{2+} import system in other organisms whose expression is also under the control of Zur (Patzer & Hantke 1998 & 2000). Inactivation of each of the *znuABC* genes resulted in mutant strains that grew poorly in the absence of Zn^{2+} added to the growth medium and such a mutant exhibited reduced uptake of $^{65}Zn^{2+}$. Evidence for Zur regulation of these genes comes from studies which showed constitutive up-regulation of *znu* genes in a *zur* knockout mutant (Pakrasi *et al.* 2001).

Two proteins with homology to MerR are also present in *Synechocystis*. A protein with homology to CueR is present however the metal sensing properties of this protein are uncharacterised. CoaR has been shown to be a Co^{2+} sensor that regulates expression of *coaT*, which encodes a Co^{2+} exporting ATPase (Rutherford *et al.* 1999). CoaR represents the fusion of an ancestral MerR-like protein and precorrin isomerase, which normally catalyses the conversion of precorrin 8-x to hydrogenobyrinic acid. Previous work showed that when the enzyme that synthesised precorrin 8-x (the substrate for precorrin isomerase) was inactivated there was an increase in expression from the *coaT* promoter (Rutherford *et al.* 1999). This established a direct link between CoaR and the B_{12} pathway with CoaR implicated in integrating metabolic demands for Co^{2+} (for insertion into the corrin ring after this step) with changes in the degree of Co^{2+} export and hence cytosolic Co^{2+} concentration (Rutherford *et al.* 1999).

Two component systems are also utilised to regulate levels of some metal ions. The *nrs* operon encodes proteins of Ni^{2+} resistance (García-Domínguez *et al.* 2000) and its expression is regulated by the two component NrsR/S system (López-Maury *et al.* 2002). The gene *mntC* encodes a component of a high-affinity Mn^{2+} uptake transporter (mntABC) which facilitates Mn^{2+} uptake under conditions of Mn^{2+} starvation (Bartsevich & Pakrasi 1995 & 1996). Its expression is under the control of ManS/R a two component Mn^{2+} sensor system (Ogawa *et al.* 2002).

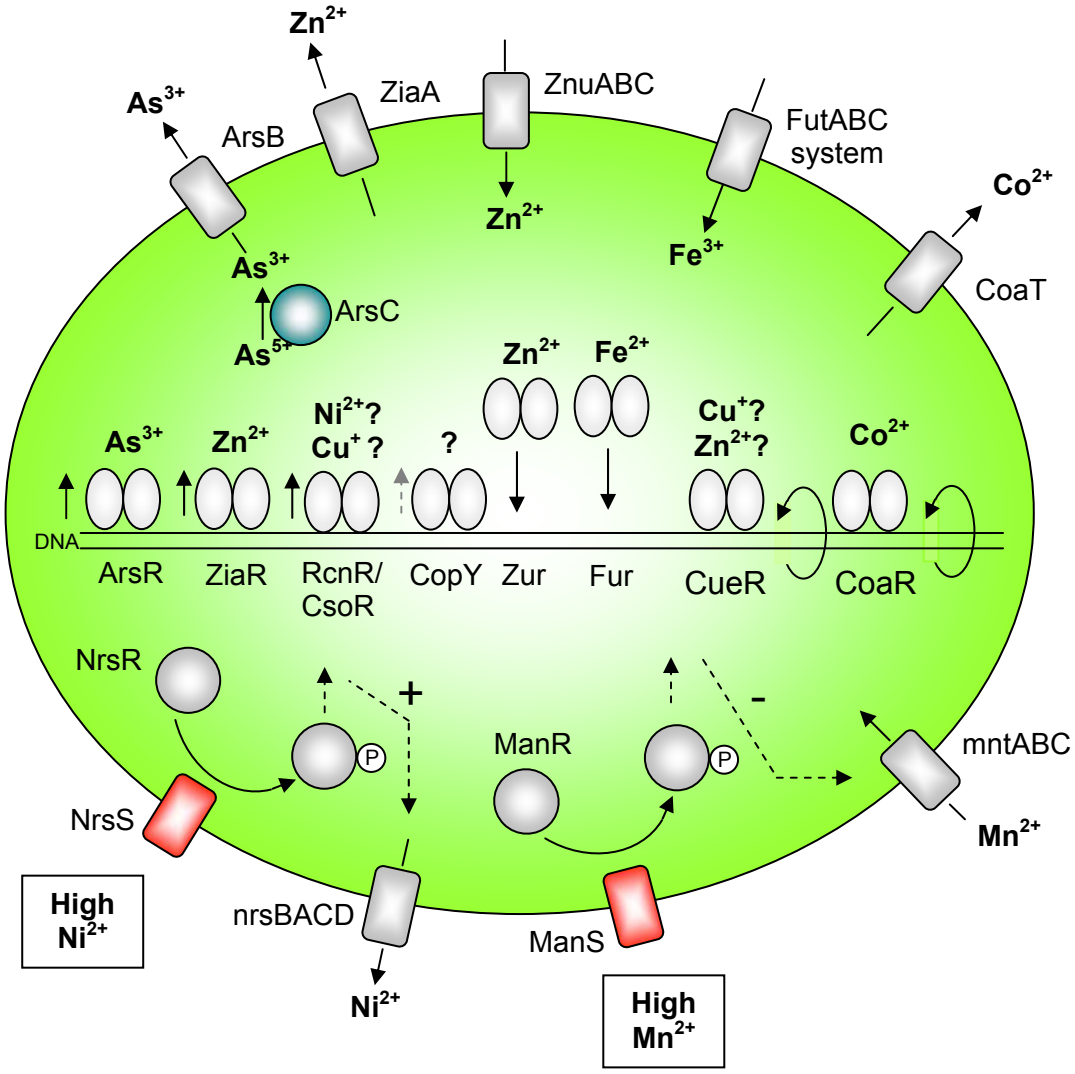

Figure 3. Summary of the metal homeostasis systems and transcriptional regulatory circuits of *Synechocystis.* The complement of single component metal sensing transcriptional regulators is shown in association with DNA. The two-component sensor systems are also shown for Ni^{2+} and Mn^{2+}. In the NrsR/S system, under Ni^{2+} replete conditions the NrsR response regulator is phosphorylated by the NrsS sensor kinase; activated NrsR binds to DNA (likely as a dimer; López-Maury *et al.* 2002) to activate transcription of the *nrsBACD* operon, which encodes components of a predicted plasma membrane Ni^{2+} export system. Under Mn^{2+} replete conditions, the two-component response regulator ManR is activated to bind DNA by the ManS sensor kinase; this inhibits transcription of an operon (*mntABC*) encoding a Mn^{2+} uptake system. The corresponding transport directions for the plasma membrane transport systems identified are also shown; iron-uptake systems have been identified in this organism (Katoh *et al.* 2001) (and are shown in this diagram) however it is not known to what extent these are regulated by the Fur homologue annotated in this genome.

1.9 Project Aims.

Investigating the roles of allostery, access and affinity in determining selective response of metal sensor proteins of *Synechocystis*

1.9.1 Analysis of the allosteric responses of ZiaR and Zur_{SS} *in vitro*

Allostery has emerged as being an important factor contributing to the generation of selective metal sensor responses *in vivo* for both metal-sensing de-repressors (Cavet *et al.* 2002) (section 1.5.5) and metal-dependent co-repressors (section 1.6.6). For metal-dependent activators and co-repressors the contribution of allostery to selectivity has been suggested to be of particular importance, as metals must bind to regulators and produce an active DNA binding adduct. Conversely, for metal-dependent de-repressors the metal ion may only need to 'trap' the protein into any of a large number of conformations suboptimal for DNA binding to prevent binding and so in some instances allostery may be less important for selectivity than for activators and co-repressors (Waldron & Robinson 2009; Waldron *et al.* 2009). Comparative *in vitro* analyses of the metal binding properties and DNA-binding responses of the Zn^{2+}-sensing proteins ZiaR and Zur_{SS} from *Synechocystis* allow this hypothesis to be investigated. Moreover, these analyses allow the apparently distinct allosteric mechanism of ZiaR, in which two metal sites are required for function *in vivo*, to be analysed.

1.9.2 Investigating the role of metallochaperones in preventing access to metals *in vivo*

Regulation of access to metal ions has come to be seen as another universal factor that governs the selectivity of metal partitioning and responses of metalloregulators (and proteins in general) *in vivo*. The comparative studies of the metal responses of NmtR and SmtB (Cavet *et al.* 2002) described in section 1.5.5, together with comparative analyses of Fur-protein activation by metal ions *in vitro* and *in vivo* described in section 1.6.6, showed that the cytosol of an organism can control access to metal ions so that the *in vivo* selectivity is not solely due to the inherent properties (e.g. metal affinity, allosteric mechanism) of the protein alone.

For highly competitive metals, such as Cu^{+} and Zn^{2+}, regulation of access of metalloregulators to these metals is of particular importance because of their ability to

readily out-compete more weakly competitive metal ions (e.g. Co^{2+}, Ni^{2+}) for binding sites on proteins. Studies of the *E.coli* Zn^{2+} sensors ZntR and Zur (Outten *et al.* 2001) and the Cu^{+} sensor CueR (Changela *et al*. 2003) have suggested cytosolic concentrations of Zn^{2+} and Cu^{+} are buffered to essentially zero free atoms per cell. Additionally, a requirement for metallochaperone-mediated metallation of copper requiring proteins such as SOD1 in yeast suggested that copper was not freely available in the cytosol (Rae *et al.* 1999). For one metal sensor, access has been shown to be regulated through specific protein-protein interactions which presumably abrogate the need for free copper ions to traverse the cytosol. In *Enterococcus hirae* the metallochaperone CopZ interacts with and delivers copper to the copper sensor CopY (Cobine *et al.* 1999).

Studies comparing the *in vitro* and *in vivo* Zn^{2+} and Cu^{2+} responses of the *B.subtilis* Zn^{2+} sensor CzrA have demonstrated the importance of access, in addition to allostery, showing the potential consequences resulting from unrestricted access to tightly binding metal ions. CzrA regulates expression of the genes *czc* and *cadA* in response to Zn^{2+} *in vivo* and Zn^{2+} also reduces the binding affinity for DNA *in vitro* (Harvie *et al*. 2006). However, in equimolar concentrations of Zn^{2+} and Cu^{2+}, Cu^{2+} readily binds to CzrA in preference to Zn^{2+} *in vitro*. Additionally, Cu^{2+} inhibits Zn^{2+} mediated relief of DNA binding *in vitro* (Harvie *et al.* 2006). Like CzrA from *S. aureus* (Eicken *et al.* 2003), *B.subtilis* CzrA was shown to have a tetrahedral α5 site; Cu^{2+} prefers tetragonal over tetrahedral coordination geometries (da Silva & Williams 2002) and so its was concluded that the likely adoption of this chelate structure by Cu^{2+} resulted in sub-optimal alignment of critical allosteric residues in the protein shown to be necessary in *S. aureus* CzrA for formation of the hydrogen bond network underpinning the allosteric switch, resulting in less effective allostery than Zn^{2+} *in vitro* (Harvie *et al.* 2006). The Cu^{2+} and Zn^{2+} binding preferences were anticipated based on their relative positions in the Irving-Williams series. Cu^{2+} bound to CzrA in preference to Zn^{2+} and prevented Zn^{2+} mediated allostery. Therefore, even though allosteric switching could confer a selective response, Cu^{2+} could inhibit this response *in vitro*. Although *B.subtilis* has no known requirement for cytosolic copper trafficking (Harvie *et al.* 2006) impairment of copper trafficking in organisms with cytosolic copper requirements would also be expected to lead to inhibition of the Zn^{2+} response; thus, restriction of access to copper in these organisms was predicted to be of particular importance.

Unlike most other bacteria, *Synechocystis* has a substantial intracellular requirement for copper principally in the form of plastocyanin, c_6 and cytochrome oxidase, all of which are localised to the photosynthetic thylakoid systems. Copper must traverse the cytosol and be taken up into the thylakoids without adventitious binding to proteins along the way. Overall copper availability in the cytosol, and more specifically localisation to the thylakoids, is determined by (at least) one P-Type ATPase, CtaA located in the plasma membrane. Another P-Type ATPase, PacS, is located in the thylakoid membrane and regulates copper import to the thylakoid lumen (Tottey *et al.* 2001). A copper metallochaperone, Atx1 interacts with the amino-terminal metal binding cytosolic domains of PacS and CtaA (Tottey *et al.* 2002) and has been shown to transfer copper to PacS (Banci *et al.* 2006). Critically, Atx1 does not interact with the analogous regions of the other P-Type ATPases present in *Synechocystis*, ZiaA and CoaT (Tottey *et al.* 2002), which export surplus Zn^{2+} and Co^{2+} respectively. In the case of ZiaA, this is likely to be due to the presence of structural features adjacent to metal binding motif distinct to those of PacS which inhibit interaction of ZiaA with the chaperone (Banci *et al.* 2010). Therefore, Cu^{+} is targeted to the thylakoid membranes by protein-protein interactions through the cytosol.

The role for Atx1 in trafficking Cu^{+} to PacS is well established however the degree to which this and other metallochaperones also prevent Cu^{+} binding to adventitious sites, including metalloregulators, in the cytosol is unclear and has not been directly analysed. The allosteric inhibition of Zn^{2+} sensing by Cu^{2+} observed for CzrA predicted that a primary role for Cu^{+} metallochaperones may be to restrict access of Cu^{+} to protein sites that bind metals (e.g. Zn^{2+}) lower in the Irving-Williams series. The *Synechocystis* system provided an ideal means of testing this hypothesis. Although ZiaR and Zur have been subject to *in vivo* characterisation nothing is known about their *in vitro* metal binding and responses. Therefore, an aim of these studies was to perform robust *in vitro* characterisation of recombinant forms of these proteins, examining their Zn^{2+} binding properties, the features of the Zn^{2+} binding sites and the effects of metal on DNA binding affinities.

It was predicted that, like CzrA (Harvie *et al.* 2006), ZiaR and Zur would bind copper in preference to Zn^{2+} *in vitro*. Additionally, given the preferred tetrahedral geometry for Zn^{2+} ions it was also anticipated that copper would form inactive complexes with proteins due to its propensity to adopt tetragonal (Cu^{2+}) and linear (Cu^{+}) geometries. These predictions were tested using recombinant forms of ZiaR and Zur. To

test the proposal that inactivation of the Cu^{+} trafficking pathway in *Synechocystis* may lead to adventitious Cu^{+} population of incorrect protein sites, responses at the ZiaR and Zur regulated promoters were compared in wild-type and mutant strains deficient in Atx1. A prediction was that copper may inhibit the Zn^{2+} effects at these promoters due to allosteric inhibition of both sensors. This would confirm a primary role for Atx1 in preventing metal mislocation in the cytosol.

1.9.3 Comparison of the relative metal binding affinities for ZiaR, Zur_{SS} and CoaR

A challenge for metal sensing transcriptional regulators is to respond selectively to the correct metal to effectively regulate homeostatic circuits that act to maintain the cytosolic concentration of the metal ion within a range optimal for metallation of target proteins. This must be achieved in the context of a cytosolic environment which may have a requirement for a range of different metal ions each with different affinities and binding preferences in accordance with the Irving-Williams series. The metal sensing requirements of *Synechocystis* exemplify this challenge; metal-sensing transcriptional regulators are present, or are predicted, from multiple regulator families (Figure 3), that must simultaneously detect changes in metals that are highly competitive (e.g. Zn^{2+} in the case of ZiaR and Zur_{SS}) and weakly competitive (e.g. Co^{2+} in the case of CoaR). The repertoire of sensors in *Synechocystis* means that for first time the factors that have evolved to maintain metal selectivity across three, distinct metalloregulator families from the same organism can be studied in detail.

In vivo ZiaR (Thelwell *et al.* 1998) and Zur_{SS} (Pakrasi *et al.* 2001) must respond to Zn^{2+} whilst CoaR also responds specifically to Co^{2+} (Rutherford *et al.* 1999). Maintaining a selective metal response for this group of sensors is likely to be particularly challenging; Zn^{2+} is expected to bind to most protein sites with an affinity substantially tighter than Co^{2+}. Moreover, there is no precedent for metallochaperone-assisted delivery of these metals to sensor proteins and so it is assumed that these sensors must compete with each other to detect changes in concentrations of these ions in free solution in the cytosol. Although allostery may facilitate selectivity, Zn^{2+} is anticipated to either allosterically inhibit the Co^{2+} response of CoaR *in vitro*, or if similar coordination geometries are adopted, may aberrantly activate CoaR.

A potential, novel mechanism by which selective responses across families of sensors may be generated is through metal partitioning based on relative affinity

(Waldron & Robinson 2009). In this model, the *in vivo* responses of metal sensors become a function of the relative metal binding affinities for particular metals. Therefore, so long as a given metal sensor has an absolute affinity for its cognate metal ion tighter than for the other sensors present in the cytosol, that metal ion will partition to the correct sensor in accordance with the affinity gradients present amongst the repertoire of sensors (Waldron & Robinson 2009). Crucially, this model does not require mechanisms of kinetic regulation (e.g. via metallochaperones) of metal delivery to sensors to be invoked. Instead, the metal responses of a set of sensors from a given organism are presumed to have evolved in a coordinated fashion through fine tuning of the metal binding properties of sensor proteins. Much like the situation for the sensors NmtR and CmtR (Cavet *et al.* 2003b), both from the same sensor family (ArsR-SmtB) (see section 1.5.5), *in vivo* responses of sensors from distinct families are expected to correlate with relative affinities for each metal. A prediction resulting from this model is that the set-point metal concentrations will differ between organisms with different repetoires of metal sensor proteins. Hence, a metal sensor protein hetrologously expressed may not produce responses as observed in the host organism as has been observed for NmtR (Cavet *et al.* 2002) (section 1.5.5).

For ZiaR, Zur_{SS} and CoaR this hypothesis would mean that even though Zn^{2+} may out-compete Co^{2+} for binding to all of the proteins, as long as the Zn^{2+} sensors each have a tighter affinity for Zn^{2+} than CoaR and conversely CoaR has a tighter affinity for Co^{2+} than each of the Zn^{2+} sensors, Zn^{2+} and Co^{2+} would partition to the correct sensors producing selective responses to these metal ions *in vivo*. Therefore, a goal of these studies was to test this hypothesis by comparison of the equilibrium binding affinities of each sensor for Zn^{2+} and Co^{2+} to test if these values correlated with the *in vivo* responses of each sensor.

Chapter 2. Methods and Materials

2.1 Reagents and chemicals

All chemicals and reagents were obtained from standard commercial suppliers (Sigma-Aldrich, Melford laboratories Ltd., BD Biosciences).

2.2 Maintenance of bacterial strains

2.2.1 Growth conditions

For all gene cloning steps, the *E.coli* strain DH5α (Genotype: F-, *φ80dlacZΔM15*, Δ(*lacZYA-argF*)*U169*, *deoR*, *recA1*, *endA1*, *hsdR17*(*rk-, mk+*), *phoA*, *supE44, λ-*, *thi-1*, *gyrA96*, r*elA1*) was used. For overexpression of recombinant proteins, the *E.coli* strain BL21(DE3) (Genotype: F–, *omp*T, *hsd*S_B (r_B–, m_B–), *dcm*, *gal*, λ(DE3), *pLysS*, Cm^r) was used. All *E.coli* cultures were grown at 37^{o}C with orbital shaking at approximately 150 r.p.m. unless stated. Bacterial cultures grown on LB agar plates were incubated at 37^{o}C overnight to allow colony formation.

2.2.2 Antibiotics

Antibiotics (supplied by Sigma and Melford laboratories Ltd.) were used as selectable markers when growing *E.coli* cells transformed to antibiotic resistance with recombinant plasmids. Antibiotics routinely used were kanamycin (50 μg ml^{-1}), carbenocillin (100 μg ml^{-1}) and chloramphenicol (15 μg ml^{-1})

2.2.3 List of plasmids

A full list of plasmid constructs used directly in this work is shown in Table 3. All subcloned DNA fragments were sequenced (Beckman Coulter Genomics, UK) to verify no mutations/errors in sequences.

Plasmid	Source	Function
pGEM-T	Promega	Used in sub-cloning of PCR products Re-circularised empty vector used as a template for PCR-amplification of EMSA control fragments
pET-29aZiaR	This work	ZiaR overexpression plasmid
pET-29aΔα3ZiaR	This work	C71S/C73S ZiaR overexpression plasmid
pET-29aΔα5ZiaR	This work	H116R ZiaR overexpression plasmid
pET-29aΔα5Δα3ZiaR	This work	Double site (H116R/C71SC/73S) ZiaR mutant overexpression plasmid
pET-29aZur_{SS}	This work	Zur_{SS} overexpression plasmid
pET-29aCoaR	This work	CoaR overexpression plasmid
pGro7	Takara bio inc.	groES-groEL chaperone overexpression plasmid
pGEM-T*znu*promoter	This work	Plasmid containing the complete *zur-znuA* intergenic region

Table 3. List of plasmids/constructs.

2.3 DNA manipulation

2.3.1 Amplification of DNA by Polymerase Chain Reaction (PCR)

A full list of primers (Sigma-Aldrich UK) used in the PCR reactions performed during the course of this work is shown in Table 4. PCR reaction solutions were prepared to a volume of 50 µl containing 2 µl dNTPs (a mixture of dATP, dCTP, dGTP, dTTP, each at a final concentration of 40 µM), 10-100 ng of plasmid or genomic DNA, 2 µl (0.4 µM) of each PCR primer, 1 µl *Pfu* polymerase enzyme (approximately 2-3 units), 5 µl of reaction buffer (Promega Pfu buffer) (containing 20 mM $MgSO_4$) and 39 µl of nH_2O. PCR reactions were performed using a variety of melting, annealing and extension temperatures and durations using a PCR thermocycler.

2.3.2 Agarose gel electrophoresis

DNA fragments were analysed by agarose gel electrophoresis performed using standard protocols and conditions (Sambrook & Russell, 2000). Concentrations of agarose were selected depending on the size of the DNA fragment to be analysed. A Tris/Borate/EDTA (TBE) buffer system was used to dissolve agarose and to run agarose gels. Agarose gels were run at 90 V prior to visualisation. DNA was stained by addition of ethidium bromide solution (~0.5 µg ml^{-1}) to gel solutions prior to setting and DNA was visualised in gels using a UV transilluminator. For preparative gel electrophoresis DNA fragments that were required for further manipulation were excised from the gel and DNA was purified from the gel matrix using a QIAquick gel extraction kit as directed by the manufacturer protocols (Qiagen).

2.3.3 Ligation into pGEM-T plasmid

To facilitate ligation into pGEM-T plasmid, blunt-ended PCR products were subject to A-tailing in which *Taq* polymerase was used to add a single adenine to the 3' end of PCR DNA products which complemented the 3' single thymidine extensions of the plasmid. Directly after completion of PCR amplification, the PCR reaction was heated

Primer	Description	Sequence (5'-3')
I	*ziaR* forward primer	GAACATATGAGTAAGTCCTCGTTGTCAAAG
II	*ziaR* reverse primer	GAAGAATTCTTAATCCGATTCCTGCAAATG GTCTGCAAC
III	*zur* forward primer	GAACATATGAGTCTTCCCACTCCTTCCCTTG CCGTT
IV	*zur* reverse primer	GAAGGATCCCTAATCACTTCCTTTGGCACA AAGTTGACA
V	*coaR* forward primer	GAACATATGAAGACTAATCACTTAACGATT AAA
VI	*coaR* reverse primer	GAAGATATCCTAAAGACAAGTGAGA TAGCAGTGGCA
VII	*zur/znu* intergenic region forward primer	CACCAAGGGGTTGGACAAAGCGGGGAA
VIII	*zur/znu* intergenic region reverse primer	GACAAGGTGGAGGAATTATGCAATGAT
IX	+ *zur* box EMSA fragment forward primer/pGEM-T T7 forward primer	TAATACGACTCACTATAG
X	*zur/znu* intergenic region + *zur* box fragment reverse primer	CCCTTTGGCATTAGGACAATAAACGAT
XI	*zur/znu* intergenic region - *zur* box forward primer	GGATAAATTTCCCATCAGCTTGATCTTCAC
XII	- *zur* box EMSA fragment reverse primer/ pGEM-T reverse primer	CAAGCTATGCATCCAACG
XIII	C71S/C73S ZiaR SDM forward primer	CGGCATTGGCCCGCCAAGAACTCAGTGTCA GTGATTTAGCAGCGGCG
XIV	C71S/C73S ZiaR SDM reverse primer	CGCCGCTGCTAAATCACTGACACTGAGTTC TTGGCGGGCCAATGCCG
XV	H116R ZiaR SDM forward primer	AGCTTGGCGCATAATCGCGTGATGAATTTG TATCGGG
XVI	H116R ZiaR SDM reverse primer	CCCGATACAAATTCATCACGCGATTATGCG CCAAGCT

Table 4. List of primers.

at 95°C for 20 minutes. Approximately 15 µl of dATP (from a 2 mM stock) and approximately 1 µl (5 units) of *Taq* DNA polymerase were added to the 50 µl PCR reaction mixture which was then incubated at 70°C for 15 minutes. The A-tailed PCR fragments were then purified from the components of the gel matrix as described in section 2.3.2.

For ligation into pGEM-T, components of the pGEM-T vector system (Promega) were used. A 10 µl ligation reaction was prepared, as directed by the manufacturer protocols, containing 3 µl of gel purified PCR product (~150 ng μl^{-1}), 1 µl of pGEM-T plasmid vector stock (50 ng μl^{-1}), 5 µl of T_4 DNA ligase reaction buffer and 1 µl of T_4 DNA ligase enzyme (3 units). Reactions were either incubated at room temperature for 1 hour or incubated at 4°C overnight. Both negative and positive control reactions were routinely performed. Negative/background control reactions were performed as described above but the PCR insert sample was not included and was replaced with nH_2O. Positive control reactions were performed as above but in place of the PCR insert a pre-prepared control insert fragment was added (2 µl) and the volume was made up to 10 µl using nH_2O. Following incubation, each reaction was used to transform cells of the *E.coli* strain DH5α to carbenocillin resistance. Between 2-5 µl of ligation reaction mixture was added to approximately 100 µl of cells and cells were subsequently treated as described in section 2.3.9.

2.3.4 Blue/white identification of transformant cells

Cells containing recombinant pGEM-T plasmids containing the desired PCR fragments were identified by screening of transformant colonies based on blue/white colour selection. Successful ligation of PCR inserts interrupts the coding sequence of the β-galactosidase gene; these clones are therefore unable to convert the colourless substrate X-gal (bromo-chloro-indolyl-galactopyranoside) into the insoluble, blue compound 5-bromo-4 chloroindole and therefore appear as white colonies. Following transformation between 100-300 µl of each transformation reaction was dispensed onto an LB agar plate containing 100 µg ml^{-1} carbenocillin. Prior to addition of the bacterial cells approximately 40 µl of 2 % w/v X-gal and 7 µl of 20 % w/v IPTG were dispensed and spread onto the plate which was then allowed to dry for 3-4 hours after which aliquots of transformations were then able to be added. Plates were incubated overnight at 37°C to allow colony growth.

2.3.5 Ligation into pET29a plasmid

Ligations of DNA fragments into the overexpression plasmid pET29a were performed using a protocol similar to that employed for ligation into pGEMT-T plasmid. Each 10 µl ligation reaction contained 1 µl of restriction digested pET29a plasmid (~1 µg μl^{-1}), 1 µl 10x T_4 ligase buffer (Invitrogen), 1 µl (5 units) T4 DNA ligase enzyme and up to 7 µl of the restriction digested DNA insert from pGEM-T. Reactions were incubated either for 1 hour at room temperature or overnight at 4^{o}C. Up to 5 µl of each ligation reaction was used to transform 100 µl of DH5α cells for subsequent manipulation of DNA and screening to confirm successful ligation. Cells were transformed (as described in section 2.3.9) to kanamycin resistance and between 100-300 µl of cells were plated out onto LB agar plates containing 50 µg ml^{-1} kanamycin. These plates were incubated overnight at 37^{o}C to allow colony growth. Colonies were screened to verify the presence of successfully ligated plasmids by diagnostic restriction digestion (see 2.3.7). Several colonies were picked from the plate and used to inoculate approximately 5 mls of LB media containing 50 µg ml^{-1} kanamycin which were then grown overnight at 37^{o}C with orbital shaking of 150 r.p.m. Plasmid DNA was isolated from each culture (as described in section 2.4.6) and each DNA sample subjected to restriction digestion. The presence of insert in each sample was verified by agarose gel electrophoresis.

2.3.6 Isolation of plasmid DNA

E.coli cell cultures were centrifuged at 8000 r.p.m for 3 minutes using a bench-top microcentrifuge for Miniprep DNA isolation and at 3000 r.p.m. for 20 minutes using a J6-HC centrifuge (Beckman) for Midiprep DNA isolation. Plasmid DNA was extracted from cells using Qiagen plasmid Mini/Midiprep kits according to manufacturer protocols (Qiagen). Recovery of plasmid DNA was confirmed by agarose gel electrophoresis.

2.3.7 Restriction digestion

Restriction digestions were used to facilitate sub-cloning of PCR inserts into pET29A plasmids. Digestions were used to generate insert fragments with ends that were complementary to those generated by analogous digestions of pET29a to allow efficient

incorporation into the plasmid. Restriction digestions were also used diagnostically to verify successful ligation of fragments into plasmids. Each 50 µl restriction digestion was prepared and performed according to manufacturer protocols and contained at least 5 µl of isolated plasmid and 1 µl of each of the pair of restriction enzymes (New England Biolabs) and the reaction was made up to volume in nH_2O. BSA was often added as directed by the manufacturer protocols. Following restriction digestion samples were analysed to verify the presence of insert by agarose gel electrophoresis using an aliquot of the sample.

In preparative analyses in which insert or digested plasmid was to be recovered, all of the reaction volume was loaded onto an agarose gel and the desired DNA fragments purified from the gel matrix as described in section 2.3.2. To prevent aberrant religation of restriction digested pET29a plasmids, 5' end dephosphorylation reactions were often performed (Sambrook & Russell 2000). To 50 µl of purified pET29A (1 µg μl^{-1}) plasmid 1 µl of calf alkaline phosphatase (CIP) (1 unit μl^{-1}) enzyme (Promega) was added. This reaction was incubated at 37^{o}C for 30 minutes. The reaction was then heated at 65^{o}C for 30 minutes in the presence of 5 mM EDTA (pH 8.0). Reactions were then analysed on a 1 % w/v agarose gel and plasmid fragments purified from gel matrix components by gel extraction as described in section 2.3.2.

2.3.8 Site Directed Mutagenesis using the 'QuikChange' method (Stratagene)

To introduce changes in the amino acid sequence of proteins the coding sequence was altered by site directed mutagenesis. This strategy involves a non-exponential, linear PCR step using pET29a plasmids as templates for amplification. Therefore, the low copy number number of pET29a plasmid constructs necessitated the use of concentrated samples of these plasmids prepared by Midiprep (Qiagen) performed as directed by the manufacturer. Each quick change PCR reaction contained 1 µl of 1 µg μl^{-1} pET29a plasmid, 2 µl of dNTP mixture (final concentration of 40 µM), 5 µl of *Pfu* reaction buffer (containing 20 mM $MgSO_4$), 0.4 µM of each primer, 1 µl of *Pfu* enzyme (2-3 units) (Promega) and the reaction was made up to 50 µl in nH_2O. Following each PCR reaction the original methylated template DNA molecules were digested by addition of 1 µl of *Dpn 1* enzyme (2-8 u μl^{-1} stock) and each reaction was incubated at 37^{o}C for 1 hour. Approximately 1 µl of each reaction was used to transform 100 µl of DH5α cells to kanamycin resistance To estimate the background number of colonies produced a

control reaction was often performed in which 1 µl of the template plasmid was digested with 1 µl of *Dpn* 1 enzyme (made up to a final reaction volume of 50 µl). An aliquot (1 µl) of this reaction was used to transform DH5α cells to kanamycin resistance.

Colonies were initially screened for mutations by diagnostic restriction digestion utilising new restriction sites engineered into the plasmid that were not present in the original parental sample. For the α3 site mutant of ZiaR the ZiaR gene in each plasmid sample was amplified by PCR reaction using primers I and II. Following agarose gel analysis and gel extraction, the DNA fragments were subjected to restriction digestion using the enzyme *Dde I* to detect a *Dde I* site introduced during mutagenesis which would cause the production of two smaller DNA fragments of similar sizes (213 and 185 base pairs). A similar strategy was used for the ZiaR α5 site mutant but in this instance a *BstU1* site was introduced into the ZiaR gene; successful mutation was confirmed by release of a DNA fragment of approximately 50 base-pairs following restriction digestion. For the combined α3α5 site ZiaR mutant a pET29a plasmid sample verified as containing the α3 site mutations was subject to another round of quick change mutagenesis using the α5 site mutagenesis primers (primers XV and XVI). Plasmids were screened for successful mutagenesis by diagnostic restriction digestion as performed for the α5 site mutant. Changes in the sizes of DNA fragments were detected by agarose gel electrophoresis analysis of the restriction digestion samples. Each plasmid verified as containing the expected novel restriction site was then sequenced to confirm correct changes had been introduced.

2.3.9 Production and transformation of competent cells

Competant cells were produced using a variation of the $CaCl_2/MgCl_2$ method. An aliquot of cells frozen at -80^{o}C was thawed and used to inoculate 5 mls LB medium. This culture was grown in the absence of antibiotic at 37^{o}C overnight. The following day 400 mls of LB media was inoculated with 4 mls of the 5 ml starter culture and this culture grown to an OD_{595} of approximately 0.3. Cultures were centrifuged in sterile 50 ml falcon tubes at 3000 r.p.m. in a J6-HC centrifuge (Beckman), at 4^{o}C. The resulting supernatant was discarded and the cell pellets resuspended in ice-cold 100 mM $MgCl_2$ (to a volume of ¼ the original culture volume). The cell resuspension was re-centrifuged as described above and the cell pellets resuspended in ice-cold 100 mM $CaCl_2$ solution (to 1/20th the initial culture volume). A further 9/20th the initial culture

volume was added and the suspension was incubated on ice for 20 minutes. The cell suspension was then centrifuged as described above and the cell pellets were resuspended in 1/50th the initial culture volume of ice cold, sterile solution of 85 mM CaCl2, 15 % (w/v) glycerol. 100 µl aliquots were dispensed into sterile 1.5 ml eppendorf tubes which were stored at -80^{o}C.

To transform *E.coli* cells to antibiotic resistance, 1-5 µl of concentrated, purified plasmid solution was added to approximately 100 µl of competent *E.coli* cells which were then incubated at 4^{o}C for 20 minutes. This mixture was then heated at 45^{o}C for 45 seconds followed by incubation at 4^{o}C for 2 minutes. This mixture was diluted to 1 ml in LB media and incubated with shaking at 37^{o}C for 1.5 hours. To select for transformant cells, approximately 100-300 µl of the transformation mixture was dispensed onto the centre of an LB agar plate and spread across the plate. Plates were incubated at 37^{o}C overnight.

2.4 Protein Manipulation

2.4.1 SDS PAGE analyses

Purity and abundance of recombinant proteins was assessed by SDS PAGE analysis using standard protocols and conditions (Sambrook & Russell 2000). For analysis of purified ZiaR and Zur_{SS}, gels were made with 17 % w/v acrylamide. For CoaR, 15 % w/v acrylamide gels were used. Gels were run at 150 V for ~1.5 - 2 hrs. For staining gels were removed from the gel tank and heated in nH_2O for 10-20 seconds. The water was discarded and gels were stained in colloidal Coomassie G250 SimplyBlue SafeStain (Invitrogen) and heated for 20-30 seconds to facilitate protein staining. The stain was discarded and gels soaked in nH_2O to allow destaining.

2.4.2 Overexpression and solubility testing

Prior to large-scale protein overexpression, small scale tests of protein expression were performed in which protein expression levels were assessed from cultures grown under different conditions. For each expression test a single *E.coli* BL21(DE3) transformant colony was inoculated into 5 mls LB growth media which was incubated at 37^{0}C overnight. The following day, 25 mls LB growth media was inoculated with 0.25 mls of

5 ml culture and cells were grown to an OD_{595} of approximately 0.7. Protein overexpression was induced by addition of IPTG to the culture. Aliquots of culture (typically 5 mls) were removed at specific timepoints and centrifuged at 3000 r.p.m. at 4^0C using a J6-HC centrifuge (Beckman). The supernatants were discarded and cell pellets frozen at -20^{o}C. To analyse pre-induction protein expression, a sample of culture was also removed immediately prior to addition of IPTG. To analyse levels of protein expression in each sample, cell pellets were thawed on ice and resuspended in 2 mls of buffer (10 mM Hepes (pH 7.8), 1 mM EDTA, 1 mM DTT, 100 mM NaCl). Cells in each sample were lysed by sonication (up to 8 x 20 second bursts performed on ice). Cell lysates were clarified by centrifugation at 15000 r.p.m. for 30 minutes in a RC-5B superspeed centrifuge (SS34 rotor) (Sorvall). Supernatants were decanted (this represented the soluble fraction) and the pelleted material was resuspended in 2 mls of resuspension buffer (this represented the insoluble fraction). Aliquots were then removed from each fraction for SDS PAGE analysis of protein expression levels in both soluble and insoluble cellular fractions.

2.4.3 Overexpression conditions for recombinant ZiaR, Zur_{SS} and CoaR in *E.coli*

All recombinant proteins produced during this work were produced as native, tag-free proteins. For overexpression of ZiaR (and mutant ZiaR proteins) and Zur_{SS}, cells of the *E.coli* strain BL21(DE3) were transformed to kanamycin resistance with the relevant pET29a expression plasmid construct (Table 3). For each protein preparation a single colony was picked from a kanamycin LB agar plate and used to inoculate 5 mls of sterile LB media containing 50 μg ml^{-1} kanamycin (present in all subsequent cultures). This culture was incubated with shaking at 37^{o}C for approximately 8 hours. 50 mls of LB media was inoculated with this 5 ml culture and grown overnight with shaking at 37^{o}C. Approximately 1 litre of LB media was inoculated with 10 mls of 50 ml overnight culture. This culture was incubated at 37^{o}C with shaking and cells were grown to an OD_{595} of approximately 0.7 (For overexpression of Zur_{SS}, slow cell growth often necessitated induction at lower OD_{595nm} values). IPTG was added to a final concentration of 1 mM to each 1 litre culture and cells grown for a further 2 hours. Cells were recovered by centrifugation at an RCF of ~6000 using a GSA rotor in an RC-5B superspeed centrifuge (Sorvall). The supernatant was discarded and the cell pellets were resuspended in LB media. This resuspension was centrifuged for 20 minutes at ~3000

r.p.m in a J6-HC centrifuge (Beckman). The supernatant was discarded and the cell pellets frozen at -20^{o}C. The quantity of cells used for each protein preparation often varied depending on the quantity of protein required. However, 1 litre of cells was usually sufficient for all forms of ZiaR and Zur_{SS} for most protein preparations.

CoaR was co-expressed in *E.coli* in the presence of the molecular chaperone GroES-EL which necessitated different overexpression conditions. In this protocol cells of the *E.coli* strain BL21(DE3) were transformed to kanamycin and chloramphenicol resistance with the plasmids pET29aCoaR and pGro7 (Takara Bio. Inc.). A single transformant colony was picked and used to inoculate 5 mls of LB media containing 15 μg ml^{-1} chloramphenicol in addition to 50 μg ml^{-1} kanamycin. This culture was grown with shaking at 37^{o}C for approximately 8 hours and was then used to inoculate 50 mls LB media. This was grown with shaking at 37^{o}C overnight and 10 mls of this culture was then used to inoculate 1 litre of LB media. In addition to kanamycin and chloramphenicol present at specified concentrations, each 1 litre culture also contained 1 mg ml^{-1} L-Arabinose to induce expression of the groES-groEL chaperone. These cultures were grown at 37^{o}C with shaking to an OD_{595} of ~0.5 and then induced with 0.2 mM IPTG. Cultures were grown for a further 3 hours and cells were collected as described for ZiaR and Zur_{SS}. Cell pellets were frozen at -20^{o}C. Each CoaR preparation typically required growth of 6-10 litres of cells.

2.4.4 Purification of recombinant ZiaR

Recombinant ZiaR was overproduced as a native, tag-free protein. Hence purification conditions were selected that exploited the inherent biochemical properties of the native protein to effect separation from contaminant protein species. Two protocols were employed to purify recombinant ZiaR protein. In the first protocol (protocol A), cell pellets were thawed on ice and resuspended in buffer A (100 mM NaCl, 1 mM DTT, 1 mM EDTA, 1 mM PMSF and 10 mM Hepes (pH 7.8)). Cells were lysed by sonication in a 15 ml chorex tube (8 x 20 second bursts on ice) and the resulting cell lysate was clarified by centrifugation at 15,000 r.p.m. The supernatant was decanted and re-centrifuged to ensure complete removal of particulate material. The supernatant was decanted, diluted into purification buffer A and loaded onto a CL-4B Heparin affinity column (GE Healthcare), pre-equilibrated in buffer A. Protein bound to the column was eluted in buffer A using a linear NaCl concentration gradient to 1M NaCl. Fractions

enriched for ZiaR were pooled and loaded onto a Superdex-75 size exclusion column (GE Healthcare) which was run in buffer B (300 mM NaCl, 1 mM DTT, 1 mM EDTA and 10 mM Hepes (pH 7.8)). Fractions were collected and those enriched for ZiaR were pooled and diluted to 50 mM NaCl in 50 mM Succinic acid buffer (pH 5.5) and 1 mM DTT and loaded onto a 1 ml HiTrap SP HP cation exchange column (GE Healthcare). Bound protein was eluted in 1 M NaCl. In this protocol, heparin affinity and size exclusion steps were performed using a pH/C-900 HPLC system (GE Healthcare).

In protocol A protein was eluted from the heparin column in the first purification step over a large number of 1 ml fractions. To maximise the quantity of protein purified by size-exclusion whilst minimising the volume of sample loaded onto the Superdex-75 column (sample volumes loaded could not exceed 1 % (~ 3 mls) of the column volume) 1 ml fractions were pooled and concentrated by cation exchange using the conditions described above. A subsequent protocol (which replaced the protocol described above) was developed which removed the requirement for this sample concentration step (protocol B). Instead of an initial heparin affinity step, the metal binding properties of the protein were exploited using an immobilised Ni^{2+} affinity chromatography step. Crude cell extract was prepared as described for the first protocol but using a buffer optimised for Ni^{2+}-affinity (buffer C, 20 mM Na_2PO_4, 500 mM NaCl, 1 mM PMSF and 5 mM DTT). Crude cell lysate was subsequently diluted and loaded onto a 5 ml HisTrap nickel-sepaharose affinity column (GE Healthcare) equilibrated in buffer C. The column was washed in 10 column volumes of buffer C and eluted using either a gradient of imidazole from 0-250 mM or as a step-elution in 250 mM imidazole made up in buffer C. Fractions containing ZiaR were pooled and purified further by size exclusion chromatography as described above (the concentration of DTT in size exclusion buffer B was 5 mM in this protocol). Fractions enriched for ZiaR were then pooled, diluted to 100 mM NaCl and loaded onto a 1 ml HiTrap heparin column (GE Healthcare). The column was washed in 10 column volumes buffer and ZiaR was eluted between 400-500 mM NaCl. This step not only acted to concentrate protein samples but also provided a third purification mechanism in addition to Ni^{2+}-affinity and size-exclusion which was effective in removing residual contaminating proteins still present after size-exclusion which would have been removed in the first step of protocol A (see Figure 7, section 3.2).

2.4.5 Purification of recombinant, mutated ZiaR proteins

For recombinant, tag-free Δα3ZiaR and Δα5ZiaR proteins, purification was achieved using a protocol effectively the same as protocol B in section 2.4.5. A similar protocol was used for the double site ZiaR mutant (Δα3Δα5 ZiaR), however in the first step crude cell extract was purified using a 1 ml HiTrap heparin column in place of the HisTrap Ni^{2+} affinity column used for the other forms of ZiaR. Cells were lysed in buffer D (100 mM NaCl, 5 mM DTT, 1 mM EDTA, 1 mM PMSF, 10 mM Hepes (pH7.8)) and cell lysate was clarified as described above and loaded onto a 1 ml heparin column. The column was washed in 10 column volumes buffer D and ZiaR protein was eluted in buffer D with 500 mM NaCl; size exclusion separation was then performed as described above.

2.4.6 Purification of recombinant Zur_{SS}

Recombinant Zur_{SS} was overexpressed as a native, tag free protein. Cell pellets were lysed to produce crude cell extract as described in section 2.4.5. However, due to poor binding on Ni^{2+} matrix, heparin affinity (as used in the first step for purification of the ZiaR double site mutant) was used as the initial purification step. Cell pellets were lysed in buffer D and crude cell extract was loaded onto a 2 ml Heparin column (2 x 1 ml heparin columns attached in series) which was then washed in 20 mls of buffer D and protein eluted in buffer D with 500 mM NaCl. Fractions enriched for Zur_{SS} were purified by size exclusion using the same conditions as for ZiaR. Final heparin affinity purification and concentration of size-exclusion fractions enriched for Zur was performed as described in section 2.4.5.

2.4.7 Purification of recombinant CoaR

E.coli cells containing over-expressed, tag-free CoaR were re-suspended in buffer C, which also contained 5 mM imidazole, and lysed by sonication. Cell lysates were clarified by centrifugation at 12000 r.p.m. for 20. Supernatants were discarded and cell pellets were resuspended in buffer C and solutions recentrifuged as described above. Cell pellets were resuspended in buffer C and the detergent n-Dodecyl β-D-maltoside (DDM) (Melford) was added to suspensions from a 10 % w/v stock solution to a final

concentration of ~ 0.8 % w/v. Suspensions were mixed by vortexing and incubated on ice for 1 hour. Suspensions were diluted in buffer C to 0.2 % DDM and incubated for a further 1 hour on ice. Suspensions were clarified by centrifugation at 12000 r.p.m. The supernatants were decanted and pelleted material was discarded. Supernatants were then applied to a 5 ml Histrap Ni^{2+} affinity column pre-equilibrated in 5-10 column volumes of buffer E (buffer C containing 0.2 % DDM). The column was washed in approximately 5 column volumes buffer B and eluted in buffer B with increasing concentrations of imidazole (typically 10, 25, 50, 100 and 250 mM imidazole). Fractions were analysed for protein content by SDS PAGE and those enriched for CoaR were pooled and diluted into buffer F (50 mM NaCl, 50 mM Hepes (pH 7.8), 5 mM DTT, 1 mM EDTA, 100 mM imidazole, 0.2 % DDM) and applied to a SP HP cation exchange column (GE Healthcare) preequilibrated in approximately 10 column volumes of buffer F. The column was washed in 10 column volumes of buffer F and protein eluted in buffer F with a range of NaCl concentrations (200, 300, 400, 500, 1000 mM). Fractions were analysed by SDS PAGE and those enriched for CoaR were diluted into buffer F and applied to a 1 ml heparin column preequilibrated in 10 column volumes of buffer F. The column was washed in 10 column volumes of buffer F and eluted in buffer F with a range of NaCl concentrations (100, 200, 300, 400, 500 and 1000 mM). Fractions enriched for CoaR were pooled to produce a working protein stock solution.

2.4.8 Estimation of protein concentration

For ZiaR, Zur_{SS} and CoaR, protein concentrations were estimated by measurement of absorbance at 280 nm and by use of the estimated protein extinction coefficients for each protein as calculated using the ProtParam tool from the Expasy website (http://www.expasy.ch/tools/protparam.html), which were 5960 M^{-1} cm^{-1}, 7450 M^{-1} cm^{-1} and 26930 M^{-1} cm^{-1}, respectively.

2.5 Anaerobic manipulation of purified protein samples

2.5.1 Production of chelex-treated, anaerobic buffers

To minimise buffer-derived metal contamination of protein samples prepared in the absence of EDTA, all buffers used to prepare protein and to perform metal binding

experiments were treated with Chelex-100 matrix (Sigma-Aldrich). Chelex matrix was prepared as directed by the manufacturer protocol by washing in two matrix volumes 1 M HCl, two matrix volumes nH_2O and two matrix volumes of 1 M NaOH. The matrix was then washed in several bed volumes of nanopure water followed by multiple washes in 100-500 mM Hepes buffer (pH 7.8). The matrix was washed in several bed volumes of nH_2O and added to buffers to a final concentration of 5 % w/v. Buffers were incubated with matrix on a roller mixer overnight. Buffers for use in anaerobic procedures were slowly purged with oxygen-free nitrogen for approximately 4 hours prior to use in an anaerobic chamber.

2.5.2 Production of anaerobic, metal free protein samples

Aliquots of purified, recombinant protein (all forms of ZiaR and Zur_{SS}) were loaded onto a 1 ml heparin column in 100 mM NaCl, 1 mM EDTA, 5 mM DTT, 10 mM Hepes (pH 7.8) In an anaerobic chamber, the 1 ml heparin column was washed with ~20 mls buffer 80 mM KCl, 20 mM NaCl, 10 mM Hepes (pH7.8) to remove EDTA and DTT and the protein was then eluted in 400 mM KCl, 100 mM NaCl, 10 mM Hepes (pH 7.8). For CoaR, purified protein was loaded onto a 1 ml heparin column in buffer containing 100 mM NaCl, 5 mM DTT, 100 mM imidazole, 1 mM EDTA and 0.2 % DDM. This column was washed and eluted in an anaerobic chamber using the same buffers employed for ZiaR and Zur_{SS} however they also contained 0.05-0.1 % DDM.

2.5.3 Determination of reduced sulphur content of proteins

The quantity of free sulfhydryl groups and therefore the amount of reduced protein was verified by assay with 5,5'-Dithio-*bis*-(2-nitrobenzoic acid) (DTNB). DTNB was dissolved to a concentration of 4 mg ml^{-1} in a buffer of 0.1 M sodium phosphate (pH 8.0), 1 mM EDTA. Standard curves were prepared from reduced glutathione (GSH). A 100 mM stock solution was prepared anaerobically in the experiment buffer (e.g. 400 mM KCl, 100 mM NaCl, 10 mM Hepes, pH 7.8) which was serially diluted to produce a range of standard concentrations incorporating the anticipated range of sulfhydryl concentrations expected in the protein sample. DTNB was added to a final concentration of 0.072 mg ml^{-1} to the samples and glutathione standards (all made up to a final volume of 1 ml). The reaction was left for 15 minutes and the absorbances of 200

µl aliquots of each solution were then measured aerobically in a 96 well microtitre plate at a wavelength of 414 nm.

2.5.4 Measurement of metal content of purified proteins

Protein was prepared anaerobically as described above and diluted to 5-10 µM in 400 mM KCl, 100 mM NaCl, 10 mM Hepes (pH 7.8). An aliquot of this sample was diluted into 2% w/v nitric acid and analysed for metal content by ICP-MS.

2.6 Experimental procedures

2.6.1 Preparation of metal stocks

All metal stocks (except for CuCl) were prepared by dissolving the metal salt into nanopure water. Metal concentrations were subsequently confirmed by ICP-MS analyses of serial metal stock dilutions. In all experiments the reduced form of copper was prepared and stored in an anaerobic chamber by dissolving solid CuCl into a solution of 0.1 M HCl and 1 M NaCl. The pH of the copper solution was adjusted by serial dilution of this stock into the experiment buffer. The concentration of Cu^{+} in solution was verified by titration against BCS and by ICP-MS analysis.

2.6.2 Fractionation of protein-bound metal complexes by size-exclusion chromatography

For experiments to resolve bound and free protein-metal complexes, protein was desalted into the specified experimental buffer and mixed with metal and reactions were incubated for 10 minutes (unless otherwise stated). Protein-bound and unbound metal ions were separated by size-exclusion chromatography using Sephadex G-25 matrix (GE Healthcare). Fractions were collected (0.5 ml) and analysed for protein content by Coomassie assay (calibrated using aliquots of known protein concentration from the same protein preparation) and the metal content of each fraction was determined by ICP-MS.

2.6.3 Measurement of the metal binding affinities of recombinant ZiaR, Zur_{SS} and CoaR

Measurement of the Zn^{2+} affinity and stoichiometry of ZiaR using the Zn^{2+} binding indicator 4-(2-pyridylazo)-resorcinol (PAR)

The metallochromic indicator PAR binds Zn^{2+} to form a PAR_2-Zn^{2+} complex which absorbs at a wavelength of 492 nm ($\Delta\varepsilon$ = 66 000 M^{-1} cm^{-1}) with a binding constant (β_2) of 3.85 x 10^{12} M^{-2} (with step-wise Zn^{2+} binding constants of 7.7 x 10^6 M^{-1} and 5 x 10^5 M^{-1}) (Hunt *et al.* 1985). In these analyses protein was desalted into experimental buffer and reactions set up in a 96-well microtitre plate. PAR (400 μM) was titrated with Zn^{2+} in the presence of ZiaR and the absorbance changes for each Zn^{2+} concentration were measured at 492 nm using a Multishon Multisoft plate reader (Labsystems). Control experiments were performed in an identical fashion but in the absence of protein.

Estimation of the Cu^+ binding affinity of ZiaR using the Cu^+ binding indicator bathocuproine disulfonate (BCS)

BCS binds Cu^+ to form a BCS_2-Cu^+ complex which absorbs at a wavelength of 483 nm ($\Delta\varepsilon$ = 13000 M^{-1} cm^{-1}) and has a reported binding constant β_2 = 6.3 x 10^{19} M^{-2} (Xiao *et al.* 2004). For these analyses protein was prepared anaerobically in buffer 400 mM KCl, 100 mM NaCl, 10 mM Hepes (pH7.8). Equimolar concentrations of BCS and protein (25 μM) were added to a sealed, anaerobic 1 ml quartz cuvette (Hellma) and titrated with CuCl using a gas-tight syringe (Hamilton). Control experiments were performed in an identical fashion but in the absence of protein. Absorbance changes at 483 nm were measured on a UV-Visible spectrophotometer.

Measurement of the Zn^{2+} binding affinities of proteins using the Zn^{2+} binding indicator Quin-2

The metallochromic indicator Quin-2 forms a Zn^{2+}-Quin-2 complex with an association constant of 2.70 x 10^{11} M^{-1} (Jefferson *et al.* 1990). To measure Zn^{2+} binding constants, protein was prepared anaerobically and diluted into buffer 120 mM KCl, 30 mM NaCl, 10 mM Hepes (pH 7.8). Protein was diluted into a sealed, anaerobic quartz cuvette in

the presence of an approximately equimolar concentration of Quin-2 and titrated with Zn^{2+}. Absorbance changes at the Quin-2 absorbance maximum of 261 nm ($\Delta\varepsilon$ = 37 000 M^{-1} cm^{-1}) (Tsien *et al.* 1980) were measured on Cary 4E UV-Visible Spectrophotometer (Varian, UK) at room temperature. Equilibration effects were routinely observed in these assays. Therefore, to ensure final measurements were made at equilibrium, after each metal addition reactions were left to equilibrate until no further change was observed in absorbance values. Control titrations were performed in an identical fashion but in the absence of protein.

Measurement of Co^{2+} binding affinities for proteins using the Co^{2+} binding indicator Fura-2

Fura-2 binds Co^{2+} to form a Co^{2+}-Fura-2 complex which has a K_d of 8.64 x 10^{-9} M at pH 7.0 (Kwan & Putney 1990). This value is not affected around neutral pH values (Grynkiewicz *et al.* 1985). On excitation of Fura-2 at 360 nm, emission spectra are produced with a maximum intensity at ~500 nm that is quenched on formation of Co^{2+}-Fura complex. For these analyses protein was prepared anaerobically and diluted into experimental buffer 400 mM KCl, 100 mM NaCl and 10 mM Hepes (pH 7.8). Equimolar protein and Fura-2 were added to a sealed, anaerobic quartz cuvette and titrated with Co^{2+} (additions made in an anaerobic chamber). Changes in the fluorescence emission spectra of Fura-2 on binding Co^{2+} were measured using a Cary Eclipse fluorescence spectrometer (Varian) with all measurements taken at room temperature. Multiple measurements were taken at time intervals for each metal concentration to verify equilibrium measurements were being obtained. Control experiments were performed in an identical fashion but in the absence of protein.

2.6.4 Analysis of protein-metal interactions by UV-Visible spectroscopy

UV-Visible spectral analyses were (unless stated otherwise) performed anaerobically in 400 mM KCl, 100 mM NaCl, 10 mM Hepes, pH 7.8. Titrations were performed using sealed, anaerobic quartz cuvettes (Hellma) with additions made using a gas-tight syringe (Hamilton) and spectra collected between 200-800 nm on a Cary 4E UV-Visible Spectrophotometer (Varian, UK).

2.6.5 Analysis of metal-binding to recombinant proteins by measurement of intrinsic tyrosine and tryptophan fluorescence

For analyses of the effects of Zn^{2+} on ZiaR intrinsic fluorescence, protein was prepared anaerobically and added to a final concentration of 25 μM in buffer 400 mM KCl, 100 mM NaCl and 10 mM Hepes (pH 7.8) in a sealed, quartz cuvette. Anaerobic titrants of Zn^{2+} were added using a gas-tight syringe. Changes in fluorescence were measured at room temperature using a Cary Eclipse fluorescence spectrometer (Varian) (λ_{Ex} = 280 nm, λ_{Em} = 305 nm). For experiments in which Zn^{2+} and Co^{2+} binding to Zur_{SS} and CoaR was monitored, anaerobic samples of protein were titrated with Zn^{2+} and Co^{2+} in buffer 400 mM KCl, 100 mM NaCl, 10 mM Hepes (pH 7.8) and 0.05-0.1% DDM in a sealed, quartz cuvette and changes in fluorescence emission measured (λ_{Ex} = 280/295).

2.6.6 Analysis of DNA binding by Fluorescence anisotropy (FA)

Production of annealed, double stranded DNA oligonucleotides

Single stranded oligonucleotides incorporating sections of conserved promoter elements for ZiaR and Zur_{SS} were synthesised commercially by Sigma. During the synthesis process, the 5' end of one of each pair of oligonucleotides was labelled with the fluorophore Hexachlorofluorocein (HEX). Lyophilised single stranded oligonucleotides were dissolved in nH_2O and serially diluted to 1 μM. To anneal the DNA oligonucleotides, 10 μl of the HEX-labelled oligonucleotide was mixed with 13 μl of the unlabelled complimentary oligonucleotide in a total volume of 100 μl of buffer containing 150 mM NaCl and 10 mM Hepes (pH 7.8). This solution was heated at 95^{o}C for 2 minutes in a PCR thermocycler and then allowed to cool slowly to room temperature overnight. The relative sizes of single- and double stranded DNA oligonucleotides were analysed by native PAGE analysis using a 12% polyacrylamide gel using a 1xTBE buffer system. Gels were run for approximately 2 hours at 90 V. Gels were stained in solution of Ethidium Bromide (~0.5 μg ml^{-1}) and DNA bands visualised on a UV-transilluminator.

Analysis of protein-DNA interactions by Fluorescence Anisotropy (FA)

Annealed, fluorescently labelled oligonucleotide was added to a 1 ml anaerobic quartz cuvette to a final concentration of 10 nM in buffer 130 mM KCl, 30 mM NaCl, 10 mM Hepes, (pH 7.8) (unless otherwise stated). For association experiments protein was prepared anaerobically (unless stated) and titrated with DNA following pre-incubation with buffer, EDTA or metal. For disassociation experiments protein-DNA complexes were pre-formed by adding protein to a final concentration of 1 μM to a quartz cuvette containing 10 nM DNA oligonucleotide. Metal was then titrated into the cuvette from concentrated anaerobic stocks using a gas-tight Hamilton syringe or by pipette additions made in an anaerobic chamber. The anisotropy of solutions was measured at 25^0C using an 8100 Fluorometer (SLM-Aminco, Urbana, USA) as described previously (Harvie *et al.* 2006).

2.6.7 Electrophoretic mobility shift assays (EMSA)

Isolation of *znu* promoter element DNA

A section of DNA containing the complete intergenic region between the *zur* and *znuA* coding regions was amplified from a sample of *Synechocystis* genomic DNA (produced by S. Dainty) by PCR. A reaction mix was prepared containing 1 μl of *Synechocystis* genomic DNA, 0.4 mM dNTP mix, 0.4 μM of each PCR primer (Primer VII and VIII), 1 x *Pfu* PCR reaction buffer and 1 μl (2-3 units) of *Pfu* enzyme made up to 50 μl in nH_2O. This reaction was heated using a PCR thermocycler at 94^oC for 5 minutes. This was followed by 30 cycles of heating at 94^oC for 30 seconds, 50^oC for 1 minute and 72^oC for 1 minute. The reaction was then heated at 72^oC for 10 minutes and held at 10^oC overnight. PCR products were analysed by agarose gel electrophoresis. DNA products were excised from the gel and purified from gel components by QIAquick gel extraction as described in section 2.3.2. A DNA fragment of the expected size was ligated to pGEM-T as described in section 2.3.3 using a 10 μl reaction volume containing 3 μl of gel-purified DNA, 1 μl pGEM-T vector (1 μg μl^{-1}), pGEM-T ligation buffer, 5 units T_4 DNA ligase, made up to 10 μl in nH_2O. Cells of the *E.coli* strain DH5α were transformed to carbenicillin resistance using 5 μl of the pGEM-T ligation

reaction diluted into 100 µl of competent cells. Transformant cells containing the PCR insert were selected by carbenicillin resistance and blue/white colony selection in section 2.3.4. Plasmids were extracted by Miniprep and the presence of insert was verified by diagnostic restriction digestion of purified plasmid preparations, utilising *NdeI* and *SphI* sites adjacent to the pGEM-T Multiple Cloning Site. Approximately 10 µl of plasmid DNA sample was mixed with 1 x reaction buffer (NEB reaction buffer 2), 1 µl *SphI* and 1 µl *NdeI* (NEB) made up to a reaction volume of 50 µl and incubated at 37^{o}C for 1 hour. Digestion reactions were analysed by agarose gel electrophoresis to verify the presence of insert DNA in the plasmid preparation. The presence of insert was also confirmed by subsequent PCR procedures in which primers IX and XII were used to amplify out the entire intergenic region.

Production of probe and control DNA fragments by PCR

DNA fragments used as probes were produced by PCR-amplification of selected regions of a pGEMT-T plasmid containing the complete *zur/znuA* intergenic region (plasmid pGEM-T*znu*promoter). For EMSA experiments monitoring binding to the complete intergenic region, the probe DNA fragment (288 base-pairs) was produced from a PCR reaction using the plasmid pGEM-T*znu*promoter and primers IX and XII. For experiments using a truncated probe fragment containing the complete predicted Zur binding box, primers IX and X were used in conjunction with the plasmid pGEM-T*znu*promoter to produce a fragment of 129 base-pairs in size. For experiments using a section of the intergenic region that did not contain the candidate Zur binding box primers XI and XII were used in conjunction with pGEM-T*znu*promoter to produce a fragment of 161 base-pairs in length.

To produce control DNA, cells of the *E.coli* strain DH5α were transformed to carbenicillin resistance with 1 µl of a pGEM-T ligation reaction that was prepared without insert DNA. Transformant blue colonies resulted from cells acquiring pGEM-T plasmids that were either undigested or which were had no 3' T overhang (the presence of which would normally inhibit plasmid religation). Blue colonies were used to inoculate LB media and plasmid DNA was extracted from the resulting cultures by Miniprep. Control fragments (136 base-pairs) were produced by PCR amplification of empty pGEM-T plasmid using primers IX and XII. In order to produce concentrated stocks of each type of DNA probe, for each fragment type multiple PCR reactions were

performed and the gel-purified DNA products were pooled to produce a working stock solution. The approximate concentrations of these stocks were estimated by comparison of band intensities to those of a 100 bp DNA ladder (Fermentas) separated on the same agarose gel.

Binding of Zur_{SS} to DNA monitored by Electrophoretic mobility shift assay (EMSA)

EMSA binding reactions were prepared to a final volume of 10 µl. In each sample DNA fragments (both probe and control fragments) were diluted to approximately 0.2 µM in EMSA binding buffer (20 mM Tris-HCl (pH 7.8), 1 mM DTT, 3 % v/v Glycerol, 0.05 mM Spermidine). Purified Zur_{SS} was buffer exchanged by loading onto a 1 ml HP heparin column in buffer containing 100 mM NaCl, 20 mM Tris-HCl (pH 7.8), 1 mM DTT and 1 mM EDTA. This column was then washed in 10 mls of buffer minus EDTA and eluted in the same buffer with 500 mM NaCl. Protein concentrations were verified by UV-Visible absorbance at 280 nm. Protein samples were serially diluted into the binding reactions to the desired concentrations. For analysis of metal dependent DNA binding effects, EDTA or Zn^{2+} were added to final concentrations of 25 mM and 200 µM Zn^{2+} respectively. Binding reactions were incubated at room temperature for 20 minutes. Each 10 µl binding reaction was then loaded onto a non-denaturing, polyacrylamide gel (6% w/v acrylamide) which was then run using an EDTA-free Tris/Borate buffer system at 120 V for approximately 1.5 hours at 4^{o}C. Gels were stained by incubation in an ethidium bromide solution (0.4 µg ml^{-1}) for 20 minutes (with shaking) and visualised using an UV transilluminator.

2.7 Bioinformatics and data analysis programs

Sequence searching for a conserved Zur-binding site in the *Synechocystis* genome

To identify potential binding elements in the *znu* promoter region the pattern search tool on the Institut Pasteur Cyanolist database website was used (http://genolist.pasteur.fr/CyanoList/index.html).

Prediction of hydrophobic regions in CoaR

Hydropathy prediction algorithms available at the ExPASy Proteomics Server (http://expasy.org/) were used to analyse the amino acid sequence of CoaR and other proteins to identify potential hydrophobic/transmembrane domains. The programs used in each case are discussed in the main text of Chapter 6.

Generation of a structural model for CoaR

Structural models of CoaR were generated using the Fugue tertiary structure prediction program (http://tardis.nibio.go.jp/fugue). Structural models were manipulated using PyMol and Swiss PDB Viewer.

Calculation of metal binding affinities by nonlinear least squares linear regression analysis

Metal binding affinities were determined from protein/metallochromic indicator titration data by non-linear least squares linear regression analysis using the program DynaFit (Biokin, Ltd) (Kuzmic *et al.* 1996).

Chapter 3. Characterisation of ZiaR-An ArsR-SmtB family zinc sensing transcriptional regulator

3.1 Multiple sequence alignment of ArsR-SmtB proteins

In previous work ZiaR was shown to require both a cysteine containing α3 site and a histidine containing α5 site for initiation of metal dependent alleviation of DNA binding and repression of transcription (Thelwell *et al*. 1998). Alignment of ZiaR with ArsR-SmtB proteins representing the main sensory paradigms shows conservation of residues shown to be important for sensing at each site (Figure 4). Critically, ZiaR contains a conserved CVC motif at its α3 site, with cysteines in this motif also shown to be crucial for sensing in the α3 site sensors BxmR, CadC and ArsR (Liu *et al*. 2008; Busenlehner *et al.* 2002b; Shi *et al.* 1996). The overall ligand set is likely the same as that in the α3N sensor AztR in which the tetrahedral α3N chelate is completed by an N-terminal cysteine and histidine residue, both of which are conserved in ZiaR. There is also conservation of the α5 site residues in ZiaR and ZiaR conserves all of the α5 site residues identified in the α5 sensor SmtB (Turner *et al.* 1996; Cook *et al.* 1998; VanZile *et al*. 2002b). ZiaR also contains a conserved arginine residue that is essential in forming the α5 hydrogen bond network that underpins the quaternary allosteric switch in α5 sensors (Eicken *et al.* 2003) (Figure 4). Therefore, the presence of two functional, structurally independent sites suggested by previous data is supported by alignment with ArsR-SmtB homologues subjected to characterisation subsequent to this initial analysis of ZiaR (Thelwell *et al.* 1998). Crucially, both metal binding sites were shown to be required for allostery *in vivo* (Thelwell *et al.* 1998).

3.2 Purification of recombinant ZiaR

The recombinant form of ZiaR produced in these studies represented the native form of the protein (a tag to aide in purification was not part of the protein-see section 2.4.5). Therefore, a range of purification strategies that exploited the inherent biochemical properties of native ZiaR were selected for purification of ZiaR (section 2.4.5). The first purification step used either heparin affinity chromatography or Ni-affinity chromatography. In heparin affinity, crude cell lysate was applied to heparin-affinity matrix and bound protein was eluted and fractionated by application of NaCl

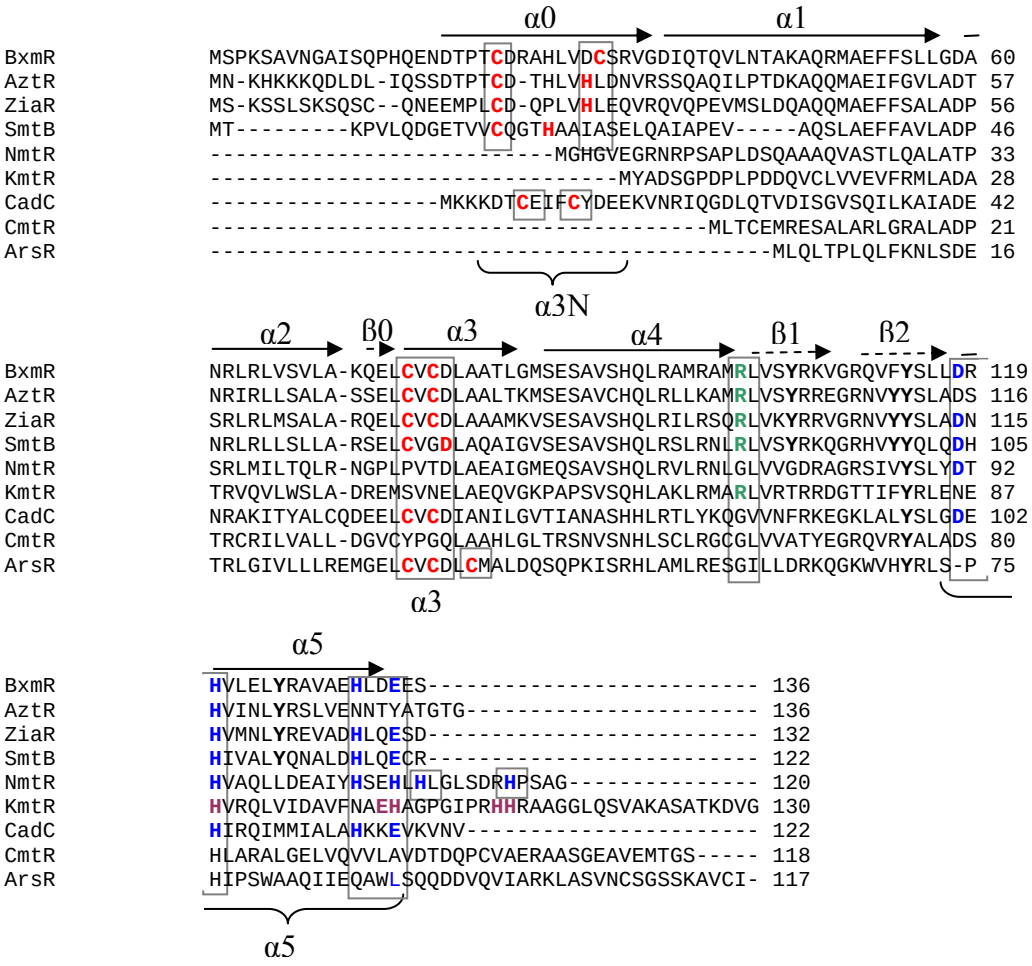

Figure 4. Multiple sequence alignment of selected ArsR-SmtB proteins. Sequences for key members of each ArsR-SmtB sensory paradigm are shown aligned with the ZiaR sequence. Sequences are ZiaR (*Synechocystis*), BxmR (α3/α5) (*Oscillatoria brevis*), SmtB (α5) (*Synechococcus* PCC 7942), AztR (α3N) (*Anabaena* PCC 7120), CadC (α3N) (*Staphylococcus aureus* pI258), CmtR (α4C) (*Mycobacterium tuberculosis*), ArsR (α3), (*Escherichia coli* R773), NmtR (α5C) (*Mycobacterium tuberculosis*) and KmtR (α5-3) (*Mycobacterium tuberculosis*). The extent of the α3, α3N and α5 sites are shown (grey boxed areas). Conserved residues which are known/predicted to be metal ligands within forms of each of the sites are shown in red (α3) and blue (α5) (the two additional ligands in NmtR in the C-terminal tail are also shown). For SmtB and CadC, which contain structurally intact but non-regulatory α3N and α5 sites respectively, residues known/predicted to ligate metal ions are also highlighted. KmtR uses some residues derived from the α5 sites (magenta) (Campbell *et al.* 2007). Conserved tyrosine residues in the α5 and β-wings are shown in bold (see section 3.4.7). The position of an arginine residue shown to be vital in hydrogen bond network formation in α5 sensors is shown (green residues in boxed region). Secondary structural features derived from the structure of CadC are shown (Ye *et al.* 2005) and helices are numbered as in Osman & Cavet *et al.* 2010. The helix-turn-helix motif in CadC is formed by the helix-4-turn-helix-5 motif (Ye *et al.* 2005).

gradient of increasing concentration (Figure 5a). Fractions determined by SDS PAGE analysis to be enriched for ZiaR (Figure 5b) were concentrated by cation-exchange chromatography for further purification. In the Ni^{2+} affinity step, crude cell lysate was applied to Ni^{2+} affinity matrix and protein eluted by addition of Imidazole (either as a gradient of increasing concentration or in a single concentration step elution) (Figure 6a,b) or as a single step elution using a high concentration of imidazole (250 mM). Fractions from both of these approaches that were enriched for ZiaR were subsequently purified by size exclusion chromatography (Figure 7a). Fractions enriched for ZiaR were concentrated and purified to homogeneity by application to heparin-affinity matrix followed by step-wise elution at various NaCl concentrations (Figure 7b). DTNB assays of thiol reactivity showed anaerobic preparations of purified ZiaR protein to contain 3.6 ± 0.4 reactive cysteine residues out of a total of four in the protein sequence confirming the production of almost completely reduced protein samples for *in vitro* characterisation. Prior to *in vitro* characterisation all samples of ZiaR (and mutant ZiaR proteins, section 3.4) were verified by ICP-MS analysis to contain <10 % Zn^{2+}.

3.3 Analysis of the metal binding properties of ZiaR

3.3.1 ZiaR binds Zn^{2+} with a stoichiometry of 2:1

Previous *in vivo* data (Thelwell *et al*. 1998) and sequence comparison with homologous ArsR-SmtB proteins (Figure 4) suggested the presence of two regulatory, metal binding sites in ZiaR. To test if there were two metal binding sites per ZiaR monomer (four per dimer), the purified, recombinant protein was subjected to metal binding assays to verify its metal binding stoichiometry. Size-exclusion chromatography was used to resolve bound and free Zn^{2+} ions following anaerobic incubation of ZiaR with a four-fold molar excess of $ZnCl_2$. In the example analysis shown in Figure 8, 10 μM protein was incubated with 40 μM Zn^{2+} prior to fractionation. In this representative analysis, the two peak protein fractions (Fractions 7 & 8), which elute just after the column void volume (2.5 mls) contain 10.5 μM protein which co-migrates with 21.8 μM Zn^{2+}. Approximately 25.6 μM Zn^{2+} is present post void as 'free' metal ions in fractions 12-30. These data suggested a Zn^{2+} binding stoichiometry of 2:1, Zn^{2+}: protein, consistent with predictions of two sites per monomer or four per dimer.

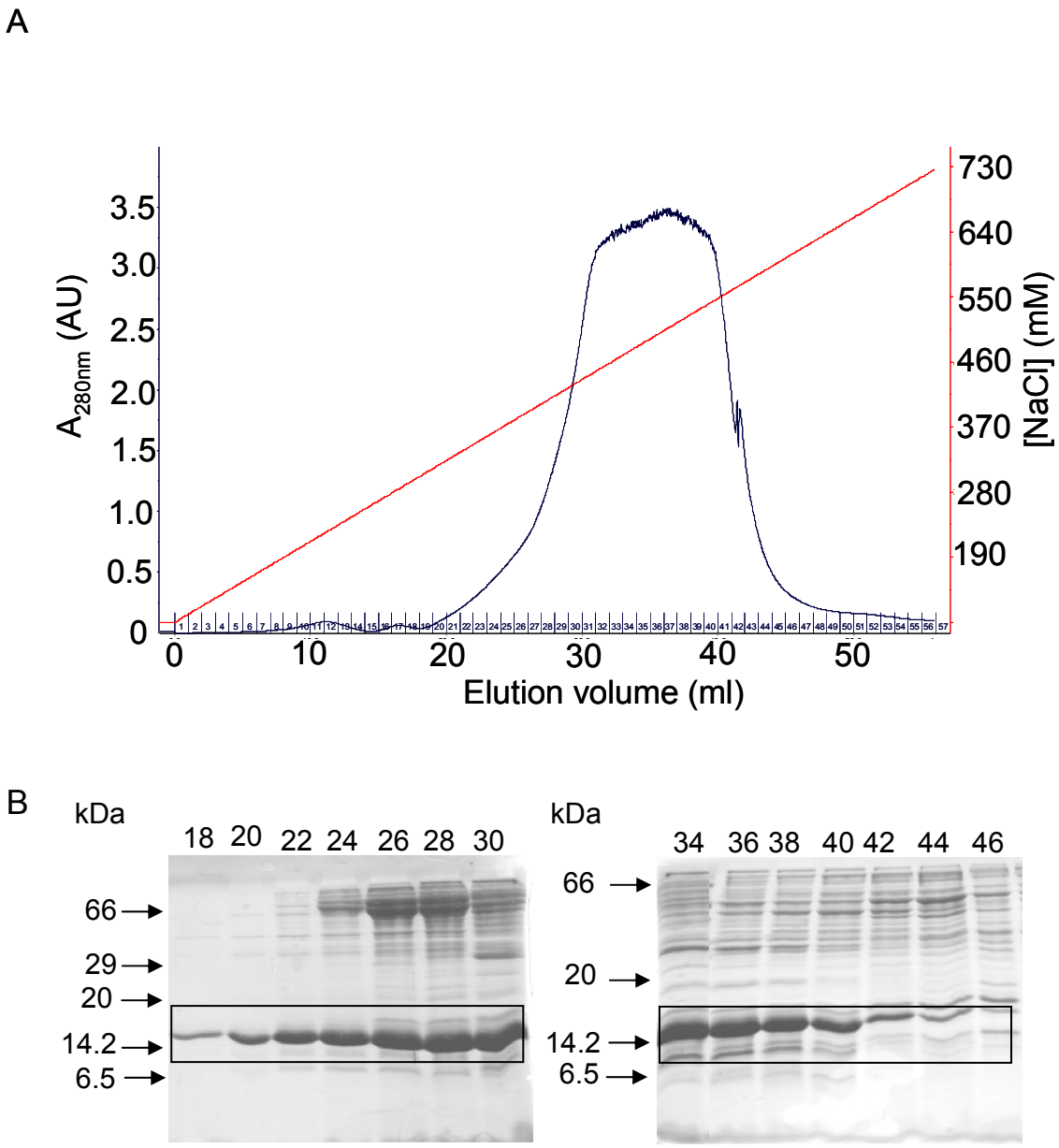

Figure 5. Purification of recombinant ZiaR by heparin affinity chromatography. A. Chromatograph showing change in total protein concentration (black line) in fractions eluted over a 0.1-1M NaCl gradient applied to a 25 ml heparin affinity column. B. SDS-PAGE gel analysis (17 % v/v acryl-bis) of heparin fractions from the separation shown in A. The highly abundant ZiaR bands are shown within boxed regions.

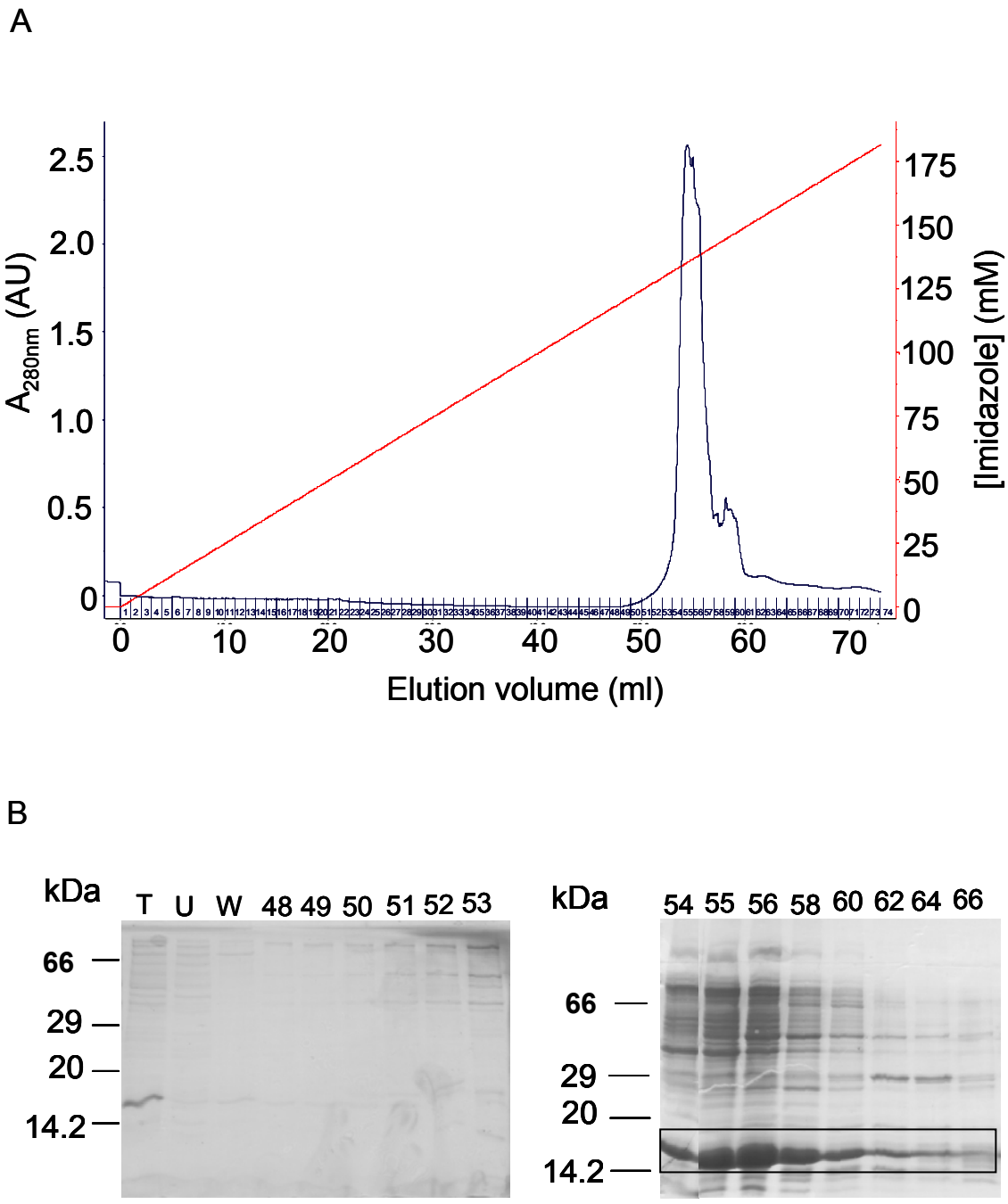

Figure 6. Purification of ZiaR by Ni-affinity chromatography. A. Chromatograph showing change in total protein concentration in fractions eluted over a 0-250 mM Imidazole gradient applied to a 5 ml HisTrap Ni affinity column. B. SDS-PAGE (17 % v/v acryl bis) analysis of selected Ni affinity fractions from A. Bands corresponding to ZiaR are highlighted in the boxed region. T; Total crude cell lysates, U; unbound protein, W; protein eluted following column wash step (see section 2.4.4)

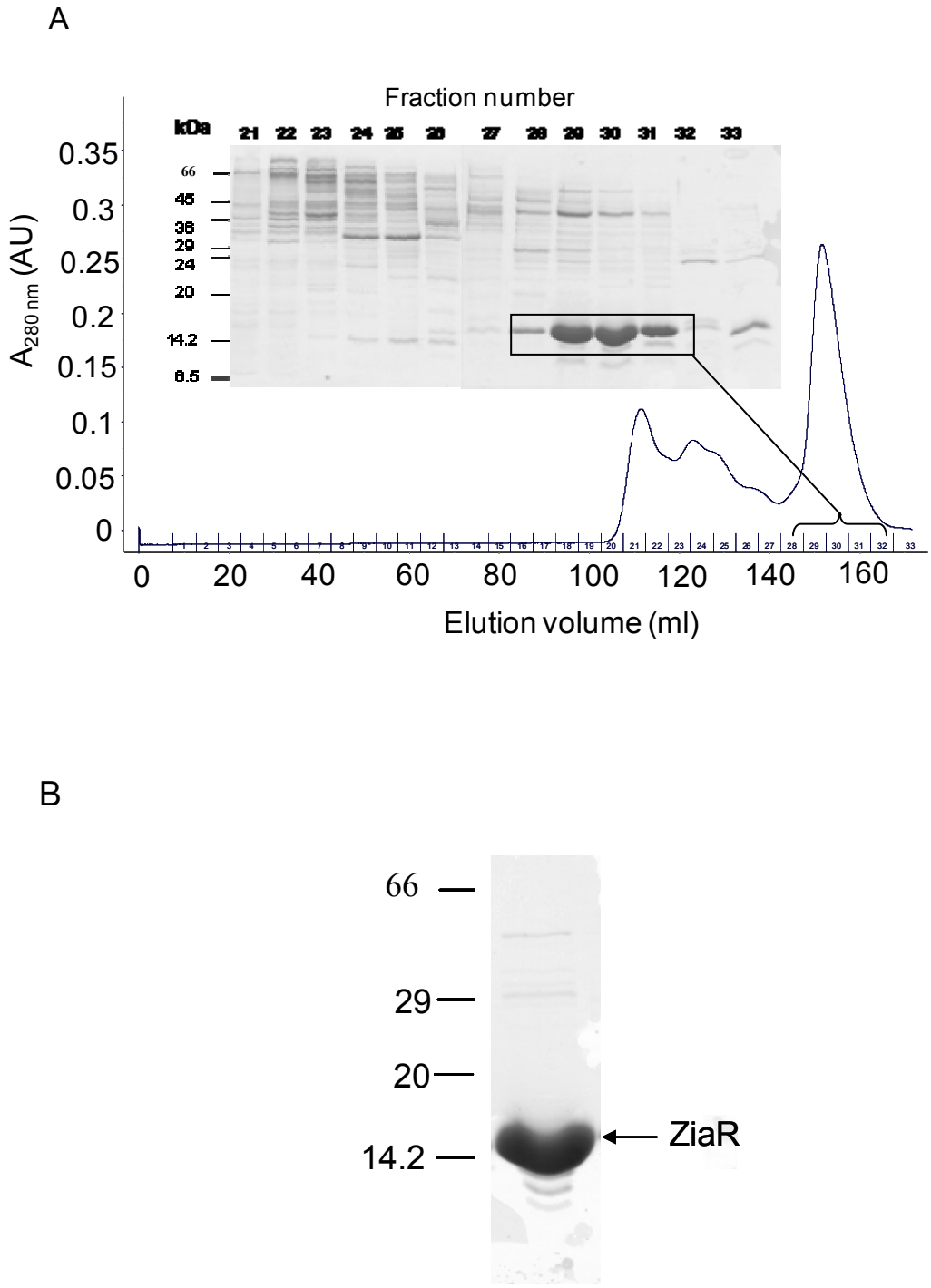

Figure 7. Purification of ZiaR by size exclusion chromatography and heparin affinity chromatography. A. Chromatograph showing change in total protein concentration in fractions eluted from a Superdex 75 gel filtration column. *Inset*; SDS PAGE analysis (17 % v/v acryl-bis) of fractions from this separation with the postion of ZiaR shown on both the gel and chromatograph (ZiaR bands are shown in the boxed region). B. SDS PAGE analysis (17 % v/v acryl bis) of fractions 21-33 eluted at different NaCl concentrations from a 1 ml heparin affinity column, loaded with size exclusion fractions enriched for ZiaR.

The 2:1 Zn^{2+} binding stoichiometry observed in gel filtration analyses was confirmed in separate analyses in which Zn^{2+} occupancy of ZiaR was measured by titration with PAR, a Zn^{2+} binding metallochromic indicator (Figure 9). Under conditions of surplus PAR, this indicator has been used previously to detect nanomolar to picomolar zinc-protein disassociation constants (VanZile *et al.* 2000; Harvie *et al.* 2006). As shown by the example analysis in Figure 9, anaerobic titration of ZiaR with increasing equivalents of Zn^{2+} in the presence of 400 μM PAR, showed that ZiaR withheld Zn^{2+} from PAR up to approximately two equivalents of Zn^{2+}, after which absorption at 492 nm increases with formation of PAR_2-Zn^{2+} complex, confirming the 2:1 Zn^{2+}: protein stoichiometry observed in gel filtration experiments. Given the high equilibrium binding affinity of PAR for Zn^{2+} and the almost complete lack of competition with the protein for Zn^{2+} up to two equivalents, these data also suggested that each of the metal binding sites on ZiaR must have a Zn^{2+} binding affinity tighter than that of the PAR_2-Zn^{2+} complex and likely close to that of SmtB, which also shows stoichiometric Zn^{2+} binding in the presence of PAR (VanZile *et al.* 2000) with an estimated $K_{Zn} \sim 10^{13}$ M^{-1} (VanZile *et al.* 2002a). In the size-exclusion analysis (Figure 8) and titration with PAR (Figure 9) ZiaR was likely to have been a dimer (see section 3.4.6); therefore, the 2:1 Zn^{2+} binding stoichiometry implied by these data is likely reporting on binding of Zn^{2+} to four sites on a ZiaR dimer (with two sites present on each dimer subunit) (see section 3.4.6 for further discussion of monomer-dimer states of ZiaR).

3.3.2 Characterisation of the metal binding sites of ZiaR using Co^{2+} as a spectral probe

Recombinant ZiaR binds Co^{2+}/Zn^{2+} in a tetrahedral geometry via an α3N and an α5 site

UV-visible spectroscopy is routinely used to interrogate the biophysical properties of metal binding sites of proteins. Although Zn^{2+} forms tight bonds to ligands, the presence of a fully occupied 3d orbital means that these bonds are spectrally silent. Co^{2+} is capable of adopting the same tetrahedral coordination geometry as Zn^{2+}. However, unlike Zn^{2+}, the presence of partially filled d-shell orbitals means that approaching ligand groups can donate electrons into these vacant orbitals. These ligand to metal

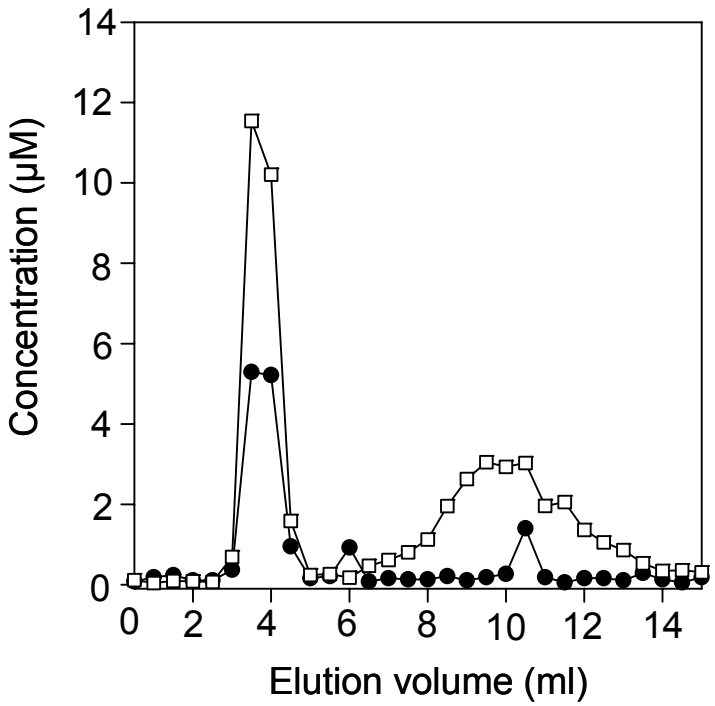

Figure 8. Size-exclusion fractionation of protein-bound and free Zn^{2+}. ZiaR protein (10 μM) was incubated anaerobically with excess Zn^{2+} (approx. 40 μM) for 10 minutes and bound and free metal resolved on Sephadex G-25 matrix. Closed circles: protein; open squares: Zn^{2+}. Conditions: 400 mM KCl, 100 mM NaCl, 10 mM Hepes (pH 7.8).

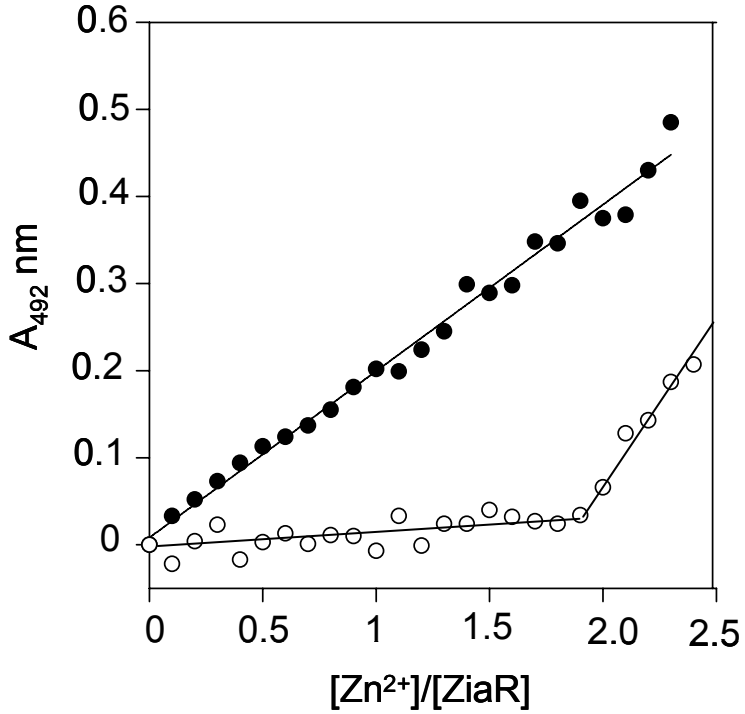

Figure 9. Zn^{2+} titration of ZiaR in the presence of the Zn^{2+} binding chelator PAR. 400 μM PAR was incubated anaerobically with increasing concentrations of Zn^{2+} in the presence (open symbols) or absence (closed symbols)) of 10 μM ZiaR. Conditions: 400 mM KCl, 100 mM NaCl, 10 mM Hepes (pH 7.8).

electron resonances have excitation energies in the UV-Visible regions of the electromagnetic spectrum producing intense absorption bands which can be identified by spectroscopy. Hence, Co^{2+} can be used as a 'surrogate' spectral probe for Zn^{2+} binding sites in proteins such as ZiaR.

A representative UV-Visible titration of ZiaR with Co^{2+} is shown in Figure 10. On titration with Co^{2+}, Co-dependent increases in absorption are observed in two key regions, a higher energy region in the near-UV, 300-400 nm wavelength range and a lower energy, broader region in the 500-800 nm range (Figure 10a). Features in the 300-400 nm region (with a peak at ~310 nm) are indicative of Ligand-Metal-Charge-Transfer (LMCT) features, diagnostic of high energy Co-S^- bond absorption (Figure 10b, left panel). It has been shown previously that molar extinction coefficients in the range 900-1300 M^{-1} cm^{-1} correlate with formation of a single Co-S-Cys bond (Brown & Collins 1991). For ZiaR peak extinction coefficients at saturation were routinely observed to be between 2000 M^{-1} cm^1 and 3000 M^{-1} cm^{-1}, suggesting the presence of at least two and potentially three cysteine residues involved in Co^{2+} binding. This result is consistent with the three predicted cysteine residues present in the ZiaR α3N site (Figure 4).

Features in the lower energy 500-800 nm region are produced by *d-d* electronic transitions and are diagnostic of the coordination sphere adopted by Co^{2+} in the metal binding sites. Ligand field theory shows that ligand groups approaching transition metal ions such as Co^{2+} cause splitting of d-orbitals, with some being promoted to higher energy and some to lower energy levels. In symmetric coordination complexes (e.g. octahedral), electronic transitions between these orbitals are spin-forbidden. Therefore, octahedral Co^{2+} complexes absorb energy extremely weakly in the UV-Visible range with *d-d* electronic transitions usually having molar extinction coefficients < 50 M^{-1} cm^{-1}. Additionally, absorbance maxima are typically at wavelengths below 600 nm with features having a broad absorption envelope of low complexity. However, transitions between split-orbitals in complexes with non-symmetric coordination geometry (e.g. tetrahedral) are not spin-forbidden and so electronic transitions with resonance energies in the UV-Visible range readily occur. These transitions are characterised by much more intense *d-d* absorption bands than seen in symmetric complexes, with extinction coefficients usually >300 M^{-1} cm^{-1}. These features also have absorbance maxima at longer wavelengths (>600 nm) and often have a high level of complexity, with multiple absorption peaks spread throughout the spectrum (Brown and Collins 1991).

For ZiaR, multiple intense *d-d* transition features are observed in the 500-800 nm region, with intensities at the peak 585 nm feature at saturation (two equivalents of Co^{2+}) typically >500 M^{-1} cm^{-1} (Figure 10b, right panel). These features are most consistent with tetrahedral or distorted tetrahedral coordination geometry (Brown & Collins 1991) at both of the metal binding sites in the protein for Co^{2+} and by inference Zn^{2+}. As expected from a tetrahedral coordination sphere, the *d-d* transitions have a high degree of complexity with multiple peaks. In addition to the primary *d-d* transition peak at 585 nm, other absorbance features are observed in this wavelength range. Notably, an intense feature is observed with maximal absorbance at approximately 655 nm. When plotted against equivalents of Co^{2+} (Figure 10b, right panel), this feature resembles the binding isotherm at 310 nm (albeit with lower intensity) and so may represent a 'red-shifted' version of this LMCT feature. Studies of Co^{2+} substituted metallothionien proteins have shown red-shifting of LMCT bands to longer wavelengths at high Co^{2+} stoichiometries associated with formation of high-sulphur content tetrathiolate Co^{2+} clusters (Vasák & Kägi 1981; Good & Vasák 1986).

Both LMCT and *d-d* features saturate at approximately two equivalents of Co^{2+} (Figure 10b). Comparison of the binding isotherms for each absorption feature (Figure 10b) reveals a linear increase in intensity at 585 nm with a sigmoidal association curve best describing data for the 310 nm LMCT feature (this is also observed for the feature at 655 nm). The linear increase in *d-d* transition feature intensity to saturation at two equivalents of Co^{2+} implies stoichiometric Co^{2+} binding to two tetrahedral metal binding sites per monomer (four per dimer). This is consistent with the Zn^{2+} binding stoichiometry determined by size-exclusion fractionation of Zn^{2+}-bound ZiaR samples (Figure 8) and by competition with the Zn^{2+} binding chelator PAR (Figure 9). The lack of a linear increase in the LMCT intensity at 310 nm implies a relatively weak association constant for Co^{2+} binding to this site and/or binding to a tighter affinity LMCT-silent site first. The α5 site of ZiaR is unlikely to contain liganding cysteine residues (Figure 4) and so Co^{2+} binding to this site would not be expected to contribute to LMCT features. Thus, these data are consistent with tetrahedral Co^{2+} (and by inference Zn) binding to both the cysteine-free α5 site and the cysteine containing α3N site, with α5 K_{Co} > α3N K_{Co}.

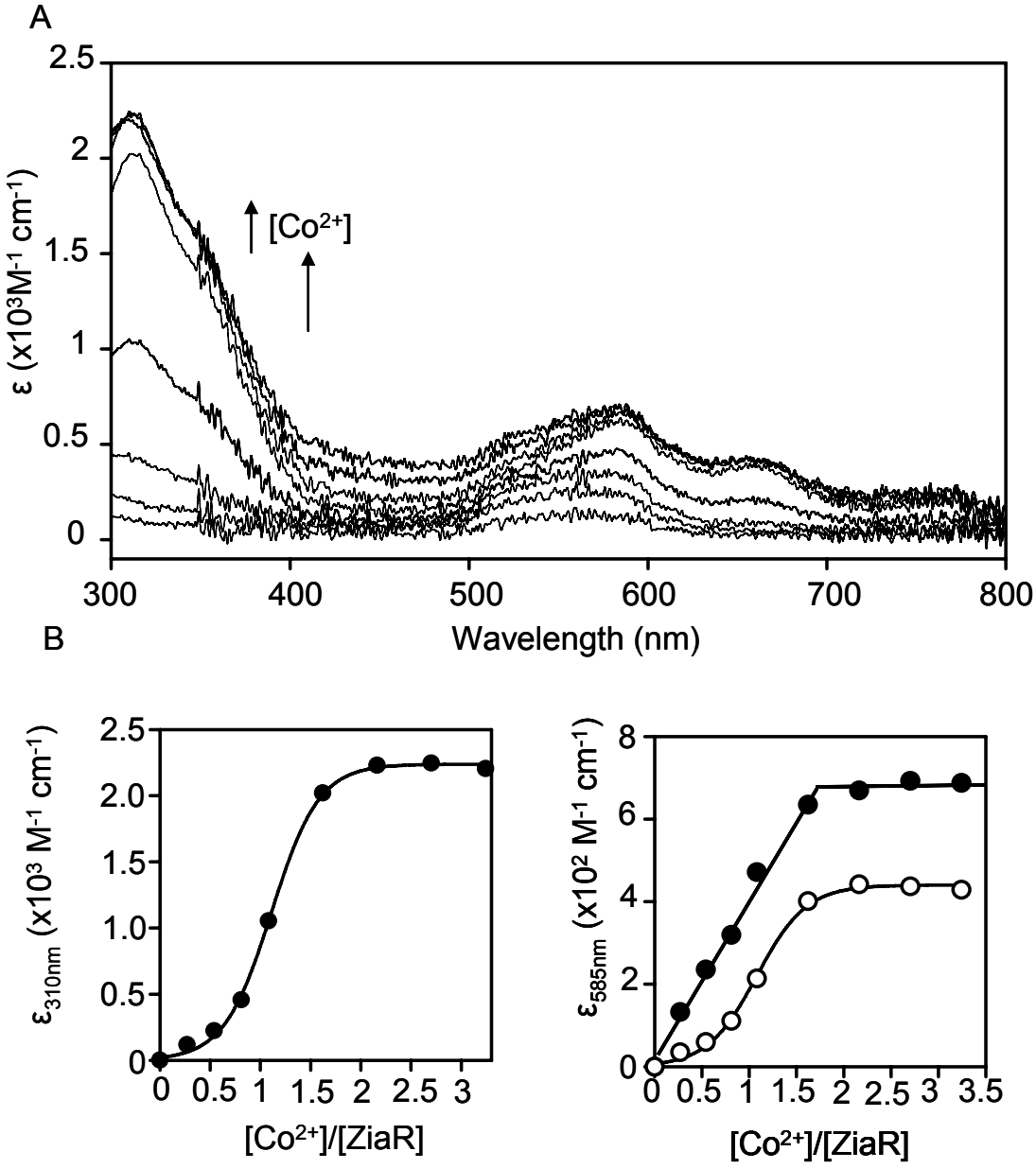

Figure 10. Anaerobic UV-Visible titration of ZiaR with Co^{2+}. 37 μM apo-ZiaR was titrated with Co^{2+} and changes in absorbance measured. A. Apo-subtracted difference spectra recorded following addition of Co^{2+}. B. Left panel; changes in molar absorbance intensities monitored at 310 nm on titration with Co^{2+}. Right panel; changes in absorbance intensities monitored at 585 nm (closed symbols) and 655 nm (open symbols) on titration with Co^{2+}. Conditions: 400 mM KCl, 100 mM NaCl, 10 mM Hepes (pH 7.8).

Zn^{2+} binds to both metal sites in ZiaR in preference to Co^{2+}

The Irving-Williams affinity series predicts that metal binding sites of organic molecules tend to have a tighter affinity for Zn^{2+} than Co^{2+}. Therefore, at equilibrium, proteins including ZiaR exposed to equivalent concentrations of Zn^{2+} and Co^{2+} are liable to preferentially bind Zn^{2+} and not Co^{2+}. The presence of strong absorbance features in the UV-Visible region in Co^{2+}-loaded ZiaR allowed this prediction to be tested using a simple spectral approach. Following addition of approximately two equivalents of Co^{2+} to apo-ZiaR protein, the Co-loaded protein was titrated with Zn^{2+} and the changes in absorbance measured (Figure 11). Addition of Zn^{2+} caused quenching of Co-dependent LMCT and *d-d* features (Figure 11a). When the fall in intensity of each feature is plotted against equivalents of Zn^{2+} added, it can be seen that complete quenching of the LMCT features occurs at ~0.8 equivalents added Zn^{2+}. However, *d-d* transitions require more added Zn^{2+} to fully saturate and are completely quenched at close to two equivalents of Zn^{2+}. This implies that Zn^{2+} first displaces Co^{2+} from the tetrahedral α3N site, accounting for the decrease in *d-d* feature intensity and the stoichiometric fall in LMCT intensity up to approximately one equivalent of Zn^{2+}, followed by displacement of Co^{2+} from tetrahedral α5 sites which requires an additional single equivalent of Zn^{2+}. These data are again consistent with α5 K_{Co} > α3N K_{Co} (Figure 10), validating the presence of structurally independent metal sites of divergent Co^{2+} binding affinities in ZiaR.

3.4 Probing the allosteric mechanism of ZiaR

It has been shown previously that both metal binding sites of ZiaR are required for metal sensing *in vivo*; mutation of certain residues at either metal site caused loss of zinc mediated de-repression of a ZiaR controlled promoter in the hetrologous host *Synechococcus* PCC 7942 (Thelwell *et al.* 1998). This is the only known instance in which both α3 and α5 sites are required to facilitate metal sensing in ArsR-SmtB family proteins and so ZiaR has come to represent one of the sensory mechanisms of this family. To verify this mechanism, mutations identical to those used in the original *in vivo* experiments were introduced into ZiaR both independently and in combination using quick-change site directed mutagenesis. At the α3N site, both cysteine residues in the conserved CVC motif were converted to serine, the resulting protein termed Δα3

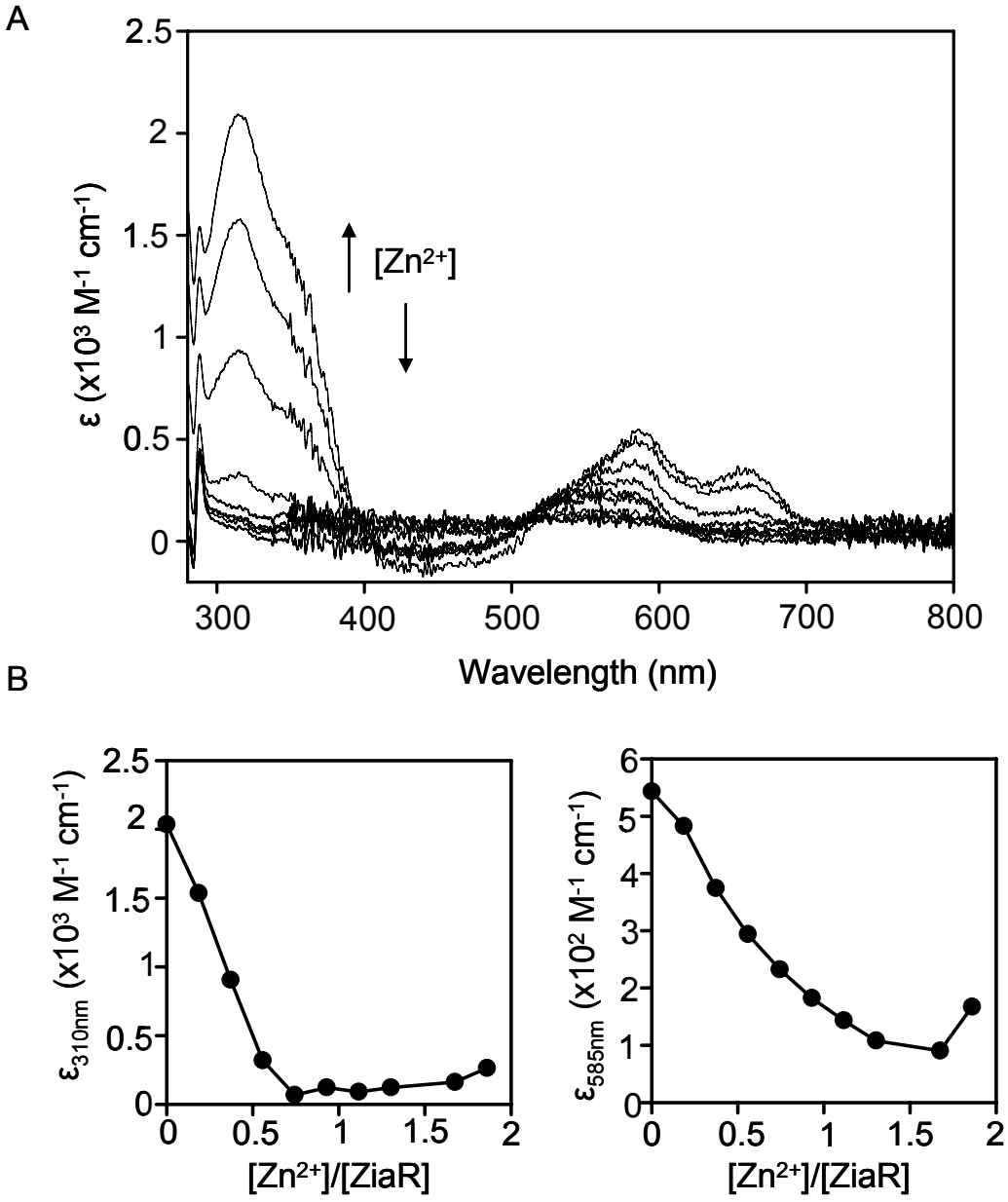

Figure 11. Zn^{2+} quenching of Co^{2+}-ZiaR spectral features. An anaerobic sample of apo-ZiaR (approx. 40 μM) was pre-loaded with a saturating concentration of Co^{2+} (two equivalents) and then titrated with Zn^{2+}. A. Apo-protein subtracted difference spectra showing changes in absorbance on titration with Zn^{2+}. B. Changes in absorbance from apo-subtracted difference spectra shown in A for 310 nm LMCT feature (left panel) and 585 nm *d-d* transition feature (right panel). Precipitation was observed beyond ~1.5 equivalents of Zn^{2+}. Conditions: 400 mM KCl, 100 mM NaCl, 10 mM Hepes (pH 7.8).

ZiaR. At the α5 site, the conserved histidine at position 116 was converted to arginine with the resulting protein termed Δα5 ZiaR. Additionally, both α3N and α5 mutations were introduced in combination to produce a protein defective in both metal sites (termed Δα3Δα5 ZiaR).

Mutated ZiaR proteins were overexpressed under conditions identical to those used for wild-type ZiaR and were purified in a similar fashion. Following an initial step in which crude cell extract was loaded and eluted on a heparin or Ni^{2+} affinity column, protein was subjected to size exclusion separation. The elution profiles for the mutated proteins were effectively the same as wild-type (Figure 12a, b). Size exclusion fractions for each protein were subjected to a further heparin affinity purification and concentration step as described previously for ZiaR (Figure 12c). DTNB assays verified the production of almost completely reduced anaerobic protein samples for characterisation; Δα3ZiaR had on average 1.74 ± 0.23 reactive cysteines (out of two predicted to present in the protein). Δα5ZiaR preparations contained 3.72 ± 0.4 cysteines (out of four predicted to be present in the protein). Δα3Δα5 ZiaR was purified as described in section 2.4.6 (data not shown); a single measurement of the cysteine content of a single Δα3Δα5 protein preparation showed a cysteine content of 2.52 (two cysteines predicted).

3.4.1 Metal binding properties of mutated ZiaR proteins

To validate the loss of metal binding properties in each of the single site mutant ZiaR proteins (Δα3ZiaR and Δα5ZiaR), UV-visible Co^{2+} binding analyses analogous to those performed for ZiaR were performed. Following anaerobic titration of Δα5ZiaR with Co^{2+}, LMCT's and *d-d* transitions were observed (Figure 13a). When the increases in intensity for each feature were plotted with a control ZiaR Co^{2+} titration, differences between the spectra are apparent. For Δα5ZiaR, the LMCT feature at 310 nm increases to saturate at just over 2000 M^{-1} cm^{-1} (Figure 13b, left panel). Critically, saturation is reached at approximately one equivalent of Co^{2+} instead of two equivalents for ZiaR, with no inflection observed in the early part of the Δα5ZiaR curve (Figure 13b, left panel) as is observed for ZiaR (Figure 10). This is consistent with a weakening of the α5 site affinity for Co^{2+} in the mutant protein resulting in stoichiometric binding of the first equivalent of Co^{2+} to the intact α3N site, directly opposite to what is observed in the wild-type protein. For *d-d* transition features, saturation is observed at approximately

Figure 12. Purification of recombinant Δα3ZiaR and Δα5ZiaR. For each protein, crude cell extract was loaded onto a 1 ml heparin affinity column. Protein was eluted in 500 mM NaCl and then applied to a Superdex 75 column for further purification. A. Example size exclusion purification chromatograph for Δα5ZiaR with SDS PAGE gel analyses of fractions shown in the inset. B. Analogous data for a preparation of Δα3 ZiaR. C. For analyses in A and B, the positions of each mutated form of ZiaR is highlighted by the boxed region and shown on the chromatograph. As for ZiaR, to purify proteins to homogeneity, size exclusion fractions were pooled, loaded onto a 1 ml heparin column and then eluted in 1 M NaCl.

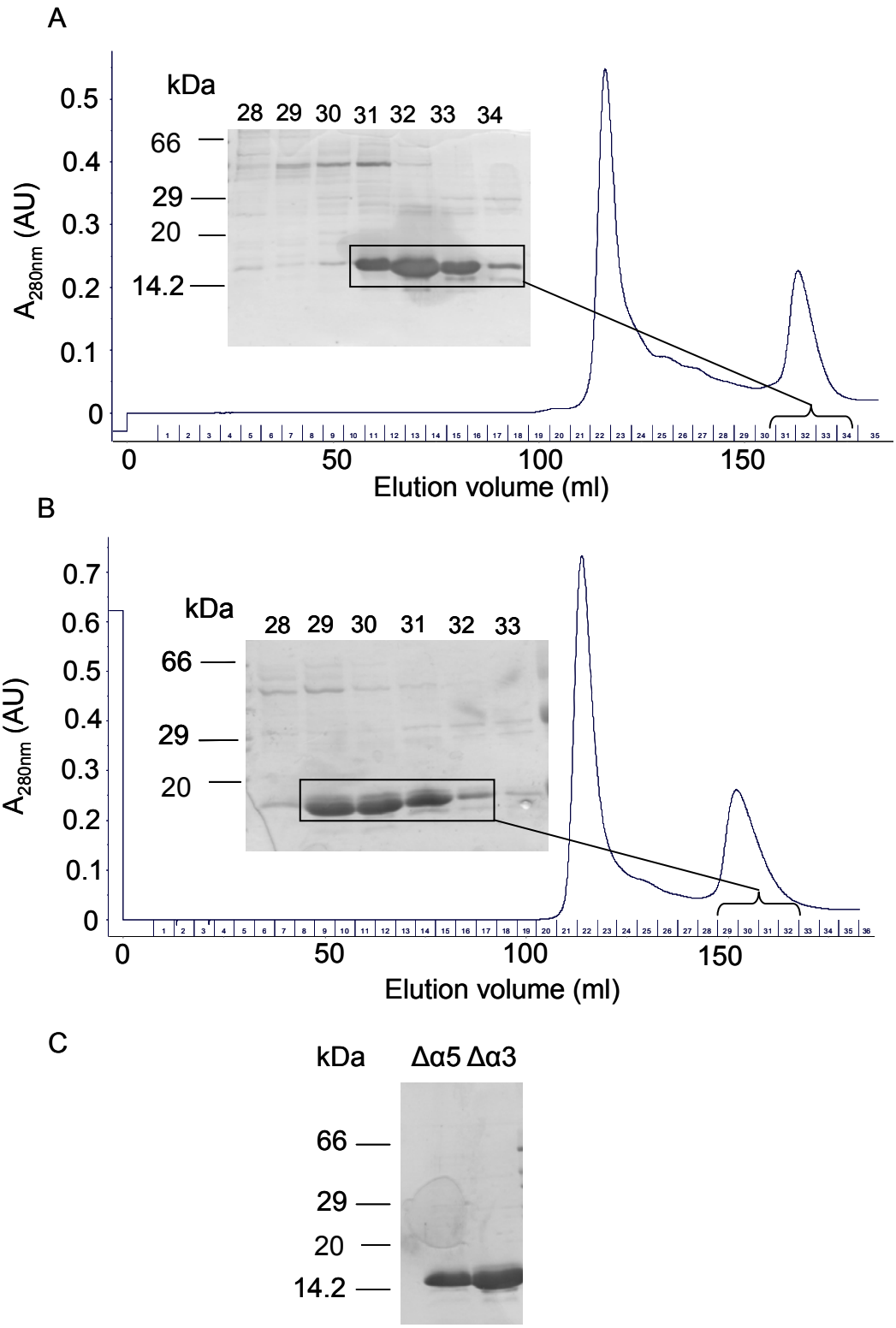
A
kDa
28 29 30 31 32 33 34
66
29
20
14.2
A_{280nm} (AU)
0.5
0.4
0.3
0.2
0.1
0
0
50
100
150
Elution volume (ml)
B
kDa
28 29 30 31 32 33
66
29
20
A_{280nm} (AU)
0.7
0.6
0.5
0.4
0.3
0.2
0.1
0
0
50
100
150
Elution volume (ml)
C
kDa
Δα5 Δα3
66
29
20
14.2

one equivalent of Co^{2+} (versus approximately two equivalents for wild-type protein) (Figure 13b, right panel). Additionally, the intensity at saturation is substantially reduced (~50 %) compared to ZiaR (Figure 13, right panel). These data are consistent with loss of tetrahedral Co^{2+} binding at the mutated α5 site with retention of tetrahedral binding at the intact α3 site. These data do not necessarily rule out Co^{2+} binding at the mutated α5 site; non-tetrahedral Co^{2+} binding, with α5 K_{Co} <<< α3N K_{Co}, would not be visible is this assay, although the preferred coordination geometries of Co^{2+} make this event unlikely.

Analogous Co^{2+} titrations with Δα3ZiaR also reveal substantial changes to the metal binding properties of this protein. As observed for Δα5ZiaR, the intensity of *d-d* transitions is substantially reduced compared to ZiaR, with saturation occurring at approximately 50 % of the ZiaR value (Figure 14a, b right panel). These data are consistent with loss of tetrahedral Co^{2+} binding at the α3N site with retention of tetrahedral binding at the intact α5 site. The magnitude of features in the LMCT regions of the spectra are also substantially reduced (Figure 14a, b, left panel). Plotting of the LMCT feature at 310 nm with equivalents of Co^{2+} added (with an analogous ZiaR control titration also shown) (Figure 14b, left panel), reveals a relatively small increase in absorbance with no apparent saturation for Δα3ZiaR. A portion of this increase may be due to increased light scatter observed towards the end of the titration (Figure 14a) potentially caused by some degree of protein precipitation. Nevertheless, at two equivalents Co^{2+}, the LMCT intensity at 310 nm is approximately 500 M^{-1} cm^{-1}, substantially less than would be expected for a single Co-S^- bond, and approximately five-fold lower than that observed for the ZiaR control titration. These data directly confirm the involvement of at least one and almost certainly both cysteines in the pair mutated (cysteine 71 and cysteine 73) in metal binding at the α3N site in ZiaR. However, it is noted that involvement of both cannot be unequivocally shown by these data alone; mutation of a single cysteine in the pair may be sufficient to lose Co^{2+} binding and thus cause a substantial reduction in LMCT intensity.

A third potential cysteine ligand at position 20 is predicted to form part of the α3N site of ZiaR (Figure 4). The upper limit for the LMCT intensities observed at saturation of Co^{2+} binding in ZiaR of ~2000-3000 M^{-1} cm^{-1} (Figure 10) strongly supports involvement of at least two cysteines (likely Cys71 and Cys73) and possibly a third, with this cysteine the likely candidate for the additional ligand. This cysteine was not mutated in the Δα3ZiaR protein, however as described above, these data are

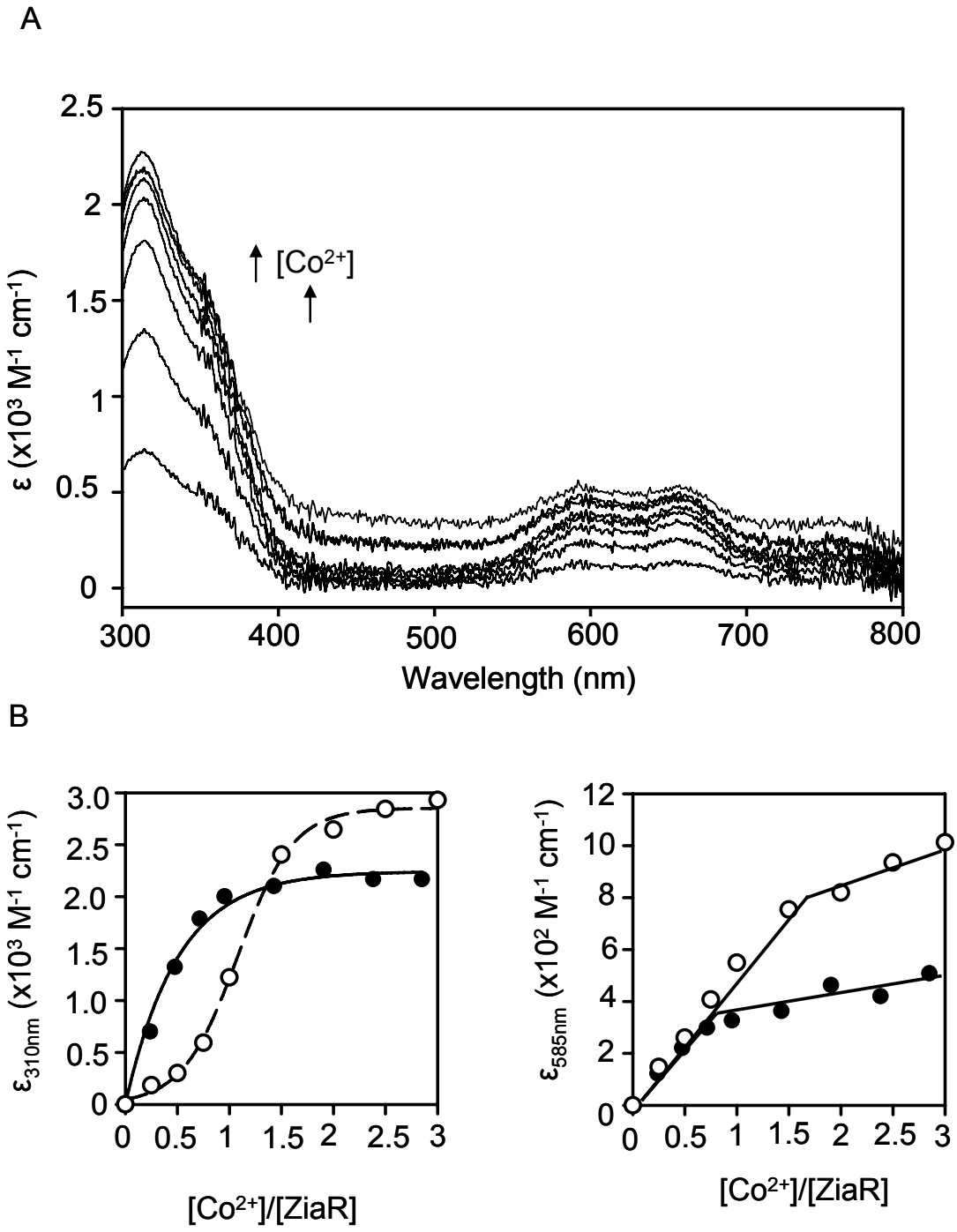

Figure 13. Anaerobic UV-Visible titration of Δα5ZiaR with Co^{2+}. A. apo-protein subtracted difference spectra produced following titration of apo-protein (42 μM) with Co^{2+}. B. Left panel; increase in intensity of the 310 nm LMCT feature with increasing [Co2+] (closed symbols). Right panel; increase in intensity of the 585 nm *d-d* transition feature with increasing [Co^{2+}] (closed symbols). Analogous data are also shown from a titration of ZiaR (40 μM) with Co^{2+} (open symbols) (wild-type data are from the same titration in both panels in B).

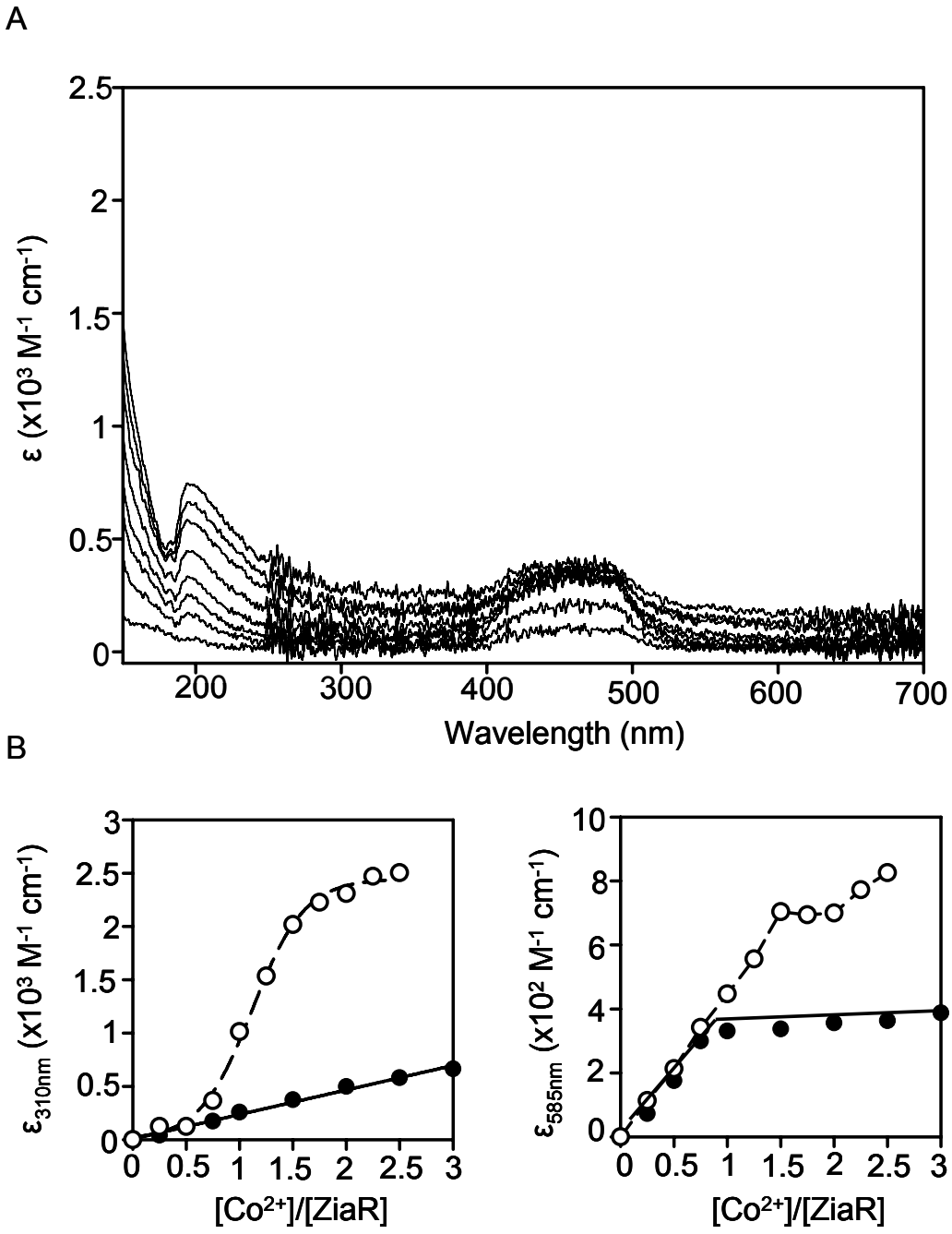

Figure 14. Anaerobic UV-Visible titration of Δα3ZiaR with Co^{2+}. Top panel; apo-subtracted difference spectra following titration of 40 μM protein with Co^{2+}. Bottom left panel; increase in intensity of the 310 nm LMCT feature with increasing Co^{2+} for Δα3 ZiaR (closed symbols) and an analogous example ZiaR titration (15 μM protein) (open symbols). Right panel; increases in intensity of *d-d* transition feature at 585 nm with increasing [Co^{2+}] for Δα5ZiaR (closed symbols). Data from an example ZiaR titration are also shown in both panels in B (open symbols).

consistent with complete loss of Co^{2+} binding at the α3N site, due to destruction of the tetrahedral ligand sphere optimal for Co^{2+} binding (Figure 14), so this residue was not expected to contribute to LMCT features in Δα3ZiaR.

3.4.2 DNA binding properties of wild-type and mutated ZiaR proteins

The *in vitro* UV-Visible analyses of Co^{2+} binding to mutated ZiaR proteins demonstrated structural changes to each of the metal binding sites which must be correlated with the changes in inducer responsiveness observed *in vivo* (Thelwell *et al.* 1998). The mutations at the α3N site removed two of the four ligands, destroying the native, tetrahedral chelate, with complete apparent loss of Co^{2+} binding to this site. The mutation at the α5 site removed one of the four metal site ligands, again causing loss of the native tetrahedral-like chelate and likely the complete loss of Co^{2+} binding to the site. To determine the effects of these mutations on the Zn^{2+} responsiveness of each protein *in vitro*, the effects of Zn^{2+} on the equilibrium DNA binding affinity of ZiaR and each of the mutant proteins was evaluated by fluorescence anisotropy.

3.4.3 Production of a DNA fragment containing a portion of the *zia* promoter sequence

The *ziaR* gene is divergently transcribed from the *ziaA* gene (encoding the Zn^{2+} exporting ATPase ZiaA). Previously it was shown using gel retardation assays that ZiaR bound specifically to a 160 bp DNA fragment incorporating the intergenic region between *ziaR* and *ziaA* within which was located a 12-2-12 hyphenated inverted repeat sequence with a high degree of similarity to characterised promoter elements recognised by other ArsR-SmtB proteins (Thelwell *et al.* 1998). Complimentary oligonucleotides were synthesised which incorporated this 12-2-12 inverted repeat sequence, with one of the pair of primers labelled at its 5' end with the fluorophore Hexachlorofluorescein (HEX) (Figure 15a). After synthesis these oligonucleotides were annealed and analysed by native PAGE analysis to confirm successful annealing. Annealed oligonucleotides were observed to routinely migrate more slowly than single stranded samples of each of the primers. As expected, the HEX-labelled oligonucleotide ran slightly slower than the

A

B

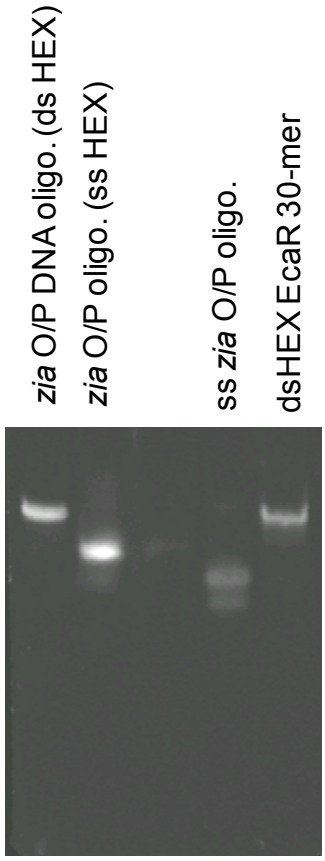

Figure 15. Production of an annealed double stranded *zia* O/P oligonucleotide for fluorescence anisotropy. A. 32-base pair DNA sequence, incorporating the conserved 12-2-12 hyphenated inverted promoter repeat sequence (bold with arrows) recognised by ZiaR, used for fluorescence anisotropy. B. Confirmation of successful annealing of single stranded *zia* O/P DNA oligonucleotides by native PAGE. Annealed and single stranded samples are shown with a sample of double-stranded HEX-labelled DNA, of approximately the same length as the double stranded *zia* oligonucleotide, containing a portion of the EcaR promoter element from *Erwinia carotavora*, also shown for comparison.

unlabelled oligonucleotide due to the presence of the relatively large fluorescent group at the 5' end of the molecule (Figure 15b).

3.4.4 Titration of ZiaR with DNA

Fluorescence anisotropy is an equilibrium DNA binding assay and is therefore ideally suited for monitoring apo-protein interaction to DNA and also for analysing the effects of potential effector species (such as metal ions), at defined concentrations, on DNA binding. On titration of *zia* O/P oligonucleotide with recombinant ZiaR an increase in the r_{obs} value was observed, implying slower rotation of the fluorescently labelled double stranded DNA, consistent with protein association to DNA (Figure 16a). Replicate analyses performed in the presence of a large excess of EDTA (1 mM) under conditions analogous to those shown in Figure 16a produced an average r_{obs} increase of 0.09556 (± 0.0038) (Table 5). For the analysis shown in Figure 16a, the estimated disassociation constant for protein binding to DNA (K_{DNA}) is approximately 50 nM, with an average value of 61 nM (±11 nM) obtained for replicate titrations performed in the presence of 1 mM EDTA. These binding parameters for apo-ZiaR compare favourably with those obtained for the α5 Zn^{2+} sensor SmtB from *Synechococcus* (VanZile *et al.* 2002b).

In previous work it has been shown that for SmtB binding to a 40-bp DNA oligonucleotide an increase in anisotropy of approximately 0.02 corresponds to the binding of a single dimer to the DNA molecule (VanZile *et al*. 2002b). ZiaR is similar in size to SmtB (15.1 kDa compared to 13.5 kDa for SmtB). The average values for increases in anisotropy from these analyses of ZiaR binding to DNA (Table 5) suggest binding of four or five protein dimers to each molecule of DNA. However, this value is only an estimation and slightly different lengths of the oligonucleotide molecules used in each study (32-bps here compared to 40-bps in studies characterising SmtB) may mean that the number of ZiaR dimers bound to each molecule may well be slightly less. Nevertheless, these data confirm the formation of higher order protein complexes observed for ZiaR in previous gel retardation analyses (Thelwell *et al*. 1998) and are consistent with the formation of higher order complexes by other members of this family.

Figure 16. Example fluorescence anisotropy titrations of *zia* O/P oligonucleotide with ZiaR. A. Aerobic titration of ZiaR protein with 10 nM *zia* O/P oligonucleotide in the presence of 1 mM EDTA and 1 mM DTT. B. Anaerobic titration of ZiaR (determined by ICP-MS prior to titration to be ~91 % Zn^{2+} free) with 10 nM *zia* O/P oligonucleotide in the presence (closed symbols) and absence (open symbols) of 1 mM EDTA. Binding parameters for the experiment performed in the absence of EDTA are shown in parenthesis C. Anaerobic titration of ZiaR protein with 10 nM *zia* O/P oligonucleotide following pre-incubation with four equivalents of Zn^{2+} (100 μM Zn^{2+}, 25 μM protein (open symbols). An analogous titration is also shown in which protein was not pre-incubated with Zn^{2+} but Zn^{2+} was present in the DNA binding reaction at a concentration sufficient to saturate the protein added (3 μM) (closed symbols); a response identical to that following pre-incubation with Zn^{2+} was produced.

A

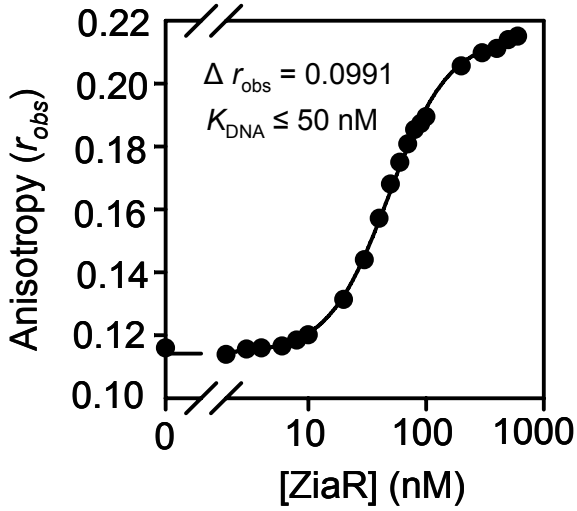
0.22
0.20
0.18
0.16
0.14
0.12
0.10
Anisotropy (r_{obs})
Δ r_{obs} = 0.0991
K_{DNA} ≤ 50 nM
0
10
100
1000
[ZiaR] (nM)

B

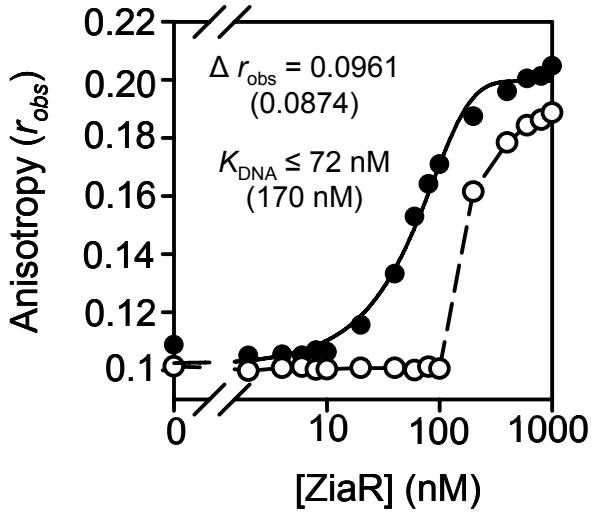
0.22
0.20
0.18
0.16
0.14
0.12
0.1
Anisotropy (r_{obs})
Δ r_{obs} = 0.0961
(0.0874)
K_{DNA} ≤ 72 nM
(170 nM)
0
10
100
1000
[ZiaR] (nM)

C

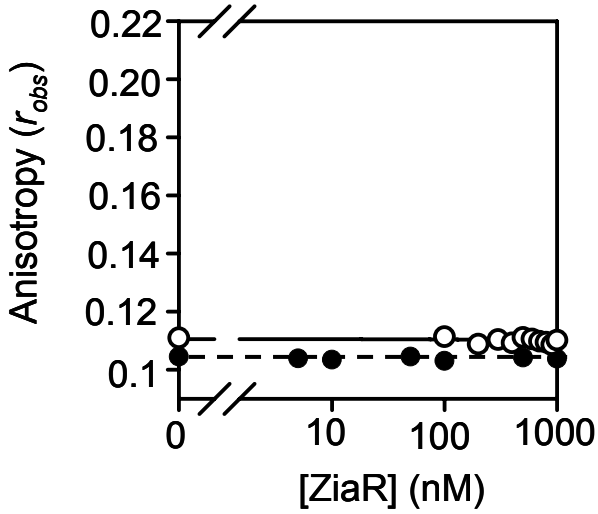
0.22
0.20
0.18
0.16
0.14
0.12
0.1
Anisotropy (r_{obs})
0
10
100
1000
[ZiaR] (nM)

Titrations analogous to those shown in Figure 16a, performed anaerobically in the presence of 1 mM EDTA, produced binding isotherms resembling those observed under aerobic conditions (Figure 16b, closed symbols). Anaerobic titrations of ZiaR with *zia* O/P oligonucleotide in the absence of EDTA also routinely showed binding to DNA and increases in r_{obs} similar to those observed following incubation in EDTA (Figure 16b, open symbols, Table 5). Titration of DNA with ZiaR protein pre-incubated in the presence of a saturating concentration of Zn^{2+} or with Zn^{2+} present at a saturating concentration in the DNA binding reaction reproducibly showed no increase in measured r_{obs} values indicating no binding of Zn-bound protein to DNA under these conditions (i.e. the K_d for DNA must be substantially weaker than 1 μM) (Figure 16c).

3.4.5 Analysis of Δα3ZiaR, Δα5ZiaR and Δα3Δα5ZiaR binding to DNA

Previously, it was demonstrated that both Δα3 and Δα5 mutations rendered ZiaR inducer non-responsive *in vivo* (Thelwell *et al*. 1998). Both mutant proteins retained wild-type-like repression of the *zia* promoter (the α5 site mutant actually repressing expression more tightly than observed with the wild-type ZiaR under low-Zn^{2+} conditions) suggesting that both mutant proteins were still capable of binding to DNA with binding affinities sufficient to mediate effective repression *in vivo*. DNA binding was confirmed *in vitro* by gel retardation assay (Thelwell *et al.* 1998). To analyse effects of Zn^{2+} on DNA binding, the mutated proteins were first titrated with *zia* O/P oligonucleotide aerobically, in the presence of DTT and EDTA, to confirm DNA binding under the conditions routinely used in the fluorescence anisotropy assays (Figure 16). Example titrations for each of the proteins are shown in Figure 17a-c, together with the associated binding parameters (Δr_{obs}, K_d) which are also summarised in Table 5. All three of the mutant proteins bound to DNA under conditions associated with ZiaR binding to DNA with the Δr_{obs} values indicating higher order complex formation for each protein (Figure 17a-c). It was reported previously that for Δα5ZiaR, protein-DNA complexes were less stable than those for ZiaR and Δα3ZiaR at higher concentrations of non-specific DNA used in gel-retardation assays (Thelwell *et al.* 1998), potentially implying a weaker DNA binding affinity *in vitro* for this protein. No evidence for this is observed in these analyses (from a single replicate at least) and a wild-type-like Δr_{obs} also observed, suggesting no apparent effect of this mutation on the oligomerisation properties of the protein. The non-equilibrium nature of the gel

retardation assays used previously may account for this apparent slightly weaker DNA binding affinity.

To determine the effects of each mutation on the *in vitro* Zn^{2+} responsiveness of ZiaR, complexes of protein and *zia* O/P oligonucleotide were preformed, the anisotropy of each complex measured and then each complex was titrated anaerobically with Zn^{2+} (Figure 18a). For ZiaR, titration with Zn^{2+} caused a decrease in measured anisotropy producing values characteristic of non-protein bound oligonucleotide, consistent with Zn-mediated disassociation of ZiaR-DNA complexes (Figure 18a). Complete disassociation with no further decrease in r_{obs} reproducibly occurred between 0.8-1.2 equivalents of Zn^{2+} (Figure 18a, Appendix A Figure 1). This apparent stoichiometry suggests that for ZiaR two metal sites per dimer must be filled by Zn^{2+} to cause complete disassociation from DNA *in vitro*. Unexpectedly, analogous titrations for Δα3ZiaR and Δα5ZiaR also showed Zn^{2+}-mediated disassociation of protein-DNA complexes (Figure 18a). For Δα3ZiaR, in the data shown in Figure 18a, a reduction in anisotropy to a value consistent with unbound DNA occurs at a lower stoichiometry than for ZiaR at approximately 0.6 equivalents. This effect was reproducible, with saturation observed to occur between 0.4 and 0.8 equivalents in replicate assays (Appendix A Figure 1). These data suggest that the intact α5 sites (in the α3 mutant protein at least) only require filling of one site within the pair on the dimer to initiate allostery; this suggested that the symmetry related α5 sites may have non-identical affinities for Zn^{2+} implying negative cooperativity between these sites in this protein as has been reported previously for other ArsR-SmtB sensors (section 1.5.4).

For Δα5ZiaR, Zn^{2+} mediated complete disassociation of protein-DNA complexes with a stoichiometry similar to that for Δα3 ZiaR (although a single replicate did show a higher stoichiometry (Figure 18a; Appendix A Figure 1). This suggests that, like the α5 sites, the α3N sites in this mutant protein may only require occupation of half the sites (one per dimer) to initiate allostery. Although both sites are required in CadC (Sun *et al*. 2002), the α3N/α5 sensor BxmR has been shown to only require occupation of half the sites on the dimer for allostery (Liu *et al.* 2008). Although apo-protein association experiments in the absence of EDTA were attempted negligible binding to DNA was observed (data not shown). This was presumably due to acquisition of Zn^{2+} from the buffer by each functional mutant protein; the potentially lower stoichiometry required to initiate allostery in each mutant may have meant that a lower quantity of Zn^{2+} was sufficient to prevent DNA binding compared to ZiaR. In

summary, these data show that *in vitro* both mutant proteins are Zn^{2+} responsive, contrary to the lack of responses observed *in vivo*.

To verify that the mutations introduced into each site had completely destroyed the metal binding and/or allosteric switching mechanism at each site (and that the responses for Δα3ZiaR and Δα5ZiaR observed in Figure 18a were reporting on allostery at the un-mutated sites only) analogous titrations were performed with Δα3Δα5 ZiaR, in which both sites were mutated. No decrease in anisotropy was observed on titration of protein-DNA complex with Zn^{2+} (Figure 18a). No change in anisotropy was observed after 10 equivalents of added Zn^{2+} (data not shown). Additionally, anaerobic titration of *zia* O/P oligonucleotide with Δα3Δα5 ZiaR in the presence of a saturating concentration of Zn^{2+} (conditions in which ZiaR did not bind to DNA, Figure 16c) showed apo-protein like binding to DNA with values for Δr_{obs} and K_d comparable to those observed for ZiaR (Figure 18b). These data showing loss of Zn-induced allostery in the double mutant protein confirmed that the individual mutations introduced into each site prevented allosteric switching at each site. Additionally, these data unequivocally show that both metal sites are not required for function, with ZiaR able to function with either an α3N or α5 site in a manor analogous to that recently described for the related sensor BxmR, which also retains strong inducer regulation at both its α3N and α5 sites *in vitro* (Liu *et al.* 2008).

The residue mutated in Δα5ZiaR (His-116) aligns with His-106 in SmtB, mutation of which has been shown to cause loss of Zn^{2+} response *in vitro* (VanZile *et al.* 2002b) and *in vivo* (Turner *et al.* 1996). However, this residue is not directly involved in hydrogen bond network formation in SmtB and so loss of allostery in ZiaR is likely due to impairment of Zn^{2+} binding to the α5 sites (supported by the reduction in metal binding stoichiometry for Δα5ZiaR (see section 3.4.6)). The two cysteine residues mutated in Δα3ZiaR comprise the α3N CVC motif that is universally conserved amongst sensors with functional α3 sites (Busenlehner *et al.* 2003) and which contains a valine residue that has been postulated to make an energetically important contact with DNA which is disrupted by cysteine-metal ligation (Arunkumar *et al*. 2009). As for Δα5ZiaR, data suggest that loss of allostery via the α3N site was likely due to impairment of Zn^{2+} binding to this site *in vitro* (see section 3.4.6).

Figure 17. Example titrations of *zia* O/P oligonucleotide with recombinant mutated ZiaR proteins. Example aerobic fluorescence anisotropy titrations of purified, recombinant Δα5ZiaR (a), Δα3ZiaR (b) and Δα3Δα5ZiaR (c) with 10 nM *zia* O/P DNA in the presence of 1 mM EDTA and 1 mM DTT.

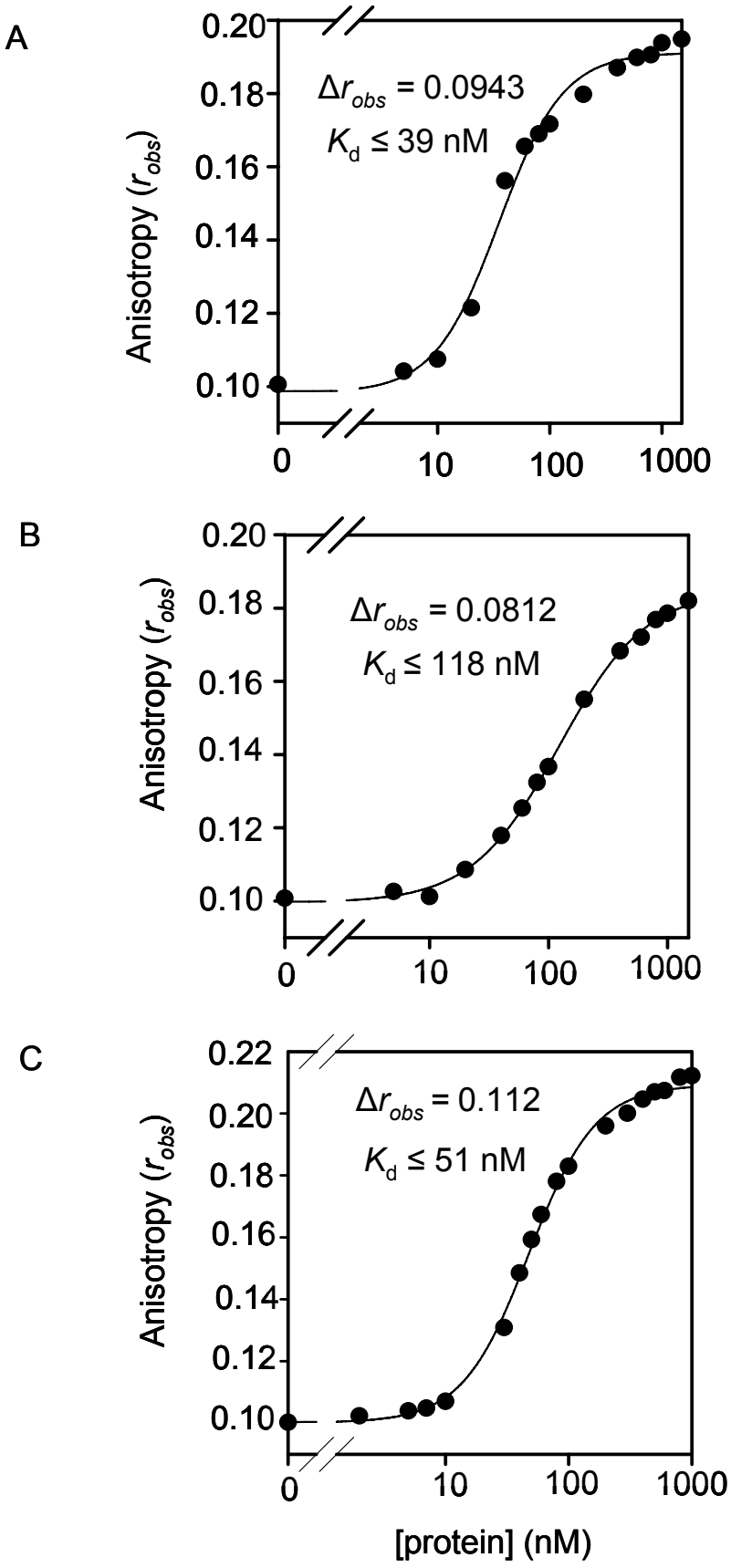
A
0.20
0.18
0.16
0.14
0.12
0.10
Anisotropy (r_{obs})
Δr_{obs} = 0.0943
$K_d \leq$ 39 nM
0
10
100
1000
B
0.20
0.18
0.16
0.14
0.12
0.10
Anisotropy (r_{obs})
Δr_{obs} = 0.0812
$K_d \leq$ 118 nM
0
10
100
1000
C
0.22
0.20
0.18
0.16
0.14
0.12
0.10
Anisotropy (r_{obs})
Δr_{obs} = 0.112
$K_d \leq$ 51 nM
0
10
100
1000
[protein] (nM)

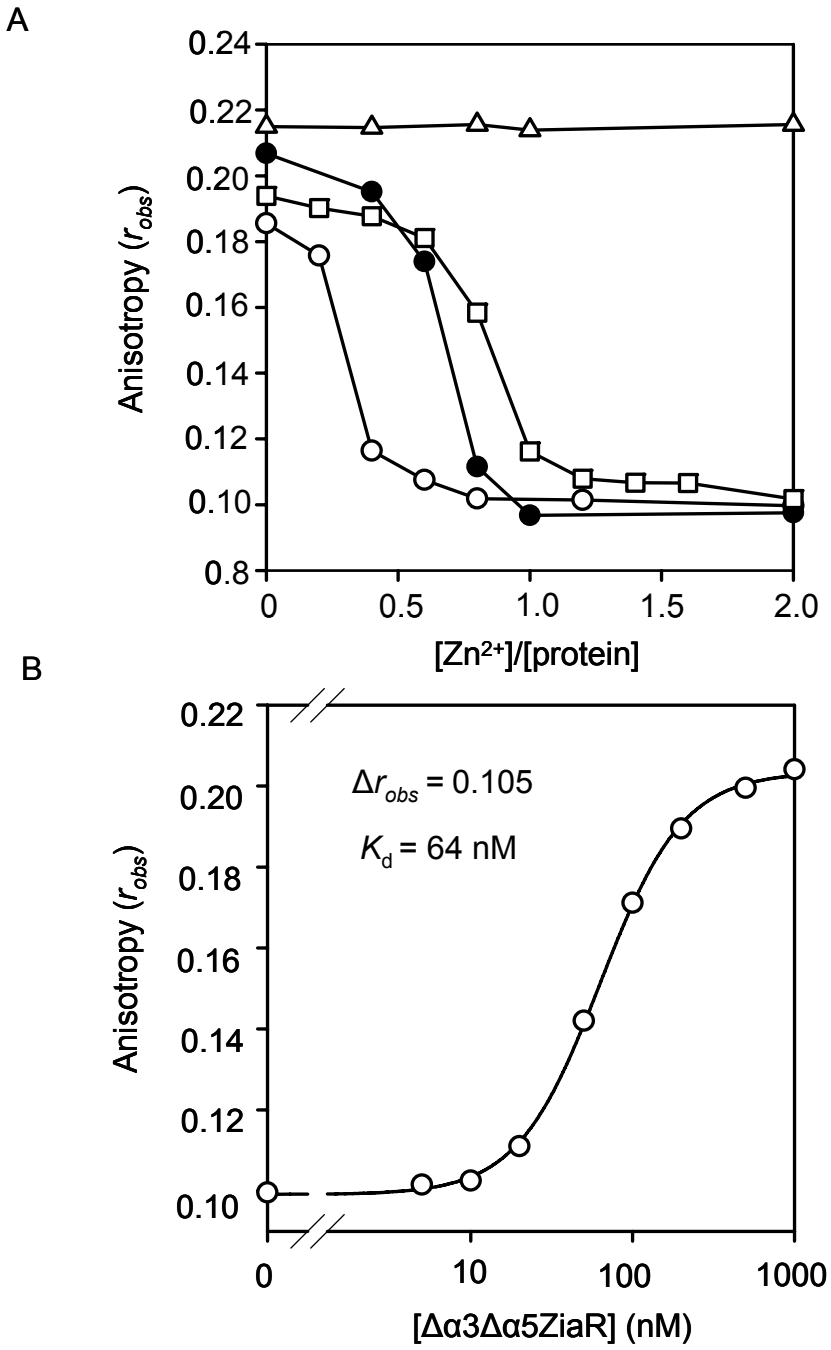

Figure 18. Comparison of the effects of Zn^{2+} on the DNA binding affinities of wild-type and mutant ZiaR proteins. A. Example anaerobic titrations of ZiaR (closed circles) Δα3ZiaR (open circles), Δα5ZiaR (open squares), and Δα3Δα5ZiaR (open triangles) *zia* O/P DNA-protein complexes (10 nM DNA incubated with 1 μM protein) with increasing concentrations of Zn^{2+}. B. Example anaerobic titration of Δα3Δα5ZiaR protein with 10 nM *zia* O/P DNA in the presence of a saturating excess of Zn^{2+} (4 μM) (open circles).

Protein	Δr_{obs}	K_{DNA} (nM)
ZiaR	0.09556 ± 0.0038 (0.1000 ± 0.01921)	61 ±11 (325 (± 193))
Δα3 ZiaR	0.0812	≤ 118
Δα5 ZiaR	0.0943	≤ 39
Δα5Δα3 ZiaR	0.112	≤ 112

Table 5. Summary of DNA binding parameters for apo-ZiaR proteins. For ZiaR the mean from three separate analyses following protein incubation in 1 mM EDTA is shown. Values from apo-protein ZiaR titrations performed in the absence of EDTA pre-incubation are shown in parenthesis (n=8). Values for other proteins are from single replicates. Note: for these proteins DNA dissassociation constants (K_{DNA}) are shown as minimal values. A single replicate for ZiaR performed in the presence of 1 mM EDTA was performed at a lower concentration of DNA (5 nM) and produced a K_{DNA} of 60 nM; therefore, the mean value quoted above for ZiaR may represent the actual affinity for DNA. All experiments were performed under identical buffer conditions (120 mM KCl, 30 mM NaCl, 10 mM Hepes (pH 7.8)).

3.4.6 Measurement of the Zn^{2+} binding affinities for wild-type, Δα3 and Δα5 ZiaR proteins

The retention of inducer responsiveness in the α3 and α5 mutants *in vitro* is contrary to previous *in vivo* data showing that loss of either site is accompanied by total loss of inducer responsiveness. One hypothesis to account for these data is that the mutations introduced into each site may have weakened the affinity of the protein for Zn^{2+}. *In vitro*, this may not necessarily impact on regulation under conditions of saturating concentrations of Zn^{2+}, where [Zn^{2+}] >>> ZiaR K_d Zn^{2+}. However, *in vivo* the presence of multiple competing ligands in the form of proteins and small molecules may mean that even a subtle weakening of the Zn^{2+} affinity may cause Zn^{2+} to aberrantly partition to other cytosolic species in preference to ZiaR, causing loss of Zn^{2+} response at a ZiaR controlled promoter. To test this model *in vitro*, the equilibrium Zn^{2+} binding affinities of wild-type, Δα3 and Δα5 ZiaR proteins were measured.

Quin-2 has been used previously to measure the affinities of other Zn^{2+} sensors of this family, such as SmtB and BxmR, with calculated Zn^{2+} association constants in the 10^{12}-10^{13} M^{-1} range (VanZile *et al.* 2002a; Liu *et al.* 2008). Figure 19 shows fitted data from two independent replicate experiments in which ZiaR and Quin-2 were titrated with Zn^{2+}. In the presence of an equimolar concentration of ZiaR, a non-linear decrease in the Quin-2 absorbance maximum at 261 nm is observed, indicative of competition between Quin-2 and the protein for Zn^{2+} (Figure 19). In the absence of protein, Quin-2 absorbance is quenched linearly to approximately one equivalent (an example control titration is shown in Appendix A Figure 2, together with non-fitted replicate titrations for each of the proteins). Non-linear least squares regression analyses were used to calculate binding constants for Zn^{2+} from these data. For the closely related homologue BxmR a four-site dimer sequential binding model has been previously used to describe competition data similar to that described in this study and which was collected under near identical solution conditions to those used in these analyses (Liu *et al.* 2008). Although, the dimerisation constant for ZiaR is unknown, studies of other ArsR-SmtB family members show the proteins in this family to be weakly dissassociable homodimers with apo-protein K_{dimer} values ranging from sub-micromolar for CadC (~0.3 μM) to low micromolar for CzrA (~6 μM). For metal-bound forms of these proteins, the K_{dimer} values are invariably tighter (in the case of Zn^{2+} loaded SmtB by more than an order of magnitude) (Busenlehner *et al.* 2003). Therefore,

considering the double-figure micromolar concentrations of protein used in these assays, for modelling of these data it was reasonable to assume ZiaR was predominantly dimeric under these conditions and such a model would best describe these data.

For ZiaR data modelled to a four-site dimer sequential binding model, a mean Zn^{2+} association constant for the first metal binding site (K_{Zn1}) was calculated to be 4.45 x 10^{12} M^{-1} (±2.85). The second binding site association constant (K_{Zn2}) was determined to be weaker than that of the first site (6.78 x 10^{11} M^{-1} ±3.72) (Table 6). In this model the final two sites on the dimer could not be modelled implying they have an affinity substantially weaker than that of Quin-2. This interpretation is supported by the points of saturation observed in the competition data (Figure 19a, b). For example, in Figure 19a, full quenching of signal is reached at just over 40 μM Zn^{2+}; approximately 20 μM Zn^{2+} must have bound Quin-2, with the remaining ~20 μM partitioning to two sites present on ~10 μM protein present in the reaction. Importantly, the presence of only two sites capable of competing with Quin-2 for Zn^{2+} on the ZiaR dimer indicates negative cooperativity occurring across the dimer, with one subunit containing a tight affinity α3/α5 pair and the other subunit containing a weaker affinity (K_a<< 2.70 x 10^{11} M^{-1}, the K_{Zn} for Quin-2) α3/α5 pair.

Experiments analogous to those for ZiaR were also performed for Δα5ZiaR (Figure 20) and Δα3ZiaR (Figure 21). For both proteins, as with ZiaR, competition for Zn^{2+} was observed between Quin-2 and protein. However, comparison of the wild-type and mutant binding curve data showed that for both mutant proteins, the observed Zn^{2+} binding stoichiometry was reduced compared to ZiaR (Appendix A Figure 2), indicating reduced Zn^{2+} binding in each of the mutant proteins. Calculation of the Zn^{2+} association constants using a four-site dimer sequential model as used for ZiaR produced mean values for the first binding site (K_{Zn1}) of 2.48 x 10^{12} M^{-1} for Δα3ZiaR and 2.36 x 10^{12} M^{-1} for Δα3ZiaR (Table 6). T-Test analyses of K_{Zn1} values used to produce the mean values shown in Table 6 produced values for $P > 0.05$ (Δα3ZiaR P=0.28, Δα5ZiaR P=0.25; determined by unpaired T-Test), suggesting that the differences in affinity between wild-type and mutant ZiaR proteins were not statistically significant. When the data shown in Figure 20 and 21 were modelled using a two-site dimer model (to take account of the loss of half of the available metal binding sites on the dimer), fits and binding parameters were produced that were effectively identical to those presented for the four-site dimer model (Appendix A Figure 4). Presumably, each model can only detect binding to the same two tight binding sites. Modelling of the

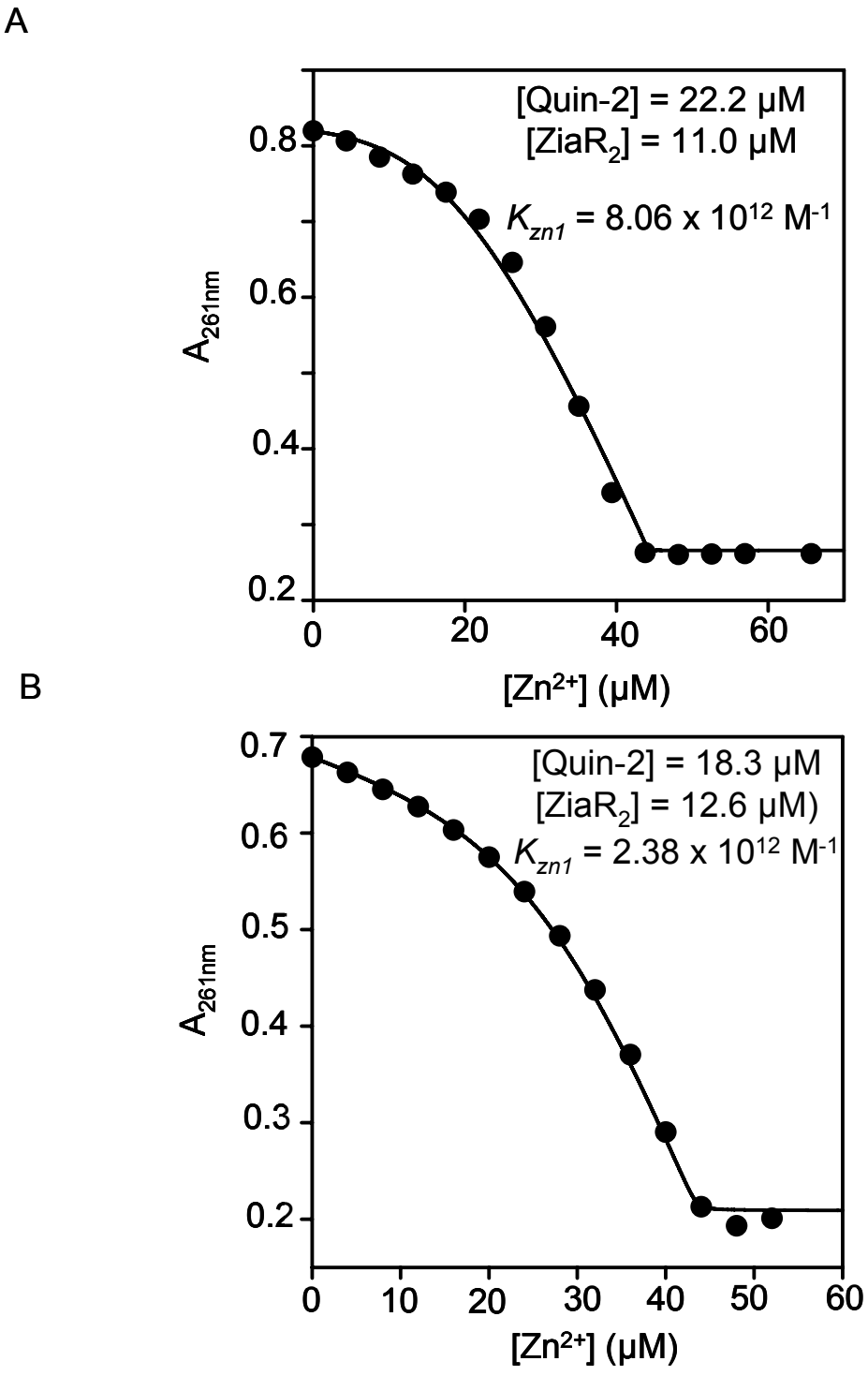

Figure 19. Measurement of the Zn^{2+} affinity of ZiaR by Zn^{2+} titration with Quin-2. Apo-protein subtracted absorbance data from two independent titrations are shown, each fitted to a four site dimer sequential binding model. In each experiment a mixture of Quin-2 and protein was titrated with Zn^{2+} under anaerobic conditions and changes in Quin-2 absorbance at 261 nm were measured. For each replicate shown, the calculated Zn^{2+} association constant for the first binding site is shown. Conditions: 120 mM KCl, 30 mM NaCl, 10 mM Hepes (pH 7.8).

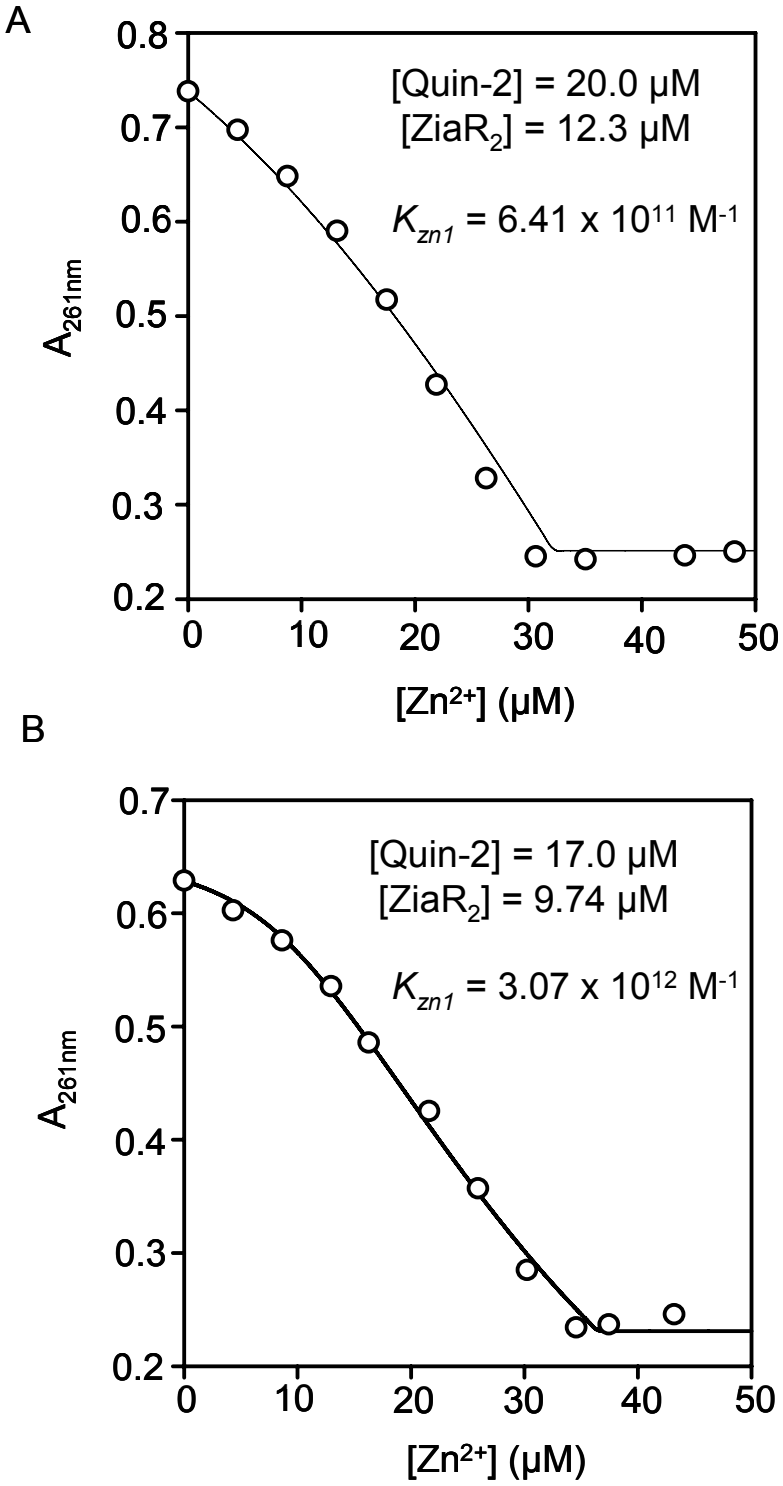

Figure 20. Measurement of the Zn^{2+} affinity of Δα5ZiaR by Zn^{2+} titration with Quin-2. Data from two independent titrations are shown with experiments performed under conditions identical to those for ZiaR. For each replicate data are fitted to the same four site dimer sequential binding model as shown in Figure 19 for ZiaR data.

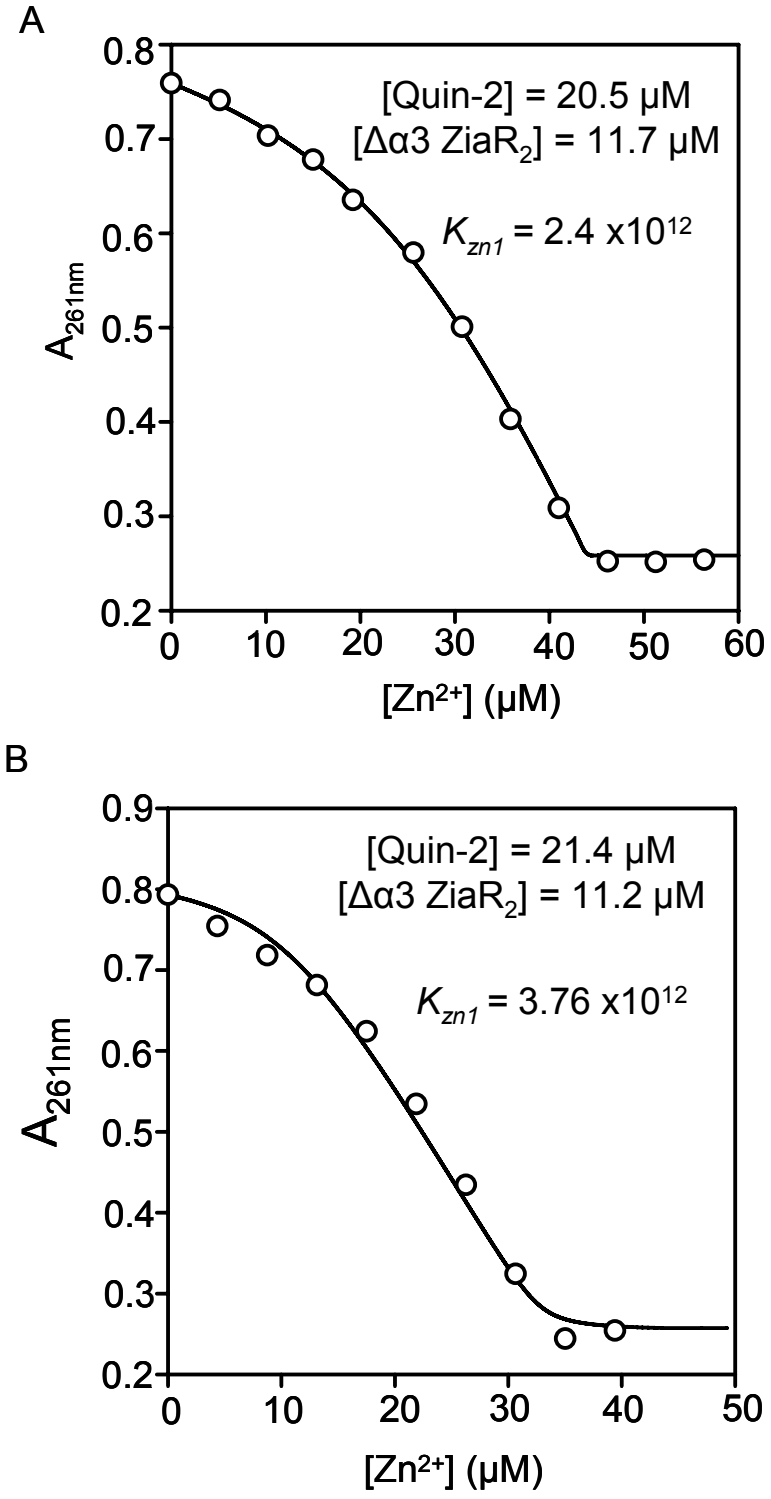

Figure 21. Measurement of the Zn^{2+} affinity of Δα3ZiaR by Zn^{2+} titration with Quin-2. Data from two independent titrations are shown with experiments performed under conditions identical to those for ZiaR. For each replicate data are fitted to the same four site/dimer sequential binding model as shown in Figure 19 for ZiaR data.

	Zn^{2+} association constants (K_{Zn}) (M^{-1})			
	K_{Zn1}	K_{Zn2}	K_{Zn3}	K_{Zn4}
ZiaR	$4.45 \times 10^{12} \pm 2.85$ $(1.69 \times 10^{12} \pm 1.2)$	$6.78 \times 10^{11} \pm 3.72$ *nd*	*nd*	*nd*
Δα3ZiaR	$2.48 \times 10^{12} \pm 1.24$ $(2.46 \times 10^{12} \pm 1.2)$	$(2.56 \times 10^{11} \pm 4.39)$* $(2.53 \times 10^{11} \pm 4.35)$*	*nd*	*nd*
Δα5ZiaR	$2.36 \times 10^{12} \pm 1.49$ $(2.36 \times 10^{12} \pm 1.49)$	1.45×10^{11} * (1.46×10^{11})*	*nd*	*nd*

Table 6. Zn^{2+} association constants for ZiaR, Δα3ZiaR and Δα5ZiaR. Mean values (all n=3 except for ZiaR which is n=4) with errors are shown and were calculated using least squares non-linear regression analysis using the program DynaFit. Values shown were calculated using a four-site dimer model which is hypothesised to most accurately reflect the behaviour of the protein in this assay. However, for ZiaR a corresponding mean value is also reported from modelling to a two-site monomer model (example fitted data shown in Appendix A Figure 3) and are shown in parenthesis. For both mutant proteins, a two-site dimer model produced fits and *Ka* values effectively identical to those reported for the four-site model (these values are shown in parentheses). Example fitted datasets from the two-site models for each of the mutant proteins are shown in Appendix A Figure 4. *nd*; binding not detected.
* The K_{Zn} value for Δα5 ZiaR represents data from two replicates, the binding constant could not be modelled in an additional replicate.

mutant data to a one-site monomer model produced poor fitting of the data. The simplest interpretation of these data is that in each mutant protein binding to each mutated site is lost, with K_{Zn1} and K_{Zn2} representing Zn^{2+} binding to each of the remaining functional sites on each subunit within the dimer. For both Δα3ZiaR and Δα5ZiaR the value of K_{Zn2} is weaker than K_{Zn1} which suggests negative cooperativity between analogous functional sites on the different dimer subunits in both mutant proteins.

3.4.7 Measurement of the effects of Zn^{2+} binding on wild-type and mutated ZiaR proteins by intrinsic tyrosine fluorescence

The possible effects of metal binding on the tertiary structure of metal sensing transcriptional regulators and the relative effects of different mutations on these structural changes have been monitored previously by measurement of changes in intrinsic tyrosine fluorescence of proteins following titration with metal (VanZile *et al.* 2002a; Liu *et al.* 2008). Although ZiaR does not contain tryptophan residues a total of four tyrosine residues are present. On excitation at 280 nm an emission spectrum with a maximum emission intensity at approximately 307 nm is produced. Titration of ZiaR with Zn^{2+} showed only a very small increase in fluorescence intensity (Figure 22). In contrast, a much larger increase in signal was observed following titration of Δα3ZiaR with Zn^{2+}, with fluorescence intensity rising to a peak between ~0.5-1 equivalents of Zn^{2+} followed by a gradual decrease after approximately one equivalent Zn^{2+}. For Δα5ZiaR, a decrease in fluorescence intensity was observed, reaching a minimum at ~0.5 equivalents of added Zn^{2+}, followed by a plateau to approximately one equivalent after which a gradual reduction in intensity is observed. Additionally, the maximum change in fluorescence intensity is smaller than for Δα3ZiaR.

It is not possible to draw firm conclusions regarding the detailed nature of the structural changes occurring in each protein from these data. However, of the four tyrosine residues present in ZiaR, three are conserved in BxmR with all four present in SmtB. One of these tyrosine residues (position 121) is predicted to be located within the α5 helix, between the two sets of α5 site ligands. The remaining residues align with those of SmtB present in a two-stranded β-sheet, N-terminal to the α5 helix (VanZile *et al.* 2002a) (Figure 4). The tyrosine residue in SmtB corresponding to tyrosine 121 in ZiaR is the only one which is buried at the dimer interface. The changes in fluorescence

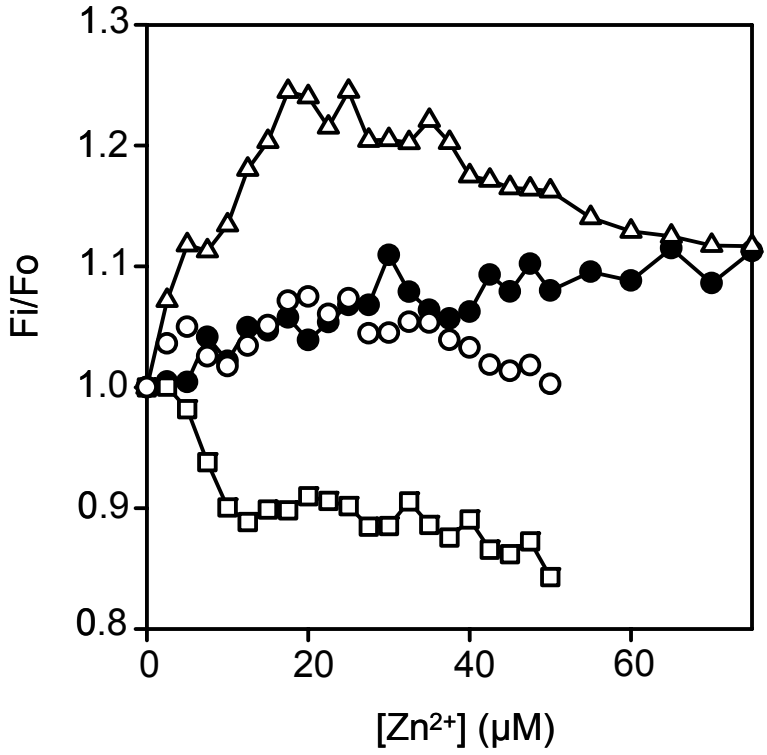

Figure 22. Measurement of Zn^{2+}-induced changes in intrinsic tyrosine fluorescence in ZiaR, Δα3ZiaR and Δα5ZiaR. Anaerobic aliquots of 25 μM of ZiaR (closed circles), Δα3ZiaR (open triangles) and Δα5ZiaR (open squares) were titrated with Zn^{2+} and the changes in tyrosine fluorescence were measured (λex = 280nm; λem = 307 nm). Data points shown as open circles represent averaged values for corresponding Δα3ZiaR and Δα5ZiaR datapoints.

yield associated with α5 site allosteric switching in ZiaR may be reporting on changes in solvent exposure of this tyrosine residue concomitant with rearrangement of the α5 helix as has been previously proposed for SmtB (VanZile *et al.* 2002a). Decreases in fluorescence emission intensity due to α3N regulation have been proposed to be due to changes in conformation of the β-wing (Liu *et al.* 2008).

Despite uncertainties about the detailed nature of the structural rearrangements that are correlated with changes in tyrosine fluorescence, it seems likely that the Zn^{2+}-induced changes at the α3N and α5 sites necessary to drive allostery in both mutant and wild-type proteins must be underpinned by different conformational changes in each case. Indeed, this is entirely expected based on the different locations of each site within the tertiary structure of the protein. Crucially, when the corresponding fluorescence intensity values for each mutant protein dataset are averaged (Figure 22, open symbols), a series of values almost identical to those observed for ZiaR is produced. The simplest interpretation of these data is that in ZiaR both α3N and α5 sites are utilised in Zn^{2+} binding and allosteric switching as has been previously reported for BxmR (Liu *et al.* 2008).

3.5 A multiple site allosteric model for ZiaR

Taken together, these data support a multiple site allosteric model for ZiaR. In this model ZiaR contains two pairs of α3N and α5 sites per dimer. One of the pair of sites on one of the dimer subunits has a 'tight' Zn^{2+} affinity (i.e. $\sim 10^{11}$-10^{12} M^{-1}) that is sufficient to compete with Quin-2 for Zn^{2+} binding. The other pair of sites on the other subunit are invisible in Quin-2 competition experiments and so must have an affinity substantially weaker than $\sim 10^{11}$ M^{-1} (Figure 23). This implies negative cooperativity for Zn^{2+} binding between pairs of sites on different subunits in ZiaR. A single equivalent of Zn^{2+} is required to disassociate ZiaR-DNA complexes *in vitro* (Figure 18a). Moreover, both α3N and α5 sites have been shown to be regulatory *in vitro,* with each having the ability to function independently of the other site (Figure 18a). These observations suggest a model for ZiaR in which Zn^{2+} first initiates regulation through an α3Nα5 pair on one dimer subunit potentially followed by population of a second, weaker pair (α3N'α5') on the second dimer subunit. This model is supported by data suggesting contributions from both the α3N and α5 sites in allosteric regulation of the wild-type protein (Figure 22). It is noted that data shown in Figure 11 suggest stoichiometric Zn^{2+}

mediated displacement of Co^{2+} from both dimer α3N sites followed by population of the α5 sites. This observation is still compatible with the model outlined above; it may be that the relatively tight affinity for Co^{2+} at the α5 sites of ZiaR (Figure 10) results in Zn^{2+} displacement of Co^{2+} from the α3N sites prior to displacement from both remaining α5 sites.

For Δα3ZiaR and Δα5ZiaR a model for allosteric function is shown in Figure 24. A reduction in Zn^{2+} binding stoichiometry for each mutant was observed (Figure 20-21; Appendix A Figure 2) consistent with some degree of reduction of Zn^{2+} binding. For both Δα3ZiaR and Δα5ZiaR negative cooperativity was implied between functional sites on each dimer subunit, as $K_{Zn1} > K_{Zn2}$. Additionally, occupation of only one of the sites in each functional pair was shown likely to be sufficient for allostery; approximately 0.5 equivalents of Zn^{2+} are required to cause complete disassociation of Δα3ZiaR and Δα5ZiaR DNA complexes (Figure 18). Intrinsic protein fluorescence quenching experiments also show a sharp inflection at ~0.5 equivalents for Δα5ZiaR. For Δα3ZiaR these analyses also show saturation at less than one equivalent of added Zn^{2+} albeit the stoichiometry is higher than for Δα5 ZiaR and the point of saturation is much broader; these data require additional replication to confirm this stoichiometry. The mean K_{Zn1} value for ZiaR was approximately two-fold tighter than K_{Zn1} values for Δα3ZiaR and Δα5ZiaR, however this difference was not statistically significant; the implications of this result in terms of the different Zn^{2+} responses of Δα3ZiaR and Δα5ZiaR *in vivo* and *in vitro* are discussed in section 7.1.

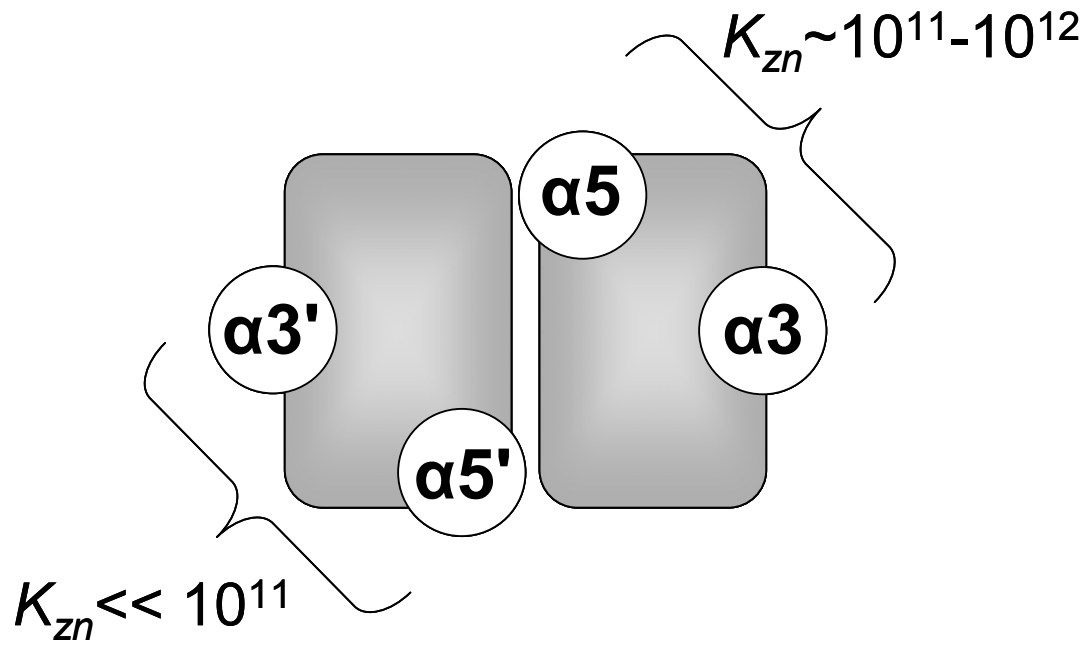

Figure 23. Schematic showing organisation of the allosteric sites in ZiaR. ZiaR is shown as a dimer with two sites per subunit (four per dimer). The extended N-terminal 'tail' from each monomer which produces an additional dimer interface close to the α3 site is not shown for clarity.

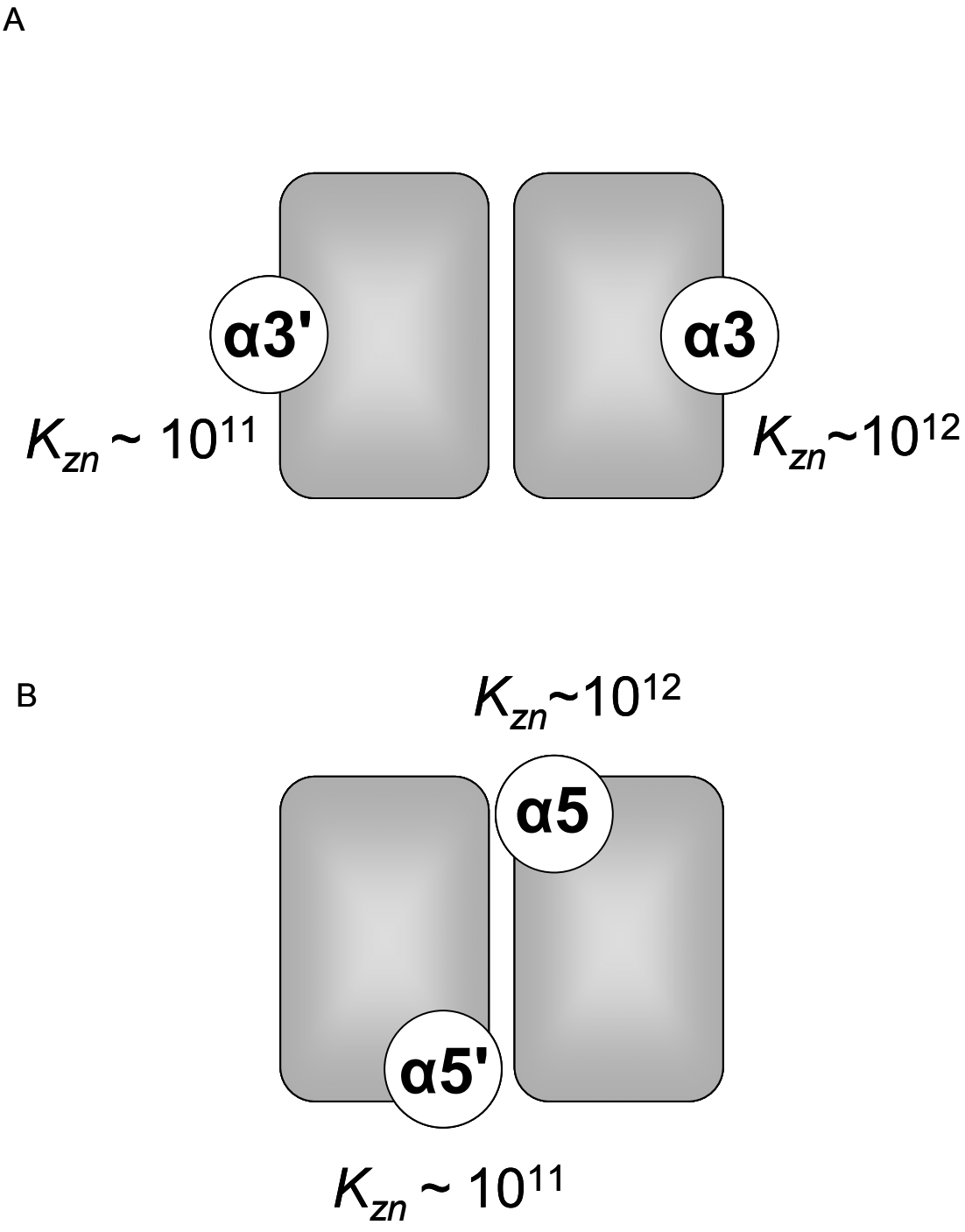

Figure 24. Schematic showing organisation of the allosteric sites in mutated ZiaR proteins. The organisation of sites in Δα5ZiaR (A) and Δα3ZiaR (B) are shown. For both proteins data is consistent with a tight affinity site on one subunit and a site of weaker affinity on the adjacent subunit.

Chapter 4. Characterisation of a Zur_{SS}: A *Synechocystis* Fur-family Zn^{2+}-sensor

4.1 sll1937 encodes a Zn^{2+}-sensing Fur family regulator

The sll1937 gene of *Synechocystis* has been annotated as a Fur-family Zn^{2+} sensor (see section 1.8.2). RT-PCR analyses (performed by Samantha Dainty) in which wild-type *Synechocystis* cultures were treated with maximum permissive concentrations of metals showed a substantial (almost complete) loss of *znuA* transcript abundance following treatment of cells with Zn^{2+} (Appendix B Figure 1). Little reproducible change in *znuA* expression, relative to the *rps1* controls, was observed following treatment with other metals shown. These data formally demonstrate that expression from the *znu* promoter is Zn^{2+} -responsive.

4.2 Purification of recombinant Zur_{SS}

To establish that the Zur-like protein from *Synechocystis* (i) binds to *znu* promoter and (ii) directly binds to (and is allosterically regulated by) Zn^{2+}, Zur_{SS} was over-expressed at high level in *E.coli* and purified to homogeneity for *in vitro* characterisation. Recombinant Zur_{SS} was produced as a native, tag-free protein and so, like ZiaR, purification strategies exploited the intrinsic biochemical properties of native Zur_{SS} to facilitate separation from contaminant proteins (These are discussed in detail in section 2.4). *E.coli* cell extracts containing overexpressed Zur_{SS} were first subjected to heparin-affinity chromatography. Following elution of bound protein a majority of the Zur_{SS} eluted in 400-500 mM NaCl (Figure 25a). Fractions enriched for Zur were further purified by size-exclusion chromatography (Figure 25b). Size exclusion fractions enriched for Zur_{SS} were pooled and concentrated by heparin affinity chromatography. This step also exerted a purification effect in addition to that performed by the initial heparin affinity step (Figure 25a) as the contaminants remaining after size exclusion (Figure 25b inset) were lost following heparin affinity (these were likely lost in the binding and wash stages of this step as little chromatography was observed during elution (Figure 25c)). Following removal of EDTA from protein samples by heparin-affinity (see section 2.5.2), ICP-MS analyses showed recombinant Zur_{SS} to be bound to approximately one equivalent Zn^{2+} (mean: 1.02 ± 0.15).

Figure 25. Purification of recombinant Zur_{SS} protein. A. SDS PAGE (17 % w/v acryl bis) analysis of samples from the first stage of purification in which crude cell extract was applied to a 1 ml heparin column and eluted in step additions of NaCl (T; sample of crude cell extract, U; unbound fraction, W; 5 column volume wash). B. Example size-exclusion separation, in which a sample enriched for Zur_{SS} eluted in an initial heparin step, was applied to a Superdex 75 column. Inset; SDS PAGE analysis of selected fractions. C. Example SDS PAGE analysis of fractions from final heparin purification and concentration of protein from pooled size-exclusion fractions showing purified Zur_{SS} protein.

A

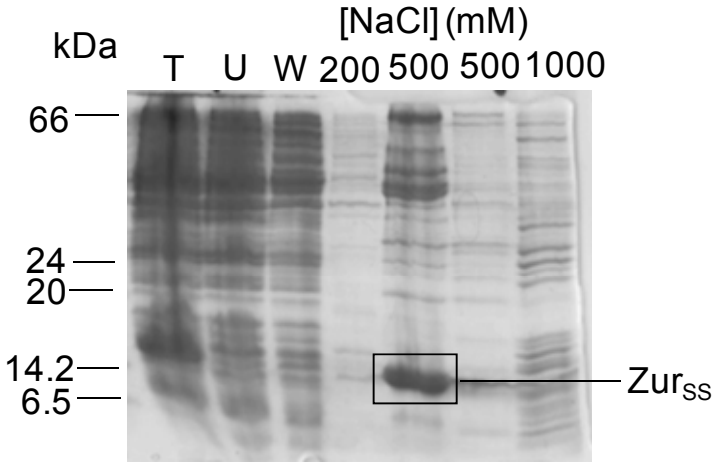
kDa
[NaCl] (mM)
T U W 200 500 500 1000
66
24
20
14.2
6.5
Zur$_{SS}$

B

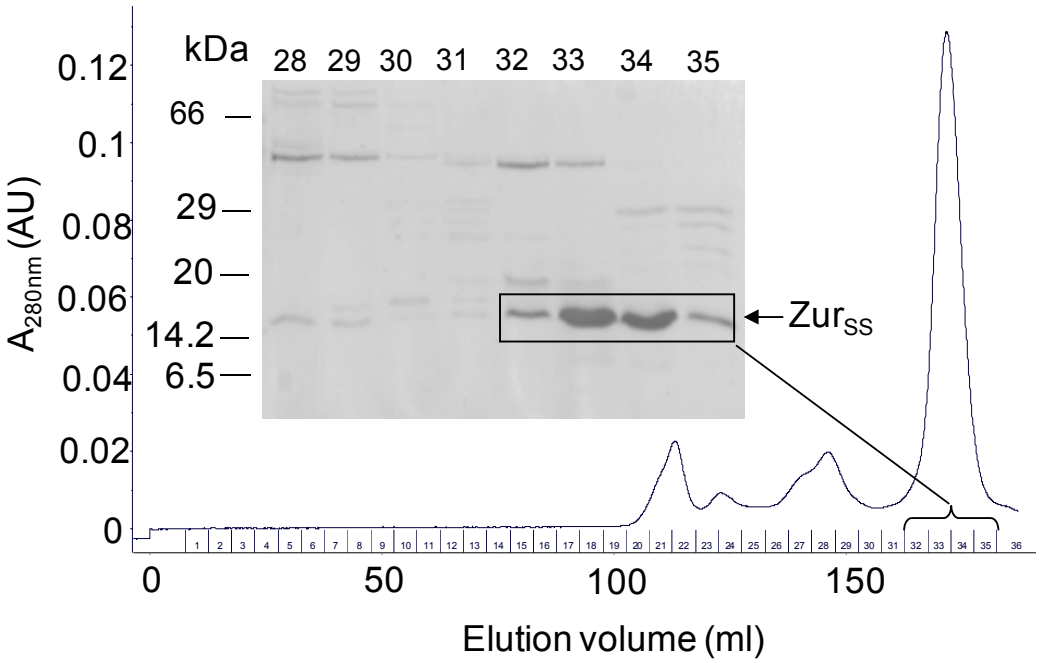
kDa
28 29 30 31 32 33 34 35
66
29
20
14.2
6.5
Zur$_{SS}$
A$_{280nm}$ (AU)
0.12
0.1
0.08
0.06
0.04
0.02
0
0
50
100
150
Elution volume (ml)

C

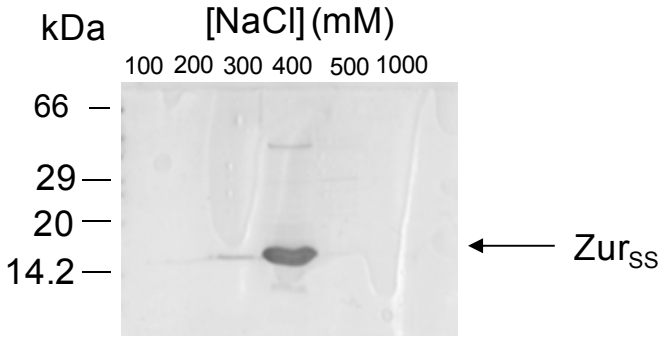
kDa
[NaCl] (mM)
100 200 300 400 500 1000
66
29
20
14.2
Zur$_{SS}$

4.3 Analysis of the metal binding properties of Zur_{SS}

4.3.1 Zur_{SS} contains a structural Zn^{2+} ion and an exchangeable metal binding site

Multiple Fur and Zur homologues have been shown to contain structural Zn^{2+} ions (see section 1.6). Shown in Figure 26a is an alignment of the protein sequences of Zur_{EC} and Zur_{SS}. The cysteine residues implicated as ligands for the structural Zn^{2+} ion in Zur_{EC} (and which are conserved in Fur_{EC} with these residues shown to be ligands for the structural Zn^{2+} ion in Fur_{EC}) are conserved in Zur_{SS} and are present in a CXXC motif. Alignment of Zur_{SS} with Zur_{MT} reveals conservation of the CXXC motif shown to be present in the structural Zn^{2+} site in Zur_{EC} and Fur_{EC}, with both cysteines in this motif verified as structural Zn^{2+} ligands in Zur_{MT} (Lucarelli *et al.* 2007) (Figure 26b). Additionally, the second CXXC motif shown to ligate the structural Zn^{2+} atom in Zur_{MT} is also conserved in Zur_{SS} (Figure 26b). However, as this motif is also conserved in Zur_{EC}, which only has an $S_3(N/O)$ structural Zn^{2+} coordination sphere (Outten *et al.* 2001), it is difficult to accurately predict the precise nature of the coordination environment of a potential structural Zn^{2+} ion in Zur_{SS} from these bioinformatics analyses. The compositions of the structural sites of Fur family proteins have experienced divergence through evolution. Nevertheless, the conservation of the first CXXC motif in Zur_{SS} (shown in red in Figure 26), implicated in binding a structural Zn^{2+} ion in both Zur and Fur homologues (and which has been structurally validated in Zur_{MT}) (Lucarelli *et al.* 2007), suggested the presence of a structural Zn^{2+} ion in Zur_{SS} with a coordination environment comprised of $S_2(N/O)_2$, $S_3(N/O)$ or possibly S_4.

Recombinant Zur_{SS} protein was routinely isolated bound to approximately one equivalent of Zn^{2+} (section 4.2). The metal binding stoichiometry of Zur_{SS} was further analysed by size-exclusion chromatography to confirm or refute the presence of a structural Zn^{2+} ion. Purified protein was incubated aerobically in the presence of a two-fold molar excess of Zn^{2+} (in the presence of 1 mM DTT but in the absence of EDTA) and bound and free metal resolved by size-exclusion chromatography (Figure 27a). Zur was found to co-migrate with approximately two equivalents (2.68 in this analysis) of Zn^{2+}, with additional Zn^{2+} (in this case approximately two equivalents) present as unbound metal ions (Figure 27a). An analogous experiment performed in the absence of added Zn^{2+} in the presence of 1 mM EDTA showed a reduction in total Zn^{2+}: protein binding stoichiometry compared to protein exposed to surplus Zn^{2+}. Co-migration of

A

```
Zur_EC          MEKTTTQELLAQAEKICAQRNVRLTPQRLEVLRLMSLQDGAISAYDLLDLLREAEPQAKP 60
Zur_SS          ---------MSLPTPSLAVRLESLTVNQRLVLQALQRETEPLSAQALFAKLRETK-KIGL 50

Zur_EC          PTVYRALDFLLEQGFVHKVESTNSYVLCHLFDQPTHTSAMFICDRCGAVKEECAEGVEDI 120
Zur_SS          ATVYRALDALKLAGFIQHQATMTGELLYQTLEQDQHC---LTCLQCGESVPIQGCPVQSL 107

Zur_EC          MHTLAAKMGFALRHNVIEAHGLCAACVEVEACRHPEQCQHDHSVQVKKKPR 171
Zur_SS          EENLQANYSFRIYYHTLEFFGLCQLCAKGSD------------------- 138
```

B

```
Zur_MT           -------MASAAGVRSTRQRAAISTLLETLDDFRSAQELHDELRRRGENIGLTTVYRTLQ 53
Zur_SS           MSLPTPSLAVRLESLTVNQRLVLQALQRETEPLS-AQALFAKLR-ETKKIGLATVYRALD 58

Zur_MT          SMASSGLVDTLHTDTGESVYRRCSEHHHHHLVCRSCGSTIEVGDHEVEAWAAEVATKHGF 113
Zur_SS          ALKLAGFIQHQATMTGELLY-QTLEQDQHCLTCLQCGESVPIQGCPVQSLEENLQANYSF 117

Zur_MT          SDVSHTIEIFGTCSDCRS--- 131
Zur_SS          RIYYHTLEFFGLCQLCAKGSD 138
```

Figure 26. Sequence alignment of Zur homologues. A. Alignment of Zur_{EC} with Zur_{SS}. Conserved cysteine residues implicated as structural Zn^{2+} ligands are highlighted in red. B. Alignment of Zur (also known as FurB) from *M.tuberculosis* (Zur_{MT}) with Zur_{SS}. Conserved cysteine residues highlighted in red represent those from the conserved motif shown in A (and which are also known to contribute to the S_4 structural site in Zur_{MT}); those shown in blue represent those present in a conserved CXXC motif shown to provide structural Zn^{2+} ligands in Zur_{MT} (in addition to those shown in red) but which do not form part of the structural site in Zur_{EC} (lucarelli *et al.* 2007).

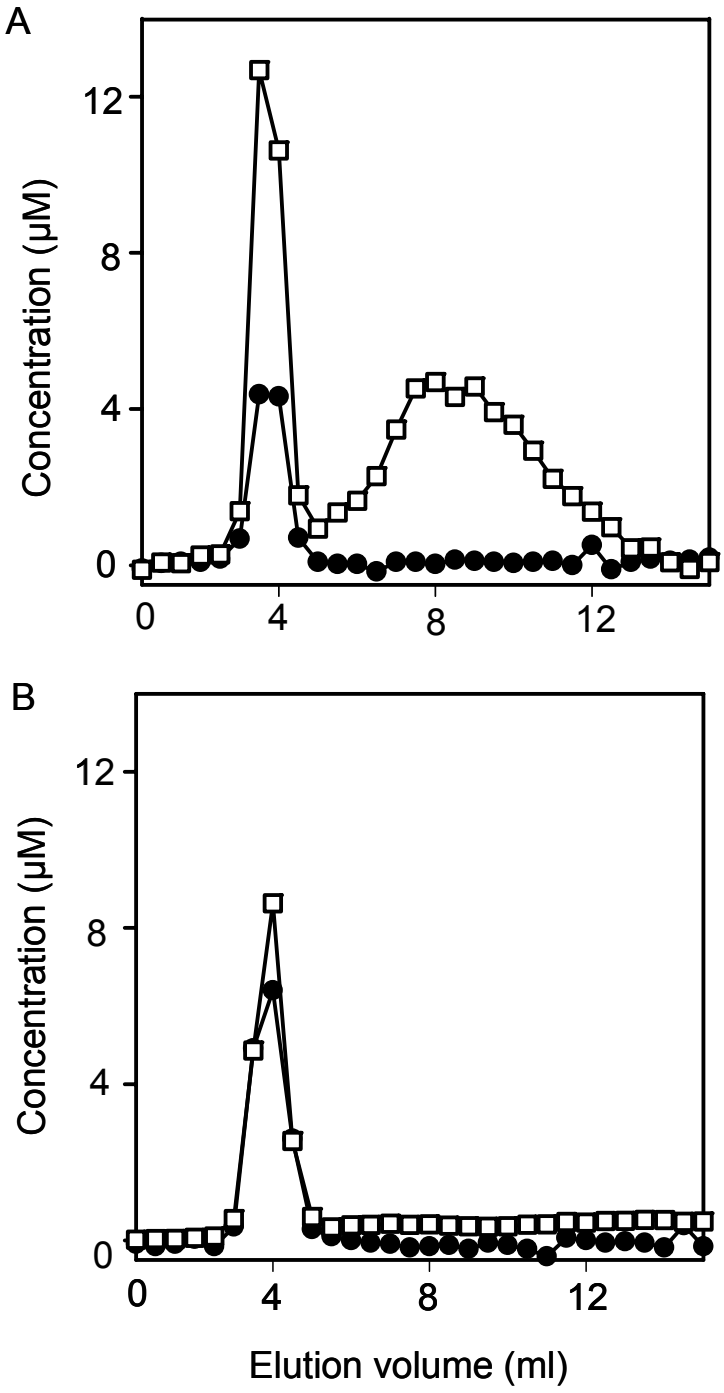

Figure 27. Size-exclusion fractionation of protein-bound and free Zn^{2+} ions. A. 10 μM recombinant Zur_{SS} was incubated with 20 μM Zn^{2+} and bound and free metal fractionated on Sephadex G-25 matrix. Zur_{SS} co-migrates with approximately two equivalents of Zn^{2+}. B. Analogous experiment with 10 μM recombinant Zur_{SS} incubated with 1 mM EDTA and bound and free metal ions fractionated. Open symbols, Zn^{2+}, closed symbols, protein.

protein with approximately one equivalent (1.19 in this analysis) of Zn^{2+} was observed (Figure 27b). These data are consistent with the presence of at least two Zn^{2+} binding sites, one of which contains a Zn^{2+} ion that is refractory to removal by a high concentration of EDTA and likely forms a structural Zn^{2+} site as found in other Zur proteins.

4.3.2 Titration of Zur_{SS} with Co^{2+} reveals a cysteine containing, tetrahedral binding site

The second, exchangeable Zn^{2+} site in Zur_{SS} is the likely sensory site in this protein. As with the allosteric sites in ZiaR, Co^{2+} was used to interrogate the structural properties of the metal sites in Zur_{SS} by UV-Visible spectroscopy. For these and other analyses, Zur_{SS} containing a single equivalent of Zn^{2+}, Zn_1Zur_{SS} (i.e. containing a structural Zn^{2+} ion only) was prepared by incubation in 1 mM EDTA (to remove metal bound at the exchangeable site) followed by elution in an anaerobic chamber during which EDTA and DTT were removed by extensive washing of a heparin affinity column, to which Zur_{SS} was bound, in chelex treated buffer. A representative anaerobic UV-Visible Co^{2+} titration is shown in Figure 28. On titration with Co^{2+} LMCT features were observed in the near-UV region (300-400 nm). The intensity of these features increased linearly to approximately one equivalent after which no further increase was observed (Figure 28b, left panel). These data show saturation at the peak LMCT wavelength of 310 nm at a molar extinction coefficient of approximately 1200 M^{-1} cm^{-1} at approximately one equivalent Co^{2+}. Similar intensities were observed in replicate analyses at saturating Co^{2+} concentrations in excess of one equivalent. Based on a range of 900-1300 M^{-1} cm^{-1} per Co-S^- bond (Brown & Collins 1991) these data are consistent with Co^{2+} binding to the site via a single cysteine residue.

Multiple, *d-d* transition features in the 500-800 nm region were also observed following Co^{2+} titration (Figure 28a, b, right panel). The peak feature at 580 nm saturates at approximately one equivalent of Co^{2+}, with a molar extinction coefficient of approximately 500 M^{-1} cm^{-1}. These data are consistent with tetrahedral or pseudo-tetrahedral Co^{2+}, and by inference Zn^{2+}, binding to Zn_1Zur_{SS}. Crucially, for both *d-d* transition and LMCT features, a binding stoichiometry of approximately 1:1, Co^{2+}: protein is observed following titration of Zn_1Zur_{SS} with Co^{2+}. In this and other replicates the presence of approximately one equivalent of structural Zn^{2+} in the protein was

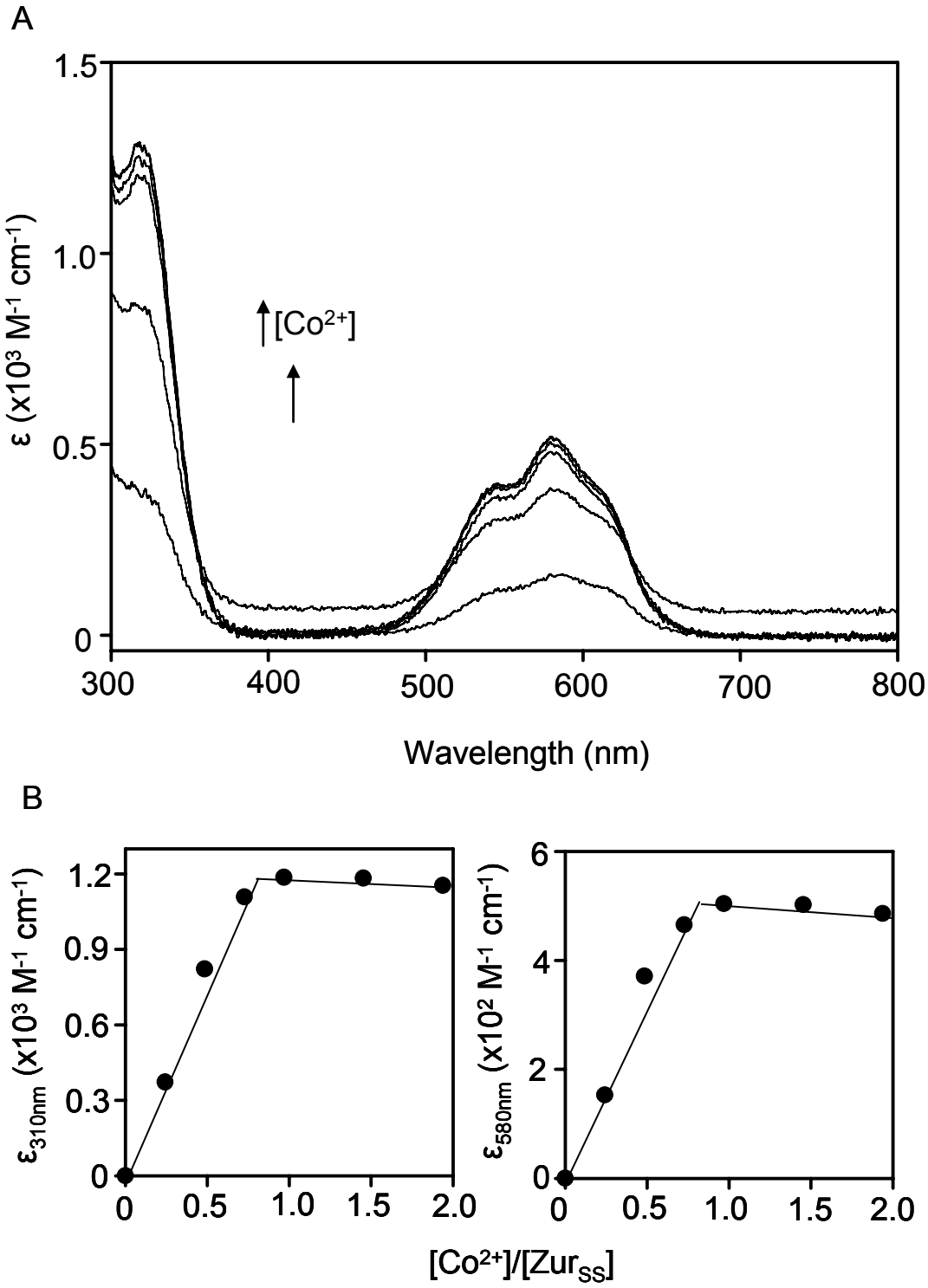

Figure 28. UV-Visible Co^{2+} titration with Zn_1Zur_{SS}. A. Apo-protein subtracted difference spectra produced following anaerobic titration of 26 μM recombinant Zn_1Zur_{SS} with Co^{2+}. B. Left panel; Increase in the LMCT feature at 310 nm with increasing [Co^{2+}]. Right panel; Increase in *d-d* transition feature at 580 nm with increasing [Co^{2+}].

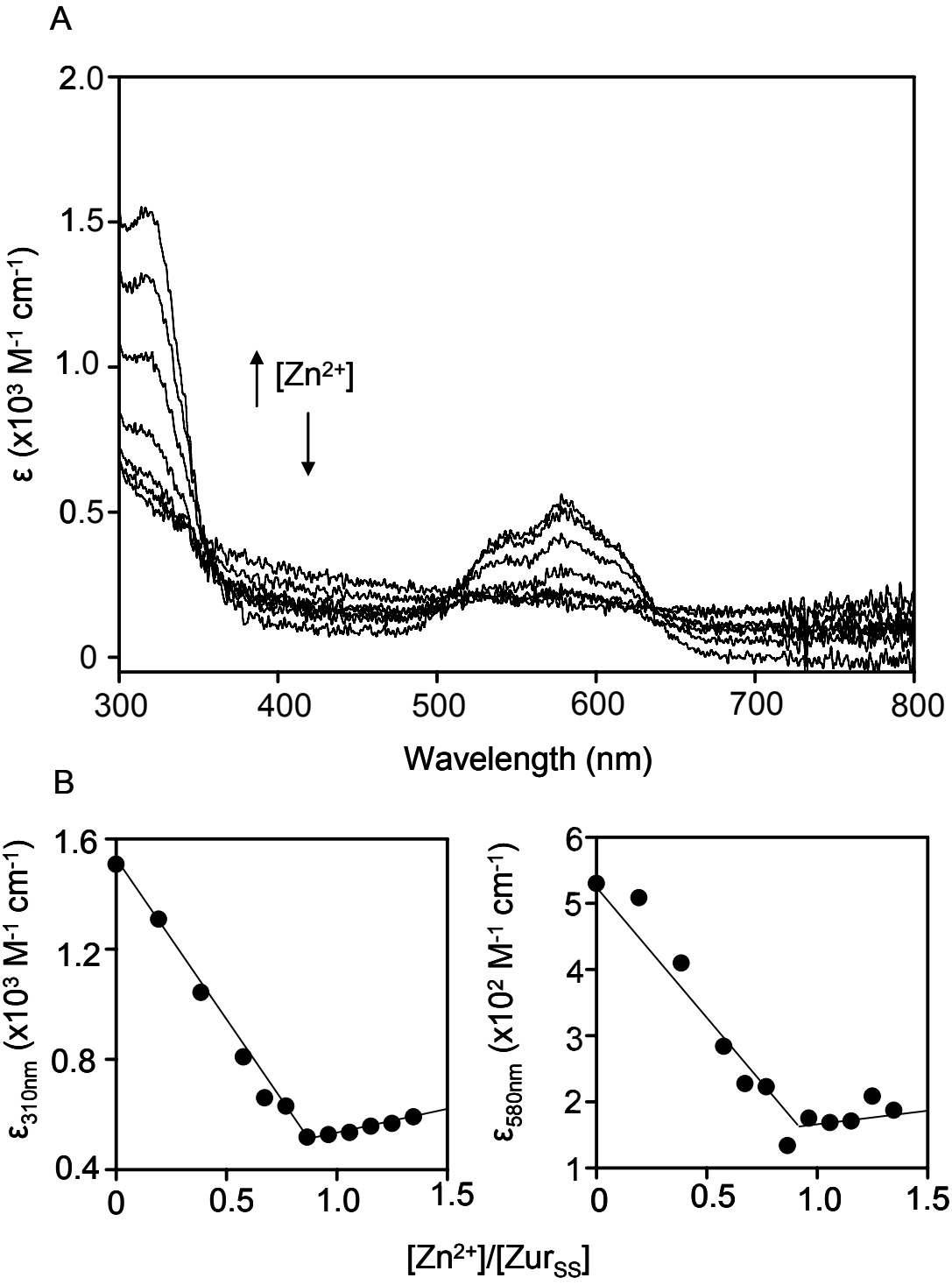

Figure 29. UV-Visible titration of Co^{2+}-loaded Zn_1Zur_{SS} with Zn^{2+}. A. example anaerobic titration of 26 μM Zn_1Zur_{SS} (pre-incubated with a saturating excess of 1.1 equivalents of Co^{2+} to produce $Zn_1Co_1Zur_{SS}$) with Zn^{2+}, showing quenching of LMCT and *d-d* features B. Changes in intensity of LMCT (310 nm) and *d-d* (585 nm) features with increasing $[Zn^{2+}]$ are shown in the left and right panels respectively.

confirmed by ICP-MS analysis following removal of EDTA from the protein and prior to Co^{2+} titration (in this analysis 0.96 ± 0.1 equivalents of Zn^{2+} were present). This confirms a total metal binding stoichiometry of ~2:1, with these UV-Visible data reporting on binding to a metal-free site (distinct to the Zn^{2+}-loaded and non-exchangeable structural site) which presumably represents the allosteric site in this protein. Taken together these data support a tetrahedral Co^{2+} (and Zn^{2+}) allosteric site with an $S(N/O)_3$ coordination environment similar to that observed in Zur_{EC}. As predicted by the Irving-Williams series, the second, exchangeable site of Zur_{SS} has an affinity for Zn^{2+} greater than that for Co^{2+}. On titration with Zn^{2+} of Zur_{SS}, pre-loaded with one equivalent of Co^{2+} ($Co_1Zn_1Zur_{SS}$), Co^{2+}-dependent spectral features decreased in intensity (Figure 29) with both LMCT and *d-d* transition features decreasing linearly to approximately one equivalent after which no further decrease was observed (Figure 29b). These data further confirm the presence of two high affinity metal binding sites on the protein one of which is rapidly exchangeable, the other being refractory to replacement.

Data from spectroscopic analysis of Zur_{SS} suggest a metal binding site model as shown in Figure 30. Each Zur_{SS} subunit has two metal sites; a single, exchangeable site and a non-exchangeable structural Zn^{2+} site. The presence of additional *bona fide* sites in Zur_{SS} appears unlikely in the light of UV-Visible analyses which showed stoichiometric Zn^{2+} and Co^{2+} binding to a single site on the protein (Figure 28 & 29). In the model shown in Figure 30, the two metal binding sites are shown at opposite ends of each of the subunits for clarity. In reality, these may be much closer together. In Fur_{PA}, both metal sites in the structure are located in the C-terminal dimerisation domain and are relatively distant from N-terminal DNA binding helix-turn-helix motif at the other side of the monomer (Pohl *et al.* 2003) (although the exact function of each site is still unclear (Lewin *et al.* 2002)). This also appears to be the case for Zur_{MT} (Lucarelli *et al.* 2007). The postulated coordination environments of these sites in Zur_{SS} are also shown in Figure 30. The exchangeable, putative allosteric site of Zur_{SS} contains at least one cysteine residue (Figure 28). The remaining three ligands are likely to be histidine/aspartate however their exact identity is difficult to assign unequivocally from data presented in these studies.

The structural Zn^{2+} site ligands were not identified however on the basis of comparison with related proteins (Figure 26) this site may have between two and four

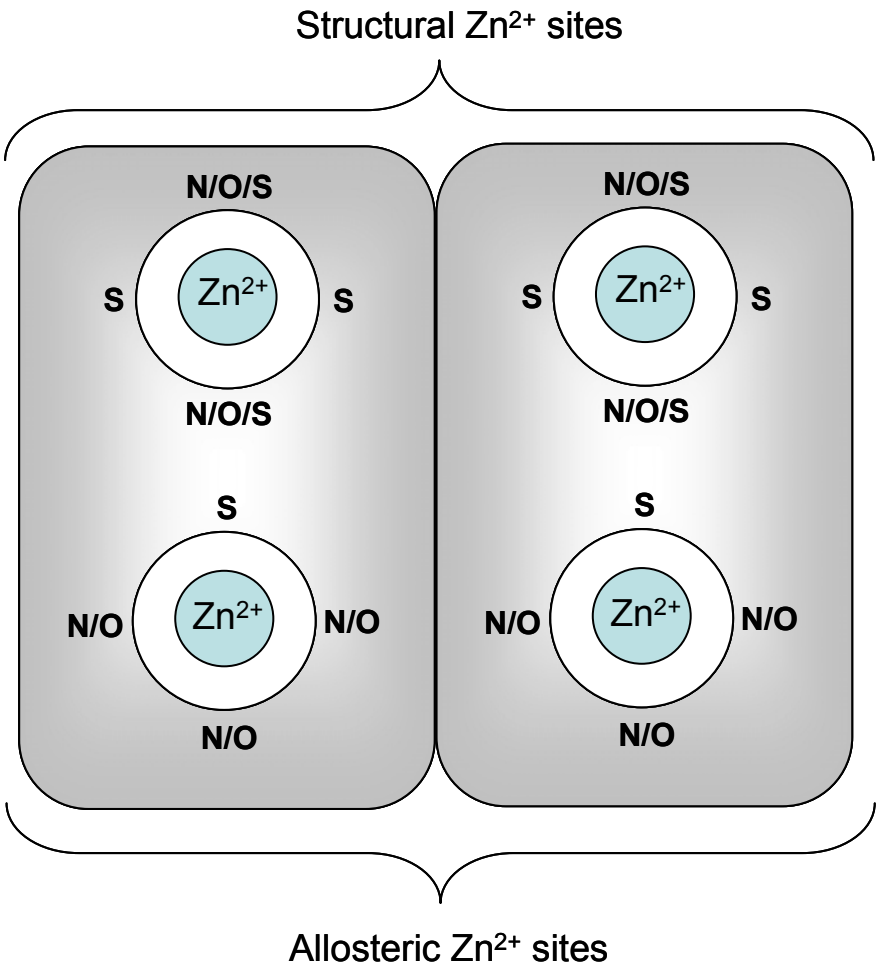

Figure 30. Multiple metal site model for Zur_{SS}. A schematic representation of a single Zur_{SS} dimer is shown, showing coordination environments thought likely in each metal site.

cysteine residues, with aspartate/histidine likely ligands in a site of lower thiol content. Zur_{SS} contains a total of six cysteine residues. DTNB reactivity assays showed an average of 7.6 ± 1.5 reactive thiol groups to be present in anaerobic samples of recombinant protein, suggesting all of the cysteine residues in anaerobic protein samples were able to react with DTNB. This suggests that the structural Zn^{2+} ion (and any associated thiol ligands) is not sufficiently buried in the protein structure to totally impede solvent exposure of liganding cysteines. The inability of EDTA to remove this Zn^{2+} ion (Figure 27) may be due to multiple factors. The octahedral metal chelate favoured by EDTA may be difficult to form around this bound Zn^{2+} ion. The site may also have a very low off-rate impeding chelation of Zn^{2+} from this site.

The sequence of Zur_{SS} was compared with that of Zur_{MT} in which allosteric site ligands have been structurally validated (Figure 31). These comparisons show a low degree of conservation in residues structurally validated as Zn^{2+} ligands in Zur_{MT}. Of the ligands in Zur_{MT} only His-82 shows evidence of conservation of function albeit this being a replacement with a cysteine residue at position 87 in Zur_{SS}. The precise ligand sets of the allosteric sites of Fur-family proteins (even for those with similar *in vivo* sensory functions) are likely to have diverged during evolution and this may have contributed to the fine tuning of metal responses amongst members of this family. The heterogeneity in the allosteric and structural site ligands in Fur-proteins has also contributed to the difficulty in characterising the metal binding sites of proteins in this family.

4.3.3 Estimation of the Zn^{2+} binding affinity of the exchangeable allosteric Zn^{2+} site in Zur_{SS}

For Zur_{EC}, it has been shown that half-maximal repression of transcription of the *E.coli znuC* gene occurs at a sub-femtomolar (~2 x 10^{-16} M) concentration of Zn^{2+}, implying a sub-femtomolar Zur_{EC} disassociation constant for Zn^{2+} (Outten & O'Halloran 2001). The other Zn^{2+} sensor from *E.coli,* ZntR (analogous in function to ZiaR) functions in a complementary fashion to Zur_{EC}, and also has a Zn^{2+} affinity also in the sub-femtomolar range (Hitomi *et al.* 2001) and half-maximal activation of transcription has been measured to occur at ~11 x 10^{-16} M (Outten & O'Halloran 2001). In *Synechocystis*, ZiaR and Zur are presumed to work in a similarly coordinated fashion to detect changes

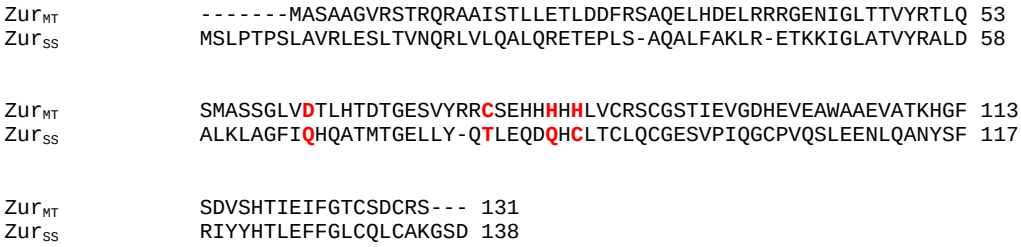

Figure 31. Multiple sequence alignment of Zur_{SS} with Zur_{MT}. Alignment of Zur_{SS} with Zur_{MT}. The residues thought to be allosteric site Zn^{2+} ligands in Zur_{MT} (together with their corresponding residues in Zur_{SS}) are highlighted in red.

to cytosolic Zn^{2+} concentrations and modulate expression of Zn^{2+} efflux (ZiaR) and influx (Zur) systems to maintain Zn^{2+} concentrations within an optimal range. Therefore, it was anticipated that Zur_{SS} would have a Zn^{2+} binding affinity closely matched to that of ZiaR.

The Zn^{2+} affinity of Zur_{SS} was measured by Zn^{2+} titrations with Quin-2. On titration of an equimolar solution of Zn_1Zur_{SS} and Quin-2 with Zn^{2+}, a non-linear decrease in the absorbance at 261 nm suggested competition with Quin-2 for Zn^{2+} binding (Figure 32), confirming a picomolar range Zn^{2+} binding affinity for Zur_{SS}. Data were modelled to either a two-site dimer sequential binding model (representative fitted data shown in Figure 32) or a one-site monomer model (Appendix B, Figure 2). The single site monomer model was found to produce poor fitting of the data (Appendix B Figure 2). This is consistent with the expectation that Zur_{SS} will be dimeric under these conditions; Fur_{EC} has been previously shown to exist as mainly a dimer in solution (Michaud-Soret *et al.* 1997: Althaus *et al.* 1999). The two-site dimer model produces an average value for the tightest Zn^{2+} site on each dimer (K_{Zn1}) of 7.75 x 10^{12} M^{-1} (± 5.94). The affinity for the second site on each dimer (K_{Zn2}) could not be modelled by least squares linear regression analyses of these data (values are summarised in Table 7).

During modelling of these Zn^{2+} binding data it was observed that the gradients of binding curves calculated by least squares non-linear regression analysis were consistently less steep than the trend implied by the individual datapoints, resulting in a possible overestimation of tightness for first affinity values (K_{Zn1}). Therefore, least squares linear regression analyses were also performed on the first five datapoints only for each dataset. This range was chosen so as to incorporate the full degree of competition between the tightest Zn^{2+} site and Quin-2 whilst minimising any distortion of the fit caused by the algorithm attempting to incorporate later datapoints into the model. This approach produced fitted binding curves that more accurately described the initial datapoints (Figure 33) with an average K_{Zn1} of 1.73 x 10^{12} M^{-1} (± 0.9) (Table 7). These data not only confirm a sub-picomolar Zn^{2+} affinity for one of the metal binding sites of dimeric Zur_{SS} but also suggest this value is closely matched to that of ZiaR (K_{Zn1}=4.45 x 10^{12} M^{-1} (four site dimer model); see section 3.4.6).

The stoichiometry of Zn^{2+} binding to Quin-2 and Zur_{SS} (with no binding detected at a second binding site on the dimer) (Figure 32) suggests that only one metal site on dimeric Zn_1Zur_{SS} was able to compete with Quin-2 for Zn^{2+} under these conditions. This observation suggests negative binding cooperativity between allosteric

sites on different subunits in the same dimer, with one site having a tighter Zn^{2+} affinity than the other (which likely has an affinity substantially weaker than Quin-2). Size-exclusion fractionation of Zur_{SS} pre-incubated in two equivalents of Zn^{2+} data showed saturation of all Zn^{2+} sites on Zur_{SS} at a protein concentration of ~5 μM (Figure 27). These data imply a Zn^{2+} disassociation constant for the second dimer site that is weaker than ~10^{-12} M but tighter than ~2.5 x 10^{-6} M. Whether this difference across the sites in the dimer is physiologically significant is unclear; a Zn^{2+} affinity for the second site on Zur_{SS} lower than affinities of competing intracellular Zn^{2+} ligands would imply that occupation of only one site per dimer may be sufficient to initiate binding to DNA. This model represents the first precedent for negative homotropic cooperativity for metalloregulation of Fur family proteins.

4.4 Characterisation of the *in vitro* DNA binding properties of Zur_{SS}

4.4.1 EMSA analyses show Zn^{2+}-dependent Zur_{SS} binding to a conserved 10-1-10 inverted repeat sequence in the znu promoter region

The Zur_{SS} gene is divergently transcribed from an operon of genes encoding the ZnuABC Zn^{2+} import system in this organism (see section 1.8.2). RT-PCR data directly demonstrated Zn^{2+} dependent repression of these genes *in vivo* (Appendix B Figure 1). For Fur-family metal responsive regulators, binding of metal to the apo-repressor facilitates binding to a cognate DNA recognition sequence in the promoter region of regulated genes. This inhibits the ability of RNA polymerase to bind to the promoter, impairing gene transcription. To confirm specific binding of Zur_{SS} to the promoter region of the *znu* divergon, electrophoretic mobility shift assays (EMSA) were performed.

The gene organisation within the *znu* divergon is shown in Figure 34a. The start of sll1937 (*zur*) is separated from the start of *znuA* (slr2043) by a 106 bp region. Searching within this region located a pallindromic, inverted repeat sequence close to the start codon (starting 41 bp upstream) of the *zur* gene. Extensive characterisation of *B. subtilis* Zur interaction with oligonucleotide probes by EMSA identified a consensus 10-1-10 inverted repeat element forming the Zur binding box (Gabriel *et al.* 2008). Introduction of symmetric mutations into each half site between positions two and nine

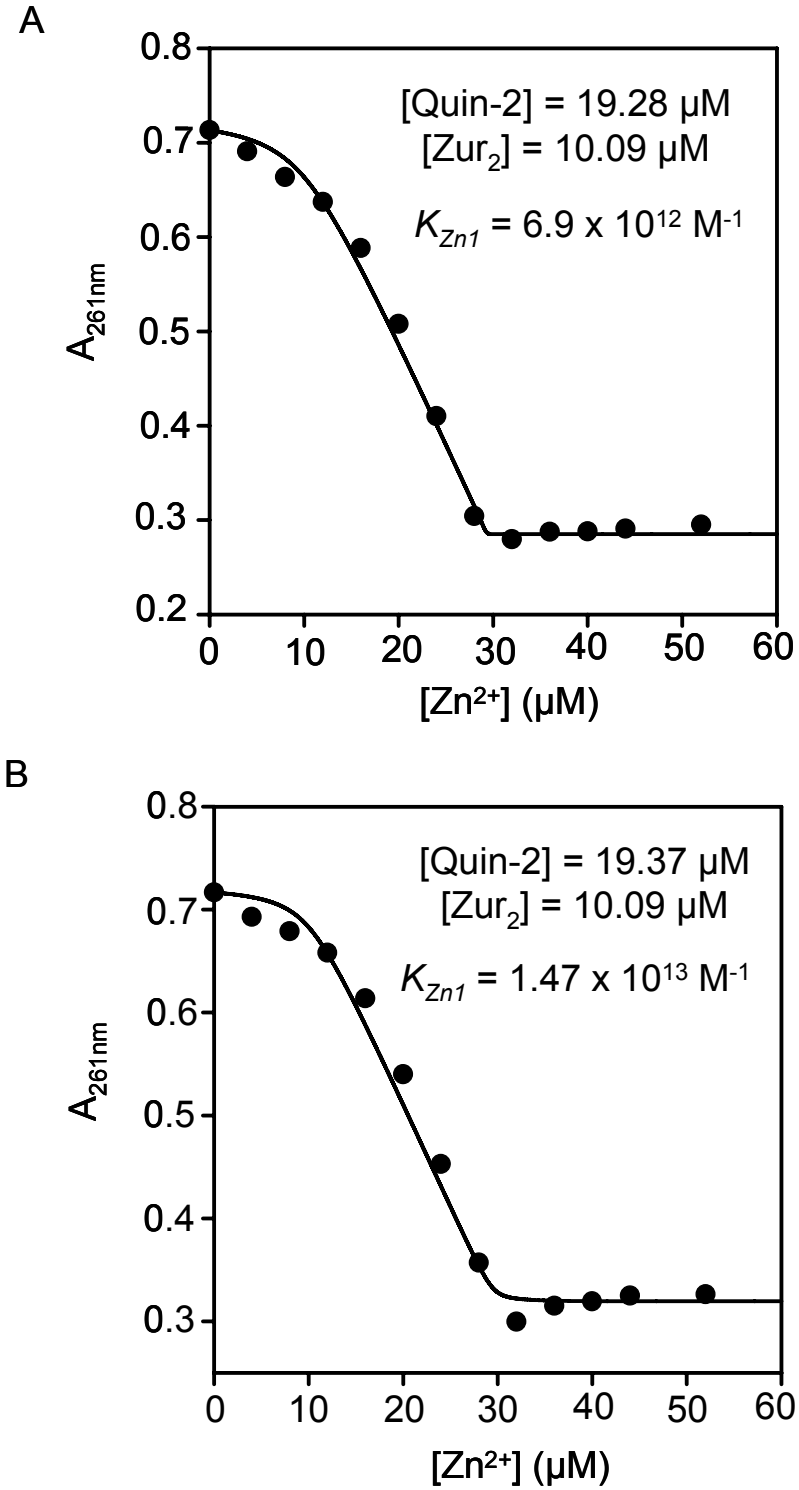

Figure 32. Measurement of the Zn^{2+} affinity of Zn_1Zur_{SS} by titration with Zn^{2+} in the presence of Quin-2. Data from two independent anaerobic titrations are shown. Experiments were performed as described for ZiaR under identical conditions. For both replicates, data are modelled to a two-site dimer sequential binding model.

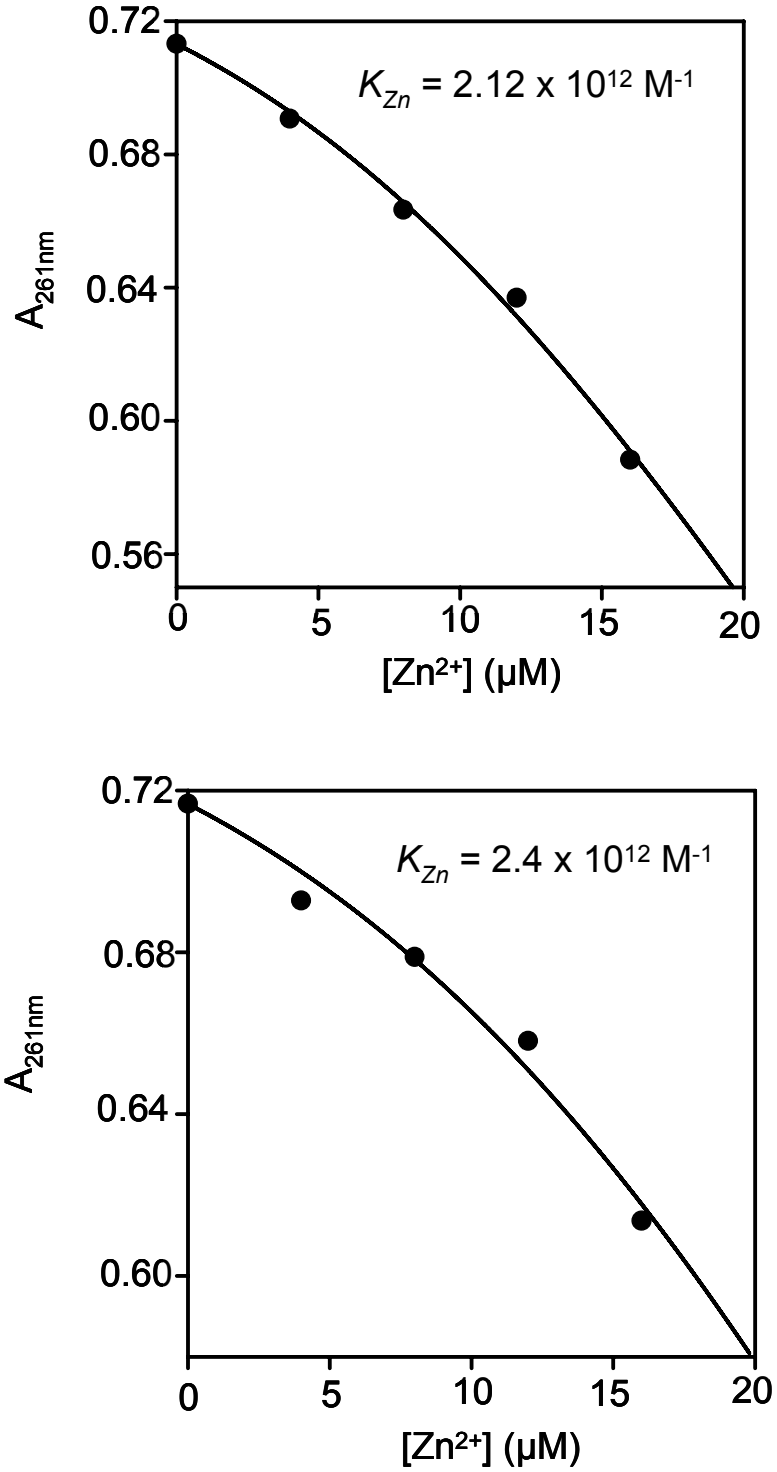

Figure 33. Optimised curve fitting for titrations of Quin-2 and Zn_1Zur_{SS} with Zn^{2+} titration data. The first five data points only for each of the two data sets shown in Figure 32 were fitted to a two-site dimer sequential binding model. All other parameters used in the curve fitting were identical to those in the analyses shown in figure 32.

	Mean Zn^{2+} association constant (K_{Zn}) (M^{-1})	
Model	K_{Zn1}	K_{Zn2}
2 site dimer	7.75×10^{12} (± 5.94)	*nd*
2 site dimer (initial points only)	1.73×10^{12} (± 0.93)	*n/a*

Table 7. Estimated Zn^{2+} association constants for Zur_{SS}. Example fits modelled to a one-site monomer model are shown in Appendix B. *nd*; binding not detected.

resulted in a substantial reduction in the binding affinity of Zur_{BS} for DNA; however, changes at position 10 in longer oligonucleotides caused no reduction in DNA binding, implying a minimal requirement for a 9-1-9 element (Gabriel *et al.* 2008). The inverted repeat sequence identified in *Synechocystis* is highly similar to the *B.subtilis* consensus sequence (Figure 34b) and also bears a striking similarity to a 7-1-7 inverted repeat consensus Zur-box sequence from *Corynebacterium glutamicum* (Schröder *et al*. 2010) (data not shown). This was the only pattern found within the intergenic region closely resembling previously characterised Zur binding sites. In *B.subtilis*, two Zur binding sites (termed C1 and C2) were implicated in regulating expression of the gene *yciC*. One of these sites (C1) is proximal to the *yciC* start codon (as is the case for the Zur box identified in *Synechocystis*) however, the other site (C2) is located approximately 200 bp upstream of the transcriptional start site (Gabriel *et al.* 2008). No sequences similar to that identified proximal to *zur* were identified upstream of the *zur* coding sequence suggesting the intergenic 10-1-10 sequence represents the Zur-box for this operon.

For gel retardation analyses to probe Zur_{SS} binding to the *znu* promoter region, oligonucleotide probes of varying lengths and compositions were produced. Example analyses for each of these probe types are shown in Figure 35. In each of these analyses recombinant, purified Zn_1Zur_{SS} was incubated at several protein concentrations aerobically (in the presence of 1 mM DTT) with either a saturating concentration of Zn^{2+} (200 μM), EDTA at a concentration (1 mM) shown to be sufficient to inhibit metal binding at the exchangeable site (Figure 27) or in buffer only. Each sample also contained an equimolar concentration of probe and control oligonucleotide (each at 0.2 μM). To confirm specific binding of recombinant Zur_{SS} to the complete *znu* intergenic region, a probe oligonucleotide (P1) containing the full intergenic region was titrated with Zur_{SS} and samples analysed by native PAGE analysis. Following incubation with Zn^{2+}, a protein-dependent retardation of the 288 bp probe fragment was observed, with no apparent decrease in the abundance of a 136 bp control fragment over the same concentration range (Figure 35a). This is consistent with the formation of a specific complex between Zur_{SS} and a region within the *zur-znu* intergenic sequence. No retardation of probe DNA was observed following incubation of recombinant Zur_{SS} in 1 mM EDTA, at a protein concentration (1 μM) shown to produce retardation of probe DNA following incubation in 200 μM Zn^{2+} (Figure 35a), demonstrating the Zn^{2+}-dependent nature of Zur_{SS} association with DNA.

An analogous analysis was performed utilising a truncated, 129 bp probe fragment (P2) which retained the candidate Zur-box element but in which a large portion of the intergenic region 5' to this section was removed. Protein-dependent retarded complexes were observed (Figure 35b), for samples pre-incubated in Zn^{2+}, in the same protein concentration range as was observed for the full length intergenic fragment (P1). Although the probe and control DNA fragment bands were poorly resolved in this analysis due to their closely matched sizes, no apparent decrease in intensity was observed for the slightly larger control DNA fragment. A decrease in intensity for the smaller probe DNA fragment, concomitant with the appearance of retarded DNA bands, was observed confirming retention of specific Zur_{SS} binding to this truncated DNA probe. No retarded DNA bands were observed in analyses using a probe fragment (P3) containing a portion of the intergenic region lacking the candidate Zur-box (Figure 35c). These data confirm that specific Zur_{SS} binding to DNA is localised to a region of 61 bp preceding the *zur* start codon with specific binding likely to be mediated by the conserved Zur-box located in this region. Moreover, these data also show Zn^{2+}-dependent association of Zur_{SS} with DNA which is consistent with Zn^{2+}-depedent regulation of *znuA* transcription observed *in vivo* (Appendix B Figure 1).

4.4.2 Production of a DNA fragment containing a 10-1-10 binding element

Fluorescence anisotropy was used to analyse equilibrium association of Zur_{SS} with its cognate DNA promoter sequence. A HEX-labelled double stranded DNA oligonucleotide was produced that incorporated the conserved 10-1-10 Zur-box binding sequence (Figure 36a). Successful annealing of single stranded oligonucleotides was confirmed by native PAGE analysis. An annealed, 33-bp *znu* O/P oligonucleotide migrated at a position similar to that of a 32-bp *zia* O/P oligonucleotide, with single stranded oligonucleotides migrating more quickly than the double stranded fragment (Figure 36b).

4.4.3 Zn^{2+} promotes high-affinity, tetrameric binding of Zur_{SS} to DNA

For fluorescence anisotropy analyses recombinant Zn_1Zur_{SS} was prepared anaerobically and pre-incubated in Zn^{2+} concentrations in the range 2.5-20 μM (present at a two-fold molar excess in all incubations). These concentrations were sufficient to ensure

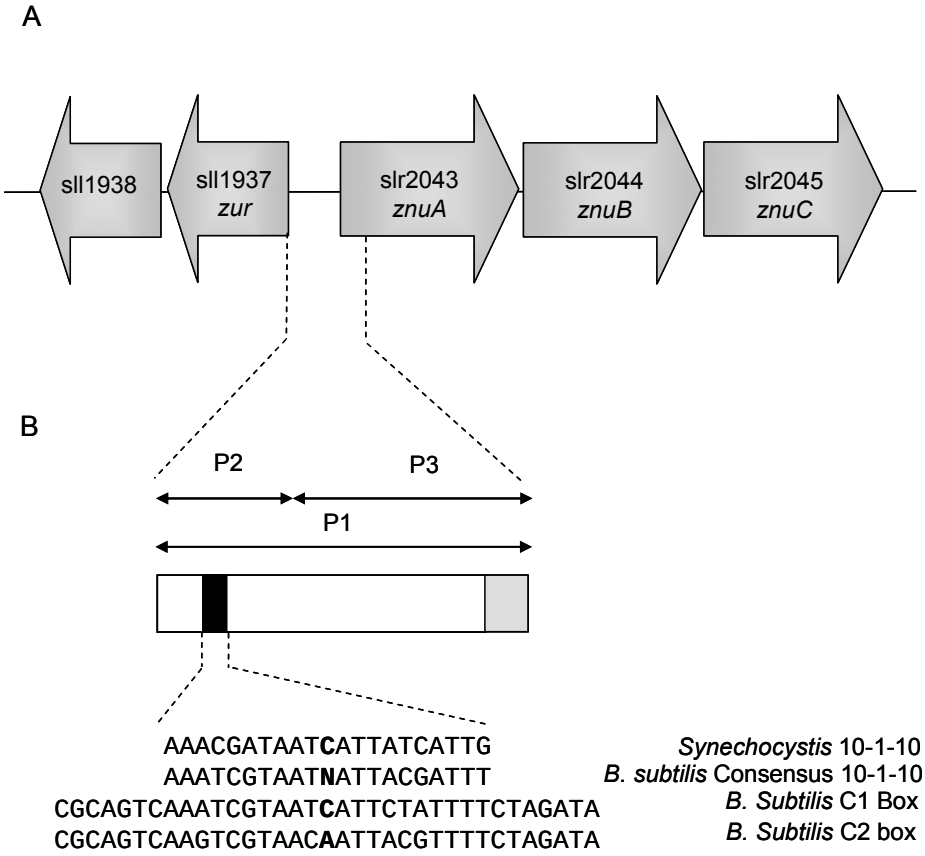

Figure 34. Organisation of the *Synechocystis znu* operon. A. Schematic showing the positions of genes within the *znu* operon (not to scale) (for details see main text). B. Summary of probe design for EMSA experiments; P1 incorporated the full intergenic region plus 46-bp of slr2043. P2 incorporated the region proximal to the Zur_{SS} start site which contained a conserved Zur box (black), which is shown aligned with elements identified in *B. subtilis* (Gabriel *et al.* 2008). P3 contained the adjacent intergenic region predicted not to contain a conserved binding site.

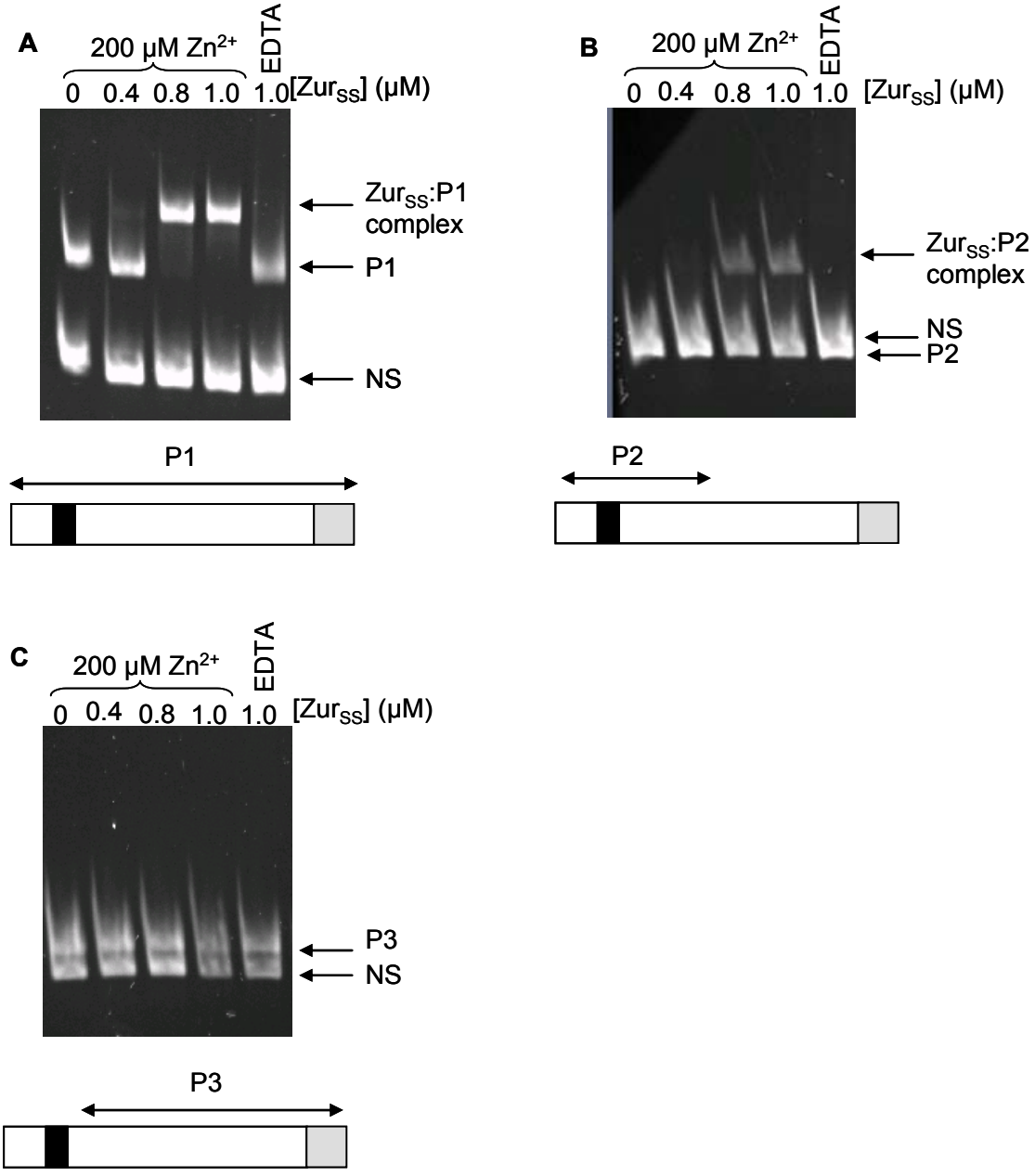

Figure 35. Identification of the Zur_{SS} DNA binding site by electrophoretic mobility shift assay (EMSA). A. Example analysis with Probe 1 (288-bp) showing metal dependent, specific formation of Zur_{SS}-P1 complex, with no retardation of a 136-bp non-specific DNA fragment (NS). B. Analogous analysis to that in A using Probe 2 (129-bp) showing decline in P2 concentration consequent with formation of retarded DNA complex. C. Example analysis using Probe 3 (P3; 161- bp) showing complete loss of DNA retardation.

saturation of the exchangeable metal binding site given a minimal estimated Zn^{2+} association constant for Zur_{SS} of 1.73 x 10^{12} M^{-1} (measured under solution conditions identical to those used in fluorescence anisotropy) (Table 7). On titration of Zn_1Zur_{SS} pre-incubated in Zn^{2+} with 10 nM of *znu* O/P oligonucleotide, an increase in anisotropy was observed consistent with association of Zur_{SS} with DNA (Figure 37a). Even at the lowest protein concentrations used in this assay (5 nM), the minimal concentration of Zn^{2+} (10 nM) was still sufficiently high enough (~four orders of magnitude greater than the Zn^{2+} disassociation constant for Zur_{SS} of 5.8 x 10^{-13} M) to ensure saturation of the exchangeable metal binding sites of Zur_{SS}. Titration of Zn_1Zur_{SS} with DNA in the presence of 1 mM EDTA showed a reduced binding affinity for DNA (Figure 37a). In the example analysis shown in Figure 37a, an increase in anisotropy was observed as the protein concentration approached 1 μM. The magnitude of this increase was not reproducible and may have been due to incomplete Zn^{2+} chelation by EDTA resulting in a low concentration of Zn-loaded Zur_{SS} (Zn_2Zur_{SS}) available for binding to DNA. The DNA association constant of ~55 nM for Zn_2Zur_{SS} (potentially a minimal value for this affinity) shown for the dataset in Figure 37a is similar to values observed for ZiaR and is consistent with specific protein interaction with DNA.

Zur_{SS} has a molecular mass close to that of ZiaR (15.4 kDa compared to 15.1 kDa for ZiaR) and is also similar in size to SmtB (13.5 kDa). Replicate titrations analogous to the example in Figure 37a in which Zur_{SS} was pre-incubated with at least two equivalents of Zn^{2+} produced an average Δr_{obs} of 0.04974 ± 0.00634 (n=6). Based on a Δr_{obs} of ~0.02 per SmtB dimer binding to a 40-mer DNA molecule (VanZile *et al.* 2002b), this value is consistent with binding of two to three (2.49) Zur_{SS} dimers to each DNA molecule. However, as for ZiaR this is only an approximate estimation; Zur_{SS} has a larger molecular mass (~10 %) than SmtB and the DNA oligonucleotide used in these studies is seven nucleotides shorter. Therefore, an expectation maybe that each Zur_{SS} dimer may cause a greater change in anisotropy than SmtB and so the actual dimer binding stoichiometry for Zur_{SS} may be somewhat less and perhaps closer to the lower estimate of two dimers. Fur family sensors have been subjected to little characterisation by this method limiting comparisons of these data with those obtained with homologous proteins. A single anisotropy study of Fur_{EC} binding to DNA showed a smaller Δr_{obs} (approximately 2-fold) consistent with dimer binding, following titration of a 25-bp oligonucleotide with dimeric *E.coli* Fur in the presence of Mn^{2+} using similar buffer conditions to those used for Zur_{SS} (D'Autraux *et al.* 2007).

A

HEX5’ GACAAT**AAACGATAATCATTATCATTG**CATAAT 3’

B

Figure 36. Production of annealed, double stranded *znu* O/P oligonucleotide. A. Section the of *znu* promoter sequence chosen for fluorescence anisotropy oligonucleotides, incorporating the conserved 10-1-10 inverted repeat sequence (shown as arrows and in bold text). B. Native PAGE analysis of annealed and single stranded 33-bp oligonucleotides. A sample of annealed *zia* O/P oligonucleotide (32-bp) is shown for comparison.

Figure 37. Example fluorescence anisotropy titrations of Zur_{SS} with DNA. A. Example anaerobic titration of 10 nM *znu* DNA with dilutions of Zur_{SS} either pre-incubated in two equivalents of Zn^{2+} (2.5-20 μM) (closed symbols) or with 1 mM EDTA. B. Analogous titration to that shown in A, performed aerobically in the presence of 1 mM DTT. 10 nM DNA was titrated with protein either pre-incubated in two equivalents Zn^{2+} (1.2-12 μM) (closed symbols), pre-incubated in 1 mM EDTA (open symbols) or with no metal/EDTA pre-incubation (red symbols). Conditions: 120 mM KCl, 30 mM NaCl, 10 mM Hepes (pH 7.8).

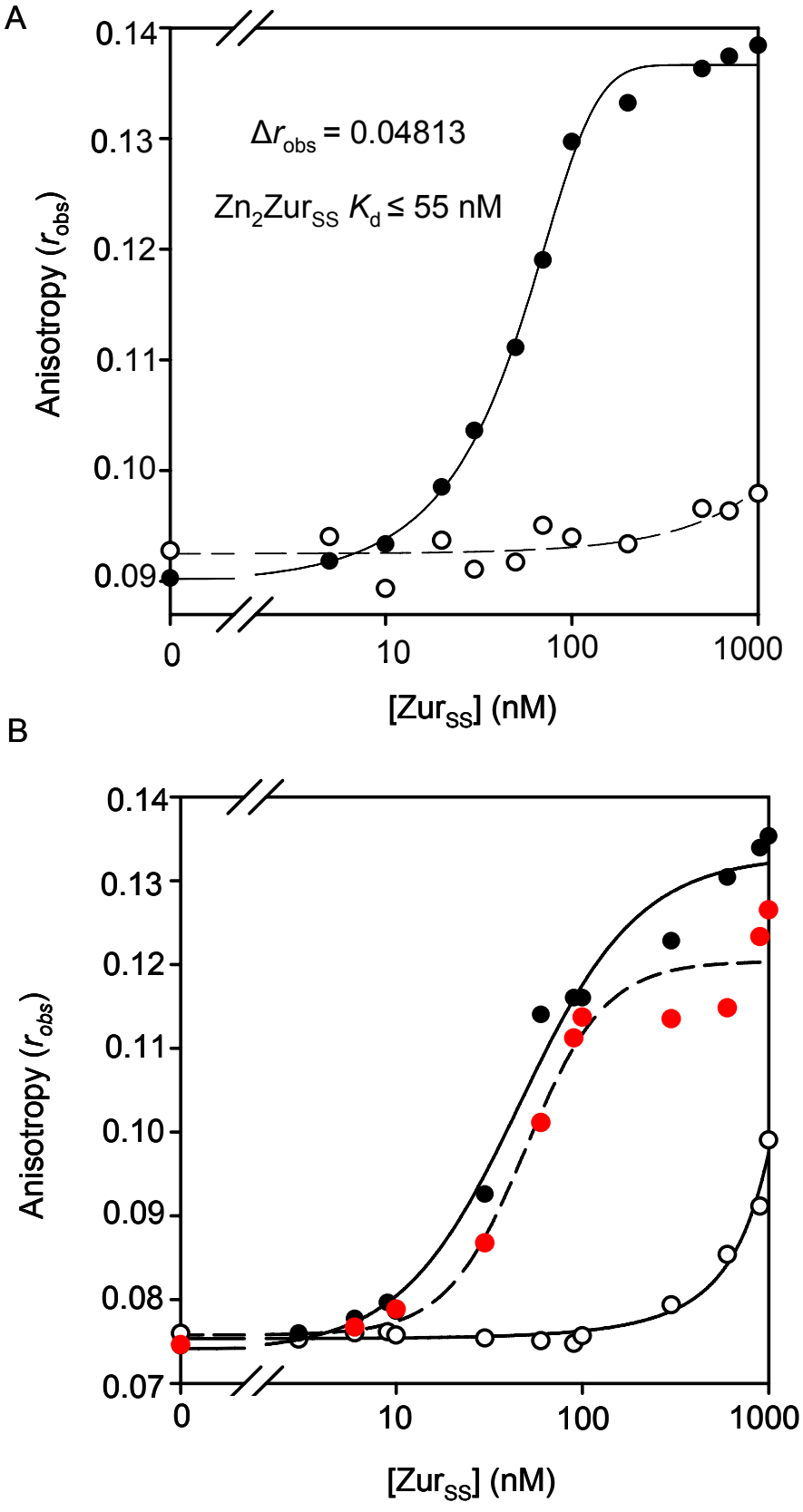
A
0.14
0.13
0.12
0.11
0.10
0.09
Anisotropy (r_{obs})
Δr_{obs} = 0.04813
Zn_2Zur_{SS} $K_d \leq$ 55 nM
0
10
100
1000
[Zur_{SS}] (nM)
B
0.14
0.13
0.12
0.11
0.10
0.09
0.08
0.07
Anisotropy (r_{obs})
0
10
100
1000
[Zur_{SS}] (nM)

Titration of DNA with Zn_1Zur_{SS} in the absence of EDTA or metal pre-treatment reproducibly produced DNA binding analogous to that observed for Zur_{SS} pre-incubated in Zn^{2+}. An example analysis performed aerobically (in the presence of 1 mM DTT) is shown in Figure 37b (similar data were also obtained under anaerobic conditions). This effect was not observed following incubation with EDTA (Figure 37a). Moreover, ICP-MS analysis of a sample of Zur_{SS} performed prior to the titrations in Figure 37b showed approximately 0.9 equivalents Zn^{2+} to be present confirming the presence of single structural Zn^{2+} ion and an unoccupied allosteric site. Therefore, the DNA binding observed in the absence of added Zn^{2+} was likely due to acquisition of contaminant metal (likely to be Zn^{2+}) by Zn_1Zur_{SS} from the buffer. Although this effect was observed to some extent for ZiaR (as a partially reduced binding affinity for DNA in the absence of EDTA pre-incubation; Table 5), apo-like binding curves could be readily produced in the absence of EDTA (Figure 16). Apo-like binding curves were never observed for Zur_{SS} titrations performed in the absence of EDTA. This effect has been observed for other members of the Fur-family (Bsat & Helmann 1999) however EMSA analyses using polyacrylamide gels pre-run in the presence EDTA have been shown to reduce this effect (Mills & Marletta 2005). These observations can likely be explained by the different modes of action of ZiaR and Zur_{SS}. Unlike Zn-loaded ZiaR, which is effectively 'invisible' in this DNA binding assay, Zn_2Zur_{SS} binds to DNA (Figure 37a) with a K_{DNA} of 10-100 nM. The picomolar equilibrium binding affinity of Zur_{SS} for Zn^{2+} means that trace amounts of buffer Zn^{2+} will be readily acquired by the protein which is then activated to bind DNA.

4.5 Models for Zur_{SS} binding to DNA

Despite the inability to regenerate an apo-like DNA binding response, these data show specific, high affinity, multimeric binding of Zur_{SS} protein to a predicted Zur-box located in the *znu* promoter region. The detailed nature of the interactions between Fur-family proteins and DNA (and also the precise nature of the Fur-box motif itself) has been controversial, primarily because of the paucity of high-resolution structural data for Fur-DNA complexes and also because of the conflicting nature of data from studies investigating the mode of interaction with DNA. Analyses of the DNA binding properties of Fur from *B.subtilus* has recently led to a model which proposes that instead of being comprised of a single 7-1-7 inverted repeat sequence (minimally

required for Fur binding to DNA), the 19-bp Fur-box is actually best described as a combination of two overlapping 7-1-7 inverted repeat sequences present on opposite strands of DNA with each inverted repeat binding a single dimer, resulting in two dimers being bound at each overlapping repeat element (Baichoo & Helmann 2002) (Figure 38a). This model for binding has a precedent in the form of the DtxR repressor; when co-crystallised with a section of DNA containing its operator promoter sequence binding of two Ni^{2+} bound dimers on opposite faces of the dimer was observed (White *et al.* 1998).

The multiple dimer binding model incorporates the minimum requirement of a 7-1-7 motif for high-affinity Fur DNA binding but also explains several other apparently contradictory observations from previous studies of Fur interaction with DNA. Notably, it has been unclear how the relatively small, compact Fur dimer binds to a region as large as 19-bp given the small size of the helix-turn-helix motif, which would be expected to bind sequences no longer than ~12-bp (Harrison & Aggarwal, 1990). Additionally, DNA footprinting data has shown Fur binding to incorporate relatively large sections of DNA (up to 30-bp), substantially more than would be expected from binding of a single Fur dimer to the Fur-box and consistent with the sizes of regions previously shown to be protected by multiple dimers of the DtxR repressor (Tao & Murphy, 1992). Furthermore, evidence for binding of multiple Fur dimers on both sides of the DNA double helix from footprinting data appeared to suggest 'wrapping' of the protein around both sides of the DNA helix with evidence also for extensive polymerisation and formation of helical arrays on binding of Fur to DNA at high protein concentrations (Le Cam *et al.* 1994; de Lorenzo *et al.* 1988). However, these data appeared inconsistent with apparently rigid structure of Fur (Saito & Williams 1991). Therefore, a model in which two dimers bind to the Fur-box region (one on each side of the double-helix), with potential for further polymerisation along the DNA molecule, could account for these observations.

Although Zur proteins have been subject to less extensive characterisation in terms of their DNA binding properties, it has been shown that Zur_{BS}, like Fur, binds to a large, extended region (~28-bp) containing a smaller 7-1-7 binding element (Gaballa *et al.* 2002). Therefore, it is reasonable to propose that Zur-boxes may also accommodate binding of multiple dimers as suggested for Fur. When the Zur_{SS} box sequence is compared to that for Fur_{EC}, an overlapping alignment of the kind found in the Fur box is immediately apparent (Figure 38b), with a portion of the 10-1-10 element also described

by two overlapping 6-1-6 inverted repeat sequences, each of which contains a single base mismatch. It is noted that in previous work it was shown that a 9-1-9 repeat motif was minimally required for Zur binding to DNA and on examination of this sequence no apparent overlapping organisation involving shorter inverted repeats is apparent (Gabriel *et al.* 2008). Nevertheless, such an organisation could provide a means by which a single 9-1-9 motif could accommodate multiple Zur_{SS} dimers (Figure 38b)

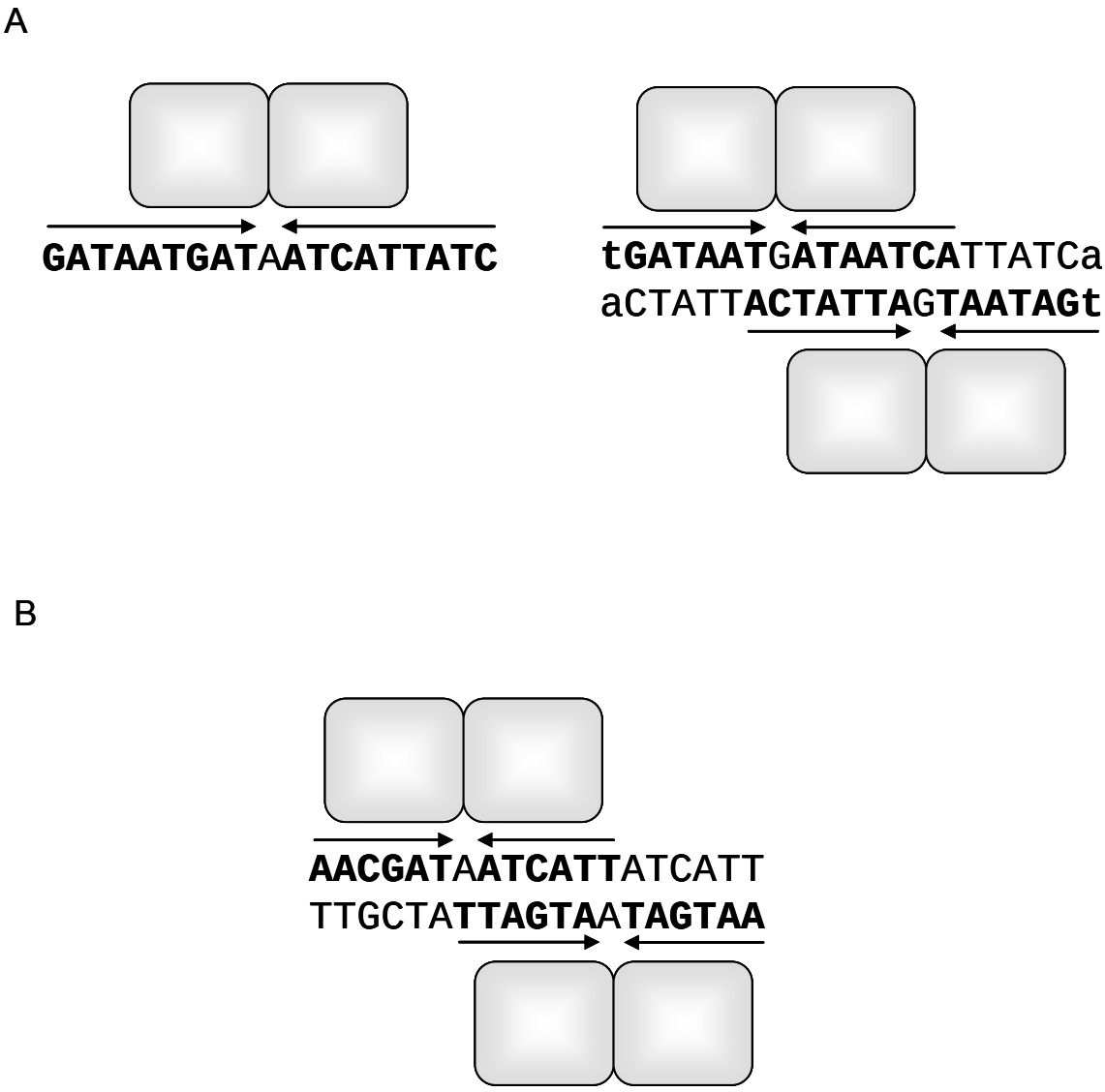

Figure 38. Models of Fur and Zur binding to their cognate DNA binding elements. A. Left; classic model of a single Fur_{EC} dimer binding to an inverted repeat element in a 19-bp conserved Fur-box. Right; Sequence of the Fur-box from *B.subtilus* in which two overlapping 7-1-7 inverted repeat sequences form an extended 21-bp binding site are able to accommodate binding of two Fur dimers, one on each strand of the DNA double helix (adapted from Baichoo & Helmann 2002). B. Analogous representation of a portion of the 10-1-10 Zur-box from *Synechocystis* showing the presence of two additional 6-1-6 inverted repeat elements which in this model are shown to accommodate binding of two Zur_{SS} dimers on opposite strands of the helix.

Chapter 5. Analysis of the contribution of access in regulation of metal partitioning *in vivo*

One aim of these studies was to investigate the contribution of kinetic factors, such as interactions with metallochaperones and other proteins involved in metal homeostasis, in facilitating specific intracellular metal partitioning. Importantly, a key prediction is that as well as trafficking metal to specific intracellular targets, metallochaperones such as Atx1 are also vital in preventing incorrect metals populating metal sites which normally bind weaker binding metals. It was hypothesised that loss of the intracellular Cu^+ chaperone Atx1 would cause aberrant partitioning of Cu^+ to adventitious protein sites, potentially including the highly exchangeable metal-binding sites of the metal-sensing transcriptional regulators that are the subject of this study. The Cu^+ binding properties of ZiaR and Zur_{SS} and the allosteric effects of Cu^+ were investigated in conjunction with comparative analyses of the responses at ZiaR and Zur_{SS} regulated promoters in wild-type and mutant strains of *Synechocystis*. Transcriptional regulation by ZiaR was analysed in a mutant strain in which the cytosolic Cu^+ chaperone Atx1 was missing (Δ*atx1*). Zur_{SS} responses were monitored in a mutant strain in which both Atx1 and glutathione synthase were absent (Δ*atx1*Δ*gshB*).

5.1 Analysis of the *in vitro* Cu^+ binding properties of ZiaR

5.1.1 ZiaR binds Cu^+ with high affinity via multiple cysteine residues

To determine if ZiaR could bind Cu^+ *in vitro*, ZiaR was prepared anaerobically and Cu^+ binding monitored by UV-Visible spectroscopy. On binding of Cu^+ to the S^- atoms on metal site cysteine residues, LMCT features are often observed in the near UV range. This has been exploited to interrogate Cu^+ binding to a range of thiol-containing Cu^+ sites in metal sensing transcriptional regulators (Liu *et al.* 2007 & 2008, Chen *et al.* 2008). Reduced Cu^+ was prepared in an anaerobic chamber and the concentrations of Cu^+ stocks were determined by ICP-MS analysis to verify the total concentration of metal and by anaerobic titration with the Cu^+-binding metallochromic indicator BCS, to confirm the stock was wholly composed of Cu^+ only (Figure 39). An example anaerobic UV-Visible titration of ZiaR with Cu^+ is shown in Figure 40. On titration with Cu^+, Cu^+-dependent electronic absorption features are visible in the near-UV wavelength

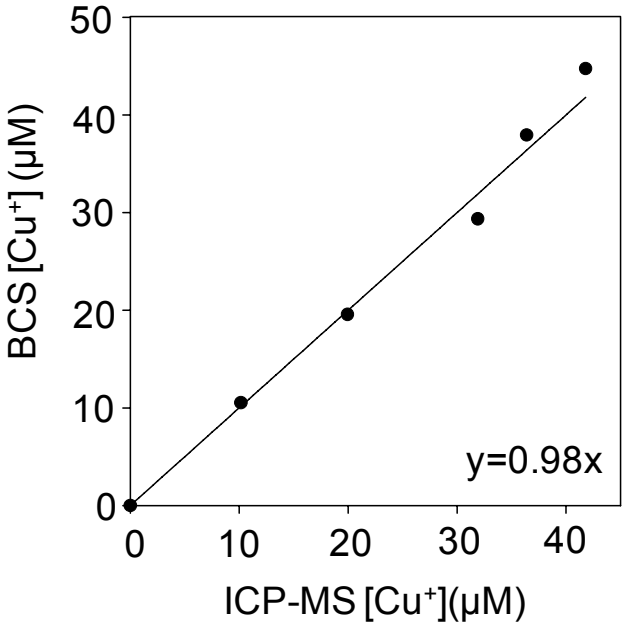

Figure 39. Validation of Cu^+ stocks by calibrated BCS assay. Stocks of Cu^+ were prepared anaerobically and analysed for total dissolved Cu^+ by ICP-MS. The proportion of Cu^+ in solution was verified as approximately 100% by titration against the Cu^+-specific metallochromic indicator BCS.

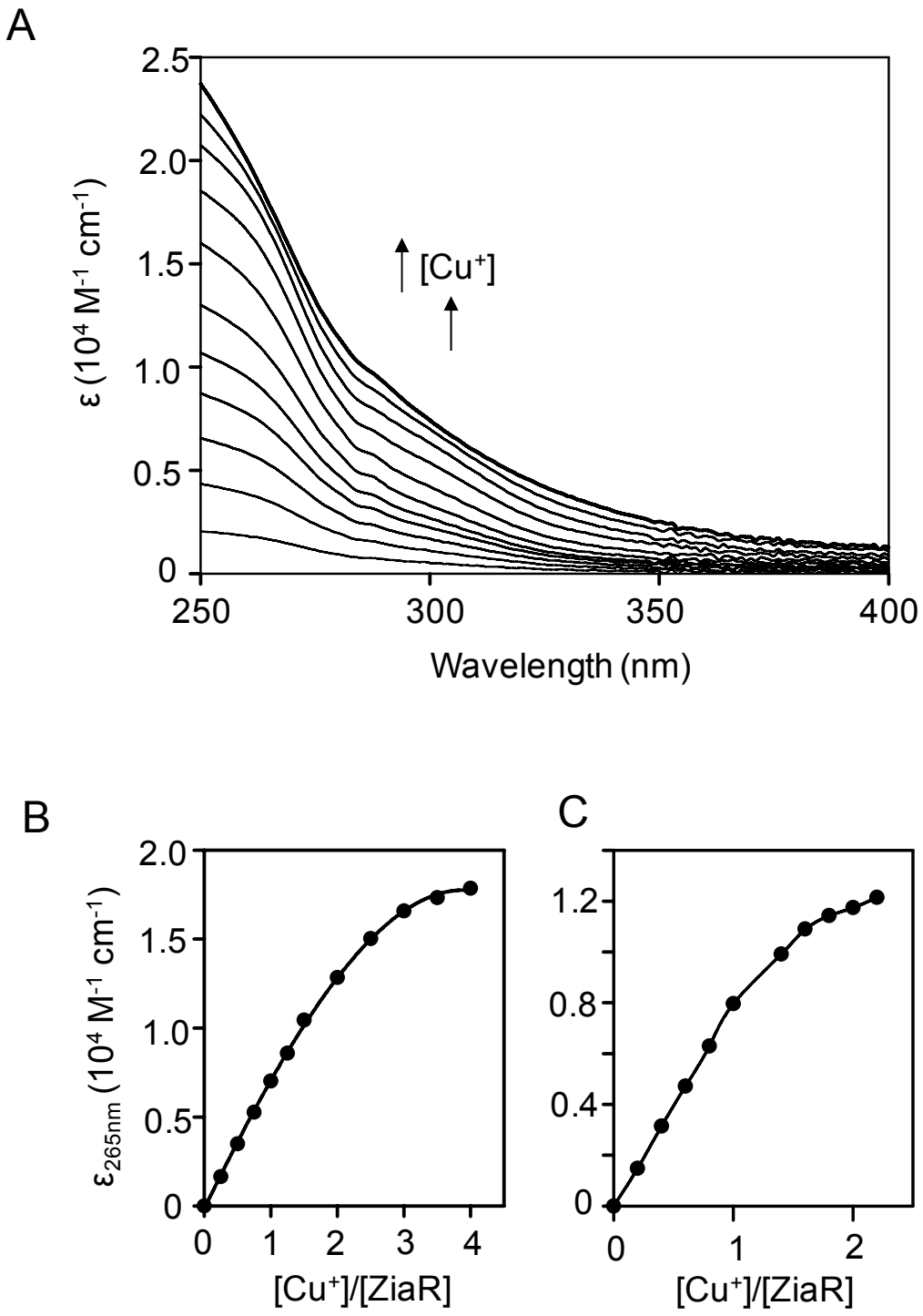

Figure 40. Anaerobic UV-Visible Cu^+ titration with ZiaR. A. Apo-subtracted difference spectra from an example titration of ~25 uM ZiaR with Cu^+. B. Increases in molar absorbance at 265 nm (from the data shown in A) plotted against increasing [Cu^+]. In analogous titrations protein precipitation was often observed beyond four equivalents of Cu^+ C. Increases in absorbance at 265 nm plotted against [Cu^+] from an analogous titration performed in the presence of 50 mM Tris-HCl. Substantial protein precipitation was observed beyond two equivalents Cu^+ in this titration. These data were published in Dainty *et al.* 2010 (Appendix E).

range between 250 and 400 nm (Figure 40a). Although these features are relatively broad, a shoulder is observed around 265 nm, the wavelength considered diagnostic for Cu^{+}-S^{-} LMCTs (Angeletti *et al.* 2005). When the changes in intensity of this feature were plotted against Cu^{+} concentration, saturation was reproducibly observed between three-four equivalents of Cu^{+} (Figure 40b). Titration of ZiaR with Cu^{+} in the presence of Tris-HCl instead of Hepes (as was used in the experiments shown Figure 40b) showed saturation of this LMCT feature at approximately two equivalents of Cu^{+} with the maximum intensity reached at saturation also lower than under Hepes buffer conditions (Figure 40c). Protein precipitation was observed under Tris buffer conditions beyond two equivalents of Cu^{+}. Tris-HCl is known to form Cu^{+} complexes (Sokołowska and Bal 2005) and may have competed with ZiaR for Cu^{+} binding to some sites under these conditions.

The magnitude of the LMCT features around the diagnostic wavelength of 265 nm has been shown to correlate with the number of Cu-S^{-} bonds formed. Studies of metallothionien proteins have shown that a molar extinction coefficient of approximately 5500 M^{-1} cm^{-1} (at a wavelength of ~262 nm) corresponds to formation of a single Cu-S^{-} bond (Pountney *et al.* 1994). For the titrations shown in Figure 40a and b, the maximum value (at four equivalents Cu^{+}) at this wavelength of ~17850 M^{-1} cm^{-1} corresponds to formation of approximately three Cu-S^{-} bonds per monomer (16500 M^{-1} cm^{1}). This value is substantially less than that expected for four Cu-S^{-} bonds (22000 M^{-1} cm^{-1}). Under Tris-HCl buffer conditions, the lower molar extinction coefficient at saturation (~11740 M^{-1} cm^{-1}) is consistent with the formation of at least two Cu-S^{-} bonds per monomer up to two equivalents of Cu^{+} (Figure 40b). Together these data confirmed that Cu^{+} can bind to ZiaR most likely via involvement of the α3N site cysteine residues. The higher Cu^{+} binding stoichiometry observed in the presence of Hepes (Figure 40b) may have been due to relatively weaker additional binding to other sites on the protein.

5.1.2 Measurement of the Cu^{+} binding affinity of ZiaR by titration with BCS

The linear increase in LMCT intensity observed on titration of ZiaR with Cu^{+} (under both sets of buffer conditions; Figure 40a, b) suggested the presence of metal binding sites of Cu^{+} affinity (K_{Cu}) too tight to measure at the protein concentrations used under these conditions. Cu^{+} has been shown to bind to cysteine containing metal sites

extremely tightly; affinities in the 10^{21} M^{-1} range have been reported for the Cu^+ sensing transcriptional regulators CueR and CsoR (Changela *et al*. 2003; Ma *et al*. 2009a). The Cu^+-specific metallochromic indicator BCS (K_{Cu} β_2= 6.3x10^{19} M^{-2}) has been used previously to estimate K_{Cu} values for proteins (Angeletti *et al*. 2005; Ma *et al.* 2009a). Titration of 25 μM BCS with Cu^+ in the absence of protein showed a linear increase in absorbance at 483 nm with saturation at approximately 12.5 μM, consistent with the formation of $CuBCS_2$ complex (Figure 42). Titration of BCS with Cu^+ in the presence of an equimolar concentration of ZiaR (25 μM) showed a much smaller increase in absorption at 483 nm compared to the BCS alone control (Figure 41). Protein precipitation observed at Cu^+ concentrations greater than 25 μM meant that the precise Cu^+ binding stoichiometry of ZiaR under these conditions was unclear. Nevertheless, these data show that ZiaR contains at least one high affinity Cu^+ binding site with an affinity for Cu^+ tighter than that of BCS.

5.1.3 ZiaR can bind Cu^+ and Zn^{2+} simultaneously via differential metal partitioning to α3N and α5 metal sites respectively

Cu^{2+} is ranked as the most competitive divalent metal element in the Irving-Williams affinity series (eq. 1) and both Cu^{2+} and Cu^+ have been demonstrated to bind to protein sites in preference to Zn^{2+} (Harvie *et al.* 2006; Borrelly *et al.* 2004b) and affinity constants for Cu^+ have been reported exceeding Zn^{2+} by up to 12 orders of magnitude (for the metal binding site of the Cu^+ sensor CsoR from *B. subtilis*) (Ma *et al.* 2009a). Therefore, a prediction is that in the presence of equimolar concentrations of Cu^+ and Zn^{2+} metals, the metal sites of proteins should become populated by Cu^+ in preference to Zn^{2+}. It is this prediction that underpins the hypothesis that Cu^+ will populate a variety of adventitious sites in the cytosol, potentially including the metal sites of ZiaR, following loss of Atx1. ZiaR can withhold at least one Cu^+ ion per monomer (two per dimer) from BCS; given the Cu^+ affinity of BCS (β_2 = 6.3 x 10^{19} M^{-1} cm) this implies a binding affinity for this Cu^+ ion tighter than the Zn^{2+} site of ZiaR (see section 3.4.6) by at least 8-orders of magnitude. This observation provided support to this prediction; however, the inability to assign affinities to each of the additional Cu^+ sites identified in ZiaR meant that more analyses were required directly comparing Zn^{2+} and Cu^+ binding to the protein. To directly determine which metal bound more tightly to ZiaR, the UV-Visible features of ZiaR were analysed following competitive binding experiments

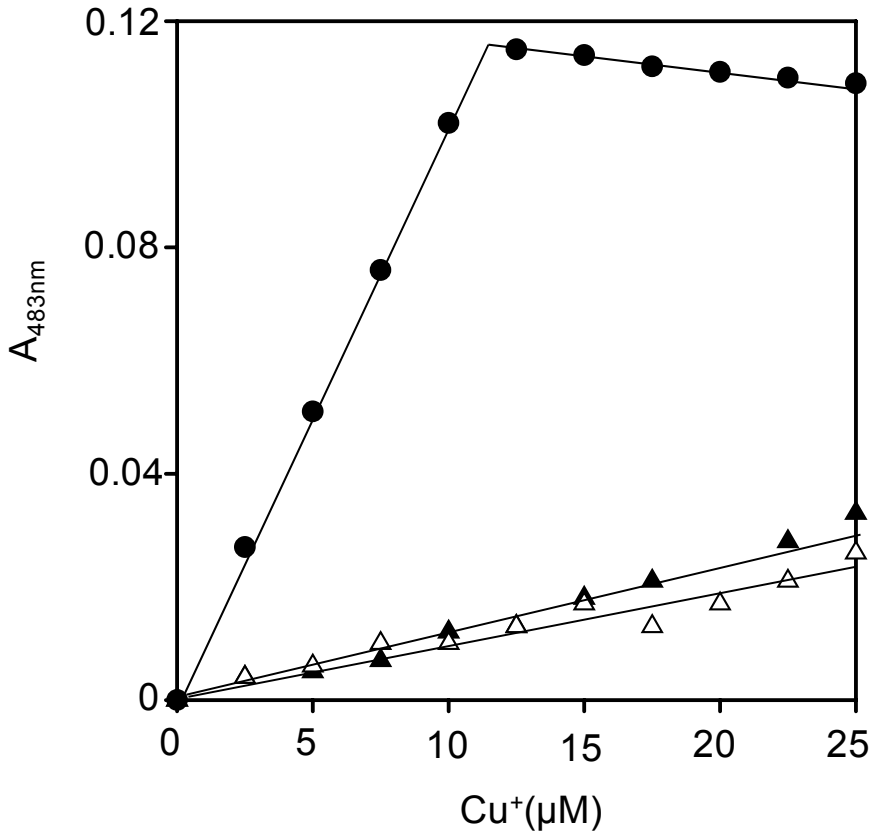

Figure 41. Anaerobic titration of Cu^+ with ZiaR and the Cu^+ chelator BCS. Titration of 25 uM BCS with Cu^+ in the presence (triangles) or absence (closed circles) of ~25 uM ZiaR. The results from two independent experiments are shown. Protein precipitation was observed after addition of 25 uM Cu^+. Conditions: 400 mM KCl, 100 mM NaCl, 10 mM Hepes pH 7.8 Hepes These data were published in Dainty *et al.* 2010.

between Zn^{2+} and Cu^{+} in which the protein was exposed to equimolar amounts of each metal; it was anticipated that the more weakly binding Zn^{2+} would fail to out-compete Cu^{+} at the metal binding sites of ZiaR resulting in spectra analogous to those produced on addition of Cu^{+} alone.

Figure 42 shows the results of several example competitive binding analyses. On titration of ZiaR with equimolar concentrations of Cu^{+} and Zn^{2+} (Figure 42a) the intensity of LMCT features increases up to ~2.5 equivalents of Cu^{+}; light-scattering indicative of protein precipitation was observed at higher metal concentrations. The magnitude of the increase in LMCT intensity at 265 nm is similar to that observed in a control experiment in which ZiaR was titrated with Cu^{+} alone (which is also consistent with values at saturation observed in other titrations of ZiaR (Figure 40) albeit with precipitation again evident after approximately 3.5 equivalents in this experiment) (Figure 42a). When ZiaR was pre-incubated with two equivalents of Zn^{2+}, sufficient to saturate the available protein metal sites, followed by titration with Cu^{+}, LMCT intensities produced (at approximately two equivalents Cu^{+}) were almost identical to those observed following addition of Cu^{+} alone and Zn^{2+} and Cu^{+} simultaneously (Figure 42a, b). These data implied that in the presence of an equimolar concentration of Zn^{2+} and Cu^{+}, Cu^{+} binding to the ZiaR sites monitored in these analyses (up to ~2.5 equivalents of Cu^{+} at least) is not inhibited by Zn^{2+}. Due to protein precipitation at high concentrations of Cu^{+} and Zn^{2+} (i.e. greater than two equivalents of each metal present), it was not possible to determine if this was also the case at the additional Cu^{+} binding sites identified on titration with Cu^{+} alone (Figure 40).

The relative affinities for Zn^{2+} and Cu^{+} of the metal binding sites of ZiaR were investigated further by size-exclusion chromatography. To directly assess metal binding, protein was incubated anaerobically with Cu^{+} and Zn^{2+} and bound and free metal ions resolved by size-exclusion fractionation on Sephadex G-25 matrix. In the example analysis shown in Figure 43, two equivalents of Cu^{+} and two equivalents of Zn^{2+} were added simultaneously to a sample of ZiaR and the UV-Visible spectrum recorded (Figure 43a). LMCT features were observed on addition of metal, with an intensity of 11318 M^{-1} cm^{-1} at 265 nm (Figure 43a), similar to that seen in analyses in which analogous quantities of Cu^{+} were added alone (12683 M^{-1} cm^{-1}) or following protein pre-incubation with Zn^{2+} (10484 M^{-1} cm^{-1}) (Figure 42a, b). A portion of this sample was then removed and fractionated by size-exclusion to resolve bound and free

Figure 42. UV-Visible titrations of ZiaR with Cu^{+} and Zn^{2+}. ZiaR was prepared anaerobically and titrated with Cu^{+} alone or in the presence of Zn^{2+}. A. Change in apo-subtracted difference spectra intensities for ZiaR (23 μM) titrated in the presence of Cu^{+} only (closed symbols) or ZiaR (19 μM) titrated with equimolar concentrations of Cu^{+} and Zn^{2+} (white symbols). Protein precipitation was observed at metal concentrations beyond the final data points for each titration shown. The intensities at 265 nm from an experiment in which ZiaR was preloaded with approximately two equivalents Zn^{2+} and then titrated with Cu^{+} are also shown (red symbols) at zero and 2.2 equivalents Cu^{+} (The corresponding difference spectrum at 2.2 equivalents Cu^{+} is shown in B). Substantial protein precipitation was observed beyond two equivalents of added Cu^{+} (Note: These data points are derived from Zn^{2+}-loaded protein subtracted difference spectra). B. Zn^{2+}-loaded ZiaR subtracted difference spectrum for addition of ~2.2 equivalents of Cu^{+} to ZiaR (23 μM) pre-loaded with approximately two equivalents Zn^{2+} (the molar absorbance at ε_{265nm} is shown in A). These analyses were performed under Hepes buffer conditions identical to those in Figure 40a & b (400 mM KCl, 100 mM NaCl, 10 mM Hepes pH 7.8).

A

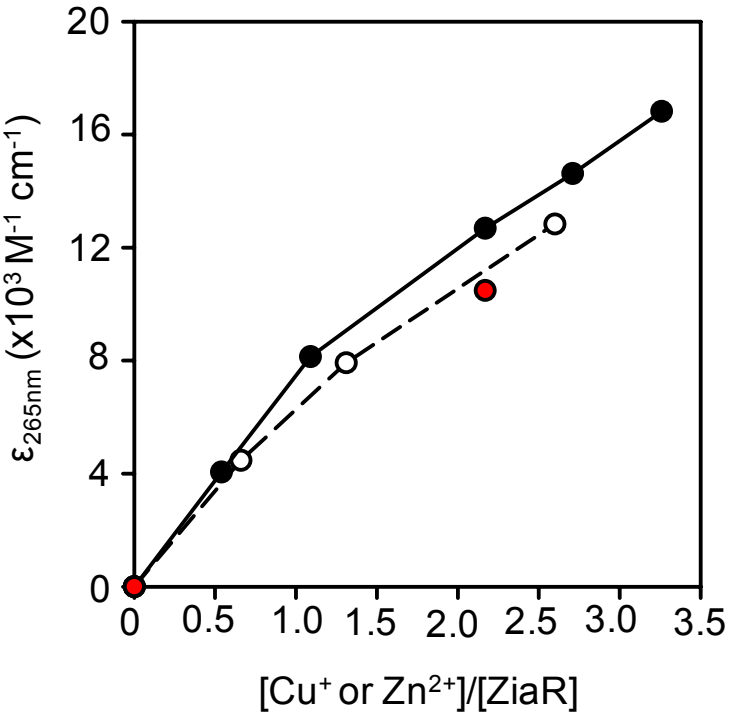
20
16
12
8
4
0
ε_{265nm} (x10^3 M^{-1} cm^{-1})
0
0.5
1.0
1.5
2.0
2.5
3.0
3.5
[Cu^+ or Zn^{2+}]/[ZiaR]

B

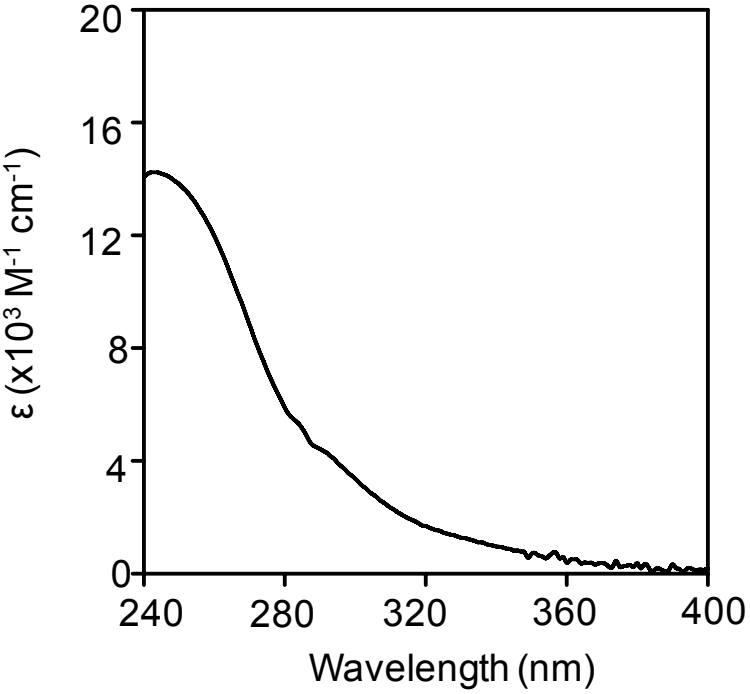
20
16
12
8
4
0
ε (x10^3 M^{-1} cm^{-1})
240
280
320
360
400
Wavelength (nm)

metal ions (Figure 43b). Unexpectedly, approximately 1.3 equivalents of Zn^{2+} was found to be associated with ZiaR in addition to approximately 1.5 equivalents of Cu^{+}.

Additional size-exclusion chromatography analyses confirmed Zn^{2+} association with Cu^{+}-loaded protein. When ZiaR was incubated with four equivalents each of Cu^{+} and Zn^{2+} and bound and free metal ions separated by size-exclusion chromatography, approximately 1.5 equivalents of Cu^{+} and 0.65 equivalents of Zn^{2+} were associated with the protein (Figure 44a). The absence of unbound Cu^{+} ions, expected if two of the four equivalents of added Cu^{+} failed to bind to ZiaR (and a smaller than expected free Zn^{2+} pool) was routinely observed. This may have been due to weak binding of metal ions by the column matrix. Analogous experiments (Figure 44b) in which ZiaR was pre-incubated with Cu^{+}-only also showed Zn^{2+} co-migration with the protein (0.62 equivalents in the analysis shown in Figure 44b). This Zn^{2+} was likely derived from size exclusion buffers which were not routinely chelex-treated. Co-migration of up to 0.64 equivalents of Zn^{2+} in the presence of Cu^{+} was also observed on replication of these assays in Hepes buffer (Appendix C Figure 1); this suggests that Zn^{2+} binding in the presence of Cu^{+} was not correlated with a potentially increased buffer chelation capacity in the presence of Tris-HCl, the conditions used for analyses shown in Figure 44 (this is also supported by data in Figure 43 showing Zn^{2+} co-migration with Cu-bound ZiaR under Hepes buffer conditions). These observations suggested the presence a non-thiol (Figure 43) metal site on ZiaR, able to bind Zn^{2+}, whilst other sites on the protein are simultaneously occupied by Cu^{+}.

During the course of these investigations, characterisation of the highly similar ArsR-SmtB protein BxmR revealed this protein to have a unique division of metal binding properties between its metal sites (Liu *et al.* 2008). Like ZiaR, BxmR has α3N and α5 sites which are fully functional to bind metal with strong allosteric regulation retained at each site. Critically, these sites are hypothesised to have distinct metal specificities; the α3N site appears to accommodate both divalent and monovalent metal ions (including Cu^{+} and Zn^{2+}), whereas the α5 site appears only to bind divalent metal ions with no binding of Cu^{+} to this site. Cu^{+} binding to the α3N site takes the form of a binuclear Cu^{+}_{2}-S_4 complex; two Cu^{+} ions were shown to bind each BxmR dimer subunit, recruiting a pair of cysteines from each subunit in the dimer (Liu *et al.* 2008). This model was consistent with many of the Cu^{+} and Zn^{2+} binding features observed for ZiaR in these studies. Binding of two equivalents of Cu^{+}/monomer (four per dimer) is observed, although adventitious binding of Cu^{+} to additional sites was implied by the

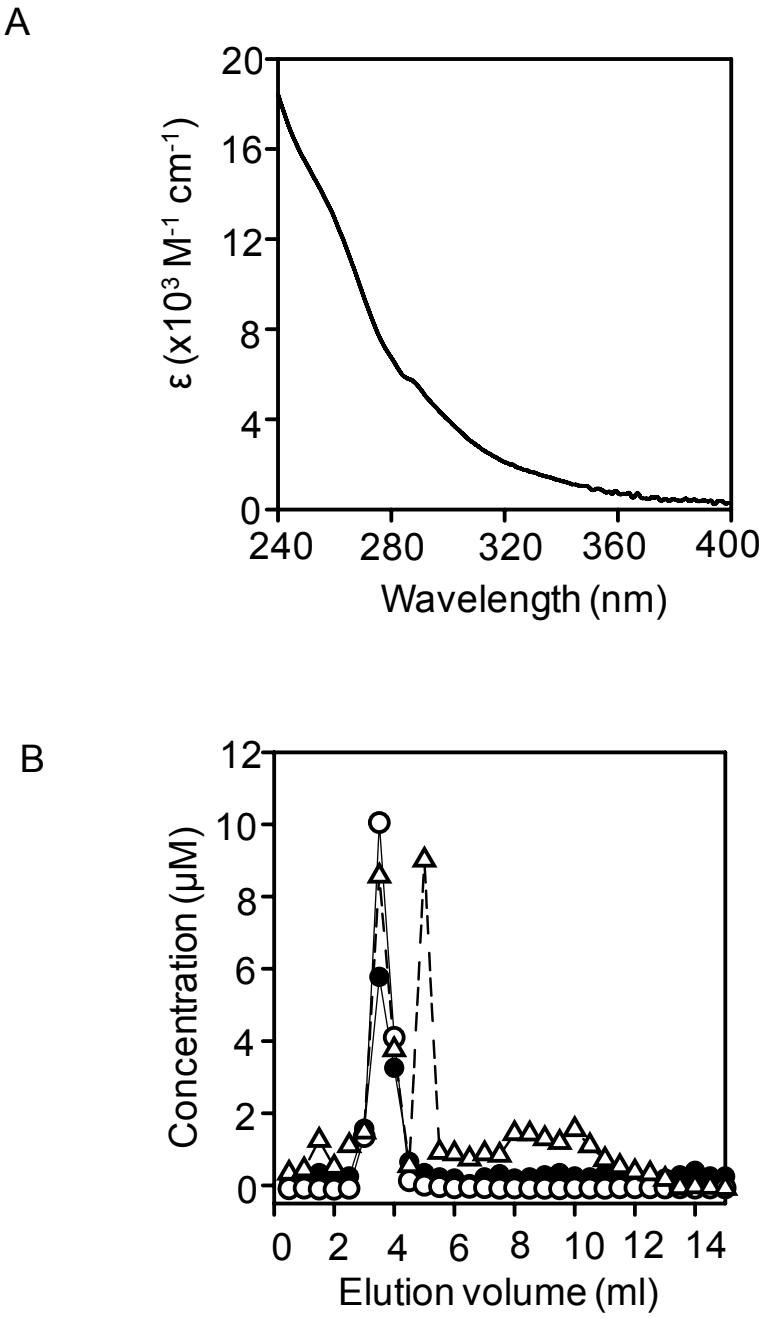

Figure 43. Zn^{2+}/Cu^{+} binding to ZiaR measured by UV-Visible titration and size-exclusion chromatography. ZiaR (23 μM) was prepared anaerobically and approximately two equivalents of Zn^{2+} and Cu^{+} were added in an anaerobic chamber. A. Apo-subtracted difference spectrum recorded following addition of 2.2 equivalents Cu^{+} and 2.2 equivalents of Zn^{2+}. B. A sample from the analysis in A was removed and bound and free metal ions separated by size-exclusion fractionation on Sephadex G-25 matrix. The concentrations of protein in each fraction were determined by Coomassie assay (closed symbols) and metal concentrations (Zn^{2+}; triangles, Cu^{+} open circles) were determined by ICP-MS (Conditions: 400 mM KCl, 100 mM NaCl, 10 mM Hepes pH7.8).

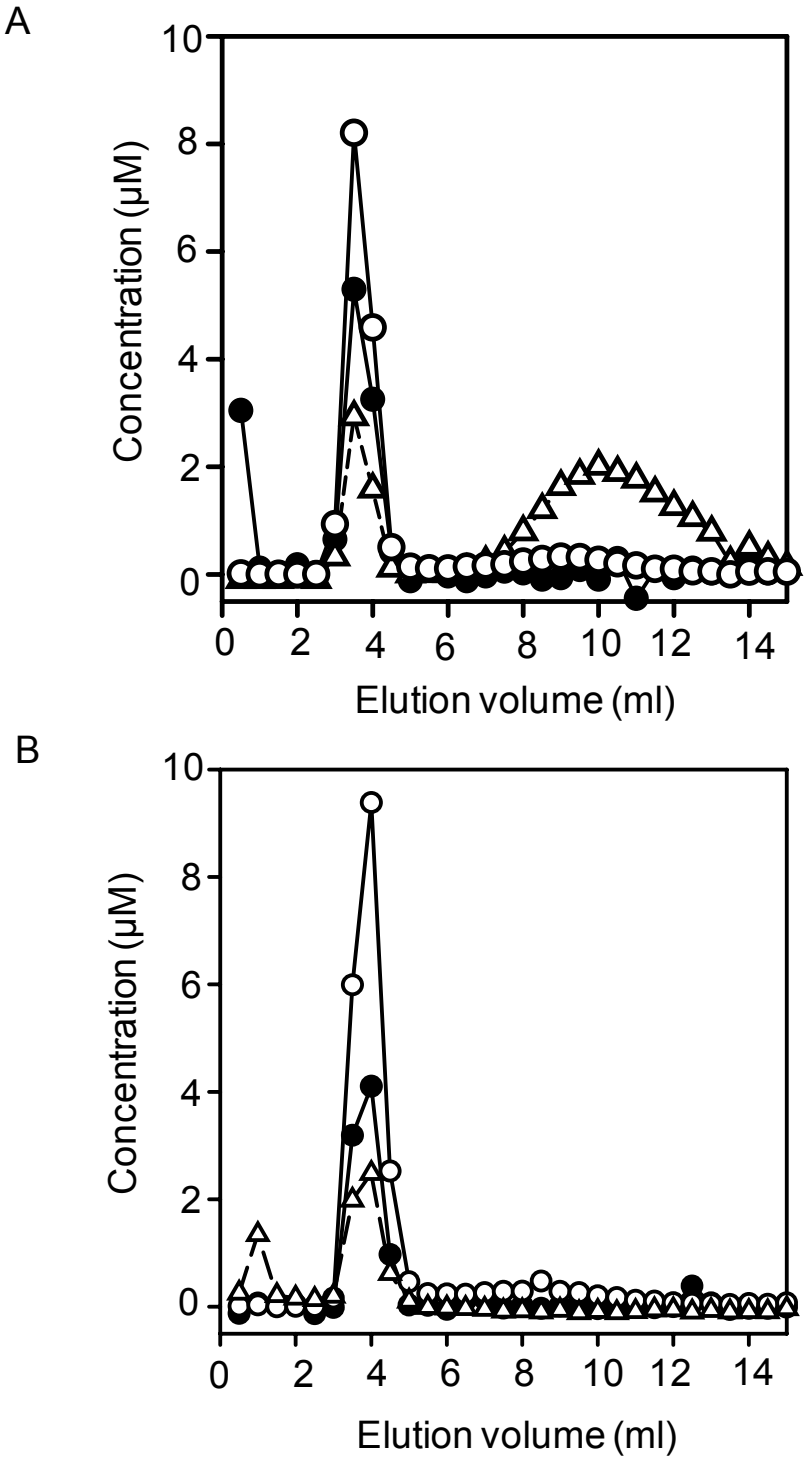

Figure 44. Size-exclusion fractionation of ZiaR-bound and free Cu^{+} and Zn^{2+} ions. ZiaR (~10μM) was prepared anaerobically and incubated with approximately four equivalents of Cu^{+} and Zn^{2+} (A) or with four equivalents of Cu^{+} only (B). Bound and free metal ions were resolved using Sephadex G-25 matrix and protein concentrations (closed symbols) determined by Coomassie assay and metal concentrations (Cu^{+}; open circles, Zn^{2+}; open triangles) were determined by ICP-MS analysis. Conditions: 500 mM NaCl, 10 mM Tris pH 7.5.

larger binding stoichiometry compared to BxmR (Figure 40a, b). The apparent binding of up to one equivalent of Zn^{2+}, almost certainly to the α5 sites of ZiaR in the presence of Cu^{+}, as shown by UV-Visible titrations and size-exclusion analyses (Figure 43) also supported a BxmR-like model.

The BxmR model predicted differential partitioning of monovalent and divalent metal ions between the α3N and α5 sites of ZiaR, with the α5 site free to bind metal ions in the presence of a fully Cu^{+}-saturated α3N site. This prediction was tested directly by UV-Visible analyses. On addition of two equivalents of Cu^{+} to apo-ZiaR, LMCT features were produced with an intensity of 14431 M^{-1} cm^{-1} at 265 nm which was comparable to values routinely observed for titration of ZiaR with Cu^{+} (12833 M-1 cm-1 in Figure 40b) at this number of added equivalents of Cu^{+} (Figure 45, black line). A single equivalent of Co^{2+} was then added to this protein sample and the spectrum re-recorded. The addition of Co^{2+} had negligible effect on the intensity of the LMCT features however, a feature indicative of *d-d* transitions appeared with a maximum intensity, in the 500-600 nm wavelength range, of approximately 400 M^{-1} cm^{-1} (Figure 45). These data are consistent with the two equivalents of Cu^{+} populating the α3N site with the Co^{2+} excluded from this site (as there is little change in the LMCT signal) and thus binding to the free α5 sites, producing *d-d* transition features analogous in intensity to those observed following addition of Co^{2+} to ZiaR (Figure 10) and to Δα3ZiaR (Figure 14) (in which binding to the α5 site only was detected). Interestingly, the *d-d* feature is also similar in shape to the low-complexity feature observed following titration of Δα3ZiaR with Co^{2+} (Figure 14); as was postulated for Δα3ZiaR, this is likely due to loss of red-shifted features in this wavelength range usually associated with sulphur-rich Co^{2+} coordination spheres.

Therefore, these studies suggest a BxmR-like model for Cu^{+} binding to ZiaR with the α3N site exclusively binding Cu^{+}. Crucially, the data in Figure 45 also suggest a binuclear Cu^{+} site similar to that in BxmR. In BxmR, the two Cu^{+} ions are each coordinated in a trigonal geometry by two cysteine residues and a single Cu-Cu bond (Liu *et al.* 2008). In this metal centre, the two pairs of cysteine residues are derived from separate subunits within the dimer (Figure 46a) (Liu *et al.* 2008). LMCT intensities observed following titration of ZiaR with Cu^{+} would suggest the formation of up to three Cu^{+}-cysteine bonds per monomer (Figure 40a,b), as opposed to the four Cu-S^{-} bonds formed per BxmR monomer. One of the cysteine residues involved in Cu^{+} binding in BxmR (Cys-31) is not present in the α3N site of ZiaR, which is consistent

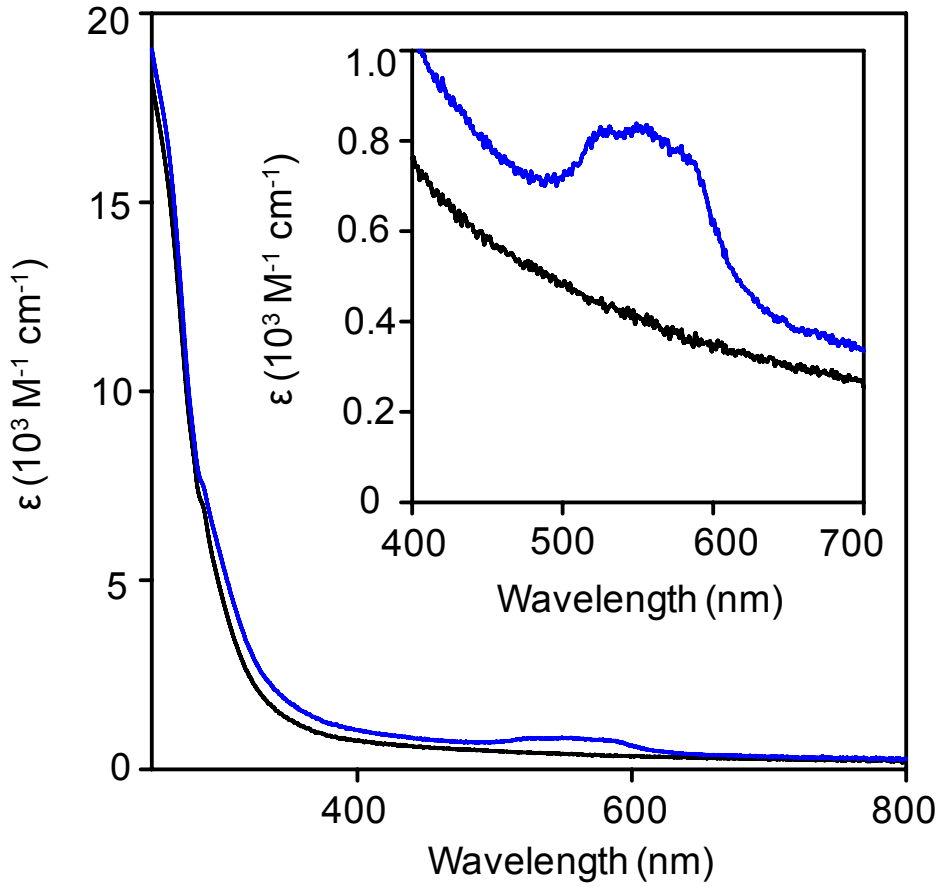

Figure 45. UV-Visible titration of ZiaR with Cu^{+} and Co^{2+}. Apo-subtracted difference spectra produced following addition of two equivalents Cu^{+} (black line) followed by a single equivalent of Co^{2+} (blue line) to ZiaR (38 μM) under anaerobic conditions. The region of the spectrum between 400-700 nm has been rescaled to show the *d-d* transitions produced on Co^{2+} binding more clearly (*inset*). Conditions: 400 mM KCl, 100 mM NaCl, 10 mM Hepes pH 7.8.

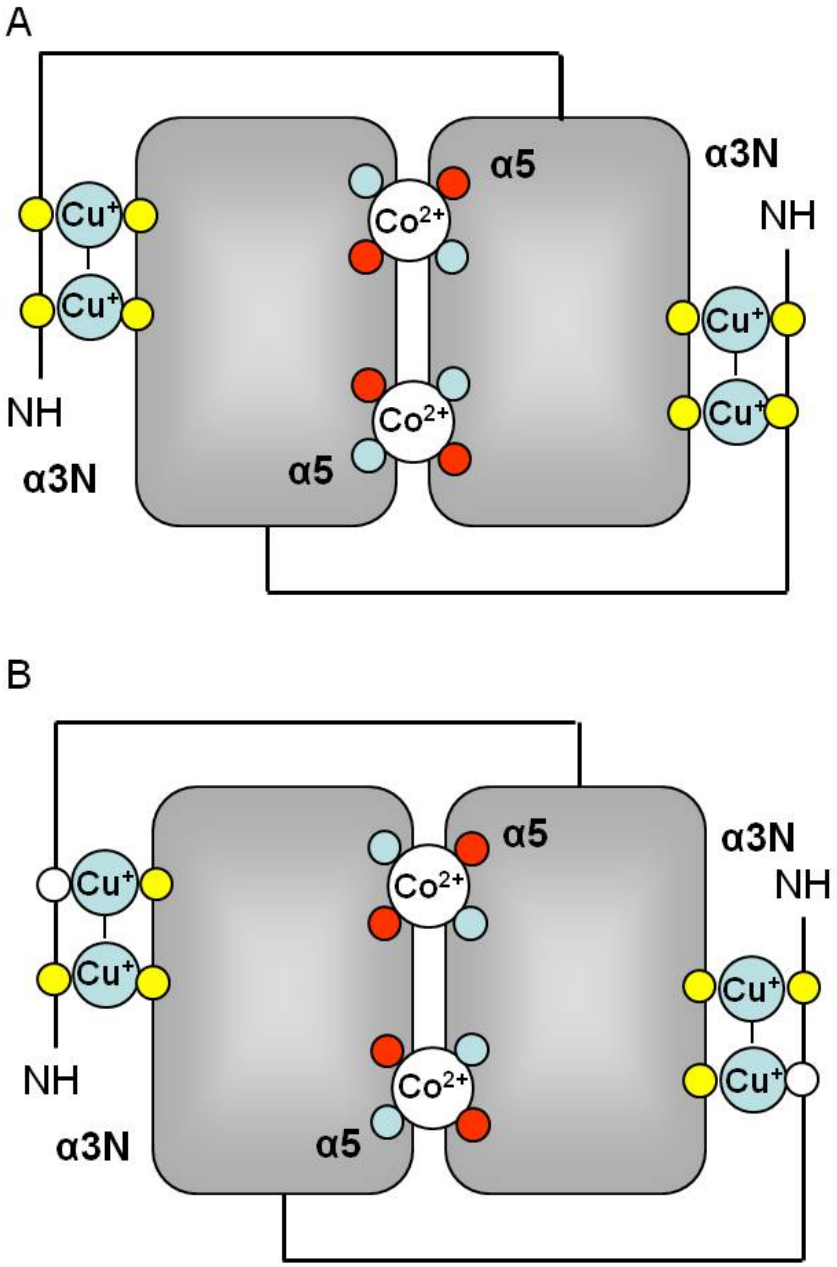

Figure 46. Models for Cu^+ binding to BxmR and ZiaR. A. In BxmR each α3N site contains four cysteine residues (yellow circles) which ligate two Cu^+ ions in a Cu_2S_4 complex. B. The α3N site of ZiaR contains only three of the four conserved cysteine residues found in BxmR. Data in this work suggests each α3N site can accommodate two Cu^+ ions (as for BxmR). However, UV-Visible data would suggest that no more than three Cu-S^- bonds per monomer are formed, consistent with involvement of fewer α3N cysteines in ZiaR. Involvement of an additional ligand (white circle) (e.g. the α3N histidine) cannot be ruled out. In the models shown in A and B the α5 sites are shown to bind Co^{2+} (simultaneously with Cu^+ binding at the α3N sites) in a tetrahedral geometry involving two histidines (blue circles), an aspartate and a glutamate residue (red circles (these ligand assignments are based on residues conserved in the α5 site of SmtB. The extent to which Cu^+ can bind to the α5 sites is unclear.

with the expectation of a maximum of three Cu^{+}-S^{-} bonds, utilising all three α3N cysteines, per ZiaR monomer. A cysteine residue is located elsewhere in the extended N-terminal arm of ZiaR (Cys-12) which could potentially be recruited with the *bone fide* α3N cysteine residues to ligate Cu^{+}. However, the maximum intensities of LMCT features observed at full Cu^{+} saturation would argue against this. Another non-thiol ligand may be recruited to accommodate trigonal coordination of each ion (perhaps His-26 or Glu-28 residue which are the likely ligands for divalent metal ions in the α3N site of ZiaR). Alternatively, perhaps one of the Cu^{+} ions in each centre is coordinated digonally in a Cu-Cu, Cu-S arrangement (Figure 46b).

The binding of the first Cu^{+} ion to the α3N site of ZiaR site must be the binding event shown to compete with the Cu^{+} chelator BCS (Figure 41). It is noted that this site has an affinity substantially tighter than the reported average step-wise Cu^{+} binding affinity reported for BxmR of approximately $1x10^{7}$ M^{-1} (Liu *et al.* 2008) and is consistent with a value minimally in the 10^{19} M^{-1} range reported for the $Cu^{+}_{2}S_{4}$ centre in MTF-1 from *Drosophilia melanogaster* (Chen *et al.* 2008). However, the value quoted for BxmR was determined from fitting of Cu^{+} binding data from UV-Visible titrations performed with protein and Cu^{+} concentrations in the micromolar range, and hence is likely a substantial underestimate of the true affinity. No competition assays with Cu^{+} binding chelators have been undertaken for BxmR.

5.1.4 Cu^{+} is less allosterically effective than Zn^{2+}

It was shown that Zn^{2+} both impairs association of ZiaR with DNA (section 3.4.4) and also promotes disassociation of ZiaR-DNA complexes (section 3.4.5). A prediction based on the BxmR-like Cu^{+} binding model outlined in Figure 46 was that if Cu^{+} was allosterically effective in a manor analogous to that of Zn^{2+} addition of at least two equivalents of Cu^{+} to a ZiaR-DNA complex would be sufficient to promote disassembly of ZiaR-DNA complexes. If Cu^{+} was able to cause a reduction in DNA binding affinity analogous to that of Zn^{2+} (of at least three orders of magnitude; Figure 16) no DNA-protein complexes would be evident after two equivalents of added Cu^{+}. This prediction was tested by anaerobic titration of ZiaR-DNA complexes with Cu^{+}. The example data shown in Figure 47 shows three replicate experiments performed under identical conditions together with a control Zn^{2+} titration. As observed in other analyses (Figure 18, section 3.4.5) a single equivalent of Zn^{2+} was sufficient to promote effectively

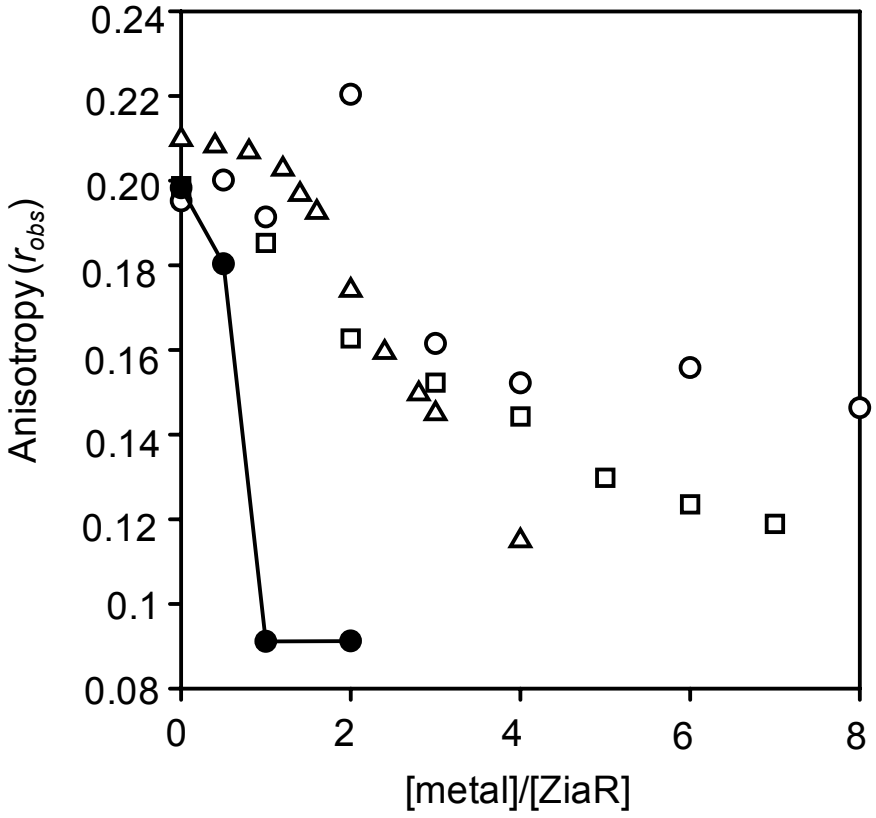

Figure 47. Titration of pre-formed ZiaR-DNA complexes with Cu^{+} and Zn^{2+}. In each experiment 1 μM ZiaR was prepared anaerobically and added to 10 nM *zia* O/P oligonucleotide DNA in a quartz cuvette. These complexes were then titrated with Cu^{+} (open symbols). The results of three independent experiments are shown. Also shown is a titration of ZiaR-DNA complexes with Zn^{2+} (closed symbols) using the same protein preparation as used for two of the Cu^{+} replicates (Conditions 120 mM KCl, 30 mM NaCl, 10 mM Hepes pH 7.8). These data were published in Dainty *et al.* 2010 (Appendix E).

complete protein-DNA complex disassembly and reduction of anisotropy values to those diagnostic of free DNA of this size. For Cu^{+}, although there is a high degree of variability between the datasets, it can be seen that complete reduction of anisotropy was never achieved with much smaller changes in anisotropy per equivalent of Cu^{+} added. Even after addition of up to eight equivalents of Cu^{+} (substantially more than the maximum saturating Cu^{+} stoichiometry from UV-Visible titrations shown in Figure 40) complete disassociation of protein-DNA complexes was not observed. Cu^{+} is therefore less effective than Zn^{+} in reducing the DNA binding affinity of ZiaR and disassociating ZiaR-DNA complexes. Association experiments performed in the presence of Cu^{+} could not be performed due to the tendency of ZiaR to precipitate at the high concentrations of protein and Cu^{+} necessary under the conditions used for fluorescence anisotropy.

An implication of the BxmR-like model for Cu^{+} binding to ZiaR is that binding of Cu^{+} to the protein (via its α3N sites) will leave the α5 sites free to bind Zn^{2+}, which as shown in Figure 18 (section 3.4.5) are fully functional to initiate allostery. Moreover, data presented in Figure 45 also support the notion that Cu^{+} does not impede the formation of the tetrahedral coordination geometry adopted Co^{2+}, and by inference Zn^{2+}, at the α5 sites that likely underpins allosteric switching at this site. Therefore, Zn^{2+} was anticipated to initiate allostery and impair DNA binding in Cu^{+}-bound ZiaR. A single experiment in which ZiaR-DNA complexes were titrated with equimolar concentrations of Zn^{2+} and Cu^{+} showed complete disassociation of complexes at approximately one equivalent of Zn^{2+}/Cu^{+} (Appendix C Figure 2). These data are similar to those observed for titration with Zn^{2+} alone however additional replication would be required to quantify this stoichiometry.

5.2 The *in vivo* Zn^{2+} and Cu^{+} responses of wild-type and Δatx1 strains of *Synechocystis*

Prior to these studies it was anticipated that because of their different preferred coordination geometries, Cu^{+} would be a much poorer allosteric effector than Zn^{2+} (Harvie *et al.* 2006). Data from DNA binding analyses confirmed this hypothesis (Figure 47). However, the presence of multiple sites on ZiaR with different metal binding preferences, resulting in ZiaR having an unusual ability to bind both Zn^{2+} and Cu^{+} with wild-type like Zn^{2+} regulation apparently retained in the Cu^{+} bound form (Appendix C Figure 2), was unexpected. Comparative analyses of the *in vivo* responses

of ZiaR in wild-type and Δ*atx1* strains of *Synechocystis* (in which data were collected by Samantha Dainty) were performed subsequent to the studies presented in Figures 39-47 to determine if any deleterious effect on *zia* regulation could be detected that would be attributable to the loss of Atx1 function. For cells of both wild-type and Δ*atx1* strains of *Synechocystis* no copper dependent increase in expression from the *zia* promoter was detected following copper treatment and no inhibition of a Zn^{2+}-dependent increase in expression was observed (see section 7.1), a result consistent with *in vitro* data showing Cu^{+} to be less allosterically effective than Zn^{2+} (Figure 47) and ZiaR able to bind both metals simultaneously (Figure 43-44) with retention of Zn^{2+}-mediated allostery even in Cu_2-ZiaR (Appendix C Figure 2). Expression from the *zia* promoter was consistently higher in the Δ*atx1* strain implying enhanced formation of Zn^{2+}-ZiaR rather than Cu^{+}-ZiaR in this strain (see section 7.1). In subsequent studies it was shown that recombinant Zn^{2+}-Atx1 could be isolated from *E.coli* cells grown with Zn^{2+} supplementation (see section 7.1). Even after copper supplementation, recombinant Zn^{2+}-Atx1 could still be recovered. Taken together these data suggested that Zn^{2+}-Atx1 can form *in vivo* (Dainty *et al.* 2010).

5.3 The *in vitro* and *in vivo* Cu^{+} binding properties of Zur_{SS}

Although the comparison of responses of ZiaR regulated promoters between wild-type and Δ*atx1* strains of *Synechocystis* showed an unexpected role for Atx1 in Zn^{2+} binding and homeostasis, no evidence was found that Cu^{+} normally bound to Atx1 in wild-type *Synechocystis* cells caused aberrant regulation at ZiaR controlled promoters in Δ*atx1* cells. Cu^{+} may not bind to ZiaR in Δ*atx1* cells or Cu^{+} may bind but have negligible effect on the Zn^{2+} response of ZiaR due to the presence of α5 sites on the protein available to bind Zn^{2+}. It was postulated that the presence of a single allosteric site on the Zur_{SS} protein may simplify interpretation of data from analyses examining the effects of copper on *znu* expression *in vivo*. Therefore, the *in vitro* Cu^{+} binding properties and the *in vivo* functional responses of Zur_{SS} were investigated.

5.3.1 Cu^{+} binds to Zur_{SS} via multiple cysteine residues

The allosteric site of Zur_{SS} contains at least one cysteine residue (Figure 28). Cu^{+} binding to the allosteric site was therefore expected to produce LMCT features

detectable by UV-Visible spectroscopy. Following UV-Visible spectral analyses in which Cu^{+} was titrated with Zn_1Zur_{SS}, LMCT features were observed diagnostic of Cu^{+}-S^{-} bond formation (Figure 48a). The intensity of the LMCT signal at 265 nm increases linearly to approximately one equivalent of Cu^{+} at which point there is a sharp upward inflection in intensity (Figure 48b). This initial increase is likely reporting on Cu^{+} binding to the single cysteine residue in the allosteric site, with recruitment of additional cysteine residues occurring after one equivalent. The molar extinction coefficient of approximately 7800 M^{-1} cm^{-1} at 265 nm would be consistent with binding to at least one cysteine residue at a single equivalent of Cu^{+}. Protein precipitation was observed beyond two equivalents of Cu^{+} and this effect is likely to have contributed to the elevated absorbance values, observed at all the wavelengths measured, approaching two equivalents of Cu^{+}.

5.3.2 UV-Visible spectroscopy and size-exclusion chromatography reveal Cu^{+} binding to Zur_{SS} in preference to Zn^{2+}

Following pre-incubation of Zn_1Zur_{SS} with a single equivalent of Cu^{+}, the UV-Visible spectrum was recorded and a single equivalent of Zn^{2+} added to the reaction. The UV-Visible spectrum was then re-recorded (Figure 49a). Negligible changes in the intensity of the Cu-dependent LMCT features were observed following addition of Zn^{2+} and there was no decrease in LMCT intensity that would be consistent with replacement of Cu^{+} by Zn^{2+}. Additionally, simultaneous addition of one equivalent each of Cu^{+} and Zn^{2+} produced LMCT features with intensities similar to those observed following addition of Cu^{+}, indicating that Cu^{+} can also out compete Zn^{2+} for binding to Zn_1Zur_{SS} (Figure 49a). These data are therefore consistent with Cu^{+} binding in preference to Zn^{2+} at the exchangeable metal binding site monitored in this assay.

To verify preferential binding of Cu^{+} to the allosteric site of Zur_{SS}, Zn_1Zur_{SS} was incubated with metal and bound and free species resolved by size-exclusion chromatography. Following incubation with two equivalents of Cu^{+} (20 μM) approximately two equivalents of Cu^{+} were found to be associated with the protein (Figure 49b), implying all of the added Cu^{+} had been bound by Zn_1Zur_{SS}. This was anticipated from UV-Visible analyses (Figure 48) which showed a continued increase in LMCT intensity beyond one equivalent of Cu^{+}. Crucially, approximately one equivalent of Zn^{2+} was also associated with the protein; no Zn^{2+} was added to the binding reaction

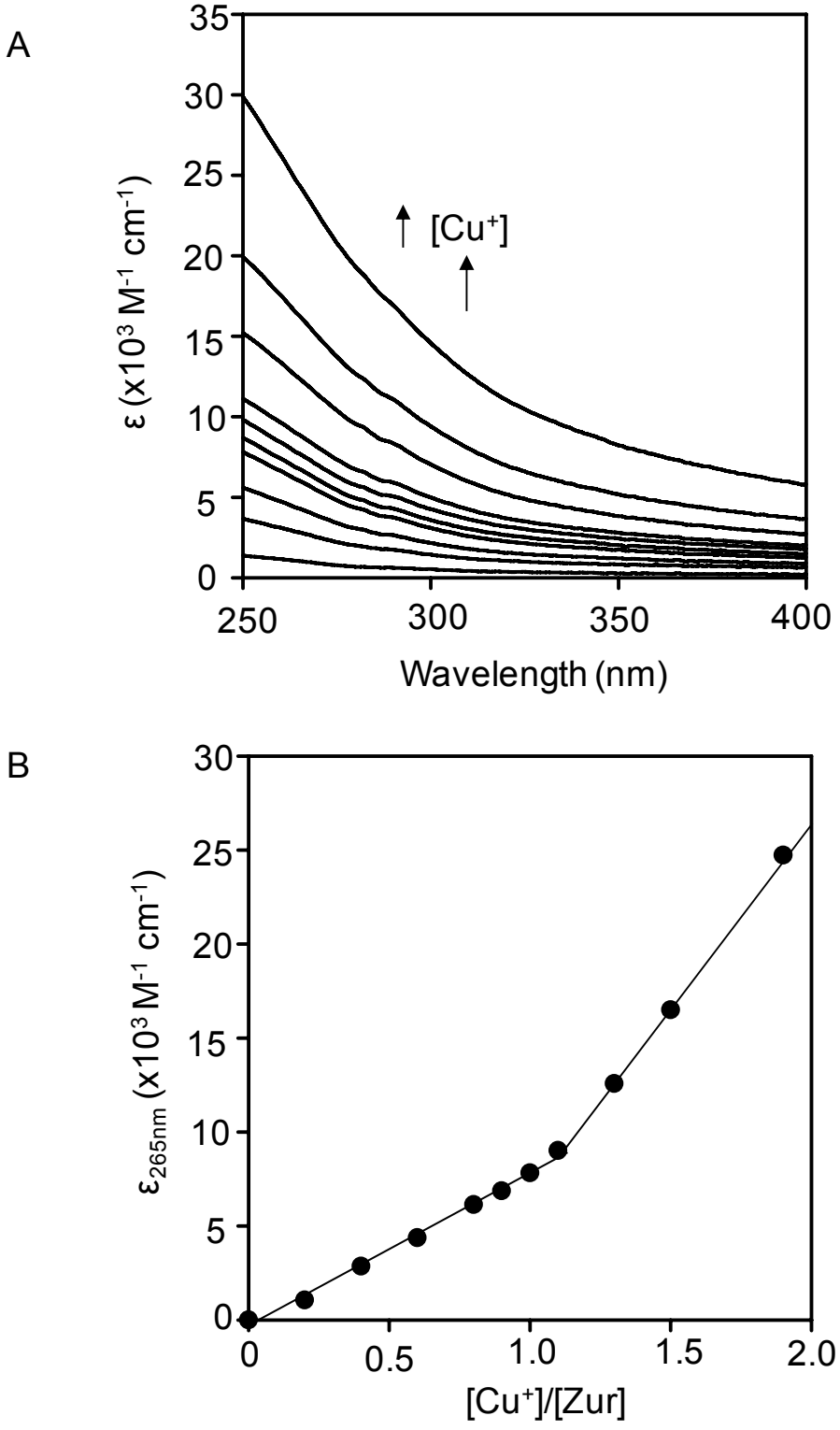

Figure 48. UV-Visible titration of Zur_{SS} with Cu^{+}. Approximately 25 μM of Zn_1Zur_{SS} was titrated with Cu^{+} under anaerobic conditions and the changes in absorbance measured. A. Apo-protein subtracted difference spectra produced on titration with Cu^{+}. B. Changes in apo-subtracted absorbance intensity measured at 265 nm with increasing $[Cu^{+}]$. Conditions: 400 mM KCl, 100 mM NaCl, 10 mM Hepes pH 7.8.

Figure 49. Measurement of the relative binding affinity of Zur_{SS} for Zn^{2+} and Cu^{+} by UV-Visible titration and size-exclusion chromatography. A. Anaerobic UV-Visible titration of Zn_1Zur_{SS} with Cu^{+} and Zn^{2+}. The black trace represents the apo-subtracted difference spectrum produced following addition of one equivalent (10 μM) of Cu^{+} to 10 μM protein. One equivalent of Zn^{2+} was then added to the reaction and the absorbance re-measured (blue line). The red line shows the apo-subtracted difference spectrum from an analogous experiment in which one equivalent (10 μM) of Cu^{+} and Zn^{2+} were added simultaneously to a sample of Zn_1Zur_{SS} (~10 μM). B. Zn_1Zur_{SS} (10 μM) was incubated under anaerobic conditions with two equivalents (20 μM) of Cu^{+} and then bound and free metal separated on Sephadex G-25 matrix (closed circles protein, open circles Cu^{+}, open triangles Zn^{2+}). C. Identical experiment to that shown in A, but with Zn_1Zur_{SS} pre-incubated in equimolar Zn^{2+} and Cu^{+} (each at 10 μM) prior to fractionation. Conditions: 400 mM KCl, 100 mM NaCl, 10 mM Hepes pH 7.8.

A

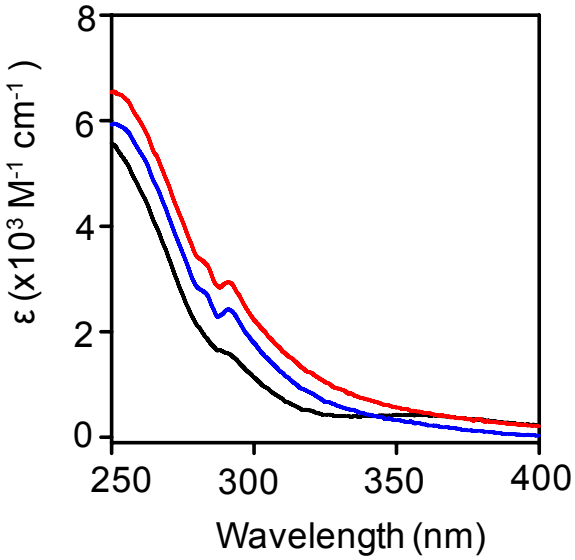
8
6
4
2
0
ε (x10³ M⁻¹ cm⁻¹)
250
300
350
400
Wavelength (nm)

B

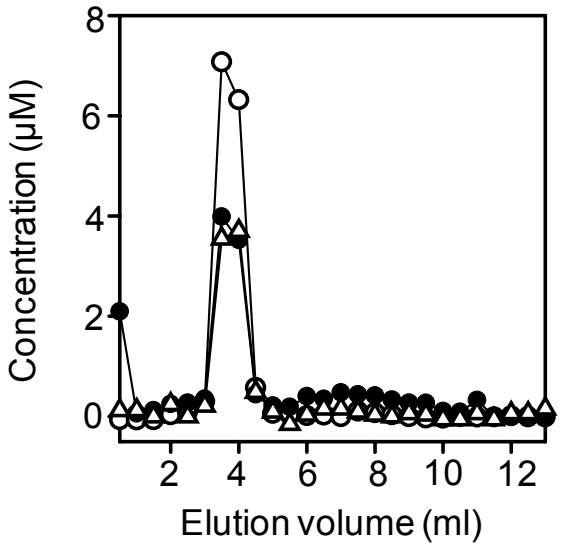
8
6
4
2
0
Concentration (μM)
2
4
6
8
10
12
Elution volume (ml)

C

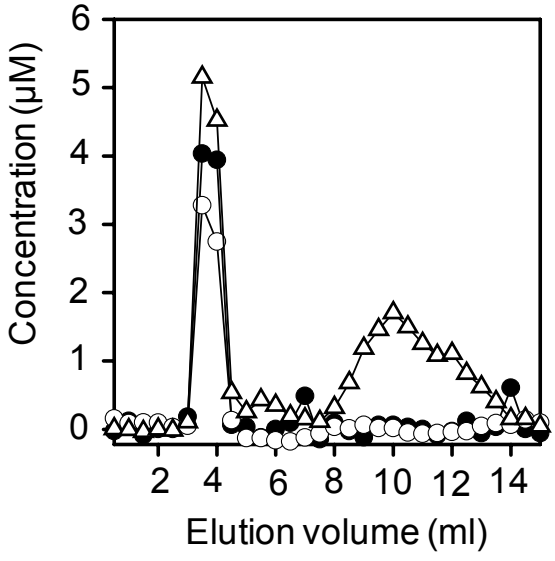
6
5
4
3
2
1
0
Concentration (μM)
2
4
6
8
10
12
14
Elution volume (ml)

however ICP-MS analysis of a sample of this anaerobic protein preparation prior to incubation with Cu^{+} confirmed the presence of approximately 0.92 equivalents Zn^{2+}. This Zn^{2+} almost certainly represents the structural Zn^{2+} ion in the protein and so these data imply that at these concentrations, Cu^{+} cannot replace the tightly bound structural Zn^{2+} ion in Zur_{SS}. Following size-exclusion fractionation of Zn_1Zur_{SS} incubated with a single equivalent of each metal (10 μM), 1.23 equivalents of Zn^{2+} was associated with the protein (consistent with approximately one equivalent of structural Zn^{2+} measured in a sample of this protein preparation prior to fractionation-see above) and 0.77 equivalents of Cu^{+}. Approximately 12 μM of Zn^{2+} is present as unbound metal, which implies that effectively all of the added Zn^{2+} failed to bind to the protein (Figure 49c). The allosteric site is predominantly occupied by Cu^{+}. Similar stoichiometries were observed in replicate experiments (see Appendix C Figure 3). These data confirm that the allosteric site in Zur_{SS} has a higher affinity for Cu^{+} than for Zn^{2+}.

5.4 Effects of Cu^{+} on the DNA binding properties of Zur_{SS}

The effects of Cu^{+} on the DNA binding affinity of Zur_{SS} were monitored by fluorescence anisotropy. Recombinant Zn_1Zur_{SS} was incubated in the presence of either EDTA or metal and was then titrated with *znu* O/P oligonucleotide under anaerobic conditions. Titration of DNA with Zn_1Zur_{SS} pre-incubated in 1.5 equivalents Zn^{2+} showed high affinity DNA binding (Figure 50a) with r_{obs} and K_{DNA} values similar to those observed previously (section 4.4.3, Figure 37). Zn_1Zur_{SS} protein that was pre-incubated in 2 mM EDTA exhibited a weaker DNA binding affinity, although some degree of binding was observed approaching 1 μM protein in this analysis (Figure 50a). To analyse the effects of Cu^{+} on DNA binding, Zn_1Zur_{SS} was pre-incubated in 1.5 equivalents of Cu^{+} and titrated with DNA in the presence of Cu^{+} (Figure 50b). It was reasoned that the trace amounts of buffer Zn^{2+}, shown in these studies to be sufficient to promote Zn_1Zur_{SS} association with DNA (section 4.4.3 Figure 37), would have negligible impact on these data because of the tighter affinity of the Zur_{SS} allosteric site for Cu^{+}. The binding isotherm for Cu^{+}-bound Zn_1Zur_{SS} is shifted compared to that for Zn_2Zur_{SS}, consistent with a weakening of the DNA binding affinity by approximately an order of magnitude in the presence of Cu^{+} (Figure 50b). However, at protein concentrations greater than approximately 100 nM, binding to DNA was observed with the magnitude of increase in r_{obs} larger than that observed at corresponding

concentrations of Zn_1Zur_{SS} pre-incubated in Zn^{2+} (Figure 50b). This may be due to Cu^+-mediated formation of higher order protein complexes on DNA, much larger than those normally observed on titration in the presence of Zn^{2+}.

The apparent binding preference of the allosteric site of Zur_{SS} for Cu^+ over Zn^{2+} (Figure 49a-c) predicted that following exposure to both metals, Zn_1Zur_{SS} would preferentially bind Cu^+ at this site producing a DNA binding isotherm analogous to that observed following incubation with Cu^+ alone. Following incubation of Zn_1Zur_{SS} with 1.5 equivalents of each metal and titration of DNA with the protein in the presence of equimolar concentrations of each metal, such an effect was observed. In the example data shown in Figure 50b, binding curves for Cu^+ alone and Cu^+/Zn^{2+} treatments were effectively identical. A tighter binding affinity for DNA was observed on replication (Appendix C Figure 4), however, the K_{DNA} for Zur_{SS} under these conditions was still substantially weaker than that measured following incubation with Zn^{2+}. These data are consistent with Cu^+ binding to the allosteric site of Zn_1Zur_{SS} in preference to Zn^{2+} and inhibiting Zn^{2+}-mediated binding to DNA. Subsequent to these studies, *in vivo* analyses (performed by Samantha Dainty) of *znuA* expression in cells of a Δ*atx1*Δ*gshB* strain of *Synechocystis* implied inhibition of Zn^{2+}-mediated repression of *znuA* expression in a Δ*atx1*Δ*gshB Synechocystis* mutant (see section 7.1).

Figure 50. Comparing the effects of Cu^{+} and Zn^{2+} on the DNA binding affinity of Zur_{SS} by fluorescence anisotropy titrations. A. Control anaerobic titration in which Zn_1Zur_{SS} was titrated with 10 nM *znu* O/P oligonucleotide following either pre-incubation with Zn^{2+} (1.5 equivalents) (closed symbols) or with 2 mM EDTA (open symbols). B. Analogous titration to that shown in A, performed on the same day and under identical conditions, in which Zn_1Zur_{SS} was titrated with 10 nM oligonucleotide following pre-incubation with either 1.5 equivalents Cu^{+} or 1.5 equivalents of Cu^{+} and Zn^{2+} (in both cases each metal was also present in the cuvette at a concentration of 3.5 μM). Conditions: metal was pre-incubated with protein in 400 mM KCl, 100 mM NaCl, 10 mM Hepes (pH 7.8) and protein then titrated with 10 nM DNA in buffer 120 mM KCl, 30 mM NaCl, 10 mM Hepes (pH 7.8).

A

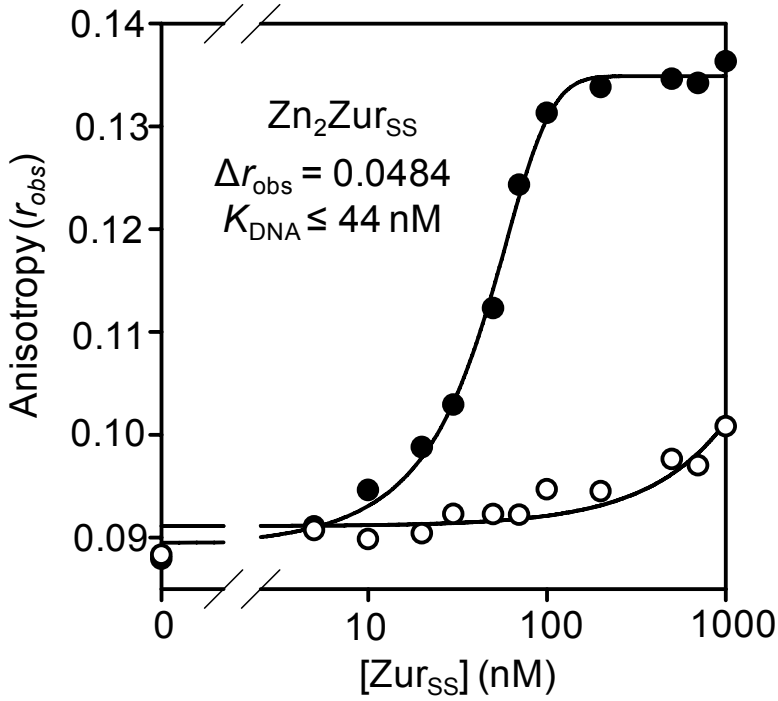
0.14
0.13
0.12
0.11
0.10
0.09
Anisotropy (r_{obs})
Zn_2Zur_{SS}
Δr_{obs} = 0.0484
K_{DNA} ≤ 44 nM
0
10
100
1000
[Zur_{SS}] (nM)

B

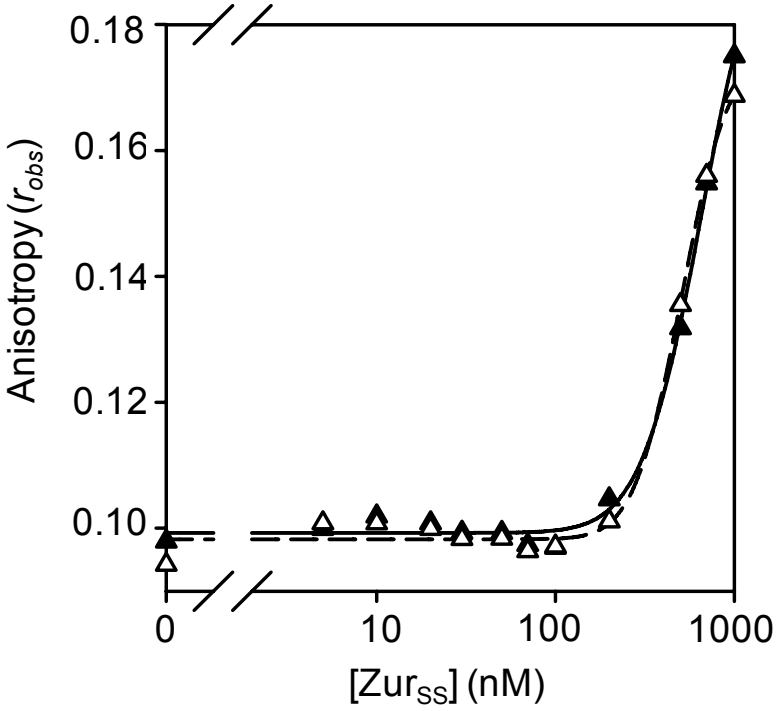
0.18
0.16
0.14
0.12
0.10
Anisotropy (r_{obs})
0
10
100
1000
[Zur_{SS}] (nM)

Chapter 6. Factors determining selective metal responses across multiple sensor families

Selectivity of responses of metal sensors based on differential allosteric responses to different metals has emerged as a key paradigm to account for the highly selective responses observed *in vivo*. Analysis of the *in vitro* effects of metals on DNA binding by metalloregulators has led to the suggestion that the ability of a metal ion to initiate allosteric switching is correlated with the ability of the metal ion to adopt a native-like coordination geometry in the allosteric site of the protein. This is exemplified by the example of the ArsR-SmtB protein NmtR described in section 1.5.5 (Cavet *et al.* 2002). Like NmtR, ZiaR is a metal-dependent de-repressor for which it has been suggested that such selectivity may be of less importance than for co-repressor proteins (such as Zur), in which metal ions must organise the formation of an active DNA binding adduct (Waldron *et al.* 2009). The formation of a Cu_2S_3-ZiaR complex correlated with a less effective allosteric effect than Zn^{2+} (section 5.1.4 Figure 47), suggesting adoption of a native-like metal complex was important for effective allosteric switching for ZiaR. The allosteric effects of additional metal ions were analysed to further examine the importance of allostery for initiation of selective metal responses.

6.1 Metal-binding and DNA-binding responses of ZiaR to non-native metals (Co^{2+}, Ni^{2+}, Cd^{2+}, Mn^{2+})

6.1.1 Estimation of the Co^{2+} binding affinity of ZiaR by titration with the Co^{2+} binding indicator Fura-2

During the course of these studies ZiaR was shown to bind Co^{2+} via both its α3N and α5 binding sites in a tetrahedral coordination geometry in both sites (section 3.3.2 Figure 10). The preferred coordination geometry adopted by Zn^{2+} is tetrahedral. Therefore, it was inferred that both Zn^{2+} and Co^{2+} adopt similar tetrahedral geometries in both of the metal sites of ZiaR. A prediction arising from this observation is that like Zn^{2+}, Co^{2+} will be allosterically effective *in vitro*. This was tested by analysis of the effects of Co^{2+} on the DNA binding affinity of ZiaR. In the Irving-Williams series, Co^{2+} is ranked lower than the more competitive ions of Zn^{2+}. Consequently, it typically has weaker binding constants for protein sites than Zn^{2+} and this property is observed directly in this work in data showing complete replacement of Co^{2+} in protein sites of ZiaR and Zur_{SS}

by Zn^{2+} (section 3.3.2 Figure 11; section 4.3.2 Figure 29). To confirm that essentially stoichiometric Co^{2+} binding to ZiaR would occur under the conditions used for fluorescence anisotropy assays (in which protein and metal concentrations in the low micromolar range were routinely used), studies were undertaken to estimate the Co^{2+} binding affinity of ZiaR.

The Co^{2+}-binding metallochromic indicator Fura-2 has been used previously to measure Co^{2+} association constants for proteins in the low nanomolar range and tighter (Wang *et al.* 2004; Iwig *et al.* 2008). On titration of an equimolar solution of ZiaR and Fura-2, Co^{2+} dependent quenching of the fluorescence emission spectra was observed (Figure 51). The shape of the binding isotherm and the shift in the point of saturation compared to an example control experiment (performed in the absence of protein) confirmed competition by ZiaR for Co^{2+} binding with Fura-2 (Figure 51). The line fitted to the data is derived from least squares linear regression analysis. For these analyses data were described using a four-site dimer model (Figure 51a) and also a two-site monomer model (Figure 51b). The average K_{Co} values calculated by each of these models were different (values summarised in Table 10, section 6.3.9). The mean K_{Co1} for the four-site dimer model was 1.1 x 10^{-9} M (± 0.61). For the two-site monomer model K_{Co1} was 8 x 10^{-9} M (± 5.4). It was observed that the four-site dimer model was more accurate at describing the data compared to the two-site monomer model, with the initial curve gradient produced by the two-site monomer model consistently underestimating the likely strength of the affinity for Co^{2+} based on the positions of the data-points (Figure 51, Appendix D Figure 1). Refitting the first six data-points only using the two-site dimer model for each replicate produced a mean K_{Co1} 2.51 x 10^{-9} M; this value is tighter than the initial estimate and the fitted curves more accurately describe the data-points (Appendix D Figure 1).

In both four-site dimer and two-site monomer models no binding to secondary binding sites was detected by least squares linear regression analyses (Table 10) implying they have an affinity substantially less than that of Fura-2. When averaged normalised fluorescence data are plotted with analogous control data as a function of the Co/protein ratio at each metal addition, the stoichiometry of Co^{2+} binding is approximately doubled in the presence of ZiaR (Appendix D Figure 2). This would suggest Co^{2+} binding to two sites on a ZiaR dimer or a single site on the ZiaR monomer, with these sites of K_{Co} tighter than that of Fura-2. Given that binding to secondary sites on a ZiaR monomer or dimer was not detected by non-linear least squares regression

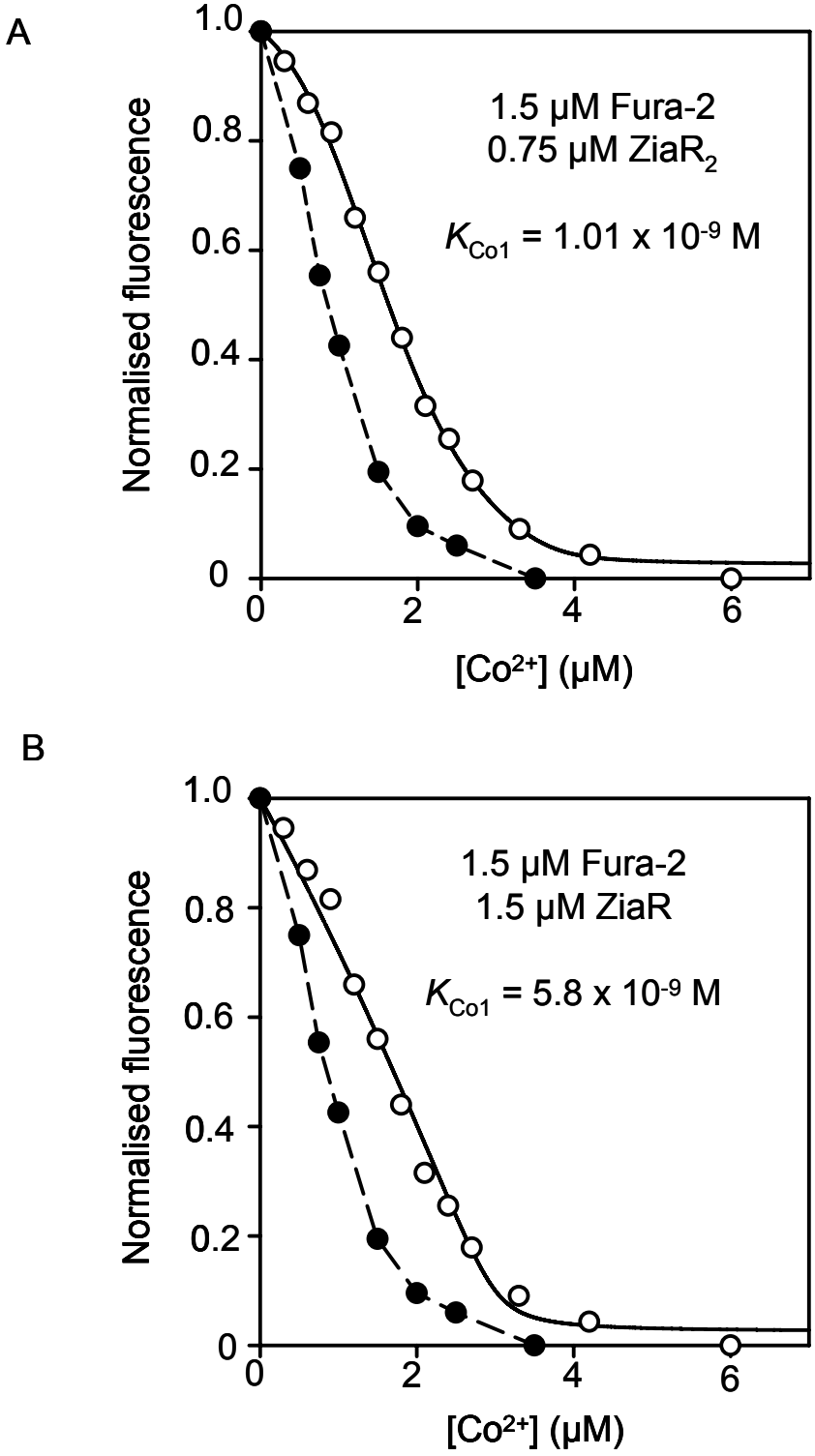

Figure 51. Determination of the Co^{2+} binding affinity of ZiaR by titration with Fura-2. ZiaR (1.5 µM) and Fura-2 (1.5 µM) were titrated with Co^{2+} under anaerobic conditions and changes in fluorescence at 500 nm measured. Data from a single replicate are shown fitted by least squares linear regression analyses to a four-site dimer model (A) and a two-site monomer model (B). Closed symbols represent an example control titration performed in the absence of protein; open symbols represent data from titrations performed in the presence of protein and Fura-2. Data were normalised using the equation $(f_i\text{-}f_f)/(f_o\text{-}f_f)$ where f_o is the fluorescence emission at zero Co^{2+}, f_i is fluorescence at a given concentration of Co^{2+} and f_f is the fluorescence at the final addition of Co^{2+}.

analyses, binding to a single site on a ZiaR monomer is the model which most accurately describes these data. Given that Co^{2+} was shown to bind to sites on ZiaR in the order α5→α3N (Figure 10) this suggests that the tightest Co^{2+} binding sites detected on titration with Fura-2 are the α5 sites. The K_{Co} values determined for ZiaR compare favourably with those determined for the homologue SmtB (0.5–2 x 10^{-9} M) (VanZile *et al.* 2002a).

6.1.2 Analysis of the effects of Co^{2+}, Ni^{2+}, Mn^{2+} and Cd^{2+} on the DNA binding affinity of ZiaR

On titration of *zia* O/P oligonucleotide with ZiaR (up to 1 μM) in the presence of a saturating concentration of Co^{2+} (4 μM), negligible binding to DNA was observed, suggesting a weaker DNA binding affinity in the presence of Co^{2+} (Figure 52a). An analogous titration of apo-ZiaR performed in the absence of metal or EDTA showed high affinity binding with the Δr_{obs} within the range previously observed (section 3.4.4) (Figure 52a). To confirm the allosteric effect of Co^{2+} disassociation experiments were also performed. When pre-formed ZiaR-DNA complexes were titrated with Co^{2+}, a decrease in r_{obs} was observed, consistent with Co^{2+} mediated disassociation of protein-DNA complexes (Figure 52b). Approximately 1-2 equivalents of Co^{2+} were required for reduction in r_{obs} values back to the range characteristic of unbound DNA (Figure 52b), however all replicates showed a majority of the decrease in r_{obs} to occur up to approximately one equivalent Co^{2+}.

The estimated K_{Co} values for ZiaR suggested that in the Co^{2+} concentration range used in these analyses, Co^{2+} binding to ZiaR was essentially stoichiometric (the minimum added concentration of Co^{2+} was 200 nM in these replicates). This implied that the DNA binding stoichiometry was not a function of the K_{Co} and was correlated with the allosteric effect of the metal at the binding sites of the protein. UV-Visible Co^{2+} titrations demonstrated that Co^{2+} bound to sites in ZiaR in the order α5→α3N (section 3.3.2 Figure 10) and the presence of Co^{2+} sites of divergent affinities supported by data in section 6.1.1. The observed stoichiometry would be consistent with a majority of the allosteric effect (i.e. up to one equivalent of Co^{2+}) being mediated through binding to the α5 sites. The small additional decrease in anisotropy observed after one equivalent of Co^{2+} may be due to 'sharing' of some of the Co^{2+} between the α5 and the lower affinity α3N binding sites. Nevertheless, these data show that Co^{2+} can inhibit binding

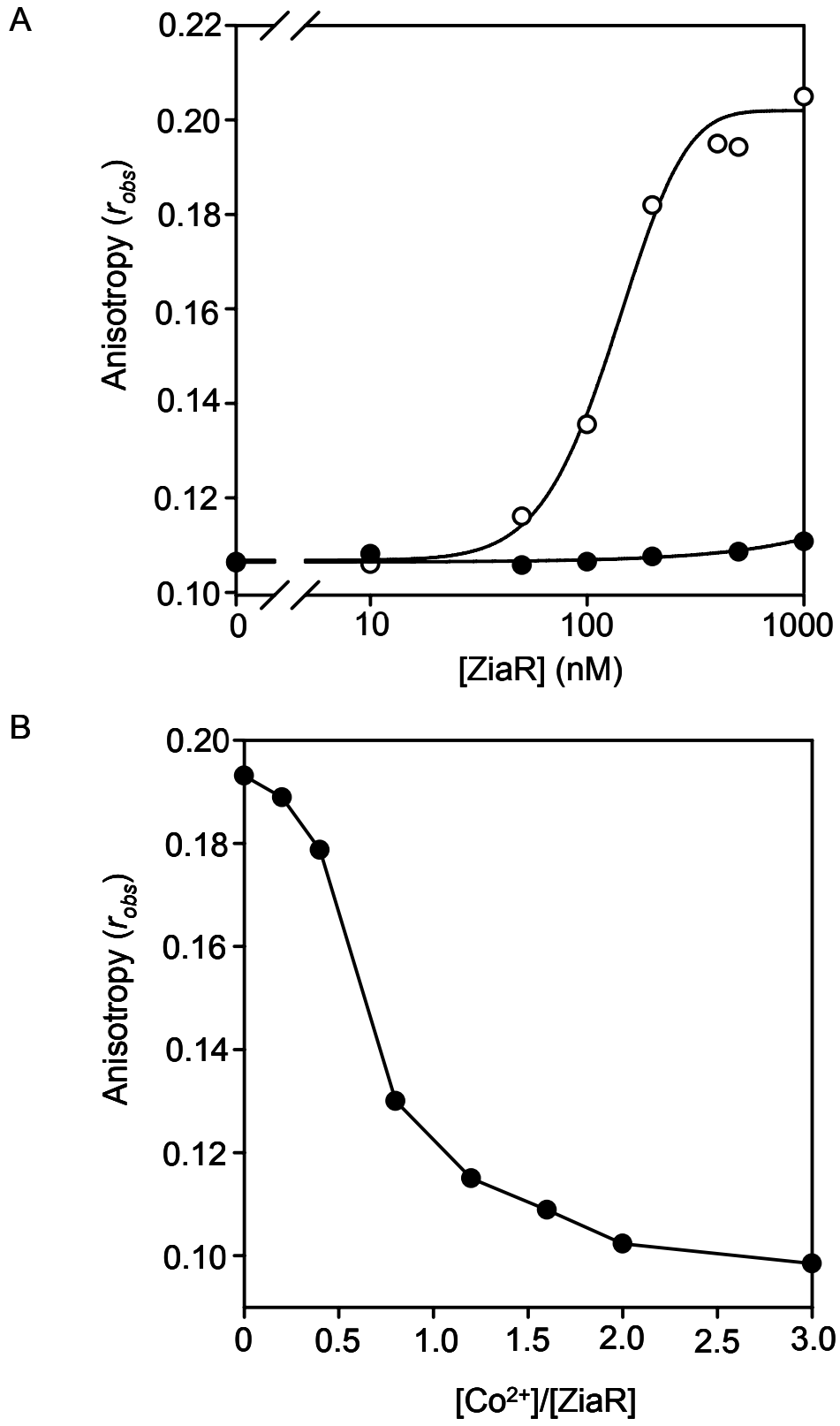

Figure 52. Analysis of the effect of Co^{2+} on the DNA binding affinity of ZiaR. A. Example anaerobic fluorescence anisotropy titration in which 10 nM *zia* O/P oligonucleotide was titrated with ZiaR protein in the presence (closed symbols) or absence (open symbols) of 4 μM Co^{2+}. B. Anaerobic titration of ZiaR-DNA complex (1 μM ZiaR, 10 nM *zia* O/P oligonucleotide) with Co^{2+}.

to DNA and that the allosteric effect is associated with adoption of a Zn^{2+}-like tetrahedral coordination geometry (Figure 10).

For Ni^{2+} ions high-spin octahedral complexes represent the dominant ligand field states (da Silva & Williams 2002). On binding to the metal sites of proteins Ni^{2+} ions also tend to adopt octahedral coordination geometries, in contrast to the tetrahedral geometries almost exclusively favoured by Zn^{2+} ions (Rulísek & Vondrásek 1998). Square-planar four coordinate geometries are also possible, are common in small-molecule complexes and can occur in proteins. This occurs notably in the case of the *E.coli* Ni^{2+} sensor NikR (Wang *et al.* 2004). Ni^{2+} rarely adopts tetrahedral geometries, however some examples are known in which Ni^{2+} can adopt a tetrahedral geometry which is enforced by a relatively rigid ligand sphere in the metal binding site (Chen *et al.* 2000) (e.g. Ni^{2+} substituted metallothionien (Vasák *et al.* 1981)). Therefore, it was predicted that on binding to ZiaR Ni^{2+} would adopt a non-native coordination geometry and hence would be a poor allosteric regulator of ZiaR. Precedent for this comes from studies of the related sensor SmtB; titration with Ni^{2+} revealed that at low Ni-protein stoichiometries, a non-native, hexacoordinate chelate is formed which is associated with low absorbance in the visible region of the spectrum although some degree of reorganisation to a lower coordination number complex may also occur at higher Ni^{2+} concentrations. The allosteric effectiveness of Ni^{2+} on SmtB was not tested (VanZile *et al.* 2000).

Ni^{2+} binding to ZiaR was analysed by UV-Visible anaerobic titration with ZiaR. Similar analyses have shown the appearance of LMCTs in the near-UV region on binding of Ni^{2+} to sites containing cysteine ligands. The Ni^{2+} sensor NikR exhibits LMCTs at approximately 300 nm (Wang *et al.* 2004). The *E.coli* Ni^{2+} sensor RcnR also displays LMCTs on Ni^{2+} binding at around 235 nm and 280 nm (Iwig *et al.* 2008). Additionally, binding of Ni^{2+} to the Cu^{+} sensor CsoR from *B. subtilis* showed LMCTs with major peaks at around 250 nm and 350 nm confirming retention of binding to cysteine residues in the binding site even in a non-native coordination geometry (Ma *et al.* 2009a). On titration with Ni^{2+}, multiple absorption bands are observed in the range characteristic of Ni-S^{-} derived LMCTs (Figure 53a). Major peaks are apparent at 237 nm, 287 nm and 325 nm (Figure 53a). When the intensities of the LMCT features were plotted as a function of Ni^{2+} concentration, saturation of binding is seen to occur at approximately two equivalents of Ni^{2+} for the features at 325 nm (Figure 53b) and 287 nm (Appendix D Figure 3). The intensity of the feature at 237 nm increased linearly and

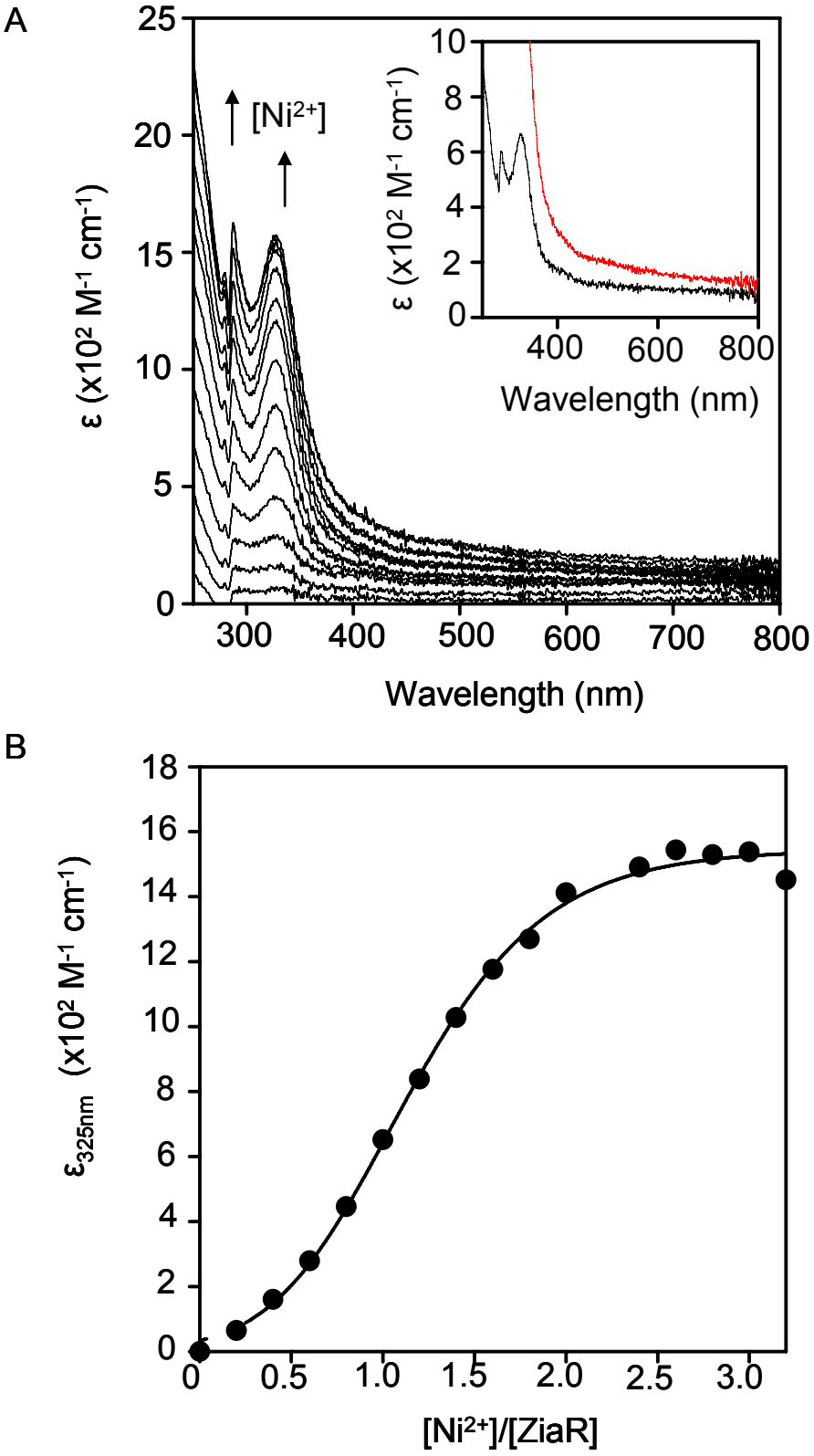

Figure 53. Anaerobic UV-Visible titration of ZiaR with Ni^{2+}. A. Apo-subtracted difference spectra produced from an example anaerobic titration of ZiaR (40 μM) with Ni^{2+}. *Inset*; spectra from one and two equivalent additions in the main figure re-plotted to provide a better view of absorbance features in the 400-800 nm region. B. Increase in intensity of the LMCT feature at 325 nm in A with increasing [Ni^{2+}].

no apparent saturation was observed even beyond two equivalents Ni^{2+} (Appendix D Figure 3). It is unclear what aspect of Ni^{2+} binding this feature is reporting on. Perhaps the increase beyond two equivalents is due to adventitious binding to multiple cysteine residues. Nevertheless, these data confirm Ni^{2+} binding to ZiaR involving thiol ligands. The non-linear shape of the Ni^{2+} binding isotherms (Figure 53b) suggests binding to additional, spectrally silent sites in addition to those containing cysteine ligands.

The features present in Ni^{2+} UV-Visible spectra can be used to assign the coordination geometry adopted by Ni^{2+} at the metal binding site. Tetrahedral Ni^{2+} sites, which are rarely adopted by Ni^{2+} in proteins, can have ligand field intensities and energies analogous to those of Co^{2+} and are characterised by broad *d-d* transition features at wavelengths longer than 700 nm (Chen *et al.* 2000). For example, in Ni^{2+}-substituted metallothionien protein, tetrahedral Ni^{2+} coordination is associated with broad *d-d* transition features increasing in intensity at smaller wavelengths, with shoulders at 750 nm and 560 nm having extinction coefficients of ~100 M^{-1} cm^{-1} and 580 M^{-1} cm^{-1} respectively (Vasák *et al.* 1981). Discrete absorption features of similar intensity (~130 M^{-1} cm^{-1} at 570 nm and 300 M^{-1} cm^{-1} at 505 nm) have been characterised in Ni^{2+}-substituted alcohol dehydrogenase enzyme (Dietrich *et al.* 1981). Square planar geometries are characterised by lack of *d-d* absorbance features at wavelengths greater than 700 nm and exhibit absorbance features between 400 and 500 nm with an intensity ranging from 50-500 M^{-1} cm^{-1} (Chen *et al.* 2000). This feature is readily apparent on titration of NikR with Ni^{2+} (Wang *et al.* 2004). In four-coordinate systems, square planar geometry is more favoured over tetrahedral geometries when thiolate or Imidazole/nitrogen ligands are present (Chen *et al.* 2000). Very weak absorption within the 400-700 nm wavelength range is typically observed on binding of Ni^{2+} ions to metal sites with a six-coordinate binding geometry (Cavet *et al.* 2002; Iwig *et al.* 2008), the environment favoured in most proteins (Rulísek & Vondrásek 1998).

The spectra for ZiaR bound to one and two equivalents of Ni^{2+} show negligible discrete absorbance features in this wavelength range (Figure 53a, inset). At one equivalent Ni^{2+} there is little change in absorbance from 800 nm to below ~400 nm, at which point LMCT absorptions dominate the spectra. The constant elevation in the baseline across the visible region was most likely caused by light scattering due to protein precipitation which was a consistent feature of these titrations. No discrete features between 400-500 nm, with intensities $\geq$ 100 M^{-1} cm^{-1} (such as those previously observed for NikR and mutants of RcnR) (Chivers & Sauer 2000; Iwig *et al.* 2008) are

present that would be consistent with a square planar geometry. These data are also inconsistent with a tetrahedral geometry; there is negligible change in absorption intensity and no discrete absorption features apparent in the visible region that would be expected from lower coordinate Ni^{2+} binding (Figure 53a, inset). At two equivalents of Ni^{2+}, an increase in intensity is observed across the spectrum even at long wavelengths; again, this may be reporting on solution light scattering. However, a weakly absorbing feature may be present at approximately 500 nm in the region often associated with square planar absorbance features. The high degree of light scattering at Ni^{2+} concentrations beyond saturation in these and replicate spectra, combined with the proximity of this region to the LMCT features, means it is difficult to unequivocally assign this feature. Taken together, these data are most consistent with adoption of a non-native, high coordinate geometry, likely octahedral, for Ni^{2+} in the metal sites of ZiaR.

The effects of Ni^{2+} on the DNA binding affinity of ZiaR were monitored by fluorescence anisotropy assays in which *zia* O/P oligonucleotides were titrated with ZiaR pre-incubated in 60 μM Ni^{2+}, a concentration determined to be sufficient to saturate the protein binding sites (Appendix D Figure 4). In the example analyses shown in Figure 54a, ZiaR bound to DNA following pre-incubation and titration in the presence of 60 μM Ni^{2+}, with the binding isotherm for Ni-bound ZiaR similar to that observed for ZiaR titrated in the absence of metal or EDTA pre-incubation (Figure 54a). ZiaR pre-incubated in Zn^{2+} showed negligible binding to DNA over this concentration range (Figure 54a). Titration of a pre-formed ZiaR-DNA complex with Ni^{2+} showed a reduction in r_{obs} of only ~30 % (relative to the average start value for the sample of DNA used) at a Ni^{2+} concentration (60 μM) sufficient to saturate the protein (Figure 54b). This is less than the decrease for analogous titrations performed using Zn^{2+} and Co^{2+} at saturating concentrations (Figures 18, 52). These data are consistent with Ni^{2+} binding to ZiaR in a non-native geometry that is ineffective in promoting the allosteric changes that lead to impaired DNA binding.

Mn^{2+} ions are characterised by a half filled $3d^5$ electron shell resulting in Mn^{2+} ions being spherically polarisable with no crystal field stabilisation energy; as a result Mn^{2+} ions prefer 6-coordinate octahedral geometries (da Silva & Williams 2002). It was therefore predicted that Mn^{2+} would bind to ZiaR but fail to initiate allostery and inhibit interaction of ZiaR with DNA. As expected from its position in the Irving-Williams series (eq. 1), the equilibrium association constants for Mn^{2+} sites are much

Figure 54. Effects of Ni^{2+} and Mn^{2+} on ZiaR DNA binding monitored by fluorescence anisotropy. A. Example anaerobic fluorescence anisotropy analyses in which *zia* O/P oligonucleotide (10 nM) was titrated with recombinant ZiaR protein following pre-incubation of between 1 and 10 μM protein with either no metal (closed circles), two equivalents of Zn^{2+} (closed triangles), 60 μM Ni^{2+} (open circles) or 1 mM Mn^{2+} (open squares). For each titration, each metal was present at the same concentration in the DNA binding reaction. B. Anaerobic titration of pre-formed ZiaR-DNA complex (1 μM protein, 10 nM *zia* O/P oligonucleotide) with Ni^{2+} showing negligible decrease in anisotropy at saturating metal concentrations. The average anisotropy value for unbound oligonucleotide from the DNA preparation used in these analyses is also shown (red circle).

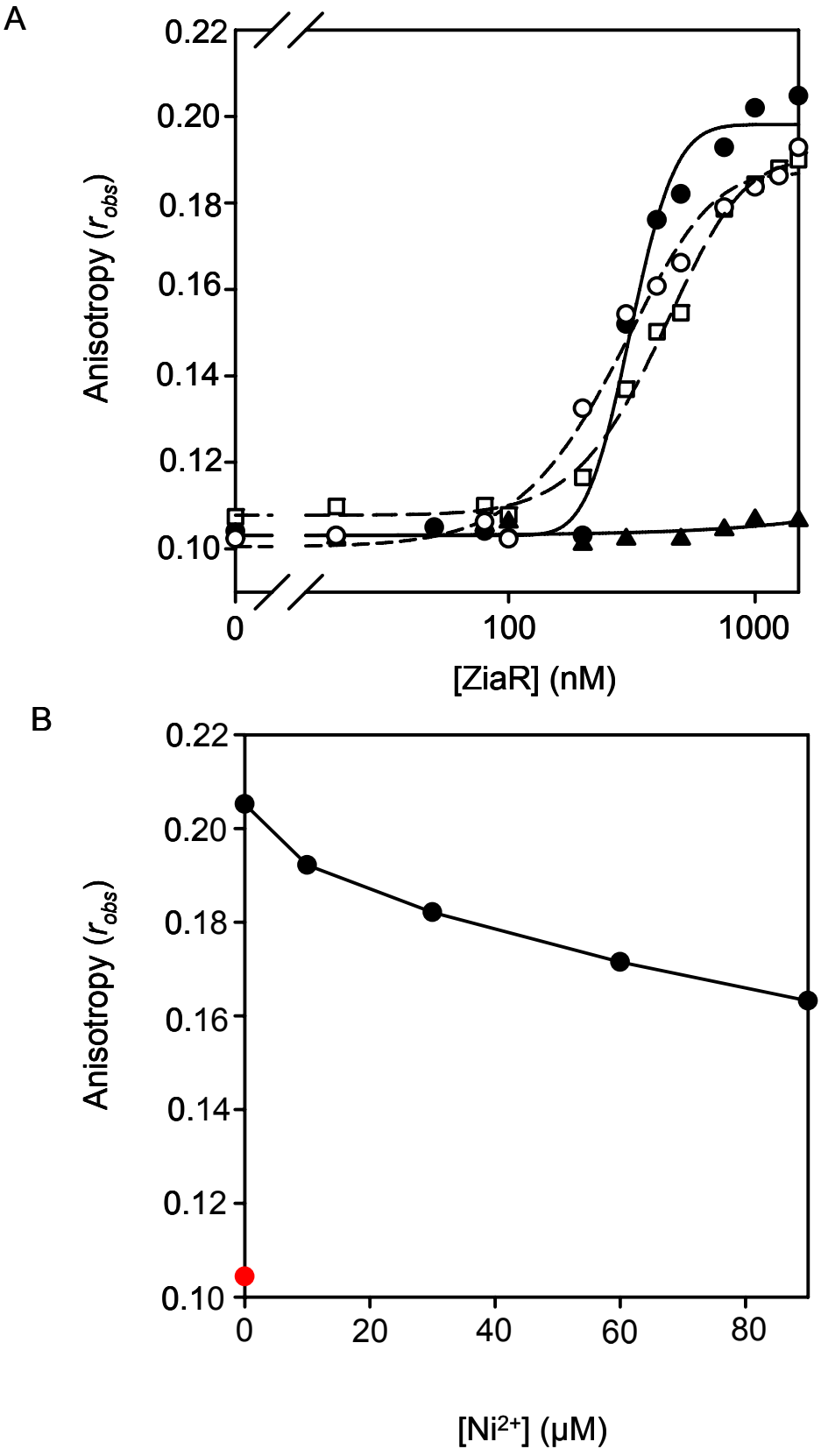
A
0.22
0.20
0.18
0.16
0.14
0.12
0.10
Anisotropy (r_{obs})
0
100
1000
[ZiaR] (nM)
B
0.22
0.20
0.18
0.16
0.14
0.12
0.10
Anisotropy (r_{obs})
0
20
40
60
80
[Ni2+] (μM)

weaker than those for Zn^{2+}, Ni^{2+} and even Co^{2+} sites. In the DtxR-like Mn^{2+} sensor MntR, in which two Mn^{2+} ions bind to the protein in dinuclear motif characterised by hexacoordinate coordination geometries (Glasfeld *et al.* 2003), an affinity for Mn^{2+} of 50-160 μM has been estimated (Golynskiy *et al.* 2006). Based on the micromolar range association constants observed for Mn^{2+} sensors (Golynskiy *et al.* 2006; Sen *et al.* 2006) a reasonable expectation was that the protein sites of ZiaR would be fully saturated following incubation in millimolar concentrations of Mn^{2+}, a concentration 1000-fold greater than the likely K_d for Mn^{2+}. To test the allosteric effect of Mn^{2+}, fluorescence anisotropy analyses were performed in which ZiaR was pre-incubated in 1 mM Mn^{2+} prior to titration with DNA. Under these conditions the binding affinity for DNA was comparable to apo-ZiaR control titrations (Figure 54a) with apo-like Δr_{obs} values also observed. These data are consistent with Mn^{2+} not being allosterically effective at these concentrations. The absence of UV-Visible spectral features correlating with coordination geometries adopted by the bound Mn^{2+} ion meant that it was not possible to unequivocally confirm the nature of the coordination environment of any bound Mn^{2+}; however, a likely model is that this lack of allostery was due to formation of a non-native octahedral-like geometry in the metal sites of ZiaR.

The effects of Cd^{2+} on the DNA binding affinity of ZiaR are of less direct biological relevance compared to Zn^{2+}, Co^{2+} and Mn^{2+}. Although some examples have been found for Cd^{2+} usage in cambialistic enzymes such as carbonic anhydrase in marine diatoms (Lane *et al.* 2005; Xu *et al.* 2008), most organisms (including *Synechocystis*) have no known Cd^{2+} requirements and have evolved efficient resistance mechanisms for this toxic metal ion (exemplified by the *cadA* system of *S. aureus* in which Cd^{2+} is expelled from the cytosol by an ATPase exporter (Nucifora *et al.* 1989)). However, the well characterised nature of Cd^{2+} binding sites and coordination geometries in proteins makes it a useful metal site probe. Both tetrahedral and octahedral coordination geometries have been found in Cd^{2+} substituted proteins, with a slightly higher number of tetrahedral sites (Rulísek & Vondrásek 1998). However, in sensor proteins closely related to ZiaR, tetrahedral geometries predominate and are correlated with allosteric function on binding the protein; CadC (Busenlehner *et al.* 2002b) and BxmR (Liu *et al.* 2005) bind Cd^{2+} in an α3N tetrathiolate complex. AztR binds Cd^{2+} tetrahedral α3N S_3N complex (Liu *et al.* 2005). Cd^{2+} is allosterically effective at the tetrahedral α5 sites of SmtB (VanZile *et al.* 2002b). Therefore, a

prediction was that Cd^{2+} would bind in a tetrahedral coordination geometry to the metal sites of ZiaR and promote allosteric switching.

On UV-Visible titration of recombinant ZiaR with Cd^{2+} LMCT features were observed (Figure 55a) with the intensity at the absorbance maximum of 230 nm showing a linear increase to approximately one equivalent of Cd^{2+}. These data are consistent with stoichiometric Cd^{2+} binding to the cysteine-containing α3N site (Figure 55b). Previous work has shown that an extinction coefficient of approximately 6000 M^{-1} cm^{-1} at the lowest energy LMCT band correlates with a single Cd^{2+}-S^- bond (Henehan *et al.* 1993). The intensity at saturation of approximately 18000 M^{-1} cm^{-1} is consistent with the involvement of three cysteine residues in binding of the Cd^{2+} ion. This value is consistent with UV-Visible titration data for both Cu^+ and Co^{2+} (Figure 40, 10) suggesting the involvement of all three cysteine residues predicted by bioinformatics analyses (Figure 4) to comprise the tetrahedral α3N site of ZiaR. The degree of Cd^{2+} binding to the tetrahedral, thiol-free α5 site cannot be determined from these data although stoichiometric binding to the α3N site would imply an α5 site with an affinity for Cd^{2+} at least an order of magnitude weaker. Characterisation of Cd^{2+} binding to BxmR suggested Cd^{2+} binding to this site albeit with an affinity weaker than Co^{2+} (Liu *et al*. 2008). The coordination geometry adopted by Cd^{2+} on binding to ZiaR cannot be assigned unequivocally from these data. However, the α3N site of ZiaR contains ligand residues identical to those previously shown to form a tetrahedral α3N Zn^{2+}/Cd^{2+} chelate in AztR (Figure 4) (Liu *et al.* 2005). Therefore, although a trigonal S_3 geometry cannot be ruled out, the four-coordinate S_3N α3N ligand sphere together with known coordination preferences of Cd^{2+} (Rulísek & Vondrásek 1998) would suggest a tetrahedral S_3N geometry for Cd^{2+}.

The effects of Cd^{2+} on DNA binding were monitored by fluorescence anisotropy analyses. On titration of preformed ZiaR-DNA complexes with Cd^{2+}, the measured anisotropy of the solution was reduced to a value consistent with unbound DNA with saturation occurring at approximately one equivalent of Cd^{2+} (Figure 55c). These data are consistent with Cd^{2+} being able to initiate allostery and mediate disassociation of protein-DNA complexes. Titration of *zia* O/P oligonucleotide with ZiaR in the presence of Cd^{2+} also showed inhibition of association with DNA (Appendix D Figure 5) Because Cd^{2+} binds stoichiometrically to the α3N sites on ZiaR (Figure 55a), the allosteric effect is likely to be mediated through these sites.

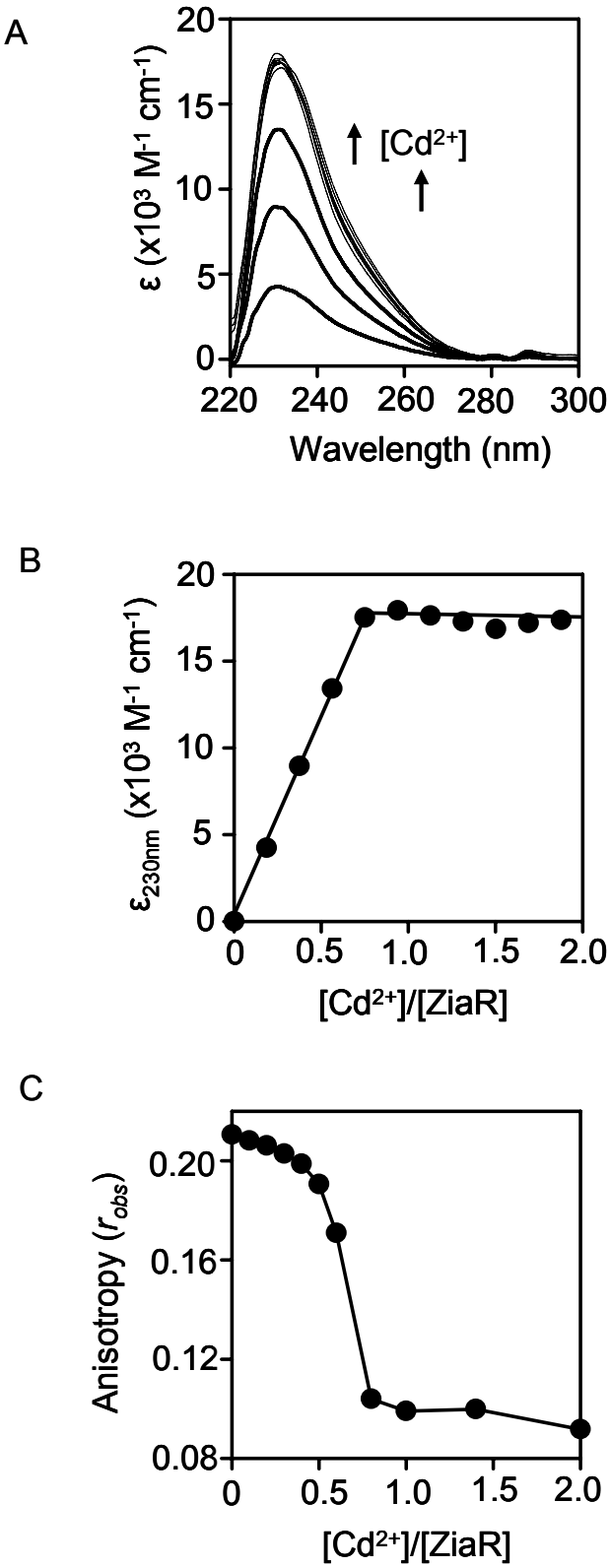

Figure 55. Analysis of the effects of Cd^{2+} binding to ZiaR. A. Apo-subtracted difference spectra produced from an example UV-Visible anaerobic titration of recombinant ZiaR (21 μM) with Cd^{2+}. B. Increase in intensity of apo-subtracted difference spectra at 230 nm (from the data in A) with increasing [Cd^{2+}]. C. Anaerobic titration of pre-formed ZiaR-DNA complexes (1 μM ZiaR, 10 nM *zia* oligonucleotide) with Cd^{2+} , showing Zn^{2+} like disassociation of protein-DNA complexes.

6.2 Analysis of non-native metal binding and activation of Zur_{SS}

6.2.1 Estimation of the Co^{2+} binding affinity of Zur_{SS} by competition with the metallochromic indicator Fura-2

During the course of these studies it was shown that Co^{2+} bound to the allosteric site of Zn_1Zur_{SS} in a tetrahedral geometry involving a single cysteine residue (Figure 28). The binding affinity for Co^{2+} was determined by titration with Fura-2. On titration of an equimolar solution of Zn_1Zur_{SS} and Fura-2 with Co^{2+}, a shift in the binding the binding isotherm relative to a control experiment was observed indicating competition with the Fura-2 for Co^{2+} binding (Figure 56, Appendix D Figure 2). Data were modelled by least squares non-linear regression analysis to either a two-site dimer model (Figure 56a) or a one-site monomer model (Figure 56b). The mean Co^{2+} disassociation constant (K_{Co1}) for data modelled to a dimer model was 0.46 x 10^{-9} M (± 0.37) compared to a value for data modelled to a single site monomer model of 2.6 x 10^{-9} M^{-1} cm^{-1} (±0.69) (Table 10). The single-site monomer model more accurately described the data; the mean K_d value for the two-site dimer model was likely an overestimate of the binding affinity due to inaccurate curve fitting which was consistently observed using this model (Figure 56a, Appendix D Figure 6). Least squares non-linear regression analysis using only the initial datapoints for each replicate produced binding curves that more accurately described the data (Appendix D Figure 6) producing a mean K_{Co1} of 1.2 x 10^{-9} (± 1.04).

In the presence of Zn_1Zur_{SS} the Co^{2+} binding stoichiometry for Fura-2 is approximately double that observed in control experiments (Appendix D Figure 2). This is consistent with Co^{2+} occupation of a single site per protein molecule in a single-site monomer model or with binding of Co^{2+} to both sites in a two-site dimer model. Given that negligible binding to secondary sites was detected by least squares linear regression analysis using a two-site dimer model (Table 10), a single-site monomer model most accurately describes the data. Nevertheless, values for Zur_{SS} are similar to those for K_{Co1} determined for ZiaR and these data imply that the allosteric site of Zur_{SS} has an affinity for Co^{2+} substantially tighter than the α3N sites of ZiaR (which do not compete with Fura-2; Appendix D Figure 2).

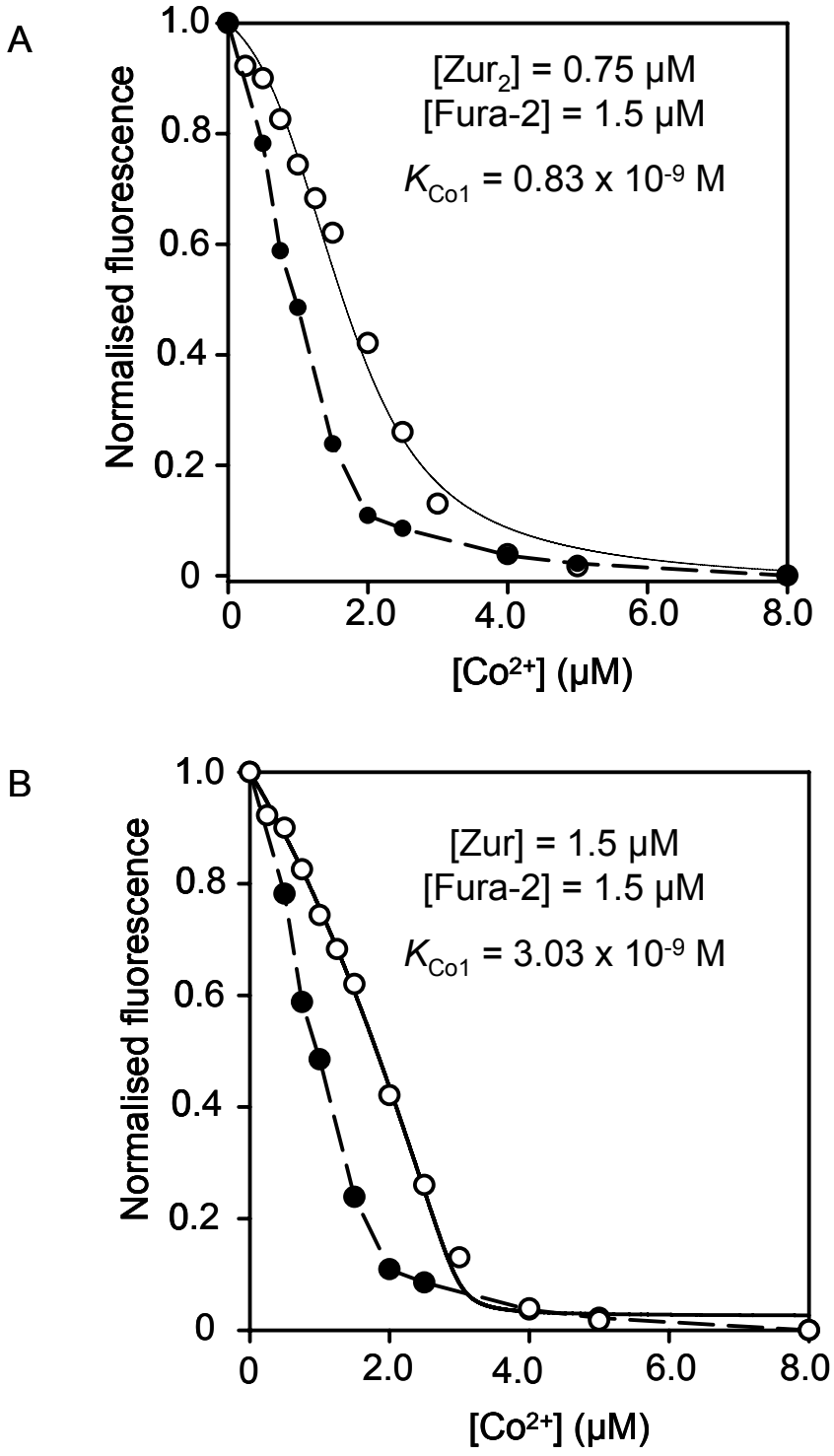

Figure 56. Determination of the Co^{2+} binding affinity of Zur_{SS} by Co^{2+} titration with Fura-2. Zn_1Zur_{SS} (1.5 µM) and Fura-2 (1.5 µM) were titrated with Co^{2+} and the changes in fluorescence at 500 nm measured. Data from a single replicate were fitted by least squares linear regression analyses to either a two site dimer model (A) or a single site monomer model (B). Closed symbols; control experiment. Open symbols; protein and Fura-2 experiment. Data were normalised as described in Figure 51.

6.2.2 Analysis of the effects of Ni^{2+}, Mn^{2+} and Co^{2+} on the DNA binding affinity of Zur_{SS}

Following UV-Visible titration of 30 μM Zn_1Zur_{SS} with Ni^{2+}, LMCT features were produced which increased linearly in intensity to approximately one equivalent (Appendix D Figure 7). These data confirmed Ni^{2+} binding to Zn_1Zur_{SS} and indicated a Ni^{2+} affinity tighter than ~15 x 10^{-6} M (Appendix D Figure 7). On titration of Zn_1Zur_{SS} pre-incubated with a saturating concentration of Ni^{2+} (60 μM), Mn^{2+} (1 mM) or Co^{2+} (30 μM) with *znu* O/P oligonucleotide, increases in anisotropy were observed that were similar in magnitude to those observed on titration of Zn_1Zur_{SS} either pre-incubated in Zn^{2+} or not subject to pre-incubation with metal ions (Appendix D Figure 8a,b). ICP-MS analysis showed that the the protein preparation used for titration with DNA in the presence of Ni^{2+} and Mn^{2+} (Appendix D Figure 8a)) contained ~1.14 equivalents of Zn^{2+} prior to this experiment. This would predict that the sample of protein not pre-incubated in metal would exhibit a K_{DNA} approximately seven-fold weaker than observed for Zn_2Zur_{SS}. However, the K_{DNA} value for Zur_{SS} not subjected to metal pre-incubation was similar to that observed for Zur_{SS} pre-incubated with Zn^{2+} (Appendix D Figure 8b) and was similar to values previously observed for Zn_2Zur_{SS} (Figure 37, section 4.4.3). This effect was probably caused by acquisition by Zn_1Zur_{SS} of competitive binding Zn^{2+} from the buffer (as observed previously in section 4.4.3) (which has an affinity tighter than that of Co^{2+}, and likely Mn^{2+} and Ni^{2+}, at the allosteric site) causing production of Zn_2Zur_{SS} activated to bind DNA. Therefore, it was not possible to draw conclusions regarding the allosteric effects on Zur_{SS} of these less competitive metal ions.

6.3 Comparing the *in vitro* and *in vivo* responses of CoaR, ZiaR and Zur_{SS}

The selective responses of ZiaR (Thelwell *et al.* 1998) and Zur_{SS} (Appendix B Figure 1)) observed *in vivo* contrast with the much broader selectivity (for ZiaR at least) observed *in vitro* (Figure 52, 55). ZiaR responds to metal ions such as Co^{2+} *in vitro* (Figure 52) but not *in vivo* (Thelwell *et al.* 1998). Whilst Zur_{SS} and ZiaR are responding selectively to Zn^{2+} CoaR, which is present in the same cytosol, is responding selectively to Co^{2+} *in vivo* (Rutherford *et al.* 1999). Partitioning of metal ions to sensors *in vivo* based on their relative affinities for metal ions was outlined as one possible explanation

to account for these highly specific responses (section 1.9.3). For these sensors this would predict that ZiaR and Zur_{SS} would have Zn^{2+} affinities much tighter than for CoaR and conversely, CoaR would have a Co^{2+} affinity much tighter than either ZiaR or Zur_{SS}. Therefore, *in vivo* Co^{2+} would selectively populate CoaR and not ZiaR or Zur_{SS} whilst Zn^{2+} would selectively populate ZiaR and Zur_{SS}. To test this hypothesis, recombinant CoaR protein was produced and its metal binding properties compared with those of recombinant ZiaR and Zur_{SS}.

6.3.1 Bioinformatics analyses of CoaR

Previous attempts at producing large quantities of native, recombinant CoaR were unsuccessful. Previous studies succeeded in producing small quantities of GST-tagged protein that was sufficient for EMSA assays that were made highly sensitive through the use of radioisotopes (Rutherford *et al.* 1999). Although recombinant CoaR could be overexpressed to a high level in *E.coli*, none of the protein was present in the soluble cell fraction following the use of a range of conditions during cell growth and induction (K.Waldron, unpublished observations). Production of larger quantities of CoaR was made possible by evaluation of its predicted biochemical properties. In previous studies it was established that CoaR was a multi-domain protein comprised of three regions. At the N-terminus residues 1-145 comprise a region with homology to MerR from *E.coli* (20 % sequence identity) which contains a helix-turn-helix motif. Immediately after this is a short, 29 residue segment with no sequence homology to other proteins and presumably links the N and C terminal domains. Immediately C-terminal to this section a region between residues 174-358 was identified with homology to precorrin isomerase (32 % identity) from *Pseudomonas denitrificans* (Rutherford *et al.* 1999). This enzyme is a component of the vitamin B_{12} synthetic pathway and catalyses the conversion of precorrin 8-x to hydrogenobyrinic acid which binds tightly to precorrin isomerase (Thibaut *et al.* 1992).

Subsequent to these previous studies (Rutherford *et al.* 1999), two precorrin isomerase homologues have been annotated in the genome of *Synechocystis*, both of which are homologous to that from *P. denitrificans* and thus also have homology to the precorrin domain in CoaR. slr1467 encodes a protein (termed precorrin isomerase A from hereon in) with 28 % identity to the precorrin domain of CoaR. sll0916 encodes a

Figure 57. Multiple sequence alignment for CoaR and both precorrin isomerase isoforms identified in the sequenced genome of *Synechocystis*. A. The whole protein sequence of CoaR was aligned with the protein sequence for precorrin isomerase A (slr1467). B. Alignment analogous to that shown in A but with the protein sequence for precorrin isomerase B (sll0916). C. Alignment of the protein sequences of CoaR and the precorrin isomerase from *P. denitrificans.* Sequences were aligned using the BLAST alignment tool (http://blast.ncbi.nlm.nih.gov/). Coloured lines indicate the positions of hydrophobic regions predicted by DAS (orange lines), TMPred (green) and TopPred (blue) (see main text). Note: the first hydrophobic region in CoaR predicted by DAS only is outside of the aligned sequence regions in B and so is not shown. In the sequence of *P. denitrificans* precorrin isomerase residues 163-170, which were shown to be important in dimer stabilisation (Shipman *et al.* 2000) are highlighted in red.

A

```
slr1467     ILRRVIYATGDFEYLNLLHFSARVLTVGAAALASRTTILVDVPMVQVGIVPTLQKTFANP  103
            +L +++ A GD   +N +  S   +     AL +   ++ DVP+V       L +T
CoaR       HLLHQLVLACGDVSLVNAVRLSQGAIASARDALKAGCPVVTDVPVVAAA----LDQTRLAH  240

slr1467     VYCATQS-ITRPQ----KERTEEAWGILNLAHRY---PDG-IFVIGHAQTALDALMELVE  154
            + C  ++ I  P     +E  +  W   +   R    P G +  IG+A + L    +L+E
CoaR       LGCTVKTLIDDPHITGLREAEQAFWHHDHWQQRLQQIPQGCVLAIGYAPSVLLTACKLIE  300

slr1467     AQRIQPALVIATATNFGDRQDVELNLQKANIPHIIVQGRKGGTEVAVAIITALVDLAWQ   215
             Q IQPALVI     F      +  L  + IPHI +QG  GG  +A   + ALV+
CoaR       QQHIQPALVIGMPIGFSHAPGAKRRLMTSPIPHITIQGSLGGGLLAAVTLNALVETLIA   359
```

B

```
sll0916     AIARGIESLRHGQTIVVDVNMVKQGIQGLVQRTFNNPIQTAIDFATI-----ADPGKTRT  123
            AIA   ++L+ G  +V DV +V   +           ++T ID   I     A+
CoaR       AIASARDALKAGCPVVTDVPVVAAALDQTRLAHLGCTVKTLIDDPHITGLREAEQAFWHH  267

sll0916     ETGMDRCIAQFPE-AIYVIGNAPTALLTLCQAIAAGKAKPALVIGVPVGFIGVLEAKKAL  182
            +    R + Q P+  +  IG AP+ LLT C+ I     +PALVIG+P+GF     AK+ L
CoaR       DHWQQR-LQQIPQGCVLAIGYAPSVLLTACKLIEQQHIQPALVIGMPIGFSHAPGAKRRL  326

sll0916     SLLPCPQIRVEGNKGGSPVAAGIVNALLMLAWRE 216
               P P I ++G+ GG  +AA  +NAL+
CoaR       MTSPIPHITIQGSLGGGLLAAVTLNALVETLIA  359
```

C

```
Isomerase   DLSRFSEEEADLAVRMVHACGSVEATRQFVFSPDFVSSARAALKAGAPILCDAEMVAHGV  85
            DLS +SE    L  ++V ACG V        S   ++SAR ALKAG P++ D  +VA  +
CoaR       DLSAYSEITIHLLHQLVLACGDVSLVNAVRLSQGAIASARDALKAGCPVVTDVPVVAAAL  233

Isomerase   TRARLPA-GNEVICTLRDPRTPAL-AAEIGNTRSAAALKLWSERL----AGSVVAIGNAP  139
             + RL   G  V   + DP    L  AE    ++      W +RL     G V+AIG AP
CoaR       DQTRLAHLGCTVKTLIDDPHITGLREAE----QAFWHHDHWQQRLQQIPQGCVLAIGYAP  289

Isomerase   TALFFLLEMLRDGAPKPAAILGMPVGFVGAAESKDALAENSYGVPFAIVRGRLGGSAMTA  199
            + L    +++     +PA ++GMP+GF  A  +K  L  +   +P   ++G LGG  + A
CoaR       SVLLTACKLIEQQHIQPALVIGMPIGFSHAPGAKRRLMTSP--IPHITIQGSLGGGLLAA  347

Isomerase   AALNSL        205
              LN+L
CoaR       VTLNALVETLIA  359
```

protein (termed precorrin isomerase B from hereon in) which has 33 % identity to the precorrin-like domain of CoaR (Figure 57). The position and extent of the precorrin isomerase-like domain in CoaR identified by these alignments is similar to that identified by the alignment in previous studies (Figure 57).

It was hypothesised that CoaR may be insoluble due to the presence of exposed regions of hydrophobicity which caused aggregation of recombinant protein. The sequence of CoaR was analysed to determine if hydrophobic regions might be present. Multiple algorithms detected hydrophobic regions in the sequence of CoaR. No regions were detected in the MerR domain; however, multiple overlapping regions were identified in the precorrin isomerase-like domain. Three main hydrophobic regions at the C-terminus of this domain were identified by multiple algorithms, with two much smaller regions also identified at the N-terminal end of the domain (Figure 58a, Table 8). Performing similar analyses on both of the precorrin isomerase isoforms identified in *Synechocystis* and the precorrin isomerase from *P. denitrificans* revealed the presence of hydrophobic regions in all three proteins (Figure 58b-d, Table 8).

Precorrin isomerase from *P. denitrificans* is a soluble protein however multiple programs predicted a hydrophobic region in the middle of the protein sequence. This region is conserved in CoaR (in hydrophobic region 2) (Figure 57c) and alignments of CoaR with precorrin isomerase A and B also show this region to be present in both of these proteins (although this region appears to be much more poorly conserved in precorrin isomerase A) (Figure 57a, b). In the crystal structure of *P. denitrificans* precorrin isomerase, homodimer interactions are stabilised by hydrophobic residues 163-170 (Shipman *et al.* 2000) which lie within this conserved hydrophobic region. Therefore, this conserved region in both precorrin isomerases and CoaR may represent a dimerisation interface. In both CoaR and precorrin isomerase B the hydrophobic patch present immediately adjacent and N-terminal to this region (hydrophobic region 1 in CoaR) is extremely close in sequence and both regions almost overlap. This suggested some potential contribution of this region to a putative dimerisation domain in these proteins (Figure 58a, d, Table 8). A striking observation is the conservation of a hydrophobic domain at the extreme C-terminus in precorrin isomerase A, B and CoaR, which is predicted to be present by multiple algorithms. This region is not conserved in *P. denitrificans* precorrin isomerase (Figure 57, 58 Table 8). This region appears distinct to the other regions described above located at positions more N-terminal.

	Amino acid positions of predicted hydrophobic regions			
Prediction algorithm	***P. denitrificans* precorrin isomerase**	**CoaR**	**Precorrin Isomerase A (slr1467)**	**Precorrin isomerase B (sll0916)**
DAS	133-146 (14) 160-166 (7)	184-198 (15) 226-229 (4) 283-294 (12) 309-312 (4) 341-354 (14)	65-76 (12) 81-90 (10) 163-164 (2) 199-210 (12)	146-153 (8) 164-175 (12) 203-211 (9)
TMpred	128-146 (19)	280-299 (20) 334-359 (26)	60-83 (24) 195-214 (20)	137-156 (20) 163-182 (20) 197-214 (18)
TopPred	128-148 (21) 152-172 (21)	277-297 (21) 302-322 (21) 334-354 (21)	77-97 (21) 195-215 (21)	159-179 (21) 196-216 (21)
SOSUI*	-	-	-	-
TMHMM†	-	-	-	-

Table 8. Hydrophobic regions predicted in *P. Denitrificans* precorrin isomerase *Synechocystis* CoaR, precorrin isomerase A and precorrin isomerase B. For each region the position in the amino acid sequence is given together with the length of the region shown in parenthesis. *SOSUI predicted no transmembrane helices in any of the proteins in the table and all of these proteins were assigned as soluble proteins. †TMHMM predicted no transmembrane regions for any of the proteins, however for *P.denitrificans* precorrin isomerase and CoaR regions of substantially increased hydrophobicity were detected between residues 120-150 and 330-355 respectively. Small increases in hydrophobicity were also detected in the sequence of precorrin isomerase A (residues 55-85 and residues 197-215 approx.) and precorrin isomerase B (residues 130-180 and residues 197-214 approx.). The algorithms used are available at the EXPASY website (http://www.expasy.ch/tools/).

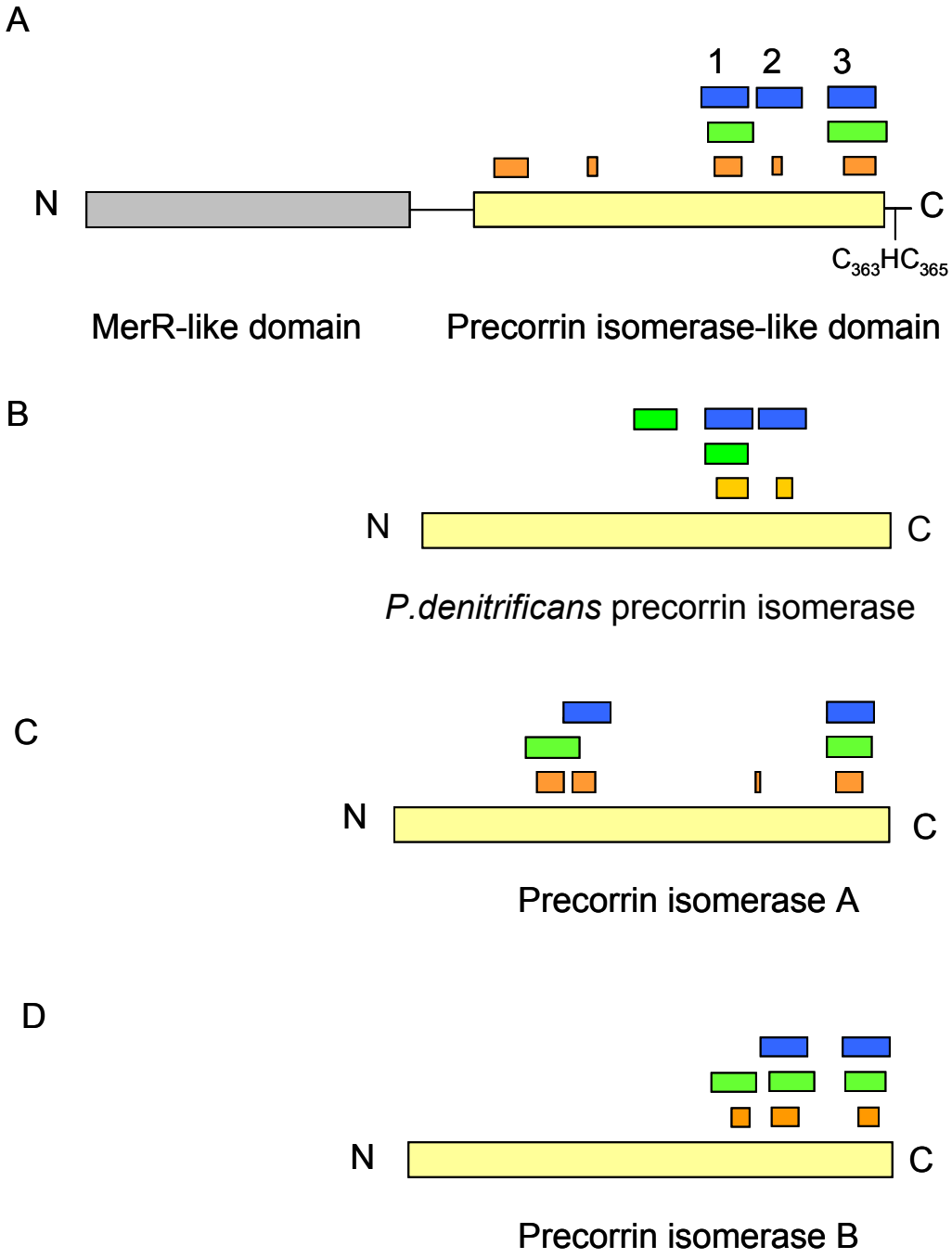

Figure 58. Positions of predicted hydrophobic regions in CoaR and precorrin isomerase sequences. The positions of hydrophobic regions predicted by DAS (orange boxes), TMPred (green boxes) and TopPred (blue boxes) are shown for CoaR (A), *P. denitrificans* precorrin isomerase (B), precorrin isomerase A (C) and precorrin isomerase B (D). For CoaR the MerR-like domain is also shown (grey boxed section) together with the position of the CHC motif previously shown to be essential for sensing *in vivo* (Rutherford *et al.* 1999). The positions and sizes of these regions and the lengths of each of the proteins are shown to scale. For CoaR, the three distinct hydrophobic regions are numbered 1-3.

6.3.2 Generation of a structural model for CoaR

The hydrophobic regions identified by bioinformatics analyses were explored further through production of a structural model for CoaR. Sections of CoaR sequence were threaded onto the solved structures for homologues of MerR and precorrin isomerase to produce a model of the structure of the CoaR protein (Figure 59). In the MerR-like domain, the helix-turn-helix motif is evident at the N-terminal end of the domain. This compact, globular region then runs into an extended α helix which is then shown linked to the C-terminal precorrin isomerase-like domain by a hypothetical linking region although this section could not be structurally modelled. The hydrophobic regions predicted to be present in the precorrin isomerase-like domain were mapped onto the predicted tertiary structure of CoaR (Figure 59b & c). Structural elements from hydrophobic regions 1 and 2 can be seen to combine to form two hydrophobic patches. The first is formed by one face of the α helix from region 1 together with the β-sheet/α-helix motif from region 2 (termed surface 1, Figure 59b & c). Another is derived from different parts of the same motifs-the N-terminal region of the region 1 α helix and the N-terminal region of the α helix that begins in hydrophobic region 2. The N-terminal region of the α helix in hydrophobic region 3 also contributes to this patch.

The hydrophobic dimerisation motif structurally validated in *P. denitrificans* (Shipman *et al.* 2001) aligns with residues in hydrophobic section 2 which run from the loop region following the single β strand to the start of the α helix (Figure 59). Parts of this sequence region could contribute to both hydrophobic surfaces identified in the protein. This supports the proposition that regions 1 and 2 contribute to a dimerisation interface. The third hydrophobic section at the extreme C-terminus of the domain is positioned at the opposite side of the domain, protrudes out of the main domain structure and does not substantially contribute to the surfaces formed by the other 2 regions (although the N-terminal of the hydrophobic α-helix does contribute to some extent to the surface 2 (Figure 59c). This supports the notion that this region may have a distinct role in the CoaR and also in precorrin isomerase A and B which also contain this motif.

Figure 59. Structural model of CoaR. A. The modelled structure of CoaR was constructed by threading residues 5-110 of the MerR-like domain and residues 174-358 of the precorrin isomerase-like domain onto the solved structures of BmrR (a MerR homologue from *B. subtilis;* PDB code: 1exj) (Heldwein & Brennan 2001) and Precorrin Isomerase (*P. denitrificans*; PDB code: 1f2v) (Shipman *et al.* 2001) using the Fugue tertiary structure prediction program (http://tardis.nibio.go.jp/fugue/). Structural models were generated independently for each domain and are shown in this representation linked by a loop region. The N-terminal five residues of the MerR domain and the C terminal 12 residues of the precorrin-like domain could not be modelled and are shown as unstructured loop segments. The approximate positions of potential metal liganding residues indentified previously (Rutherford *et al.* 1999) are highlighted. The locations of regions within the precorrin isomerase domain predicted to be hydrophobic are shown as coloured sections. Using the number designations from Figure 58, hydrophobic section 1 is shown in red, section 2 is shown in green and section 3 is shown in yellow. The modelled precorrin isomerase-like domain is shown viewed from alternative angles in B and C to show the relative positions of the predicted hydrophobic patches (the positions of the N terminal region of the precorrin domain are also shown for each orientation). The position of the sequence that aligns with the hydrophobic patch structurally validated as facilitating dimerisation in *P. denitrificans* precorrin isomerase is shown as a boxed region.

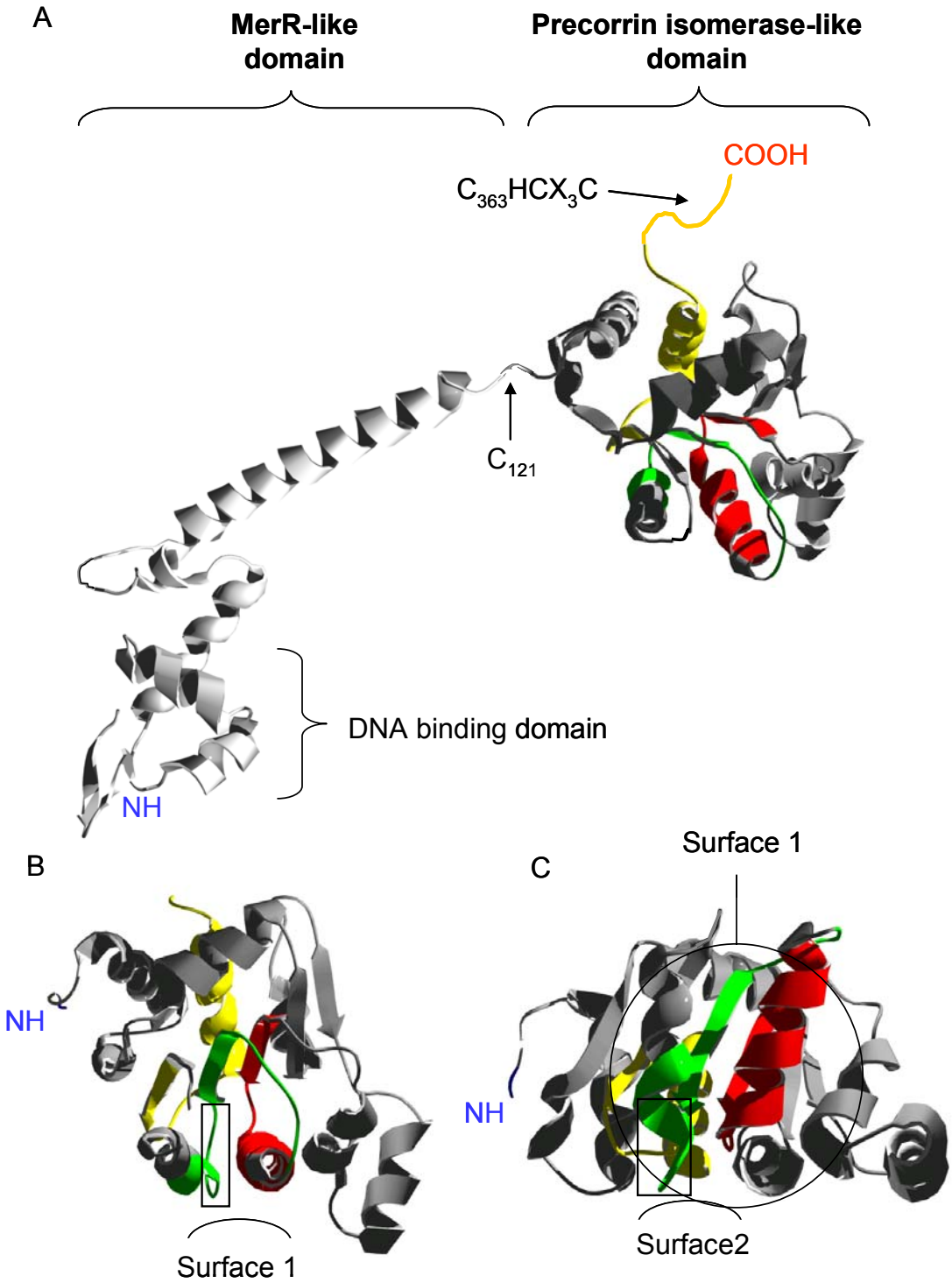
A
MerR-like domain
Precorrin isomerase-like domain
COOH
$C_{363}HCX_3C$
C_{121}
DNA binding domain
NH
B
NH
Surface 1
C
Surface 1
NH
Surface2

6.3.3 CoaR is a candidate membrane-associated protein in *Synechocystis*

It was hypothesised that the predicted hydrophobic region 3 in CoaR may mediate association with the membrane *in vivo*. Thus, protein precipitation facilitated by exposure of this (or another) hydrophobic motif to solution may have contributed to the previous failure to purify native CoaR. This region was conserved in precorrin isomerase A and B and so it was predicted that these proteins may also localise to the membrane *in vivo*. Evidence was therefore sought in support of this prediction. A literature survey confirmed that precorrin isomerase A has been shown to be membrane associated by *in vivo*; studies in which membrane proteins were isolated from total *Synechocystis* cell membrane preparations by interaction with a thioredoxin 'probe' identified precorrin isomerase A to be present in a fraction representing loosely associated membrane proteins (Mata-Cabana *et al*. 2007). Precorrin isomerase B and CoaR were not detected in this study however localisation to the membrane cannot be ruled out (e.g. intracellular concentrations may have been below detection level or they may have been lost altogether from the membrane fraction due to loose association with the membrane).

A literature survey revealed that multiple steps in the vitamin B_{12} synthesis pathway are localised to the membrane. Notably, in *Salmonella enterica,* CobS protein, a component of the CobNST cobaltochelatase complex and the oxidoreductase enzyme CbiB have both been shown to be integral membrane proteins (Maggio-Hall *et al.* 2004; Zayas *et al.* 2007). The detailed nature of the vitamin B_{12} pathway is poorly characterised in *Synechocystis* however, proteins homologous to those identified in the well characterised B_{12} pathway of *P. denitrificans* are present in *Synechocystis*; these proteins were identified by bioinformatics analyses the results of which are summarised in Table 9. The sequences of the homologues identified were analysed for the presence of hydrophobic/membrane spanning regions using programs also used in similar analyses for CoaR and precorrin isomerase (section 6.3.1). A majority of these homologues are predicted to have a low level of hydrophobicity (see Table 9). However, sll0378 and slr0636 both encode proteins predicted to contain multiple transmembrane helices. slr0963, a homologue to CobG (which is predicted to contain two transmembrane helices although it has not been reported as being membrane bound (Heldt *et al.* 2005; Schroeder *et al*. 2009)), also has predicted transmembrane helices and has been shown to be membrane associated by two previous studies (Mata-Cabana

et al. 2007; Pisareva *et al*. 2007). The proteins previously identified as being membrane localised in other organisms have homologues in *Synechocystis* either shown directly or predicted to be membrane bound. CobD and CobS (homologous to CbiB and CobS in *S. typhimurium* respectively) both contain candidate transmembrane helices predictive of membrane localisation. Notably, in all genome sequences of prokaryotic organisms analysed in previous work, both CobD and CobS are predicted to be hydrophobic proteins and thus are likely membrane associated (Maggio-Hall *et al.* 2004); there has likely been extensive selective pressure to maintain membrane localisation of the pathway throughout evolution. In summary, as in other organisms (Maggio-Hall *et al.* 2004) some components of the B_{12} pathway, including precorrin isomerase, are also likely to be membrane localised in *Synechocystis.* This provides support to the hypothesis that CoaR is also localised to the membrane (perhaps in association with other B_{12} pathway proteins) via its conserved hydrophobic region in the precorrin-isomerase like domain.

The length of the conserved C-terminal hydrophobic region in CoaR calculated from prediction algorithms varied between a minimum of 14 to a maximum of 26 residues (Table 8). Given that approximately 20 residues in an α-helix are required to span the 30 Å width of a typical membrane hydrocarbon core (Berg *et al.* 2002), the C-terminal hydrophobic region predicted to contain a helical segment is in theory long enough to traverse the membrane to form a single pass membrane protein. However, an alternative model, supported by the apparently weak association of precorrin isomerase A with the membrane (Mata-Cabana *et al.* 2007), is for this region to weakly associate with the inner membrane leaflet so as not to completely traverse the lipid bilayer (this is discussed in section 7.3).

6.3.4 Isolation and purification of native, recombinant CoaR protein using a non-ionic detergent

In light of the likely membrane association of CoaR *in vivo*, conditions previously used for purification of CoaR were optimised. Following overexpression, cells were lysed in buffer containing the non-ionic detergent n-Dodecyl β-D-maltoside (DDM). This detergent is routinely used to purify and reconstitute functional membrane proteins allowing *in vitro* characterisation of their native biochemical properties. DDM has been shown to be more effective than other commonly used detergents in retaining membrane

Table 9. Survey of components of the vitamin B_{12} biosynthetic pathway in *Synechocystis*. Summarised in the table are the main enzyme components of the aerobic B12 synthesis pathway characterised in *P. denitrificans* (from the scheme outlined in Heldt *et al.* 2005) together with their likely homologues in *Synechocystis* identified by BLAST search. Each of the homologues identified in *Synechocystis* were analysed for the presence of hydrophobic regions possibly correlated with membrane localisation using DAS, SOSUI, TMHMM, TMpred and TopPred. Proteins annotated as having low hydrophobicity were characterised by either no predicted regions of increased hydrophobicity or small regions (e.g. 2-10 residues predicted by DAS) scattered throughout the amino acid sequence thought to be unlikely to contribute to membrane associated regions. Cellular localisation remains to be verified for most proteins unless already directly demonstrated (e.g. precorrin isomerase).

Protein	Function	Homologue in *Synechocystis*	Possible Membrane domains/localisation
CobA	Methyltransferase	sll0378	Up to 6 transmembrane helices predicted in sll0378 by multiple algorithms (including SOSUI); Fewer in CobA, shown to be soluble (Blanche *et al.* 1989)
CobI	Methyltransferase	slr1879	Low hydrophobicity predicted
CobG	Monooxygenase	slr0898/slr0963	Annotated as nitrite & sulphite reductases respectively; slr0963 is membrane bound (likely loosely associated) (Mata-Cabana *et al.* 2007; Pisareva *et al.* 2007)
CobZ	Monooxygenase	No homologue Identified	CobZ replaces CobG in *Rhodobacter capsulatus*; membrane associated (McGoldrick et. al., 2005: Heldt *et al.* 2005)
CobJ	Methyltransferase	slr0969	Contains multiple predicted hydrophobic regions
CobM/F	Methyltransferase	slr0239	Low hydrophobicity predicted
CobK	Reductase	slr0252	Low hydrophobicity predicted
CobL	Methyltransferase & decarboxylase	sll0099	Low hydrophobicity predicted
CobH	isomerase	slr1467/slr0916	slr1467 is membrane associated (Mata-Cabana *et al.* 2007), predicted hydrophobic regions in each
CobB	Synthase	sll1501	Low hydrophobicity predicted
CobNST	Cobalt chelatase complex	N:slr1211 S:slr0636 T: No homologue	CobN predicted to have low hydrophobicity slr0636 has predicted transmembrane regions (8 predicted by SOSUI); Integral membrane protein in *S. enterica* (Maggio-Hall *et al.* 2004)
CobR	Reductase	slr0001 (Top hit)	CobR is soluble (Lawrence *et al.* 2008); slr0001 has no predicted TMHs/hydrophobic regions
CobO	Transferase	slr0260	Low hydrophobicity predicted
CobQ	Synthase	slr0618	Low hydrophobicity predicted
CobD	Oxidoreductase	slr1925	slr1925 has predicted TMHs (7 detected by SOSUI); *S. enterica* CbiB homologue is membrane bound (Zayas *et al.* 2007)
CobC	Aminotransferase	sll1713	Low hydrophobicity predicted
CobP	Oxidoreductase	slr0216	Low hydrophobicity predicted
CobU	Phospho-ribosyltransferase	slr0692	Low hydrophobicity predicted
CobV	Synthase	slr0636	Contains predicted transmembrane helices (8 predicted by SOSUI)

protein structure and stability (Casey & Reithmeier 1993; Taanman & Capaldi 1992). This agent was present in buffer used during cell lysis, protein purification and in buffers used for protein characterisation (See section 2.4.7 for a detailed description of protein purification protocols). By using this detergent it is was possible to successfully isolate large quantities of CoaR following overexpression in *E.coli* (see description below); this was not possible in the absence of detergent. In the first step of purification, crude cell extract was prepared and loaded onto Ni-affinity matrix which was subsequently eluted step-wise by application of Imidazole (Figure 60a). Fractions produced by Ni-affinity separation that were enriched for CoaR were pooled and purified further by cation-exchange chromatography. Most of the CoaR bound to the cation exchange matrix was eluted between 400-500 mM NaCl (Figure 60b) and fractions enriched for CoaR were purified to homogeneity by heparin affinity chromatography (Figure 60c).

6.3.5 Confirmation of functional CoaR in the presence of non-ionic detergent

To verify that functional CoaR had been produced the DNA binding affinity of the protein was analysed by fluorescence anisotropy. In previous studies, EMSA assays confirmed specific binding of both recombinant and endogenously expressed CoaR to a 77-bp fragment containing the *coa* operator-promoter region (Rutherford *et al.* 1999). Within this region a 13-6-13 hyphenated inverted repeat sequence was identified which overlapped the sub-optimally spaced -35 and -10 promoter elements which have been shown for other members of the MerR family to define the protein binding site (Figure 61a) (Hobman *et al.* 2005). A fragment of DNA with a sequence which incorporated the full extent of this inverted repeat motif was designed for use in fluorescence anisotropy (Figure 61a). Labelled and unlabelled complimentary oligonucleotides were annealed and formation of double-stranded, probe DNA was confirmed by Native PAGE analysis (Figure 61b).

Purified, recombinant CoaR protein was titrated with *coa* O/P oligonucleotide aerobically in the presence of DTT (5 mM) and the metal chelators EDTA (1 mM) and imidazole (200 mM) and the changes in anisotropy recorded. Increases in measured r_{obs} in the 0-100 nM concentration range indicated binding consistent with specific association of CoaR to DNA (Figure 62). The apparent disassociation constant for binding to *coa* DNA from these data of approximately 50 nM may be a minimal value

Figure 60. Purification of recombinant CoaR from the soluble cell fraction. A. SDS-PAGE analysis (15 % w/v acryl bis) of fractions from an example purification of recombinant CoaR from crude cell extract by Ni-affinity chromatography. Protein was eluted in increasing step-wise additions of Imidazole. B. SDS PAGE analysis of fractions produced from an example cation exchange purification of protein from fractions enriched for CoaR from the heparin step in A. C. SDS PAGE analysis of fractions from a heparin affinity purification of pooled fractions enriched for CoaR from the separation shown B.

A

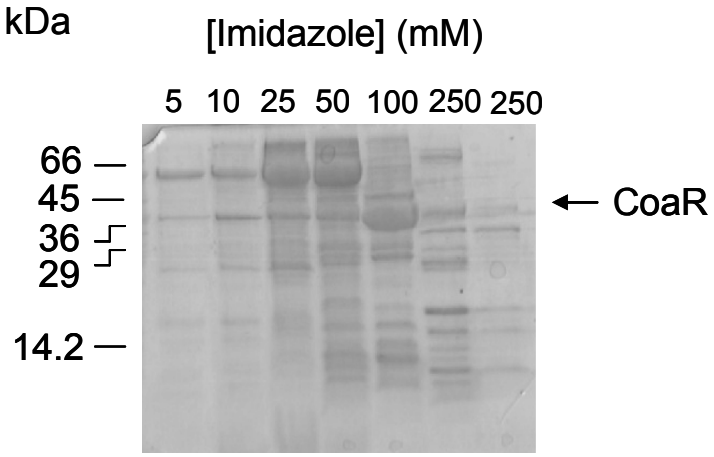
kDa
[Imidazole] (mM)
5 10 25 50 100 250 250
66
45
36
29
14.2
CoaR

B

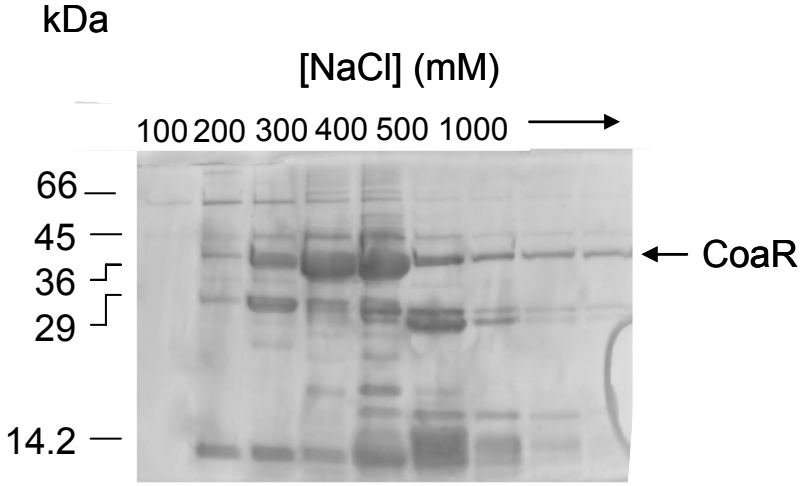
kDa
[NaCl] (mM)
100 200 300 400 500 1000
66
45
36
29
14.2
CoaR

C

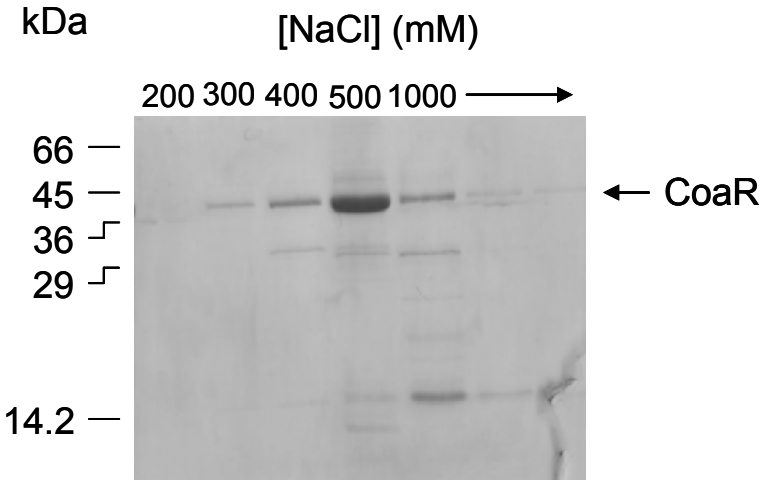
kDa
[NaCl] (mM)
200 300 400 500 1000
66
45
36
29
14.2
CoaR

with the true value being much tighter; however, additional replication would be needed to confirm this prediction. Nevertheless, this value is within the range of K_{DNA} values previously reported for soluble MerR family members and which were derived from equilibrium fluorescence anisotropy analyses. PbrR has affinities in the range 23 nM (holo) to 43 nM (apo) (Andoy *et al.* 2009). CueR has affinities in the range 17 nM (apo) to 25 nM (holo) (Stoyanov *et al.* 2001), derived from EMSA analyses. However, recent fluorescence anisotropy analyses for CueR have produced values an order of magnitude tighter than this for both apo (~6 nM) and holo (~1.9 nM) proteins (Andoy *et al.* 2009) an observation that again suggest the actual CoaR K_{DNA} may be substantially tighter than observed in these titrations.

The increases in r_{obs} observed are consistent with the formation of higher order CoaR complexes on binding DNA. After correcting for the much larger mass of CoaR relative to SmtB, an increase of approximately 0.2417 produced in this analysis (Figure 62) suggests binding of at least four CoaR dimers to DNA, a stoichiometry higher than expected given that previously characterised members of this family have been shown to be dimeric and to bind to their cognate promoter elements as functional homodimers (O'Halloran & Walsh 1987; Hobman *et al.* 2005). Recent analyses of binding of the MerR regulators CueR and PbR to DNA using fluorescence anisotropy have also shown much smaller increases in r_{obs} than observed here (Andoy *et al.* 2009). The relatively large Δr_{obs} values measured for CoaR may be due to effects of interaction with the detergent micelles which are unique to CoaR (This is discussed in detail in section 7.3).

To further confirm selective binding to the *coa* promoter element, *zia* O/P oligonucelotide was titrated with CoaR. Although substantial binding to this promoter element was observed, the apparent binding affinity for DNA was approximately an order of magnitude weaker suggesting this was due to non-specific association with DNA (Figure 62). In some experiments using protein produced by refolding, CoaR also showed binding to *coa* O/P oligonucelotide, albeit with a weaker K_{DNA}, with negligible binding to the *zia* O/P oligonucleotide. Analyses of reduced cysteine content of these refolded protein stocks by DTNB assay showed much lower reactivity indicative of oxidation of thiols to a much greater extent than that observed for CoaR preparations characterised in this work (see below). This effect may account for the weaker affinity for DNA measured for these protein preparations (N.Cant, data not shown).

A

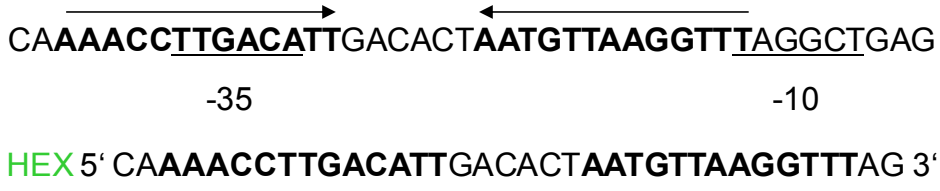

B

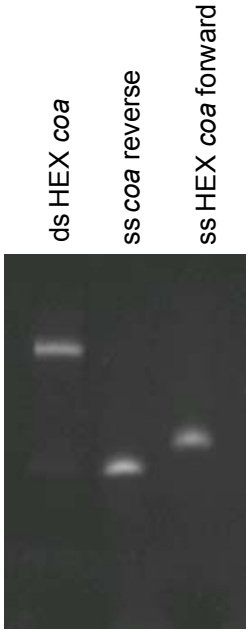

Figure 61. Production of annealed, double stranded *coa* DNA. A. Organisation of the CoaR promoter sequence showing positions of the -35 and -10 sites (underlined) and the inverted repeat sequence previously identified as the likely CoaR binding site (bold) (Rutherford *et al.* 1999). The sequence of the HEX labelled forward primer used for fluorescence anisotropy is also shown. B. Native PAGE analysis of annealed and single stranded fluorescence anisotropy primers confirming successful annealing.

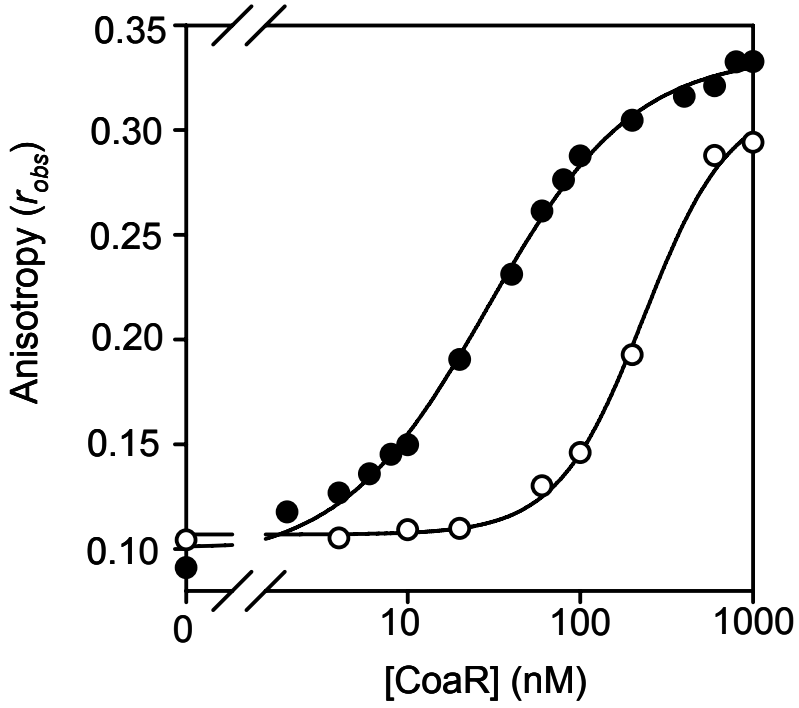

Figure 62. Example titration of recombinant CoaR with *coa* O/P oligonucleotide. CoaR was titrated with either 10 nM annealed *coa* O/P oligonucleotide (closed circles) or 10 nM *zia* O/P oligonucleotide (open circles), aerobically in the presence of 5 mM DTT, 1 mM EDTA and 200 mM Imidazole.

6.3.6 Measurement of reduced cysteine content of anaerobic, recombinant CoaR

Recombinant CoaR was prepared anaerobically using a protocol similar to that employed for ZiaR and Zur_{SS} (see section 2.5.2). For anaerobic CoaR stocks used for *in vitro* analyses presented in this work, DTNB assays estimated a mean value of 7.8 ± 1.3 (n=3) cysteines to be reduced out a total of nine in the protein. Substantially lower values were often observed for protein preparations produced by both refolding and using the soluble purification protocol described in 2.4.7; analyses of these preparations often showed much weaker metal dependent absorbance features in the UV-Visible spectrum compared to preparations with near 100 % reduction of thiol groups, indicative of oxidation of key cysteine ligand residues. Therefore, data from these preparations is not presented in this work.

6.3.7 Co^{2+} binding to CoaR monitored by UV-Visible and fluorescence spectroscopy

In previous work it was shown that mutation of a C-terminal pair of cysteines in the motif $C_{363}HC_{365}$ caused loss of CoaR sensing *in vivo* (Rutherford *et al.* 1999). Although these residues may not have bound Co^{2+} directly, if they did contribute to the primary ligand sphere Co^{2+} binding would be associated with intense LMCT features. Recombinant CoaR was titrated anaerobically with Co^{2+} and the UV-Visible spectra recorded. On addition of a single equivalent of Co^{2+} to CoaR LMCTs and *d-d* transitions were observed indicative of tetrahedral binding with a cysteine containing primary ligand sphere. CoaR was therefore able to bind Co^{2+} under these conditions (Figure 63). An intensity of approximately 3300 M^{-1} cm^{-1} at a wavelength of 310 nm characteristic of LMCT formation is most consistent with involvement of three cysteine residues. The tetrahedral geometry implied by *d-d* transitions (450 M^{-1} cm^{-1} at 650 nm) indicates involvement of a fourth non-thiol ligand to complete the tetrahedral chelate. The individual cysteine residues cannot be unequivocally assigned from these data. However, a model in which two of the cysteines in the chelate are derived from the C-terminal CHC motif, shown previously to be critical for sensing (Rutherford *et al.* 1999), would not be inconsistent with these data. A cysteine residue is positioned C-terminal to the CHC motif in the precorrin domain of CoaR however its role (if any) is not known. CoaR also contains a conserved cysteine residue at the extreme C-terminus

of the MerR-like domain (cysteine 121) which reporter gene assays performed subsequent to the *in vitro* analyses in this work suggesting this residue may be important for Co^{2+} sensing *in vivo* (see section 7.4 for further discussion).

UV-Visible titration of recombinant CoaR (5 μM) with multiple additions of increasing Co^{2+} concentration under anaerobic conditions produced Co^{2+} dependent increases in LMCT and *d-d* transition intensities (Figure 64a) with an apparent saturation of the LMCT signal (at 310 nm) at approximately one equivalent of Co^{2+}, although it is noted that the binding isotherm is defined by relatively few data points (few Co^{2+} additions were made to minimise Co^{2+}-dependent protein precipitation) (Figure 64b). The linear increase in LMCT intensity to approximately one equivalent suggests that no free Co^{2+} was present in this assay, which would indicate a $K_{Co} < 2.5$ μM. Addition of Zn^{2+} to the sample of CoaR at the end of this experiment resulted in a decrease in the intensities of both the LMCT and *d-d* transition signals (Figure 64a). The *d-d* transitions appear to be completely abolished after addition of one equivalent of Zn^{2+} with little change on addition of a second equivalent. LMCTs are reduced by approximately 75 % after one equivalent of Zn^{2+}, but addition of a second equivalent resulted in a small increase in signal. The almost complete loss of *d-d* transitions indicates complete replacement of Co^{2+} by Zn^{2+} at the binding site. The reason for the retention of some degree of Co^{2+}-S bonding implied by residual LMCTs post addition of Zn^{2+} is not clear; perhaps Co^{2+} displaced by Zn^{2+} bound weakly to additional thiols on the protein. Nevertheless, these data indicate that Zn^{2+} binds to CoaR with an affinity tighter than that of Co^{2+}.

Metal binding to proteins has been monitored previously by measurement of changes in intrinsic tyrosine and tryptophan fluorescence that occur on binding of metals to protein sites (VanZile *et al.* 2002a; Campbell *et al.* 2007). CoaR contains a total of seven tyrosine and three tryptophan residues (two are located in the precorrin isomerase-like domain and one in the linking domain, 28 residues C-terminal to Cys-121) and so it was anticipated that metal binding may be accompanied by measurable changes in intrinsic protein fluorescence. The changes in fluorescence emission (following excitation at 280 nm) of the CoaR sample used for UV-Visible analyses in Figure 64 were measured following each addition of Co^{2+}. Apo-CoaR produced an intense emission spectrum with an emission maximum at 340 nm (Figure 65a). This signal was quenched on titration with Co^{2+} (Figure 65a, b). This change appeared to saturate at approximately 1.5 equivalents of Co^{2+} however a change in the rate of

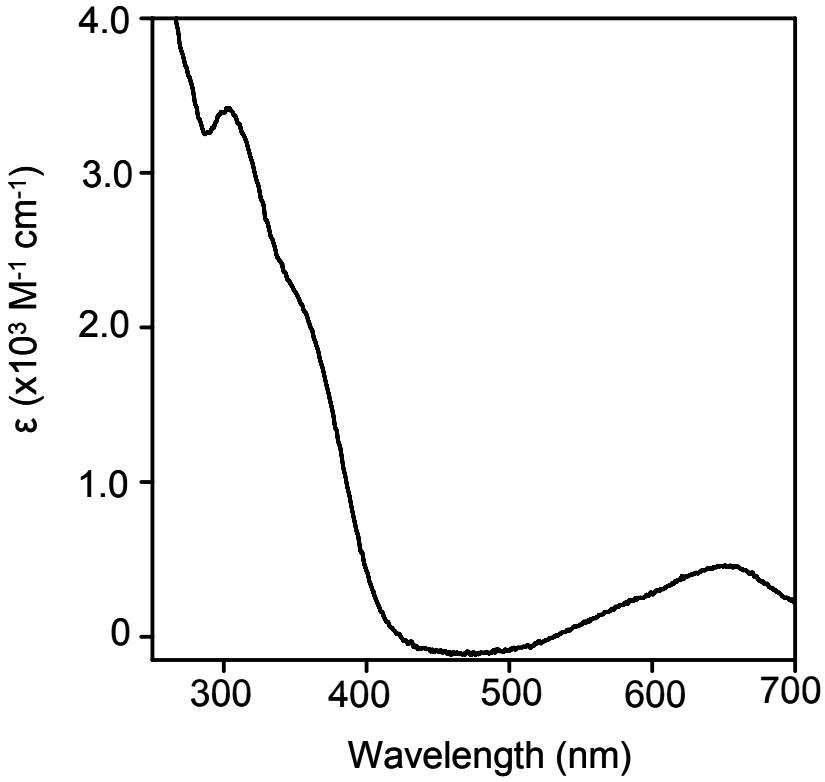

Figure 63. UV-Visible analysis of Co^{2+} binding to CoaR. Apo-subtracted difference spectrum recorded following addition of 1.1 equivalents of Co^{2+} to CoaR (9.3 μM) under anaerobic conditions.

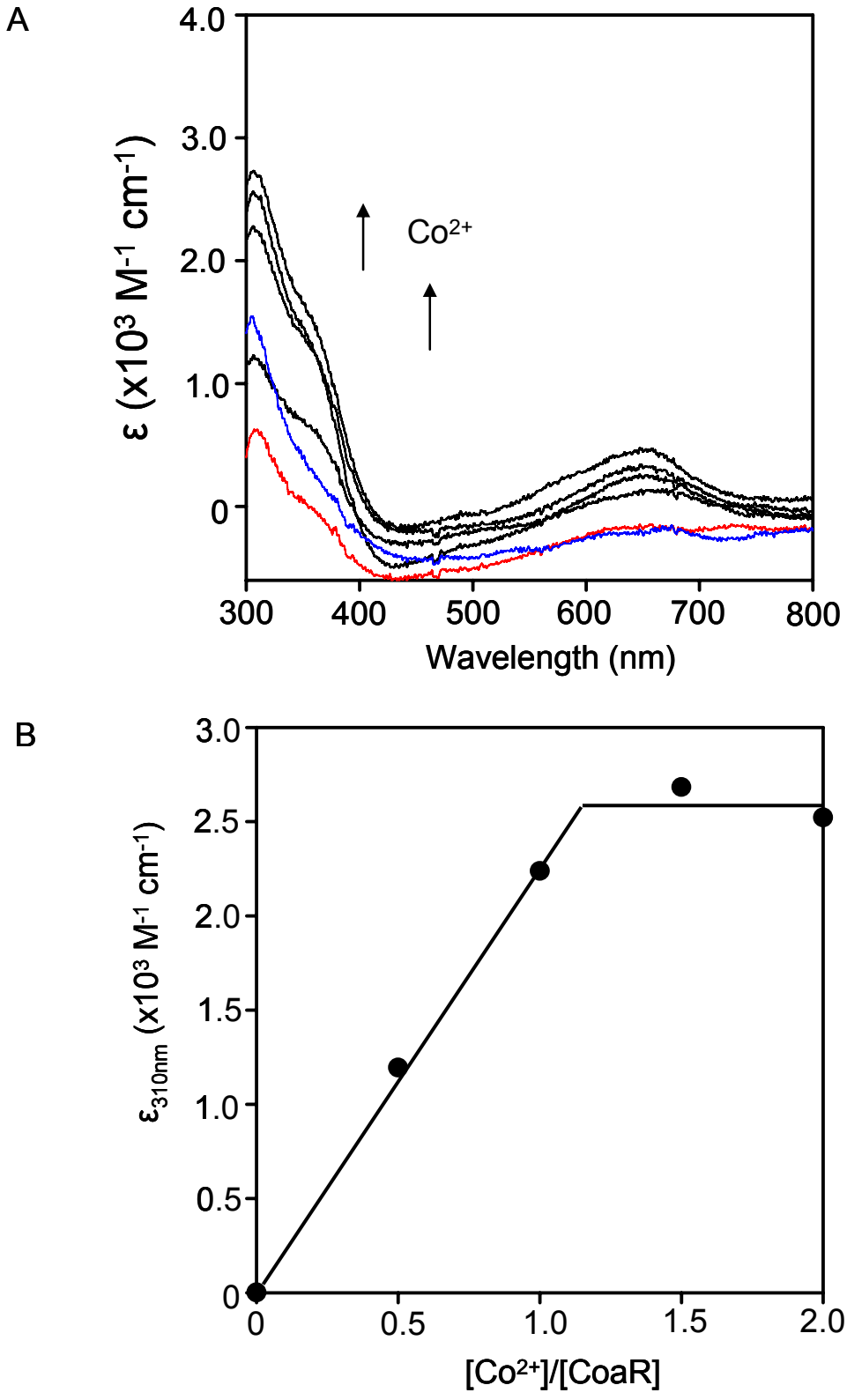

Figure 64. UV-Visible titration of CoaR with Co^{2+}. A. Apo-protein subtracted difference spectra produced following titration of 4.7 μM CoaR with Co^{2+}. Spectra produced by one equivalent (red line) and two equivalents (blue line) of Zn^{2+} added to the solution after the final addition of Co^{2+}, are also shown. B. Change in intensity of the LMCT feature at 310 nm with increasing [Co^{2+}].

quenching at the first equivalent of Co^{2+} is also apparent (Figure 65b). This contrasts with the much clearer saturation at one equivalent evident in absorption spectra from this sample (Figure 64).

The nature of the biochemical changes correlated with the changes in fluorescence emission intensities on Co^{2+} addition to CoaR remain unclear; they may be reporting on changes in the degree of solvent shielding of the tryptophan residues; a decrease in fluorescence emission intensity is consistent with increased solvent exposure. The complete loss of *d-d* transition features following addition of two equivalents of Zn^{2+} to this sample of CoaR (Figure 64) implied complete displacement of Co^{2+} from the tetrahedral binding site in CoaR after addition of one equivalent of Co^{2+}. The associated fluorescence emission spectrum following addition of the first equivalent of Zn^{2+} was similar to that produced following addition of a single equivalent of Co^{2+} (Figure 65). Addition of the second equivalent of Zn^{2+} caused no further change in the fluorescence emission spectrum (Figure 65). The d^{10} electron configuration of Zn^{2+} makes this ion spectrally silent in contrast to Co^{2+} which readily undergoes ligand-metal charge transfer. The increase in fluorescence emission following Zn^{2+} replacement of Co^{2+} on CoaR may have been due to a Förster-dipole coupling mechanism as outlined in Figure 66 and which has recently been suggested to account for differences in fluorescence quenching by Zn^{2+} and Cu^{2+} for the copper protein CucA (Waldron *et al.* 2010). Additionally, the observation that Zn^{2+} replacement of Co^{2+} in CoaR does not re-produce the apo-protein fluorescence emission spectrum (Figure 65) supports a model in which a proportion of the fluorescence quenching caused by Co^{2+} binding to CoaR is caused by changes in conformation which alter the environment of the tryptophan residue(s) being monitored (see above). Zn^{2+} is likely to adopt a Co^{2+}-like tetrahedral binding geometry and so it would be anticipated that conformational changes induced by the two ions in CoaR may be similar.

6.3.8 Estimation of the Co^{2+} affinity of CoaR by titration with the Co^{2+} binding indicator Fura-2

It was predicted that CoaR may have an affinity for Co^{2+} tighter than that of ZiaR and Zur_{SS}; Co^{2+} would therefore partition specifically to CoaR in preference to either ZiaR or Zur_{SS} *in vitro* and this property would underpin the differential responses of the sensors to Co^{2+} observed *in vivo*. To test this hypothesis, the Co^{2+} binding affinity for

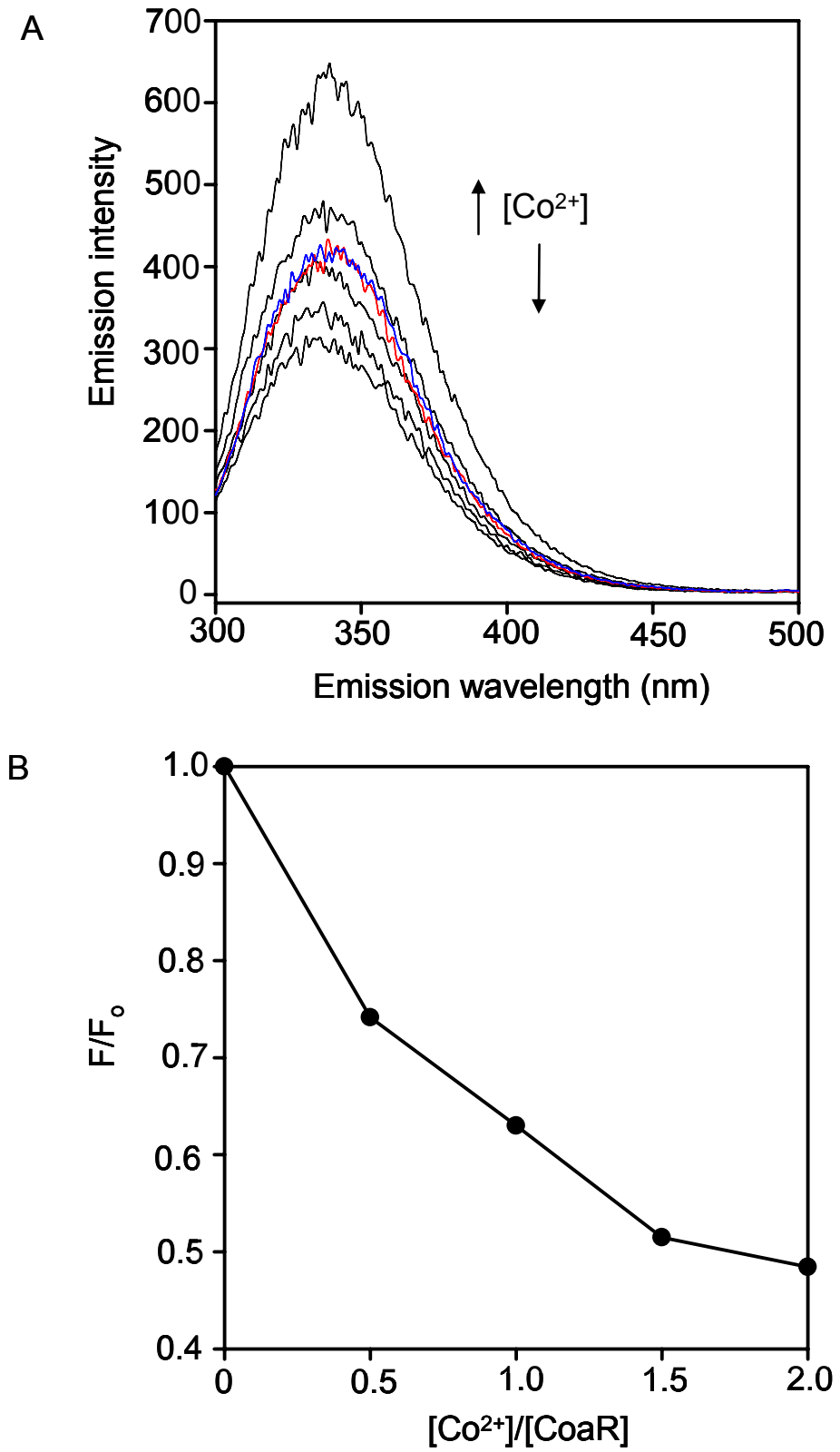

Figure 65. Measurement of changes in intrinsic protein fluorescence of recombinant CoaR following titration with Co^{2+}. A. CoaR (4.7 µM) was prepared anaerobically and titrated with Co^{2+} and emission spectra recorded following excitation at 280 nm. Emission spectra produced at one equivalent (red line) and two equivalents of Zn^{2+} added after Co^{2+} additions are also shown. B. Normalised changes in fluorescence for each concentration of Co^{2+} showing change in emission intensity at the peak wavelength of 340 nm.

Figure 66. Model for Förster-dipole coupling in CoaR. A. In apo-CoaR tryptophan is excited at a wavelength of 280 nm; this incident light is absorbed by the delocalised π electrons in the aromatic ring of tryptophan residues and re-emitted as fluorescence (λ_{em} max = 340 nm). B. The three Co-S^- bonds produced on Co^{2+} binding to CoaR absorb radiation in the UV range of the spectrum. Some of the emitted fluorescence following excitation at 280 nm is absorbed by the Co-S^- bonds resulting in reduced fluorescence emission intensity in Co^{2+} bound CoaR compared to apo-CoaR. A contribution to fluorescence quenching may also come from the protein adopting a different conformation (shown as the circle versus the square used in A) with an altered local tryptophan environment on binding Co^{2+}.C. Zn^{2+} can readily adopt the tetrahedral geometry adopted by Co^{2+} however Zn^{2+} is spectrally silent; the metal-ligand bonds do not absorb fluorescence emitted by tryptophan leaving more available for detection, producing an emitted fluorescence of greater intensity than for Co^{2+}-loaded CoaR. The intensity of emitted fluorescence may still be lower than for apo-CoaR in (A) because Zn^{2+} may promote Co^{2+}-like conformational changes in the protein which alter the local tryptophan environment and reduce the fluorescence emission intensity.

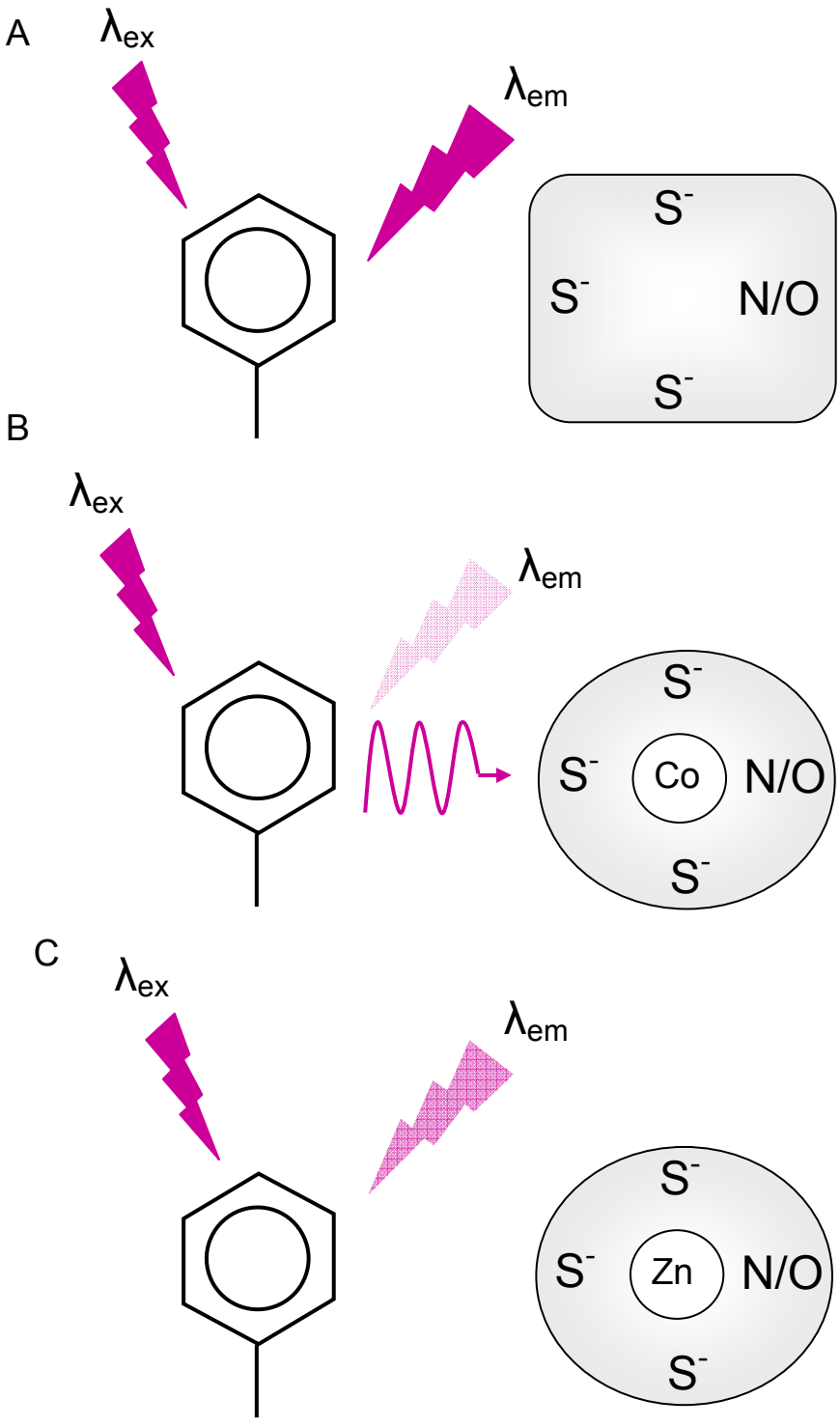
A
λex
λem
S-
S-
N/O
S-
B
λex
λem
S-
S-
Co
N/O
S-
C
λex
λem
S-
S-
Zn
N/O
S-

CoaR was determined under conditions identical to those used for ZiaR and Zur_{SS} (albeit in the presence of DDM to maintain native CoaR function). Upon titration of an equimolar solution of CoaR and Fura-2 with Co^{2+}, stoichiometric quenching of the Fura-2 fluorescence emission signal to one equivalent of Co^{2+} was reproducibly observed in three separate experiments with data similar to control experiments performed in the absence of protein (Figure 67), suggesting little competition with Fura-2 for Co^{2+}. In summary these data suggest CoaR has a weaker measured affinity for Co^{2+} than the allosteric site of Zur_{SS} and the tightest Co^{2+} binding site (α5) of ZiaR.

6.3.9 Competitive Co^{2+} binding analyses between Zur_{SS} and CoaR

The partitioning of Co^{2+} and Zn^{2+} to CoaR in the presence of an equimolar concentration of Zur_{SS} was analysed. On the basis of the Co^{2+} affinities for ZiaR, Zur_{SS} and CoaR (Table 10), it was predicted that Co^{2+} would bind to Zur_{SS} in preference to CoaR. If the Zn^{2+} affinities were correlated with the *in vivo* selectivities of these sensors another expectation was that Zn^{2+} would bind preferentially to Zur_{SS}. In previous studies the sensor proteins KmtR and NmtR from *M. tuberculosis* were mixed and the differential fluorescence changes following metal binding to each of the proteins used to assess Co^{2+} and Ni^{2+} partitioning to each protein (Campbell *et al.* 2007). In this work the fluorescence emission features associated with metal binding to CoaR were exploited to monitor the metal binding in the presence of Zur_{SS}.

Zn_1Zur_{SS} was prepared anaerobically and DDM was added to a final concentration of 0.1 % (identical to that routinely used for CoaR). Zur_{SS} contains five tyrosine residues but contains no tryptophan residues and so it was anticipated that Zur_{SS} would have a substantially smaller fluorescence yield following excitation at 280 nm. Following excitation of a 5 μM solution of Zn_1Zur_{SS} at 280 nm, the fluorescence intensity at the peak emission wavelength (305 nm) was ~200, approximately 1/3 rd the value previously obtained for CoaR (albeit at a lower emission wavelength than for CoaR) (Appendix D Figure 9). Addition of one equivalent of Co^{2+} substantially quenched this signal confirming Co^{2+} binding to the protein. During this work it has been shown that Zn^{2+} displaces Co^{2+} from the allosteric site of Zn_1Zur_{SS} (Figure 29). Addition of one equivalent of Zn^{2+} to $Zn_1Co_1Zur_{SS}$ in this analysis had little effect on the fluorescence signal suggesting that Zn_2Zur_{SS} and $Zn_1Co_1Zur_{SS}$ were spectrally identical in this assay (Appendix D Figure 9).

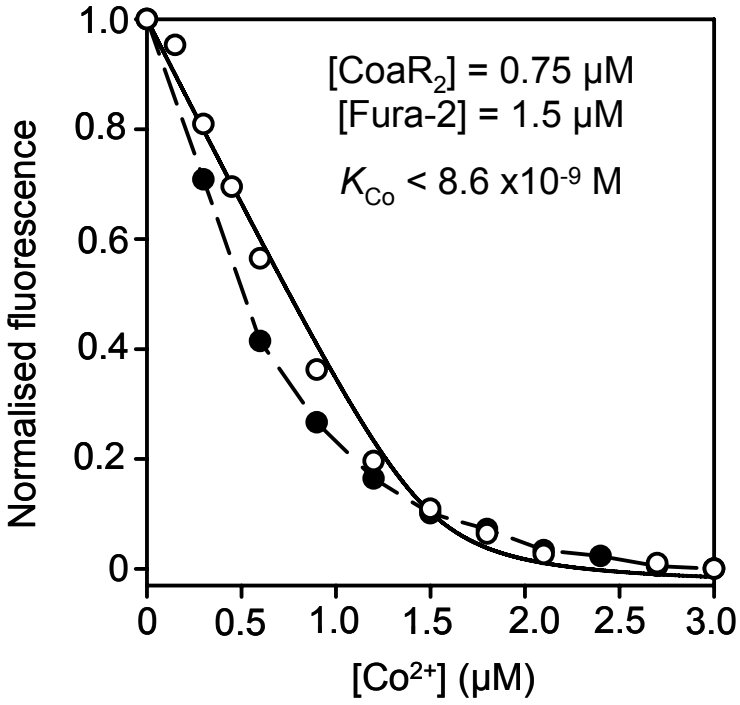

Figure 67. Measurement of Co^{2+} binding affinity of CoaR by Co^{2+} titration with Fura-2. CoaR (1.5 µM monomer) and Fura-2 (1.5 µM) were titrated with Co^{2+} and the changes in fluorescence at 500 nm were measured. Closed symbols; control data points, open symbols; protein and Fura-2. The line fitted to data from the protein/Fura-2 experiment was produced by least squares non-linear regression analysis using a two-site dimer model (assuming CoaR to be present as a dimer (0.75 µM) under these conditions); the binding constant was too weak to be modelled. Data were normalised as described in Figure 51.

	Co^{2+} disassociation constant (M)			
	K_{Co1}	K_{Co2}	K_{Co3}	K_{Co4}
ZiaR	a.1.1 x10^{-9} ± 0.61	*nd*	*nd*	*nd*
	b. 8 x10^{-9} ± 5.4	*nd*	-	-
	c. 2.51 x 10^{-9} ± 0.92	-	-	-
Zur_{SS}	a. 0.46 x 10^{-9} ± 0.37	*nd*	-	-
	b. 2.6 x 10^{-9} ± 0.69	-	-	-
	c. 1.2 x 10^{-9} ± 1.04	-	-	-
CoaR	< 2.5 x 10^{-6}	-	-	-

Table 10. Collated Co^{2+} disassociation constants (K_{Co}) for ZiaR, Zur_{SS} and CoaR. All values for ZiaR and Zur_{SS} are derived from Fura-2 competition experiments and represent means from n=3 datasets (example data shown in Figure 51 & 56). Values quoted are from dimer (a) and monomer models (b). Mean values are also shown for titration data in which only a subset of initial points were fitted (c) (see Figure 1 & 6 in Appendix D). The value for CoaR represents an upper limit and is derived from UV-Visible titration data (Figure 64). No Co^{2+} binding to CoaR was evident on titration with Fura-2. *nd*; no binding detected.

Optimal conditions for comparison of CoaR and Zur_{SS} would ensure minimisation of the fluorescence emission signal from Zur_{SS} (i.e. effectively zero for both apo- and metallated forms) whilst retaining a strong emission signal for apo-CoaR. At a longer excitation wavelength of 295 nm the emission signal from tyrosine residues is often substantially reduced whilst tryptophan emission is largely retained (Campbell *et al.* 2007). Adjusting the excitation wavelength to this value successfully reduced Zur_{SS} emission spectra intensities whilst retaining substantial emission from CoaR (albeit reduced by approximately 50 % compared to excitation at 280 nm) (Figure 68b). Emission spectra for Zur_{SS} following addition of Co^{2+} and then Zn^{2+} (one equivalent of each) were also of negligible intensity at this wavelength (Figure 68a). Following addition of one equivalent of Co^{2+} to CoaR, quenching of the fluorescence emission spectrum was again observed, albeit with a smaller relative decrease than observed at 280 nm (Figure 68b).

Following excitation at 295 nm of an equimolar solution of apo-CoaR and Zn_1Zur_{SS} (both 5 uM) (Figure 68c), the emission spectrum produced was almost identical in intensity to that obtained for CoaR alone (Figure 68b). On addition of one equivalent of Co^{2+} negligible decrease in the emission spectrum was observed as would have been expected if the Co^{2+} had bound exclusively to CoaR. These data are consistent with Co^{2+} populating the tighter affinity allosteric site of Zur_{SS} in preference to that of CoaR. These preliminary data are consistent with Zur_{SS} having a substantially tighter measured binding affinity for Co^{2+} than CoaR (Figure 56, 67; Table 10). It was thought that Zur_{SS} may have a tighter affinity for Zn^{2+} than CoaR and so addition of Zn^{2+} to the solution would displace Co^{2+} bound to Zur_{SS} (as shown in Figure 29). This Co^{2+} would then be available to bind to CoaR and cause quenching of the fluorescence emission signal. On addition of Zn^{2+} no change in emission intensity was observed at both one and two equivalents (data not shown). Zn^{2+} may have failed to displace Co^{2+} from Zur_{SS} (and there was no Zn^{2+} binding to CoaR) or the Co^{2+} displaced by Zn^{2+} may have failed to bind to CoaR. Both results are inconsistent with previous data showing rapid replacement of Co^{2+} by Zn^{2+} on Zn_1Zur_{SS} (Figure 29) and with data showing CoaR being fully capable of binding both Co^{2+} and Zn^{2+} under these conditions (Figure 64). The degree of quenching of CoaR fluorescence induced by Zn^{2+} was not measured at the excitation wavelength (295 nm) used for these comparative analyses however, the magnitude of quenching by Co^{2+} at this excitation wavelength was lower than when measured using an excitation wavelength of 280 nm (Figure 65, 68). In an alternative

model in which the Zn^{2+} binding to CoaR is associated with reduced (i.e. negligible) fluorescence quenching following excitation at 295 nm, immediate binding of the first added equivalent of Zn^{2+} to CoaR could account for these data. In the absence of additional competing ligands (e.g. CoaR), Zn^{2+} can rapidly replace Co^{2+} on Zn_1Zur_{SS} (Figure 29); however, the contribution of potentially slow exchange kinetics, for example, beween Zn^{2+}-bound CoaR (which may have a slow-off rate for Zn^{2+}) and Co^{2+}-bound Zur_{SS} may have affected these data. Some degree of protein precipitation may have occurred during this sequence of additions. These preliminary data require replication to clarify the nature of metal partitioning following this sequence of additions.

To further investigate the relative Zn^{2+} binding affinities of CoaR and ZiaR a separate converse experiment was performed in which 0.9 equivalents Zn^{2+} was added first to an equimolar solution of apo-CoaR and Zn_1Zur_{SS}. No change in emission intensity was observed on addition of Zn^{2+} whereas subsequent addition of 1.1 equivalents of Co^{2+} to this solution caused a decrease in emission intensity of approximately 27 % (slightly higher than the ~ 17 % decrease observed on addition of fewer equivalents (0.9) of Co^{2+} to CoaR alone) (Figure 68c). Zn^{2+} binds in preference to Co^{2+} at the binding sites of both Zn_1Zur_{SS} (Figure 29) and CoaR (Figure 64). Thus, these data imply that the Zn^{2+} added first must have bound to Zur_{SS} and not CoaR with the Co^{2+} added subsequently binding to CoaR. These preliminary results show that under these conditions, the allosteric site of Zur_{SS} has a tighter affinity for Zn^{2+} than CoaR.

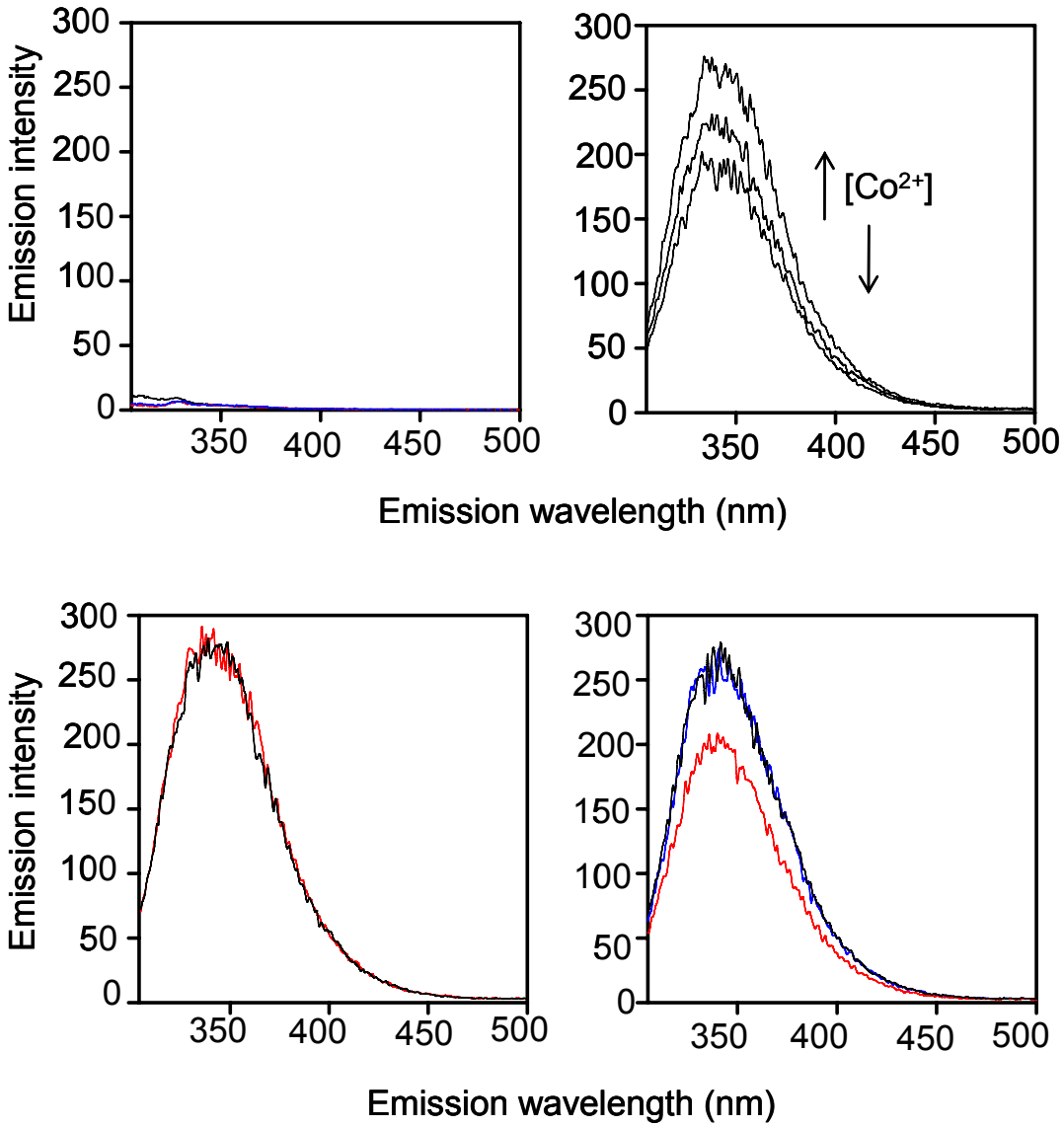

Figure 68. Measurement of Co^{2+} and Zn^{2+} binding to CoaR and Zur_{SS} following direct competition for metal binding. CoaR and Zur_{SS} were prepared anaerobically and excited at 295 nm. A. Emission spectra recorded for 5 μM Zn_1Zur_{SS} (black line), one equivalent Co^{2+} (red line) and one equivalent Zn^{2+} (blue line). B. Emission spectra for apo-CoaR (5 μM) and following addition of 0.9 and 1.8 equivalents Co^{2+}. C. Emission spectra recorded for a mixture of CoaR and Zn_1Zur_{SS} (both 5 μM) at 0 metal (black line) and following addition of one equivalent of Co^{2+} (red line). D. Emission spectra recorded for a mixture of CoaR and Zn_1Zur_{SS} (both 5 μM) for 0 metal (black line), 0.9 equivalents Zn^{2+} (blue line), which was added first and 1.1 equivalents of Co^{2+} (red line) added after the Zn^{2+} addition.

Chapter 7. Discussion and Further Work

7.1 ZiaR is an α3N/α5 sensor that does not sense Cu^{+}

The data presented in these studies show that ZiaR can be allosterically regulated by Zn^{2+}, Co^{2+} and Cd^{2+} but not Ni^{2+}, Mn^{2+} and Cu^{+} *in vitro* (section 6.1). Co^{2+} (and by inference Zn^{2+}) bind in tetrahedral geometries (Figure 10) and Cd^{2+} prefers tetrahedral geometries and spectral data were consistent with formation of this type of complex (Figure 55). However, Ni^{2+} adopted a non-tetrahedral geometry (likely six-coordinate) (Figure 53). Although the structural features of Mn^{2+} binding were not investigated Mn^{2+} also prefers 6-coordinate geometries. These data highlight the importance of allostery in metal-sensing de-repressor proteins, such as ZiaR; for ZiaR, the efficacy of metal ions to inhibit DNA binding is correlated with the adoption of a native-like metal coordination geometry. Zn_1Zur_{SS} could not be produced in fluorescence anisotropy analyses and so it remains to be determined whether or not allostery is generally more important for co-repressor and activator type sensors (Waldron *et al*. 2009).

The data presented in these studies show that ZiaR has functional α3N and α5 sites and on mutation of either site the protein retains metalloregulation through the other unaltered binding site (Figure 18). Therefore, ZiaR does not require both sites for metalloregulation *in vitro* as was initially anticipated and has been shown to be the case *in vivo* (Thelwell *et al.* 1998). Instead of representing a distinct sensory paradigm in which both sites are absolutely required for function as previously suggested (Thelwell *et al.* 1998), allosteric regulation can occur via either the α3N or the α5 site *in vitro*. The experiments described in section 3.4.6 were initially undertaken to test the hypothesis that the loss of sensing by each mutant *in vivo* was caused by a reduction in Zn^{2+} binding affinity in the mutant proteins. The mean K_{Zn1} values for both the Δα3ZiaR and Δα5ZiaR were approximately two-fold weaker than for ZiaR (Table 6) and the initial gradients of the binding curves for both Δα3ZiaR and Δα5ZiaR were slightly steeper than for ZiaR (Appendix A Figure 2); however statistical analyses showed these differences not to be statistically significant. It is possible that a relatively small weakening in the Zn^{2+} binding affinities of Δα3ZiaR and Δα5ZiaR (i.e. substantially less than order of magnitude) may have been beyond the limits of detection of this assay. The different fluorescence emission changes observed on the binding of Zn^{2+} to

ZiaR, Δα3ZiaR and Δα5ZiaR (Figure 22) provides a means of identifying Zn^{2+} occupancy of each protein following direct pair-wise competition of the proteins for Zn^{2+} binding. This approach may allow any subtle differences in affinity for Zn^{2+} to be detected. In a model in which the mutant proteins do have significantly weaker, comparable affinities for Zn^{2+} relative to ZiaR, the model described in Figure 23-24 would have to be adapted to accommodate some degree of positive cooperativity between the α3N and α5 sites in the wild-type protein which was lost on mutation of either site. The loss of positive cooperativity, and associated decrease in Zn^{2+} affinity, would therefore be proposed to underpin the loss of responses observed *in vivo* for each metal-site mutant.

ZiaR has a Zn^{2+}-induced allosteric mechanism similar to that proposed for BxmR, which is the homologue most closely related to ZiaR and which shares an identical α5 site and a similar α3N site (Figure 4). BxmR has been proposed to be a Cu^{+}-sensing ArsR-SmtB protein based on studies showing a response to Cu^{+} *in vivo* (Liu *et al.* 2004) and *in vitro* (Liu *et al.* 2008). Crucially, unlike BxmR, ZiaR does not respond to Cu^{+} *in vitro* (Figure 47). Moreover, there is no evidence that copper is allosterically effective i*n vivo*; in previous studies no evidence was obtained that would suggest copper-mediated de-repression of expression from the ZiaR regulated *ziaA* promoter and there is no evidence to suggest that a Cu^{+} transport function has evolved in ZiaA (Thelwell *et al.* 1998).

Further *in vivo* analyses (in which expression from a *zia-lacZ* promoter fusion was monitored by β-galactosidase assays and *ziaA* transcript abundance was analysed by RT-PCR) performed subsequent to the work presented in this thesis confirmed that ZiaR did not sense Cu^{+} even in a mutant strain of *Synechocystis* missing the cytosolic copper chaperone Atx1 (Δ*atx1*) in which it was anticipated that Cu^{+} normally trafficked by Atx1 may interfere with regulation at the *ziaA* promoter (Figure 69; these data were collected by Samantha Dainty). No significant increase in *lacZ* expression was observed up to inhibitory concentrations of copper (1 μM) in wild-type and Δ*atx1* cells (Figure 69a) implying Cu^{+} does not inhibit ZiaR binding to DNA *in vivo*. The absence of any increase in *ziaA* expression with increasing concentrations of exogenous copper also ruled out copper dependent displacement of Zn^{2+} from intracellular pools which could potentially be detected by ZiaR. No copper dependent inhibition of Zn^{2+}-induced *zia* expression was also observed in either strain (Figure 69) suggesting two possibilities; (i) in Δ*atx1* cells, Cu^{+} normally bound to Atx1 either binds to ZiaR via its α3N sites failing

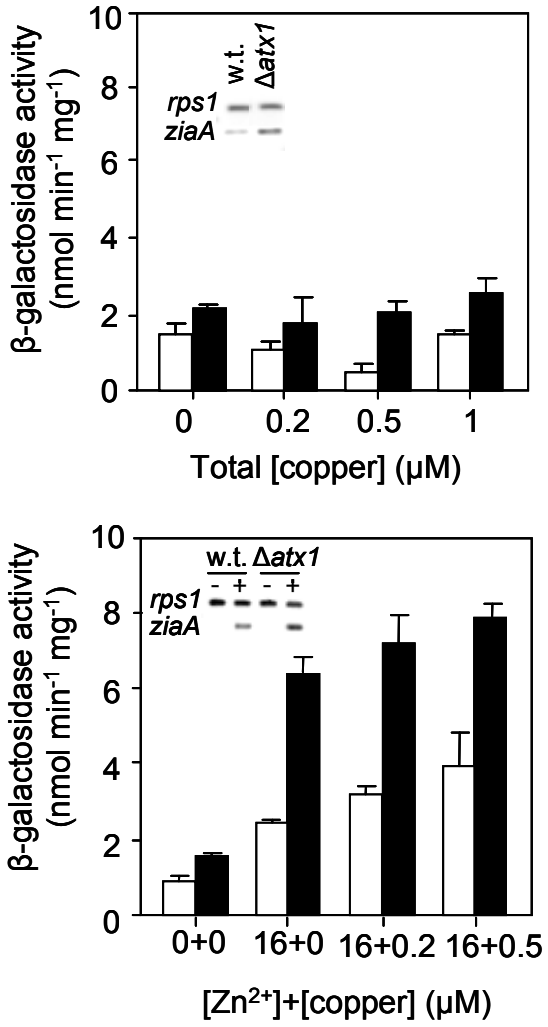

Figure 69. *LacZ* assays monitoring zinc and copper induced changes in *zia* promoter regulation in *Synechocystis*. A. Wild-type (open bars) and Δ*atx1* (closed bars) cells were cultured in the specified amount of copper for 48 hr prior to assay of β-galactosidase activity. RT-PCR analyses of *ziaA* transcript abundances in each strain are shown in as insets. B. Wild-type (open bars) and Δ*atx1* (closed bars) cells cultured in the presence of indicated concentrations of zinc and copper prior to assay of β-galactosidase activity. RT-PCR analyses of *ziaA* transcript abundance is again shown in the inset. These data were collected by Samantha Dainty and published in Dainty *et al.* 2010 (Appendix E).

to activate allostery whilst retaining Zn^{2+} allostery at the α5 sites or (ii) that Cu^{+}-ZiaR does not form *in vivo.*

The absence of a Cu^{+}-dependent increase in expression from the *zia* promoter (Figure 69a, b) argues against a Cu^{+}-dependent 'potentiation' of the Zn^{2+} response of ZiaR associated with Cu^{+} occupation of the α3N sites, an effect which may have been predicted to occur given the lower Zn^{2+} concentration required to disassociate Δα3 ZiaR-DNA complexes (Figure 18) (although *in vitro* data showing a wild-type like stoichiometry on titration of Cu-loaded ZiaR-DNA complex with Zn^{2+} would also suggest that the Zn^{2+} stoichiometry of Cu^{+}-bound and Δα3 ZiaR are not the same potentially arguing against this possibility (Appendix C Figure 2)). Given that previous work showed mutation of the α3N site completely abrogated Zn^{2+} induction *in vivo* in *Synechococcus* PCC 7942 (Thelwell *et al*. 1998) and that this is associated with loss of Zn^{2+} binding to this site *in vitro* (Appendix A Figure 2) one expectation was that binding of copper in preference to Zn^{2+} to the α3N site may lead to loss of Zn^{2+} induction *in vivo*. Although the effects on ZiaR function of such a mutation in the context of the *Synechocystis* host used in this work were not analysed, there was no inhibition in Zn^{2+} sensing *in vivo* by copper in either strain analysed (Figure 69). These observations provide support to model (ii) described above, with Cu^{+}-ZiaR not formed *in vivo*.

What could account for the apparent differences in the *in vitro* Cu^{+} responses for ZiaR and BxmR? One explanation may be due to the different ligand sets of the α3N sites in each protein. ZiaR contains an AztR-like trithiolate α3N site (Figure 4) (which also shows Zn^{2+} but not Cu^{+} regulation *in vivo* (Liu *et al.* 2004)) whereas BxmR has a tetrathiolate site. Consequently, the Cu^{+} binding properties of both proteins are different; the ZiaR α3N site is predicted not to be capable of supporting the formation of the complete Cu_2S_4 complex observed in BxmR and *in vitro* data are consistent with formation of a Cu_2S_3 complex in the α3N site of ZiaR (Figure 40, 45). Such a complex may be predicted to be less effective at driving allostery compared to the complete cluster formed in BxmR. *In vitro* DNA binding data for the two proteins are not directly comparable as robust association experiments in which ZiaR was pre-incubated in a saturating concentration of Cu^{+} were unable to be performed; conversely, disassociation experiments monitoring Cu^{+}-mediated release of BxmR-DNA complexes have not been published. Therefore, the difference in the magnitude of Cu^{+}-dependent weakening of

the DNA binding affinity of each protein remains to be tested. A prediction is that K_{DNA} for ZiaR pre-incubated in Cu^{+} will be tighter than for BxmR.

An alternative explanation to account for the differences between ZiaR and BxmR is that BxmR is in fact not a *bona fide* Cu^{+} sensor. A reinterpretation of previous data supports this proposal. BxmR was shown to regulate expression of a CPx-ATPase (Bxa1) (Liu *et al.* 2004) that confers resistance (and is postulated to export) both monovalent (Cu^{+} and Ag^{+}) and divalent (Zn^{2+} and Cd^{2+}) metal ions (Tong *et al.* 2002) in addition to regulating expression of *bmtA*, encoding a Cd^{2+}/Zn^{2+} inducible metallothionein that conferred resistance to these metals *in vivo* (Liu *et al.* 2003). However, rQRT-PCR analyses showed that Zn^{2+} was the most effective inducer of Bxa1 mRNA (five times more effective than Cu^{+}) (Tong *et al.* 2002). Subsequent rQRT-PCR analyses showed metal concentration-dependent increases in expression of *bxmR, bmtA* and *bxa1* in response to Cu^{+} (as well as Zn^{2+}, Cd^{2+} and Ag^{+}) *in vivo* (Liu *et al.* 2004). This effect may have been due to displacement of intracellular Zn^{2+} pools which were subsequently detected by BxmR. Experiments using coupled *in vitro* transcription/translation systems showed increased Bxa1 synthesis in response to these metals (Liu *et al*. 2004) however, this assay may have been subject to the same effects (Zn^{2+} pools may have been displaced from proteins present in the *E.coli* S30 cell lysate used in this system). Critically, these *in vitro* analyses were performed aerobically using Cu^{2+} salts instead of Cu^{+} which is the likely oxidation state of this ion *in vivo*.

Although the Cu^{+}-dependent allosteric effect for BxmR was abrogated by mutation of α3N cysteine residues in BxmR, only a modest Cu^{+}-dependent decrease in the DNA binding affinity for wild-type BxmR (approximately five-fold) was observed (Liu *et al.* 2008). Fluorescence anisotropy analyses of the CsoR-family Cu^{+} sensor from *M. tuberculosis* have shown a weakening of 1-2 orders of magnitude in the DNA binding affinity for the Cu^{+} bound form (Ma *et al.* 2009a). A reduced protein-DNA binding stoichiometry is also apparent for Cu^{+}-bound CsoR and it has been proposed that inducer effectiveness may correlate with the degree of inhibition of formation of a higher order octameric complex by Cu^{+} in addition to changes in the DNA binding affinity. Nevertheless, the reduction in binding affinity for CsoR is much greater than that for BxmR. Additionally, although DNA association curves for Zn^{2+}-bound BxmR were not presented in previous work (Liu *et al.* 2008) those for α3N site mutants (in which α5 Zn^{2+} site regulation was retained) were presented and they showed a substantially greater weakening in DNA binding affinity for Zn^{2+}-bound mutant α3N

BxmR compared to Cu^{+}-bound wild-type BxmR (Liu *et al.* 2008); this would suggest more potent regulation by Zn^{2+} for BxmR which is exactly what is observed for ZiaR (Figure 47). Perhaps, like ZiaR, BxmR is instead primarily a Zn^{2+} sensor *in vivo* and *in vitro*. It was suggested that the Cu^{+} resistance conferred by the BxmR/Bxa1/BmtA system may have a role in mediating resistance to copper containing algaecides routinely used to control *O. brevis* growth in water used in catfish aquaculture (Liu *et al.* 2008). The Bxa1 Cpx-ATPase confers resistance to Zn^{2+}, Cd^{2+} and also Ag^{+} and Cu^{+} (Tong *et al.* 2002) and the SmtA-like metallothionein BmtA confers resistance to Cd^{2+} and Zn^{2+} *in vivo* (Liu *et al.* 2003). Perhaps selective pressure has acted to optimise monovalent ion transport functions in Bxa1 instead of monovalent ion sensing in BxmR.

It is unclear why ZiaR retains potent divalent metal ion regulation through both its α3N and α5 metal binding sites. A recently proposed hypothesis has suggested that some metalloregulator proteins may contain ligands at or nearby the metal binding sites which may act to 'lure' incorrect metals into binding the protein in a non-native coordination geometry that is not allosterically effective (Waldron *et al.* 2009). Both ZiaR and Zur_{SS} both contain cysteine residues in at least some of their metal binding sites (the α3N site but not the α5 site in ZiaR). In both proteins, Cu^{+} binding is accompanied by binding to multiple cysteine residues within the metal site for ZiaR (Figure 40, 46) and both inside and likely outside the site for Zur_{SS} (Figure 48). For both proteins Cu^{+} is not regulatory (Figure 47, 50) and in ZiaR this was shown to be accompanied by formation of a non-native α3N chelate structure (Figure 45). Perhaps the high cytosolic Cu^{+} demands of *Synechocystis* have driven the conservation of cysteine ligands in/around metal binding sites which can bind and trap aberrantly released, thiophilic Cu^{+} into allosterically ineffective complexes. At α3 sites of ArsR-SmtB proteins, conserved cysteine residues (notably in the CVC motif) (Figure 4) are correlated with conservation of metalloregulation at that site. Therefore, in the case of ZiaR, this may have contributed to the conservation of two functional metal sites with the advantage that even on formation of allosterically ineffective Cu^{+} complexes at the α3N sites, allosteric regulation by Zn^{2+} at the α5 sites is retained. It is interesting that the related ArsR-SmtB sensor SmtB, also from a photosynthetic cyanobacterium, contains an α3 site that can bind metals in addition to metal binding and regulation via the *bona fide* α5 allosteric sites. The Cu^{+} binding properties of this site remain to be analysed.

Another explanation to account for the retention of two functional metal sites in ZiaR may be to expand the sensory abilities of the protein. In these studies it was shown that Cd^{2+} binds stoichiometrically to the α3N sites in ZiaR and impairs DNA binding (Figure 55) most likely through formation of an S_3N tetrahedral complex akin to that formed by Zn^{2+} and Co^{2+}. In previous work in which transcription from the *zia* promoter was monitored in *Synechococcus* PCC 7942 in response to metals, enhanced expression was detected following treatment of Zn^{2+} only (Thelwell *et al.* 1998). However, a two-fold increase in Cd^{2+} tolerance was detected in the cells of the same strain containing *ziaA* and *ziaR*, suggesting ZiaA could export Cd^{2+} ions. Perhaps ZiaR can function as a Cd^{2+} sensor under certain conditions to facilitate removal of this ion by up-regulation of ZiaA expression. This function may be facilitated by the presence of intact α3N sites that bind highly thiophilic Cd^{2+} ions.

7.2 The factors determining selective metal responses of ZiaR, Zur_{SS} and CoaR-access, affinity and allostery

7.2.1 Atx1 restricts access to Zn^{2+} *in vivo*

In vivo analyses of ZiaR-regulated expression from the *zia* promoter showed higher β-galactosidase activity for cells of the Δ*atx1* strain of *Synechocystis* compared to those of the wild-type strain and this was accompanied by an increased abundance of *ziaA* transcript in the Δ*atx1* strain (Figure 69). Because Cu^{+} is not an allosteric effector of ZiaR *in vitro* (Figure 47) and because expression from the *zia* promoter displays no copper-dependency *in vivo* (Figure 69), these data implied that this effect was due to enhanced formation of Zn^{2+}-ZiaR, rather than Cu^{+}-ZiaR, in the Δ*atx1* strain missing the Atx1 chaperone. The increase in formation of Zn^{2+}-ZiaR due to the loss of Atx1 implied Zn^{2+} binding to Atx1 *in vivo*. Evidence in support of this was obtained from subsequent experiments in which protein-bound and free metal ions from cell extracts containing Atx1 were separated by size-exclusion chromatography (data was obtained by K. Waldron). The abundance of both Zn^{2+} and Cu^{+} in native Δ*atx1* cell extracts was reduced (Figure 70, panels a, b) at the elution volume of Atx1 expressed in *E.coli* (Figure 70, panels c, d). The presence of plastocyanin in these fractions combined with the likely low level of expression of Atx1 from its endogenous promoter means that it was not possible to unequivocally determine the metal content of Atx1 expressed in

Figure 70. *In vivo* Zn^{2+} binding properties of Atx1. Crude cell extracts from *Synechocystis* wild-type and Δ*atx1* strains (a and b respectively) were separated by size-exclusion chromatography on Sephadex G-75 matrix. Eluted fractions were analysed for copper (triangles) and Zn^{2+} (squares) by ICP-MS and for protein by Coomassie assay. Analogous separations are shown for extracts from *E.coli* cells expressing recombinant Atx1 under conditions of Zn^{2+} (0.5 mM) (c) and copper (1 mM) supplementation (d). A control separation is shown using cell extracts from *E.coli* cells (grown with 1 mM copper supplementation) containing the pET29a expression plasmid without *atx1* (e); the metals can be seen to run at the total volume (Vt) and the proteins at the column void (Vo). These data were collected by Kevin Waldron and published in Dainty *et al.* 2010 (Appendix E).

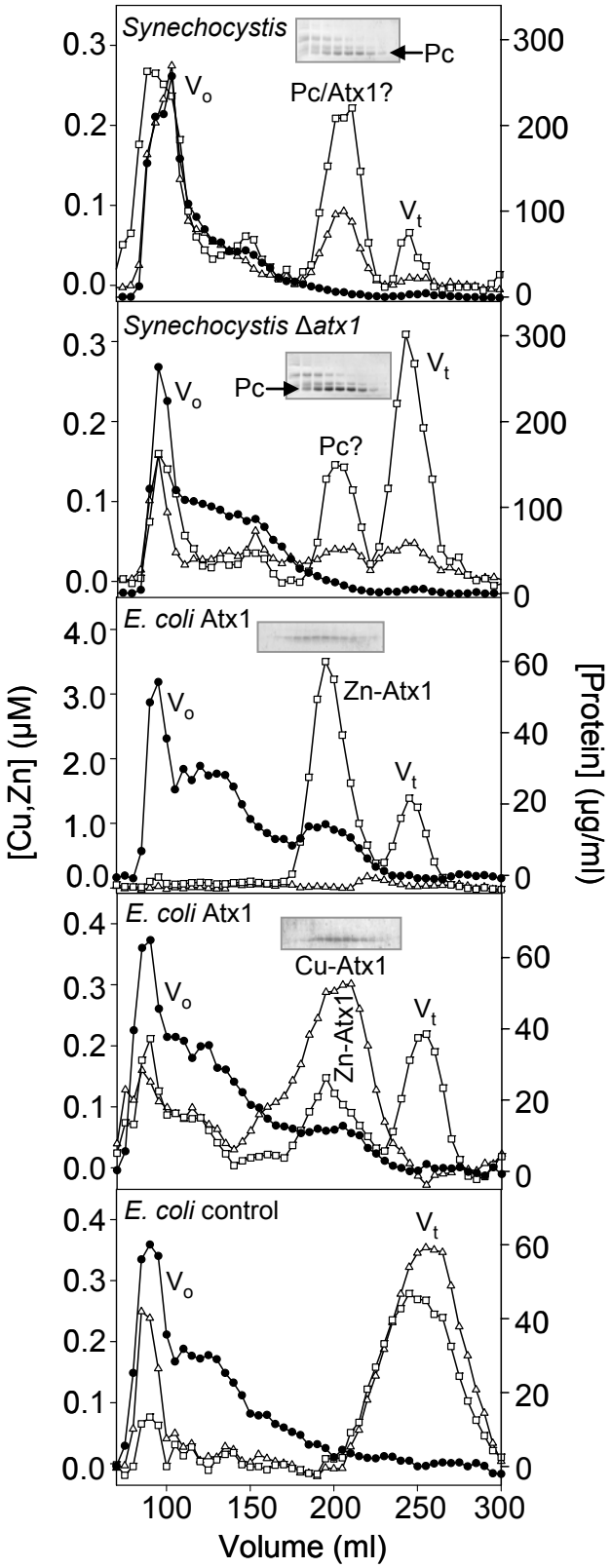
Synechocystis
Pc
Pc/Atx1?
Vo
Vt
Synechocystis Δatx1
Pc
Pc?
E. coli Atx1
Zn-Atx1
E. coli Atx1
Cu-Atx1
Zn-Atx1
E. coli control
[Cu,Zn] (μM)
[Protein] (μg/ml)
Volume (ml)

Synechocystis. However, an increase was observed in low molecular weight Zn^{2+} complexes in Δ*atx1* concomitant with the loss of Zn^{2+} in the Atx1 region of the chromatogram (Figure 70 panels a, b). Following overexpression in *E.coli* cells, Zn-Atx1 only was isolated following growth of cells *E.coli* cells in growth medium containing Zn^{2+} at non-inhibitory concentrations (0.5 mM) (Figure 70, panels d, e) and Zn^{2+}-Atx1 was also recovered in addition to Cu-Atx1 from cells grown with non-inhibitory concentrations of copper (1 mM) without Zn^{2+} supplementation. These observations suggested Atx1 could bind Zn^{2+} in addition to Cu^{+} and that access of ZiaR to this Zn^{2+} pool was restricted in wild-type *Synechocystis*.

7.2.2 Potential novel functions for Zn^{2+}-Atx1

During the course of these investigations evidence was obtained that implied Atx1 bound Zn^{2+} *in vivo*. Given the primary role of Atx1 as a Cu^{+} chaperone this was unexpected and is almost without precedent in characterised Cu^{+} metallochaperones. Although synthetic peptides designed to incorporate the metal binding site sequence MxCxxC, conserved in Atx1-like metal binding domains, have been shown to bind a range of metal ions including Zn^{2+} (Rousselot-Pailley *et al.* 2006) only a single copper chaperone from *Archaeoglobus fulgidus* has been shown to bind Zn^{2+}. However, this protein is unusual in structure containing an atypical N-terminal domain containing a 2Fe2S cluster and which binds Zn^{2+} in an unusual four cysteine motif (Sazinsky *et al.* 2007). Comparison of the structural properties of characterised metal binding sites Cu^{+} metallochaperones suggests that the Zn^{2+} binding feature of *Synechocystis* Atx1 may well be rare. *Synechocystis* Atx1 binds copper in a trigonal coordination geometry involving two cysteine residues and third histidine ligand (Borrelly *et al.* 2004a; Banci *et al.* 2004). On interaction with PacS it is this residue which is thought to provide the 'trigger' for Cu^{+} transfer; this residue is forced out of the Cu^{+} coordination sphere by steric hindrance on binding of the proteins, facilitating transfer of the Cu^{+} ion (Banci *et al.* 2006). This histidine is atypical for metal binding sites of Cu^{+} metallochaperones. However, a similar coordination environment has been characterised in the Sco1, the Cu^{+} chaperone that delivers Cu^{+} to cytochrome c oxidase (Nittis *et al.* 2001). Perhaps Sco1 shares a similar Zn^{2+} binding function.

It is unclear what advantage Zn^{2+} bound Atx1 would confer to *Synechocystis* cells. One possible role may be that Zn^{2+} protects the cysteinyl thiols of Atx1, keeping

them in a reduced state ready to receive Cu^+; on Cu^+ acquisition the Zn^{2+} would be displaced from the binding site. In the copper sensor CopY from *Enterococcus hirae* Zn^{2+} binds Cu^+ binding cysteine residues and is displaced upon acquisition of Cu^+ from the Cu^+ chaperone CopZ (Cobine *et al.* 1999). However, in this instance the Zn^{2+} ion appears to have a structural role, facilitating formation of a DNA binding conformer which is converted to a lower affinity state on binding of Cu^+ (Portmann *et al.* 2004). Other copper chaperones have been shown to have thiol disulphide oxidoreductase activity in which electrons are exchanged with Cu^+ acquiring proteins (Furukawa *et al.* 2004; Abriata *et al.* 2008). This may be the case for Zn^{2+}-Atx1; Zn^{2+} may maintain thiols in the metal biding site of Atx1 in a reduced state. On interaction with PacS disulphide exchange may occur causing Zn^{2+} release from Atx1 and promoting acquisition of Cu^+ from Cu^+ bound forms of Atx1.

7.2.3 The metallochaperone Atx1 restricts access to Cu^+ *in vivo*

In these studies it was shown that Cu^+ was less effective than Zn^{2+} at promoting binding of Zur_{SS} to DNA (Figure 50). Cu^+ ions tend to adopt trigonal or digonal coordination geometries in proteins and so on binding to Zn_1Zur_{SS}, Cu^+ likely adopted a coordination geometry that failed to organise the protein into a DNA binding conformation analogous to that produced on Zn^{2+} binding. The effects on the DNA binding affinity of Zur_{SS} of metal ions that are less competitive than Cu^+ or Zn^{2+} could not be determined due to inability to produce Zn_1Zur_{SS} in fluorescence anisotropy analyses (Figure 37). However, the Cu^+ responses of Zur_{SS} would predict that, as for ZiaR, allosteric regulation is correlated with adoption of a native-like coordination geometry.

Cu^+ ions were shown to bind to the allosteric site of Zur_{SS} in preference to Zn^{2+} (Figure 49) and inhibited Zn^{2+} mediated allostery *in vitro* (Figure 50). It was predicted that binding of Zur_{SS} to Cu^+ *in vivo* would cause inhibition of Zn^{2+}-dependent regulation of expression from the Zur_{SS} regulated *znu* promoter. In a *Synechocystis* mutant (Δ*atx1*Δ*gshB*) with a defective cytosolic Cu^+ trafficking and buffering capacity it was therefore anticipated that inhibition of Zn^{2+}-regulated *znu* promoter expression would be observed. Coincident with these studies, RT-PCR (data obtained by Samantha Dainty) was used to monitor *znuA* expression in cells of wild-type and Δ*atx1*Δ*gshB* strains of *Synechocystis*. Zn^{2+}-dependent repression of *znuA* expression in wild-type *Synechocystis* was observed, however, in a Δ*atx1*Δ*gshB Synechocystis* mutant levels of

znuA expression following treatment with Zn^{2+} were analogous to those observed in the absence of metal treatment (Figure 71). No increase in *znuA* expression was detected in Δ*atx1*Δ*gshB* cells that would indicate association with Zn^{2+} released due to loss of Zn^{2+}-bound forms of Atx1. These data are consistent with inhibition of Zn^{2+}-mediated repression of *znuA* expression in a Δ*atx1*Δ*gshB Synechocystis* mutant and are consistent with a model in which impaired cytosolic Cu^{+} trafficking in Δ*atx1*Δ*gshB* results in Cu^{+} mis-localisation to Zur_{SS}, inhibiting Zn^{2+} binding and regulation *in vivo*. Thus, a primary role for Atx1 (and other copper chaperones) may be to restrict access of proteins (including metal-sensing transcriptional regulators) to highly competitive metal ions.

The importance of this role is further highlighted by analyses conducted in parallel to these studies. In cells of the *Synechocystis* strain Δ*atx1*Δ*gshB* wild-type copper supply to plastocyanin was retained (Figure 71a, b) however, cells of this strain also exhibited copper sensitivity (Figure 71c). This phenotype is consistent with Cu^{+} movement to the thylakoid via adventitious transfer between cytosolic protein sites (e.g. Zur_{SS}) with a greater propensity for damage caused by Cu^{+} ions *en route*. In *E.coli* a primary mechanism of acute Cu^{+} toxicity is displacement of Fe from Fe-S clusters, with the iron released proposed to accelerate secondary damage via production of reactive oxygen species (ROS) (Macomber & Imlay 2009). Similar disruption to Fe-S cluster assembly has also been shown for *E.coli* cells exposed to toxic levels of Co^{2+} (Ranquet *et al.* 2007) suggesting these proteins are uniquely vulnerable to damage by metals released into the cytosol. Such a mechanism may account for the Cu^{+} toxicity in Δ*atx1*Δ*gshB Synechocystis*.

7.2.4 *In vivo* responses of ZiaR, Zur_{SS} and CoaR correlated with their relative affinities for Zn^{2+} but not Co^{2+}

An aim of these studies was to investigate the factors which determined selective metal responses for each transcriptional regulator. For metals such as Co^{2+}, for which no precedent exists for kinetic regulation of metal partitioning to sensors, it has been hypothesised that *in vivo* responses of sensors may be correlated with the equilibrium binding affinity for the cognate metal (section 1.9). The availability of Zn^{2+} and Co^{2+} sensor proteins of different sensor families from the same organism allowed this hypothesis to be tested *in vitro*. Unexpectedly, the relative affinities of ZiaR, Zur_{SS} and CoaR for Co^{2+} were not correlated with *in vivo* responses. Both ZiaR and Zur_{SS} were

Figure 71. Characterisation of the Cu^+ supply pathways in wild-type and mutant strains of *Synechocystis*. A. Surface plot data showing the relative concentrations of copper associated with plastocyanin and GSH following native separation by HPLC of components of cell extracts from various strains of *Synechocystis*. B. Quantity of copper associated with plastocyanin (left panel) and P1 (right panel) following isolation from each mutant strain of *Synechocystis*. C. Comparison of growth rates for various strains of *Synchechocystis*. D. RT-PCR analyses monitoring expression of *znuA* in wild-type and mutant strains following metal treatment. These data were collected by Steve Tottey and Samantha Dainty (manuscript in preparation).

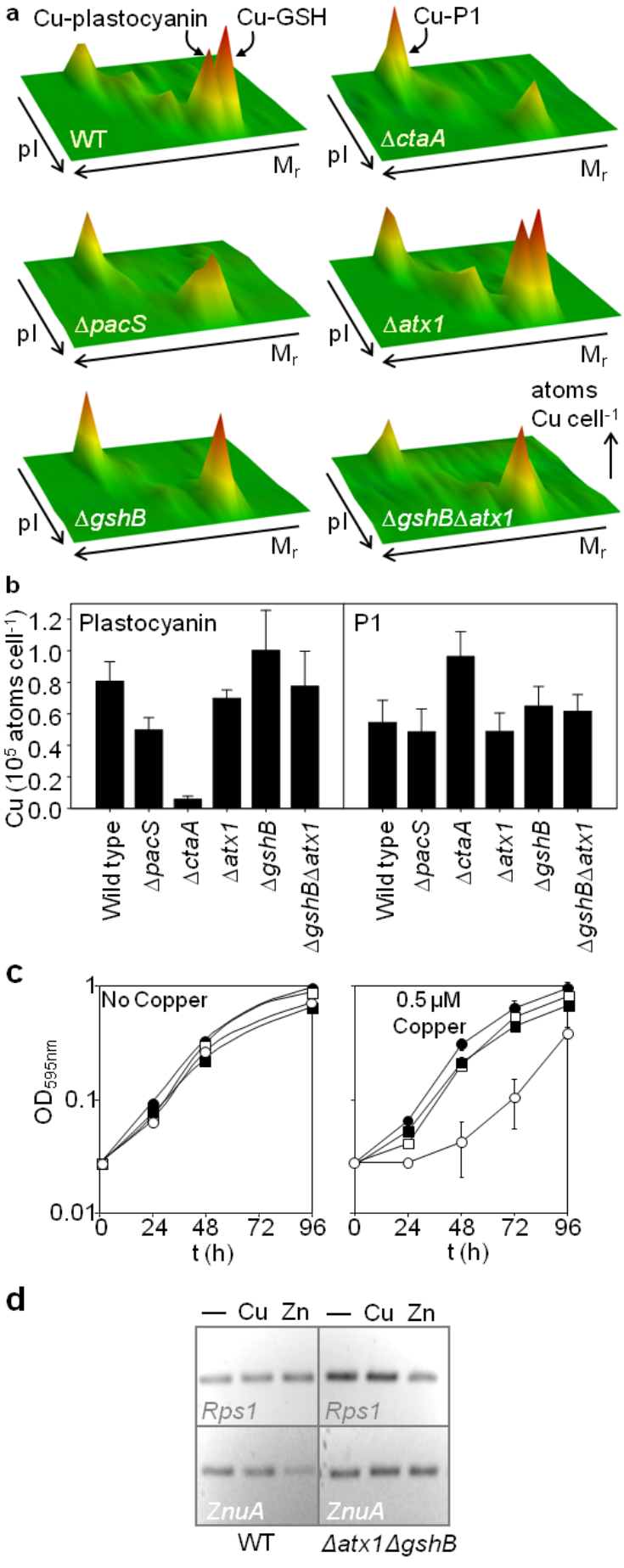
a
Cu-plastocyanin
Cu-GSH
Cu-P1
WT
ΔctaA
ΔpacS
Δatx1
ΔgshB
ΔgshBΔatx1
pI
Mr
atoms Cu cell-1
b
Plastocyanin
P1
Cu (10^5 atoms cell^-1)
1.2
1.0
0.8
0.6
0.4
0.2
0.0
Wild type
ΔpacS
ΔctaA
Δatx1
ΔgshB
ΔgshBΔatx1
c
No Copper
0.5 µM Copper
OD595nm
1
0.1
0.01
0
24
48
72
96
t (h)
d
— Cu Zn — Cu Zn
Rps1
ZnuA
WT
Δatx1ΔgshB

shown to have equilibrium Co^{2+} affinities substantially tighter than CoaR (Figure 51, 56, 67, Table 10). Furthermore, Zur_{SS} acquires Co^{2+} in preference to CoaR when the two proteins are competed (Figure 68). In contrast to Co^{2+}, evidence was obtained to suggest that the Zn^{2+} affinity of Zur_{SS} and likely ZiaR are correlated with *in vivo* responses; Zur_{SS} acquired Zn^{2+} in preference to CoaR following direct competition of the two proteins for Zn^{2+} (Figure 68) implying a Zn^{2+} affinity for CoaR at least an order of magnitude weaker than 1.73×10^{12} M^{-1} (the K_{Zn1} for Zur_{SS}). The Zn^{2+} affinity of ZiaR is similar to that of Zur_{SS} (Table 6) and so is also inferred to have a Zn^{2+} affinity substantially tighter than that of CoaR. Direct measurement of the Zn^{2+} binding affinity of CoaR by titration with Quin-2 would precisely quantify the differences in Zn^{2+} affinities value. Nevertheless, these data show that for this set of sensors, correct perception of Zn^{2+} may be imparted by the relative Zn^{2+} affinities of the proteins.

7.3 Sub-cellular protein localisation is a factor regulating metal partitioning to sensors *in vivo*

The measured equilibrium binding affinities for ZiaR, Zur_{SS} and CoaR suggest a model in which Zn^{2+} partitions to higher affinity sites on Zur_{SS} (and likely ZiaR) in preference to CoaR *in vivo* (with Co^{2+} unable to out-compete Zn^{2+} for sites on ZiaR and Zur_{SS}) thus leaving the allosteric sites of CoaR free to bind Co^{2+}, despite having a tighter affinity for Zn^{2+} over Co^{2+} *in vitro*. However, these observations only partially account for the specificities observed *in vivo*. Previous studies have shown that CoaR does not respond to Zn^{2+} *in vivo* and there is no evidence that Zn^{2+} inhibits Co^{2+} responses in *Synechocystis* cells (Rutherford *et al.* 1999). Critically however, both ZiaR and Zur_{SS} have substantially tighter Co^{2+} affinities compared to CoaR (Table 10). ZiaR (Figure 52) (and potentially Zur_{SS}) can also be allosterically regulated by Co^{2+} *in vitro*, however, there is no evidence to suggest Co^{2+} association with either Zur_{SS} (Appendix B Figure 1) or ZiaR (Thelwell *et al.* 1998) in *Synechocystis.*

How do ZiaR and Zur_{SS} fail to respond to Co^{2+} whilst CoaR remains fully responsive to this metal? This organism does contain a CbiX cobaltochelatase (Leech *et al.* 2003) which inserts Co^{2+} into sirohydrocorrin during the synthesis of vitamin B_{12}. However, there is no precedent for metallochaperone-mediated delivery of Co^{2+} to a Co^{2+}-sensor protein which could potentially provide a selective means of Co^{2+} acquisition by CoaR. By implication, CoaR must sense Co^{2+} that is freely available in

the cytosol. CoaR was estimated to have a Co^{2+} disassociation constant in the range ~ 9.6 x 10^{-9} <<< K_{Co} < 2.5 x 10^{-6} M (section 6.3.7/8). Therefore, for CoaR and not ZiaR or Zur_{SS} to be activated by Co^{2+} CoaR must exist in an environment in which the Co^{2+} concentration exceeds this value. Evidence was obtained during these studies supporting localisation of CoaR to the membrane in *Synechocystis* (section 6.3.3). ZiaR and Zur_{SS} are soluble and thus localised to the cytosol. Therefore, from these observations a model emerges in which CoaR and ZiaR/Zur_{SS} have different intracellular localisations. In the model shown in Figure 72 CoaR experiences local concentrations of Co^{2+} at the membrane domain which must be higher than the K_{Co} range implied by direct measurements of affinity and thus are sufficient to activate CoaR and facilitate up-regulation of Co^{2+} export in conditions of surplus intracellular Co^{2+}. Thus, surplus Co^{2+} is quickly removed from the cytosol and so does not accumulate in the cytosol to a concentration sufficient to activate cytosolic ZiaR and Zur_{SS}. Zn^{2+} partitions specifically to ZiaR and Zur_{SS} (in preference to CoaR) due to their tighter affinities for Zn^{2+}; thus, highly competive Zn^{2+} is prevented from binding (in preference to Co^{2+}) at the metal binding site of CoaR.

The high local concentrations of Co^{2+} necessary for CoaR activation at the membrane are shown in this model to be due to high-affinity Co^{2+} uptake into the cytosol via as yet unidentified Co^{2+} import proteins. Perhaps CoaR associates with components of these systems *in vivo*. Interactions mediated by exposed hydrophobic patches between CoaR and other proteins *in vivo* (e.g. components of the vitamin B_{12} synthetic pathway), which are not retained following purification of recombinant CoaR, could in theory account for the interaction of exposed hydrophobic segments on purified CoaR with detergent micelles *in vitro*. However, this model is unlikely as CoaR remains responsive to Co^{2+} when expressed in *E.coli* suggesting native-function is retained even in this distantly related organism (Rutherford *et al.* 1999). *E.coli* is also incapable of synthesising the corrin macrocycle of vitamin B_{12}, lacking many of the enzymes required for its synthesis (vitamin B_{12} is also not required for cell growth) (Raux *et al.* 1996). Previous work demonstrated that one mechanism of selective metallation of proteins is by regulation of the folding location of proteins which utilise different metal cofactors (Tottey *et al*. 2008). The model described in this work (Figure 72) also implies protein localisation can determine responses of metal sensors, but that this can be achieved within the same cellular compartment which can contain niches of different metal set-point concentrations.

Figure 72. Localisation of CoaR to the cell membrane in *Synechocystis*. CoaR is shown in association with the inner leaflet of the plasma membrane (but not as an integral protein-see section 7.3.1) in close proximity to components of the vitamin B_{12} synthesis pathway (slr1467 is membrane associated and CobS is a predicted transmembrane protein) and as yet unidentified Co^{2+} import systems. Consequently CoaR experiences a local concentration of Co^{2+} at the membrane that is sufficient to activate the protein. The mechanism by which this occurs is unknown; in this model Co^{2+} is shown to induce a conformational change in the protein that leads to burial of an exposed hydrophobic patch that mediates interaction with the membrane which results in movement into solution. The Co^{2+}-bound protein can then bind to repeat elements within the *coaA* promoter, which presumably leads to promoter under-winding (thus realigning the -10 and -35 elements so they are in optimal positions for contact with RNA polymerase) and relief of DNA bending. Hydrogenobyrinic acid is shown to bind to CoaR to inhibit Co^{2+} binding by either causing a conformational change which occludes the Co^{2+} binding site (arrow a), as suggested in Rutherford *et al.* 1999, and/or by promoting release from the membrane into the cytosol so that the protein experiences local concentrations of Co^{2+} lower than required for activation (arrow b). ZiaR and Zur_{SS} are shown localised to the cytosol.

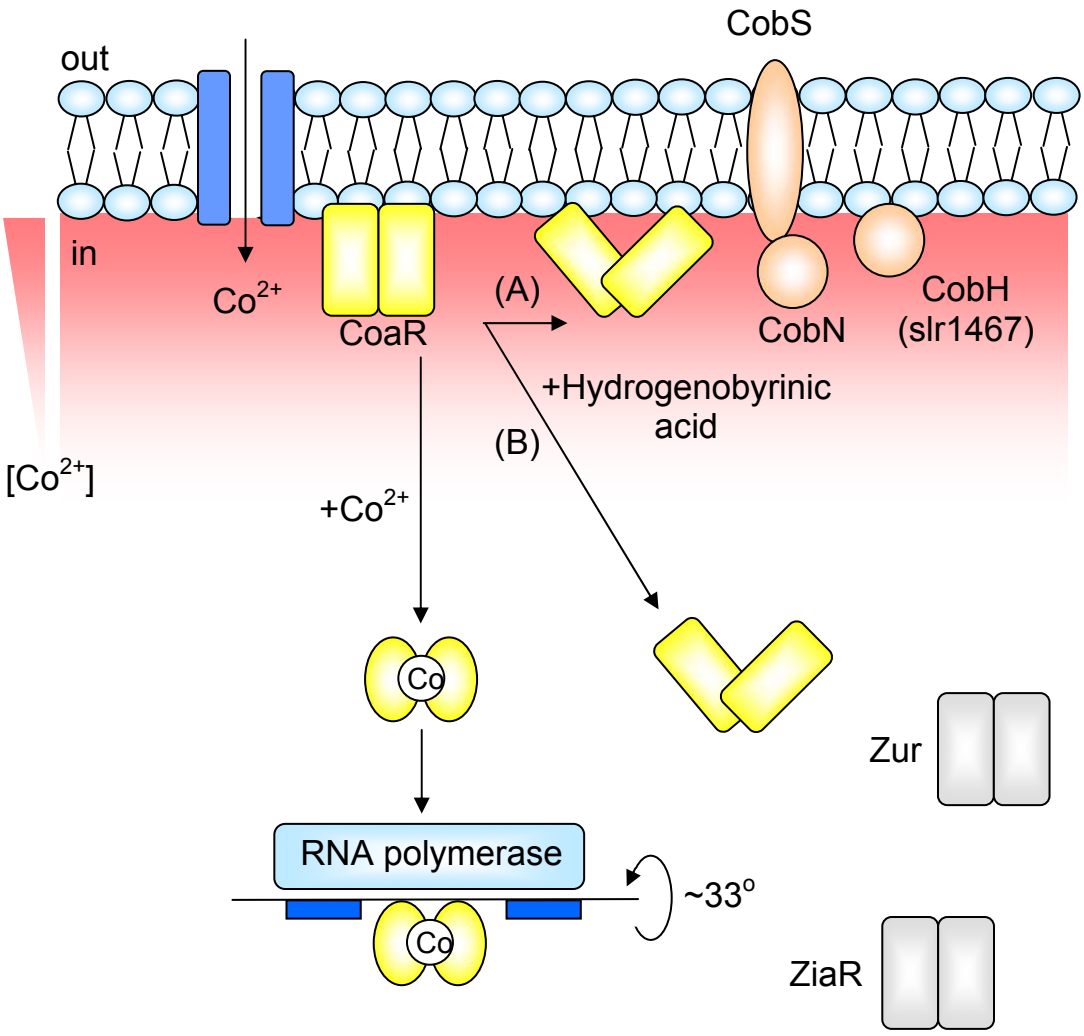
CobS
out
in
Co^{2+}
CoaR
(A)
CobN
CobH
(slr1467)
+Hydrogenobyrinic
acid
(B)
$[Co^{2+}]$
$+Co^{2+}$
Co
Zur
RNA polymerase
~33°
Co
ZiaR

7.3.1 Possible membrane topologies for CoaR

An obvious problem with the model outlined above (Figure 72) is the requirement for CoaR to bind the membrane and bind to and regulate expression from a DNA promoter. Single-component systems are the dominant form of signal transduction system in bacteria but a majority of these proteins are predicted to be soluble (Ulrich *et al.* 2005). However, examples of single component membrane associated proteins have been identified in the form of the ToxR-like family; these proteins are characterised by a cytosolic N-terminal DNA binding domain, a single transmembrane helix and a C-terminal extracellular domain and include proteins such as ToxR itself (Miller *et al.* 1987), which controls expression of the toxin gene in *V. cholerae* (Miller & Mekalanos 1984) and CadC (distinct to the ArsR-SmtB repressor from *S. aureus*), which senses extracellular concentrations of lysine indirectly through association with membrane bound lysine permease and regulates expression of genes encoding a lysine decarboxylase and a lysine antiporter (Tetsch *et al.* 2008).

In *Enterococcus faecalis* resistance to the antimicrobial polypeptide bacitracin is mediated by the ABC transporter BcrABD which is regulated by the protein BcrR (Manson *et al.* 2004). The BcrR regulator contains an N-terminal DNA binding helix-turn-helix motif and a C-terminal domain containing four predicted transmembrane α-helices. BcrR protein was purified using *n*-dodecyl-β-D-maltoside and was shown to bind to an inverted repeat sequence within the promoter region of *bcrABD* (Gauntlett *et al.* 2008). Subsequent analyses confirmed Zn^{2+}-bacitracin bound to the protein and induced upregulation of *bcrABD* transcription. Critically, a truncated form of the protein in which the transmembrane domain was removed was unable to bind DNA and regulate transcription *in vitro* or *in vivo*, suggesting membrane localisation was vital for function (Gebhard *et al.* 2009). Consistent with these observations a model was proposed in which membrane-bound BcrR protein was permanently bound to DNA; binding of Zn^{2+}-bacitracin to the extracellular domain would then be transduced into a change in the regulation at the bound promoter element via the cytosolic C-terminal domain. Like members of the MerR family (possibly including CoaR), changes in transcriptional regulation induced by Zn^{2+}-bacitracin were not correlated with changes in DNA binding affinity of BcrR; instead, a conformational change resulting in a change in the mode of interaction with RNA polymerase was proposed (Gauntlett *et al.* 2008; Gebhard *et al.* 2009).

A mechanism of DNA interaction and signal transduction for CoaR bound to the plasma membrane as an irreversibly bound integral protein, that is similar to that outlined above for BcrR and other membrane bound single component systems, seems unlikely given the architecture of the cyanobacterial cell. Cyanobacteria such as *Synechocystis* contain highly differentiated intracellular membrane systems which house the electron transport chains involved in photosynthesis and respiration. These membranes are arranged in multiple, concentric shells within the cytosol. Like other cyanobacteria, *Synechocystis* contains multiple copies of its chromosome (between six and eight copies per cell (Williams 1988)). The DNA and carboxysomes are both located in a cytosolic 'cavity' at the centre of these membrane stacks (Nierzwicki-Bauer *et al.* 1983). Recent studies have shown the membranes within the different layers to be interconnected, forming a continuous, enclosed thylakoid lumen. Within this structure small perforations (10-150 nm in diameter) have been observed linking the cytosol in the centre of the cell to that near the external membrane. Multiple components including ribosomes, lipid bodies and carbohydrate granules were observed to traverse the cell through these perforations (Nevo *et al.* 2007).

Although in theory the presence of at least one chromosome in the outer layer of the cytosol, proximal to the plasma membrane, could allow simultaneous membrane and DNA binding to CoaR there is no evidence that DNA itself approaches the cell membrane to allow for transcription proximal to the cell surface; confocal microscopy analyses of DNA localisation in *Synechocystis* have shown the DNA to be localised to the central region of the cytosol encompassed by the thylakoid membranes (Schneider *et al.* 2007). Given this organisation it is unclear how the chromosome structure would reorganise to facilitate transit through the perforations in the thylakoid membrane layers. Previous studies also suggest that the thylakoid and plasma membranes are not contiguous and represent separate structures (Liberton *et al.* 2006; Schneider *et al.* 2007). This would seem to rule out migration of CoaR to regions of the membrane structure proximal to DNA or rearrangement of the membrane structure to facilitate close approach of the plasma membrane-bound CoaR and DNA. It seems unlikely that CoaR is associated with thylakoid membrane; precorrin isomerase has been shown to be localised to the plasma membrane in *Synechocystis* (Mata-Cabana *et al.* 2007).

Although multiple algorithms predicted membrane interacting regions in similar sequence locations it is notable that two, SOSUI and TMHMM, did not. TMHMM uses the hidden Markov model to predict the location of transmembrane α helices in integral

membrane proteins (Krogh *et al.* 2001). SOSUI detects α helices that are likely to be membrane spanning using a range of parameters including hydropathy index, amphilicity index (i.e. clustering of polar amino acids adjacent to transmembrane regions in integral membrane proteins) and sequence length (Hirokawa *et al.* 1998). These results suggest a model in which the hydrophobic regions present in CoaR (and which are detected by other algorithms) are not organised into integral membrane spanning helices, thus leading to CoaR being assigned as a soluble protein by TMHMM and SOSUI. Therefore, a likely alternative model is that the membrane associated regions of CoaR do not completely traverse the membrane bilayer. In this model, the protein would not form an integral topology and the hydrophobic region may instead insert rather loosely into the inner leaflet of the membrane in similar fashion to prostaglandin H_2 synthase enzyme which is anchored to the outer surface of the plasma membrane by three short, consecutive amphipathic α-helices which protrude out of the main protein structure and are ideally positioned to insert into the outer membrane leaflet (Picot *et al.* 1994). The three α-helices in this protein cause the protein to be firmly anchored into the membrane.

It is striking that the C-terminal hydrophobic region in CoaR conserved in the membrane bound precorrin isomerase homologue in this organism and which is implicated in mediating membrane association in this work is predicted to be composed of a single α-helix (Figure 59); perhaps this causes relatively weak anchoring in the membrane. This would be consistent with the apparent weak association of precorrin isomerase with plasma membrane shown in other work (Mata-Cabana *et al.* 2007). The other hydrophobic regions in CoaR (regions 1 and 2) are predicted to combine to form a hydrophobic patch (Figure 59) that is denoted as a likely dimerisation domain in this work (Figure 59). This was not demonstrated unequivocally and it remains possible that this region could also be a candidate site for membrane binding. Again, this region was predicted to contain only a single sizeable α-helix (from region 1) (Figure 59) which if inserted laterally into the plane of the membrane leaflet could potentially mediate interaction with the membrane.

This membrane association model is also supported by several lines of evidence based on the known *in vivo* functions of CoaR and also from *in vitro* data presented in these studies. If CoaR was an integral membrane protein two possible topologies, N-terminal out or N-terminal in, would in theory be possible (Figure 73). An N-terminal-out organisation is unlikely *in vivo* as it would locate much of the precorrin isomerase

domain into the periplasm which would be inconsistent with interaction of CoaR with the cytosolic components of the B_{12} pathway implied by previous studies (Rutherford *et al.* 1999). Additionally, the whole of the MerR-like domain would also be in the periplasm and thus the protein would be unable to interact with DNA *in vivo*. However, it is acknowledged that the DNA binding observed in fluorescence anisotropy analyses in this work (Figure 62) could be accommodated by such a topology following reconstitution into DDM micelles *in vitro*. Although the r_{obs} increases recorded for CoaR association with DNA could be consistent with binding of four dimers to the DNA (Figure 62), given a mass range for DDM micelles estimated to be between 70-72 kDa (Strop & Brunger 2005; VanAken *et al.* 1986) these data could also be accounted for by binding of two CoaR dimers each localised to a separate DDM micelles. These increases in r_{obs} could also be produced by micelles containing multiple CoaR dimers (e.g. three dimers with two interacting with DNA). However, the number of molecules of CoaR per micelle is unknown.

A C-terminal-out orientation *in vivo* would place most of the precorrin isomerase-like domain and the MerR-like domain in the cytosol (Figure 73) and would localise the C-terminal CHC motif, shown to be essential for sensing *in vivo* (Rutherford *et al.* 1999) (plus Cys-369) to the periplasm. In theory, such an orientation *in vitro* could accommodate Co^{2+} binding as observed in UV-Visible analyses (Figure 63, 64). However, this would locate the DNA binding domain to the interior of the micelle, precluding interaction of the protein with DNA observed in these studies (Figure 62). Mutation of Cys-121 (S. Dainty, unpublished observations-see section 7.4) and the C-terminal CHC motif (Rutherford *et al.* 1999) in CoaR impairs Co^{2+} sensing *in vivo*. Given that these essential sensory residues are located on either side of the C-terminal hydrophobic region postulated to mediate interaction with the membrane (Figure 58,59), a model in which they are localised to opposite sides of the membrane appears unlikely (although it remains formally possible that some may be required for sensing/allosteric transduction in the protein, but may not be required for direct metal ligation).

The thiol reacting agent DTNB is a dianion over a wide pH range (Riddles *et al*. 1979) and so is incapable of traversing lipid membranes. As a consequence it has found uses in mapping membrane protein topologies by localisation of reactive cysteine residues in transmembrane proteins (Gostimskaya *et al.* 2006; Nara *et al.* 2007). In this

Figure 73. Possible modes of membrane association for CoaR. CoaR is shown as a multi-domain protein comprised of the N-terminal DNA binding MerR-like domain (grey box) and the C-terminal precorrin isomerase-like domain (yellow box) which is shown to contain a single hydrophobic region that mediates association with the membrane (red box). Three possible orientations are shown that could result from this (assuming the region is of sufficient length to traverse the membrane); an N-terminal in orientation (left), an N-terminal out orientation (middle) and an orientation in which the hydrophobic region 'dips' into the inner leaflet of the membrane. The approximate relative positions of the cysteine residues which are known to be required for Co^{2+} sensing (Cys-121, Cys-363, Cys-365) together with the C-terminal cysteine (Cys-369) for which a role in Co^{2+} binding/sensing is not yet known, are annotated.

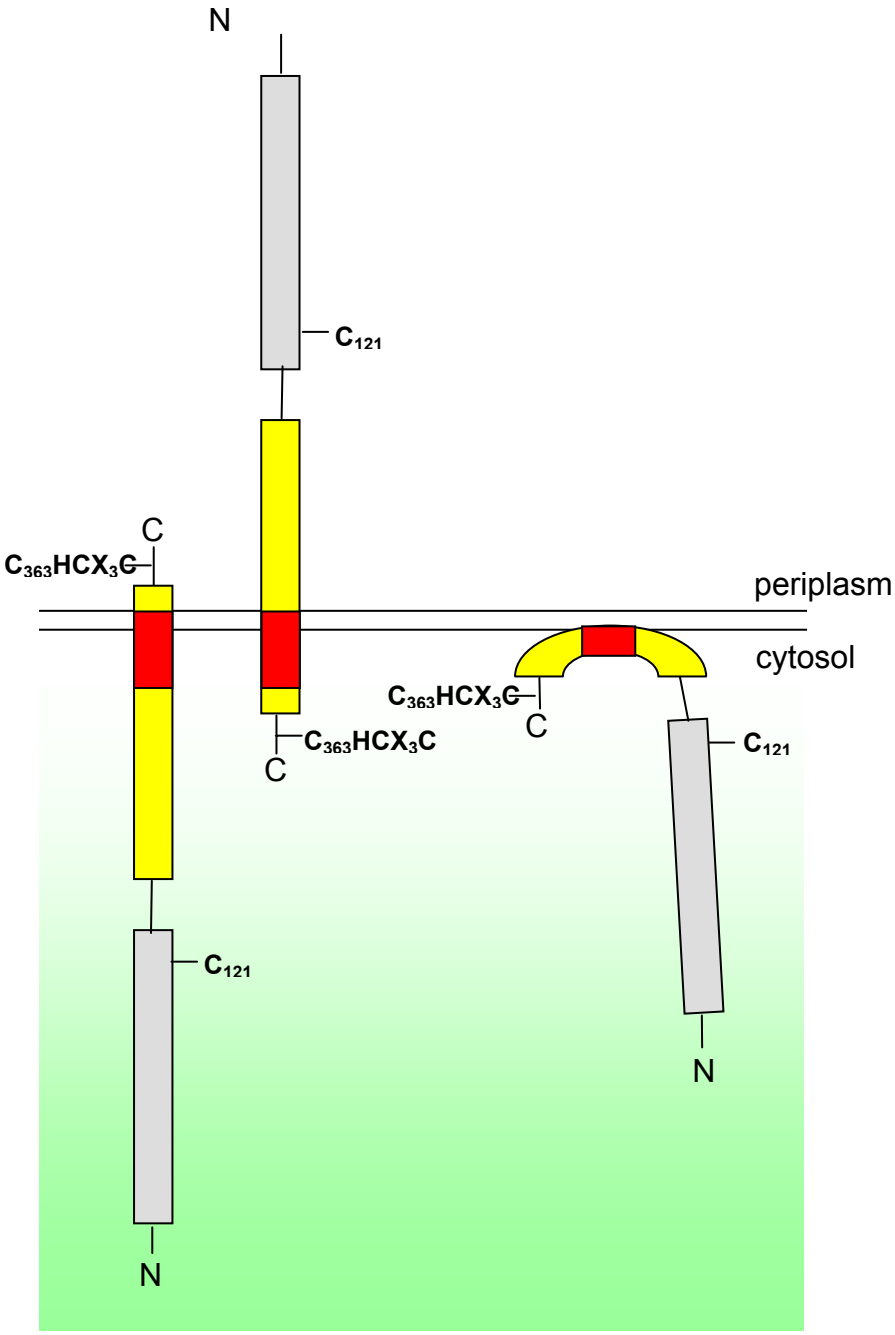
N
C121
C
C363HCX3C
periplasm
cytosol
C363HCX3C
C
C363HCX3C
C
C121
C121
N
N

work DTNB reactivities for purified CoaR close to 100 % were often observed which would suggest that effectively all of the cysteine residues in these protein preparations were solvent exposed. These preparations were associated with high affinity DNA binding and Co^{2+} binding mediated by three solvent exposed cysteine residues. Crucially, a reduced thiol content close to 100 % was observed for a protein preparation for which high-affinity binding to the *coaA* promoter was observed (Figure 62) and this affinity was apparently weaker for refolded CoaR which had a lower degree of reactivity with DTNB. Either N-terminal in or out orientations would produce substantially lower DTNB reactivities. During these studies protein preparations often did produce values much lower than the protein preparations characterised in this work. Based on predictions of hydrophobic regions (Table 8) and assessments of the feasibility of N-terminal out/in orientations described above protein preparations which produced high DTNB reactivities were concluded to represent the most physiologically relevant form of the protein. Complete exposure of all of the cysteines in this protein would be consistent with the monotopic membrane association model described above.

A model in which CoaR is in loose association with the inner leaflet of the membrane raises the possibility that on binding Co^{2+}, the resultant conformational changes would cause the protein to become soluble allowing it to re-localise and bind to DNA in other regions of the cytosol (Figure 72). Another possibility is that the MerR-like DNA binding domain could become detached via a proteolytic cleavage event induced following Co^{2+} binding to the protein (perhaps caused by exposure of a proteolytic cleavage site). This model also provides a means by which hydrogenobyrinic acid could negatively regulate the response of CoaR to Co^{2+} *in vivo* (Rutherford *et al.* 1999) (see section 1.8.2). Previously it was proposed that hydrogenobyrinic acid may bind to the precorrin isomerase domain inhibiting Co^{2+} binding or Co^{2+}-dependent conformational changes that are required for activation of the protein (Rutherford *et al.* 1999). In an alternative model, hydrogenobyrinic acid binding to CoaR may trigger a conformational change resulting in burial of the hydrophobic region that mediates interaction with the membrane (Figure 72). The resulting, solubilised form of CoaR would then be localised to the cytosol where the local concentration of Co^{2+} is substantially less than the Co^{2+} binding affinity of CoaR; hence, Co^{2+}-activation of CoaR is inhibited. A prediction is that binding of hydrogenobyrinic acid to CoaR *in vitro* will increase the solubility of recombinant CoaR. Alternatively, occlusion of the Co^{2+} binding site by conformational changes

induced on hydrogenobyrinic acid binding would be predicted to result in reduced Co^{2+} occupation of recombinant CoaR *in vitro* (e.g. reduced co-migration of Co^{2+} with protein following size-exclusion fractionation or reduced LMCT intensities following UV-Visible Co^{2+} titration).

7.4 Future Work

The regulation of sub-cellular localisation of CoaR potentially represents a novel strategy for ensuring selective responses of metal sensors to weakly competitive (e.g. Co^{2+}) and highly competitive (e.g. Zn^{2+}) metal ions are maintained within a common cytosol. Many facets of this model remain to be explored. Data obtained during the course of these studies suggests that CoaR is likely not to be an integral membrane protein but is membrane associated (discussed in 7.3.1). Unequivocal identification of membrane interacting motifs and determination of the mode of CoaR interaction with the membrane remain key priorities. In previous analyses of membrane protein topology amino acid residues have been covalently labelled and labelled and unlabelled forms subjected to proteolytic digestion. Comparison of the mass changes in each set of peptide fragments by mass spectroscopy allows identification of exposed protein segments and assignment of topology (Pan & Konermann 2010). In methods avoiding covalent labelling, mass spectroscopy has been used to determine the mass and sequences of peptides produced by proteolytic digestion of soluble segments of protein located outside the membrane and insoluble peptides located within the membrane can be recovered for analysis by reverse phase separation (Wu *et al.* 2003; Barnidge *et al*. 1997). For CoaR a potential strategy may be to perform proteolytic digestion of micelle-reconstituted CoaR. The resulting protected peptides could then be resolved by peptide SDS PAGE analysis or reverse phase chromatography followed by mass spectrometry based identification of protected peptide species.

Systematic identification by mutation of the candidate cysteine ligands that form the tetrahedral Co^{2+} site in CoaR may allow the unequivocal confirmation of the association model, in which CoaR is not integrally bound to the membrane to form a transmembrane protein. Candidate ligand residues are located at positions 363 and 365 (in the C-terminal CHC motif required for sensing (Rutherford *et al.* 1999)), position 369 (these are C-terminal to the hydrophobic region) and at position 121 at the C-terminal end of the MerR domain (N-terminal to the hydrophobic regions). Cys-121

aligns with a cysteine residue in ZntR that has been shown to be a Zn^{2+} ligand in ZntR that is required for sensing (Kahn *et al.* 2002; Changela *et al.* 2003) (Appendix D Figure 10). *In vivo* reporter gene assays performed in an *E.coli* host showed loss of CoaR response to Co^{2+} following mutation of this residue to serine (S. Dainty unpublished observations). It remains to be tested whether this protein is functional to bind DNA; comparison of its *in vitro* DNA binding properties with wild-type CoaR is a priority.

Cysteine 193 and 220 align with liganding cysteines in ZntR and CueR respectively, they are located within the precorrin isomerase-like domain predicted by alignment with precorrin isomerase A and B although cysteine 193 is just outside the domain predicted by alignment with the more distantly related *P. dentrificans* precorrin isomerase (Appendix D Figure 10). Structural modelling data for CoaR (Figure 59) would suggest that cysteine residues within the precorrin domain may not be expected to contribute to the Co^{2+} binding site; the compact, globular structure of the domain may provide substantial steric constraints on potential liganding cysteines which may be much larger than those experienced by cysteines at the C-terminus (which may represent a flexible loop) and by Cys-121 at the C-terminus of the MerR-like domain. A crucial experiment will be to analyse Co^{2+} binding to cysteine mutants of recombinant CoaR. A decrease in LMCT intensity associated with mutation of residues on both sides of the predicted hydrophobic region would confirm that cysteine residues from both sides of the predicted hydrophobic region ligate Co^{2+} and would therefore confirm that they are located in the cytosol and hence the CoaR is also associated with the inner surface of the plasma membrane.

An intriguing possibility arising from the model shown in Figure 72 is that by modifying the solubility of CoaR the *in vivo* responses may be modified so that they become a product of the local metal concentrations experienced by newly solubilised protein. A priority is to systematically mutate and convert the hydrophobic residues to relatively hydrophilic counterparts to enhance the solubility of CoaR. Subsequent purification of these recombinant forms of CoaR will allow any changes in solubility to be directly assessed. *In vivo* a prediction is that such a protein will lose Co^{2+} responsiveness due to relocation to a part of the cytosol of $[Co^{2+}] <<< K_{Co}$. This may also be accompanied by a response of Zur_{SS} and ZiaR to Co^{2+} *in vivo*; both have tighter affinities for Co^{2+} than CoaR and so it would be expected that they would acquire Co^{2+} in preference to CoaR when exposed to the same intracellular Co^{2+} pool.

For CoaR, like other MerR regulators, the allosteric effectiveness of metal ions are likely to be correlated with the adoption of a native like coordination geometry that allows the protein to be organised into an activated conformation (section 1.7.5). Zn^{2+} readily adopts tetrahedral geometries in protein sites and so is anticipated to a form a chelate similar in structure to that formed by Co^{2+} (Figure 63) and some evidence for similar conformational changes induced on Zn^{2+} binding was obtained on titration of recombinant CoaR with Zn^{2+} (Figure 65). Therefore, a prediction is that soluble CoaR may become activated by Zn^{2+} *in vivo* in the absence of *bona fide* Zn^{2+} sensors which have been removed by mutation or in which the metal-binding ligands have been mutated to reduce their metal binding affinity.

In the case of Co^{2+} partitioning to sensors in *Synechocystis,* the challenge of ensuring selective responses of CoaR to this weakly competitive metal may have been solved by spatial organisation of different metalloregulator functions. However, an outstanding question is how selectivity is maintained for soluble regulators which must compete with each other in the cytosol for strongly and weakly competitive metal ions. As for the archetypal ArsR-SmtB sensor NmtR, allostery is a key control point (Cavet *et al*. 2002), however as observed for both ZiaR and Zur_{SS}, additional mechanisms must also operate to ensure selective responses; ZiaR binds Co^{2+} and likely Zn^{2+} in tetrahedral geometries (Figure 10) and Co^{2+} can promote Zn^{2+} like allostery (Figure 52). The allosteric mechanism induced by Zn^{2+} binding to Zur_{SS} is inhibited by more tightly binding Cu^{+} ions (Figure 49, 50). It remains possible that selectivity of responses based on relative affinity may well operate between these and other soluble cytosolic sensors. *Synechocystis* contains a complement of soluble, metal sensing transcriptional regulators that are ideally suited to answering this question (see section 1.8.2). Efforts are underway to characterise the *in vitro* and *in vivo* responses of these sensors to allow for comparative analyses of their relative affinities for metal, to confirm or refute the predictions associated with this hypothesis. For example, the iron sensing Fur protein in *Synechocystis* may be expected to have an Fe^{2+} affinity tighter than that of the other cytosolic sensor proteins in this organism. Similarly, the arsenic sensor ArsR may be expected to have a Zn^{2+} affinity substantially weaker than the both Zur_{SS} and ZiaR. The metals sensed *in vivo* by the RcnR/CsoR homologue in this organism are unknown however sequence comparison with other members of this family suggest Ni^{2+} and Cu^{+} (for which no sensor has yet been identified in this organism) are likely candidates and a Zn^{2+} sensing function is unlikely. With analogy to Fur and ArsR, a prediction is that

RcnR will have a weaker affinity for Zn^{2+} than both Zur_{SS} and ZiaR. Evidence in support of this prediction comes from preliminary analyses suggesting a tighter Zn^{2+} binding affinity for ZiaR (data not shown).

Little is know about the intracellular abundances of metal sensor proteins from the major prokaryotic sensor families. Previous studies have shown that there are approximately 2500-7500 molecules of Fur protein per cell in *V. cholerae* (Watnick *et al.* 1997) and between 5000-10000 per cell in *E.coli* (Zheng *et al.* 1999). However, these abundances are much greater than observed for other transcriptional repressors (e.g. only 50-300 copies of the Trp apo-repressor are present in *E.coli* cells (Kelley & Yanofsky 1982)); this may be atypical for prokaryotic metalloregulators and may be explained by the high number of Fur binding sites in genomes, the high binding stoichiometries at these sites or the presence of weak affinity sites in some promoters necessitating higher intracellular protein concentrations (Watnick *et al.* 1999). The complement of sensor proteins from this organism (section 1.8.2) provides an ideal opportunity to study the abundance of sensor proteins from multiple families and the contribution of this factor to the generation of selective metal responses *in vivo*.

Elucidation of the factors governing selective metal responses for a set of sensors derived from the same organism represents a key priority for ongoing efforts in synthetic biology. A mechanism of selective metal partitioning to sensors based on relative affinity would imply that the metal binding properties (e.g. affinity, exchange kinetics) of metal-binding sites of sensors derived from a particular organism have been optimised in a coordinated fashion during evolution to maintain concentration ranges of metal ions optimal for metal co-factoring in that organism. Through modification of these properties (e.g. ligand sets of binding sites) it may therefore be possible to specifically engineer the metal set-point concentrations in a given organism to produce novel, useful phenotypes. Because such a high proportion of proteins require metal cofactors it is essential that in engineered organisms these requirements are at least met and ideally optimised to facilitate efficient cell function. Such considerations are likely to be of particular importance in attempts to re-engineer the high-metal demand systems of photosynthesis to optimise energy conversion and generate commercially valuable organic molecules and also to produce recombinant proteins in bioprocessing.

References

Abriata L.A., Banci L., Bertini I., Ciofi-Baffoni S., Gkazonis P., Spyroulias G.A., Vila A.J. & Wang S. (2008) Mechanism of Cu_A assembly. *Nat. Chem. Biol.* 4: 599-601.

Adrait A., Jacquamet L., Le Pape L., Gonzalez de Peredo A., Aberdam D., Hazemann J.L., Latour J.M. & Michaud-Soret I. (1999) Spectroscopic and saturation magnetization properties of the manganese- and cobalt-substituted Fur (ferric uptake regulation) protein from *Escherichia coli. Biochemistry.* 38: 6248-6260.

Ahmad R., Brandsdal B.O., Michaud-Soret I. & Willassen N.P. (2009) Ferric uptake regulator protein: binding free energy calculations and per-residue free energy decomposition. *Proteins.* 75: 373-386.

Ahmed M., Borsch C.M., Taylor S.S., Vázquez-Laslop N. & Neyfakh A.A. (1994) A protein that activates expression of a multidrug efflux transporter upon binding the transporter substrates. *J. Biol. Chem.* 269: 28506-28513.

Ahmed M., Lyass L., Markham P.N., Taylor S.S., Vázquez-Laslop N. & Neyfakh A.A. (1995) Two highly similar multidrug transporters of *Bacillus subtilis* whose expression is differentially regulated *J. Bacteriol.* 177: 3904-3910.

Ahn B.E., Cha J., Lee E.J., Han A.R., Thompson C.J. & Roe J.H. (2006) Nur, a nickel-responsive regulator of the Fur family, regulates superoxide dismutases and nickel transport in *Streptomyces coelicolor. Mol. Microbiol.* 59: 1848-1858.

Akanuma G., Nanamiya H., Natori Y., Nomura N. & Kawamura F. (2006) Liberation of zinc-containing L31 (RpmE) from ribosomes by its paralogous gene product, YtiA, in *Bacillus subtilis. J. Bacteriol.* 188: 2715-2720.

Althaus E.W., Outten C.E., Olsen, K.E., Cao H. & O'Halloran T.V. (1999) The ferric uptake regulation (Fur) repressor is a zinc metalloprotein. *Biochemistry.* 38: 6559-6569.

Amábile-Cuevas C.F. & Demple B. (1991) Molecular characterization of the *soxRS* genes of *Escherichia coli*: two genes control a superoxide stress regulon. *Nucleic Acids Res.* 19: 4479-4484.

An Y.J., Ahn B.E., Han A.R., Kim H.M., Chung K.M., Shin J.H., Cho Y.B., Roe J.H. & Cha S.S. (2009) Structural basis for the specialization of Nur, a nickel-specific Fur homolog, in metal sensing and DNA recognition. *Nucleic Acids Res.* 37: 3442-3451.

Anderson L.A., Palmer T., Price N.C., Bornemann S., Boxer D.H. & Pau R.N. (1997) Characterisation of the molybdenum-responsive ModE regulatory protein and its binding to the promoter region of the *modABCD* (molybdenum transport) operon of *Escherichia coli. Eur. J. Biochem.* 246: 119-126.

Andoy N.M., Sarkar S.K., Wang Q., Panda D., Benítez J.J., Kalininskiy A. & Chen P. (2009) Single-molecule study of metalloregulator CueR-DNA interactions using engineered Holliday junctions. *Biophys. J.* 97: 844-852.

Andreini C., Bertini I., Cavallaro G., Holliday G.L. & Thornton J.M. (2008) Metal ions in biological catalysis: from enzyme databases to general principles. *J. Biol. Inorg. Chem*. 13: 1205-1218.

Angeletti B., Waldron K.J., Freeman K.B., Bawagan H., Hussain I., Miller C.C., Lau K.F., Tennant M.E., Dennison C., Robinson N.J. & Dingwall C. (2005) BACE1 cytoplasmic domain interacts with the copper chaperone for superoxide dismutase-1 and binds copper. *J. Biol. Chem.* 280: 17930-17937.

Ansari A.Z., Chael M.L. & O'Halloran T.V. (1992) Allosteric underwinding of DNA is a critical step in positive control of transcription by Hg-MerR. *Nature.* 355: 87-89.

Ansari A.Z., Bradner J.E. & O'Halloran T.V. (1995) DNA-bend modulation in a repressor-to-activator switching mechanism. *Nature.* 374: 371-375.

Arunkumar A.I., Campanello G.C. & Giedroc D.P. (2009) Solution structure of a paradigm ArsR family zinc sensor in the DNA-bound state. *Proc. Natl. Acad. Sci. U S A*. 106: 18177-18182.

Auld D.S. (2001) Zinc coordination sphere in biochemical zinc sites *Biometals* 14: 271-313.

Bagchi A., Roy D. & Roy P. (2005) Homology modelling of a transcriptional regulator SoxR of the Lithotrophic sulfur oxidation (Sox) operon in alpha-proteobacteria. *J. Biomol. Struct. Dyn*. 22: 571-577.

Bagg A. & Neilands J.B. (1987) Ferric uptake regulation protein acts as a repressor, employing iron (II) as a cofactor to bind the operator of an iron transport operon in *Escherichia coli. Biochemistry.* 26: 5471-5477.

Baichoo N., Wang T., Ye R. & Helmann J.D. (2002) Global analysis of the *Bacillus subtilis* Fur regulon and the iron starvation stimulon. *Mol. Microbiol.* 45: 1613-1629.

Baichoo N. & Helmann J.D. (2002) Recognition of DNA by Fur: a reinterpretation of the Fur Box consensus sequence. *J. Bacteriol.* 184: 5826-5834.

Banci L., Bertini I., Ciofi-Baffoni S., Su X.C., Borrelly G.P. & Robinson N.J. (2004) Solution structures of a cyanobacterial metallochaperone: insight into an atypical copper-binding motif. *J. Biol. Chem.* 279: 27502-27510.

Banci L., Bertini I., Ciofi-Baffoni S., Kandias N.G., Robinson N.J., Spyroulias G.A., Su X.C., Tottey S. & Vanarotti M. (2006) The delivery of copper for thylakoid import observed by NMR. *Proc. Natl. Acad. Sci. U S A*. 103: 8320-8325.

Banci L., Bertini I., Cantini F., Ciofi-Baffoni S., Cavet J.S., Dennison C., Graham A.I., Harvie D.R. & Robinson N.J. (2007) NMR structural analysis of cadmium sensing by winged helix repressor CmtR. *J. Biol. Chem.* 282: 30181-30188.

Banci L., Bertini I., Ciofi-Baffoni S., Poggi L., Vanarotti M., Tottey S., Waldron K.J. & Robinson N.J. (2010) NMR structural analysis of the soluble domain of ZiaA-ATPase and the basis of selective interactions with copper metallochaperone Atx1. *J Biol Inorg Chem*. 15: 87-98.

Baranova N.N., Danchin A. & Neyfakh A.A. (1999) Mta, a global MerR-type regulator of the *Bacillus subtilis* multidrug-efflux transporters. *Mol. Microbiol.* 31: 1549-1559.

Barbosa R.L. & Benedetti C.E. (2007) BigR, a transcriptional repressor from plant-associated bacteria, regulates an operon implicated in biofilm growth. *J. Bacteriol.* 189: 6185-6194.

Barnidge D.R., Dratz E.A., Sunner J. & Jesaitis A.J. (1997) Identification of transmembrane tryptic peptides of rhodopsin using matrix-assisted laser desorption/ionization time-of-flight mass spectrometry. *Protein Sci.* 6: 816-824.

Bartsevich V.V. & Pakrasi H.B. (1995) Molecular identification of an ABC transporter complex for manganese: analysis of a cyanobacterial mutant strain impaired in the photosynthetic oxygen evolution process. *EMBO J.* 14: 1845-1853.

Bartsevich V.V. & Pakrasi H.B. (1996) Manganese transport in the cyanobacterium *Synechocystis* sp. PCC 6803. *J. Biol. Chem.* 271: 26057-26061.

Bellini P. & Hemmings A.M. (2006) *In vitro* characterization of a bacterial manganese uptake regulator of the fur superfamily. *Biochemistry.* 28: 2686-2698.

Berg J.M., Tymoczko J.L. & Stryer L. (2002) *Biochemistry*. 5th ed. New York: W. H. Freeman and company.

Binet M.R. & Poole R.K. (2000) Cd(II), Pb(II) and Zn(II) ions regulate expression of the metal-transporting P-type ATPase ZntA in *Escherichia coli. FEBS Lett.* 473: 67-70.

Blanche F., Debussche L., Thibaut D., Crouzet J. & Cameron B. (1989) Purification and characterization of S-adenosyl-L-methionine: uroporphyrinogen III methyltransferase from *Pseudomonas denitrificans*. *J. Bacteriol*. 171:4222-4231.

Bloom S.L. & Zamble D.B. (2004) Metal-selective DNA-binding response of *Escherichia coli* NikR. *Biochemistry.* 43: 10029-10038.

Borrelly G.P., Blindauer C.A., Schmid R., Butler C.S., Cooper C.E., Harvey I., Sadler P.J. & Robinson N.J. (2004a) A novel copper site in a cyanobacterial metallochaperones. *Biochem. J.* 378: 293-297.

Borrelly G.P., Rondet S.A., Tottey S. & Robinson N.J. (2004b) Chimeras of P-type ATPases and their transcriptional regulators: contributions of a cytosolic amino-terminal domain to metal specificity. *Mol. Microbiol.* 53: 217-227.

Borremans B., Hobman J.L., Provoost A., Brown N.L. & van Der Lelie D. (2001) Cloning and functional analysis of the *pbr* lead resistance determinant of *Ralstonia metallidurans* CH34. *J. Bacteriol.* 183: 5651-5658.

Brocklehurst K.R., Hobman J.L., Lawley B., Blank L., Marshall S.J., Brown N.L. & Morby A.P. (1999) ZntR is a Zn(II)-responsive MerR-like transcriptional regulator of *zntA* in *Escherichia coli. Mol. Microbiol.* 31: 893-902.

Brocklehurst K.R., Megit S.J. & Morby A.P. (2003) Characterisation of CadR from *Pseudomonas aeruginosa*: a Cd(II)-responsive MerR homologue. *Biochem. Biophys. Res. Commun.* 308: 234-239.

Brown D.C. & Collins K.D. (1991) Dihydroorotase from *Escherichia coli*. Substitution of Co(II) for the active site Zn(II). *J. Biol. Chem.* 266: 1597-1604.

Bsat N. & Helmann J.D. (1999) Interaction of the *Bacillus subtilis* Fur (ferric uptake repressor) with the *dhb* operator *in vitro* and *in vivo. J. Bacteriol.* 181: 4299-4307.

Busenlehner L.S., Cosper N.J., Scott R.A., Rosen B.P., Wong M.D. & Giedroc D.P. (2001) Spectroscopic properties of the metalloregulatory Cd(II) and Pb(II) sites of *S. aureus* pI258 CadC. *Biochemistry.* 40: 4426-4436.

Busenlehner L.S., Apuy J.L. & Giedroc D.P. (2002a) Characterization of a metalloregulatory bismuth(III) site in *Staphylococcus aureus* pI258 CadC repressor. *J. Biol. Inorg. Chem.* 7: 551-556.

Busenlehner L.S., Weng T.C., Penner-Hahn J.E. & Giedroc D.P. (2002b) Elucidation of primary (α_3N) and vestigial (α_5) heavy metal-binding sites in *Staphylococcus aureus* pI258 CadC: evolutionary implications for metal ion selectivity of ArsR/SmtB metal sensor proteins. *J. Mol. Biol.* 319: 685-701.

Busenlehner L.S., Pennella M.A. & Giedroc D.P. (2003) The SmtB/ArsR family of metalloregulatory transcriptional repressors: Structural insights into prokaryotic metal resistance. *FEMS Microbiol. Rev.* 27: 131-43.

Campbell D.R., Chapman K.E., Waldron K.J., Tottey S., Kendall S., Cavallaro G., Andreini C., Hinds J., Stoker N.G., Robinson N.J. & Cavet J.S. (2007) Mycobacterial cells have dual nickel-cobalt sensors: sequence relationships and metal sites of metal-responsive repressors are not congruent. *J. Biol. Chem.* 282: 32298-32210.

Carlin A., Shi W., Dey S. & Rosen B.P. (1995) The *ars* operon of *Escherichia coli* confers arsenical and antimonial resistance. *J. Bacteriol.* 177: 981-986.

Carrington P.E., Chivers P.T., Al-Mjeni F., Sauer R.T. & Maroney M.J. (2003) Nickel coordination is regulated by the DNA-bound state of NikR. *Nat. Struct. Biol.* 10: 126-130.

Casey J.R. & Reithmeier R.A. (1993) Detergent interaction with band 3, a model polytopic membrane protein. *Biochemistry.* 32: 1172-1179.

Cavet J.S., Meng W., Pennella M.A., Appelhoff R.J., Giedroc D.P. & Robinson N.J. (2002) A Nickel-Cobalt-sensing ArsR-SmtB Family Repressor. *J. Biol. Chem.* 277: 38441-8.

Cavet J.S, Borrelly G.P. & Robinson N.J. (2003a) Zn, Cu and Co in cyanobacteria: selective control of metal availability. *FEMS Microbiol. Rev*. 27: 165-181.

Cavet J.S., Graham A.I., Meng W. & Robinson N.J. (2003b) A cadmium-lead-sensing ArsR-SmtB repressor with novel sensory sites. Complementary metal discrimination by NmtR and CmtR in a common cytosol. *J. Biol. Chem.* 278: 44560-44566.

Champier L., Duarte V., Michaud-Soret I. & Covès J. (2004) Characterization of the MerD protein from *Ralstonia metallidurans* CH34: a possible role in bacterial mercury resistance by switching off the induction of the *mer* operon. *Mol. Microbiol.* 52: 1475-1485.

Changela A., Chen K., Xue Y., Holschen J., Outten C.E., O'Halloran T.V. & Mondragón A. (2003) Molecular basis of metal-ion selectivity and zeptomolar sensitivity by CueR. *Science* 301; 1383-1387.

Checa S.K., Espariz M., Audero M.E., Botta P.E., Spinelli S.V. & Soncini F.C. (2007) Bacterial sensing of and resistance to gold salts. *Mol. Microbiol.* 63; 1307-1318.

Chen X., Chu M. & Giedroc D.P. (2000) Spectroscopic characterization of Co(II)-, Ni(II)-, and Cd(II)-substituted wild-type and non-native retroviral-type zinc finger peptides. *J. Biol. Inorg. Chem.* 5: 93-101.

Chen X., Hua H., Balamurugan K., Kong X., Zhang L., George G.N., Georgiev O., Schaffner W. & Giedroc D.P. (2008) Copper sensing function of *Drosophila* metal-responsive transcription factor-1 is mediated by a tetranuclear Cu(I) cluster. *Nucleic Acids Res.* 36: 3128-38.

Chivers P.T. & Sauer R.T. (2000) Regulation of high affinity nickel uptake in bacteria. Ni^{2+}-Dependent interaction of NikR with wild-type and mutant operator sites. *J. Biol. Chem.* 275: 19735-19741.

Chivers P.T. & Sauer R.T. (2002) NikR repressor: high-affinity nickel binding to the C-terminal domain regulates binding to operator DNA. *Chem. Biol.* 9: 1141-1148.

Cobine P., Wickramasinghe W.A., Harrison M.D., Weber T., Solioz M. & Dameron C.T. (1999) The *Enterococcus hirae* copper chaperone CopZ delivers copper(I) to the CopY repressor. *FEBS Lett.* 445: 27-30.

Cook W.J., Kar S.R., Taylor K.B. & Hall L.M. (1998) Crystal structure of the cyanobacterial metallothionein repressor SmtB: a model for metalloregulatory proteins. *J. Mol. Biol.* 275: 337-46.

Cromie M.J. & Groisman E.A. (2010) Promoter and riboswitch control of the Mg^{2+} transporter MgtA from *Salmonella enterica. J. Bacteriol.* 192: 604-607.

Dainty S.J., Patterson C.J., Waldron K.J. & Robinson N.J. (2010) Interaction between cyanobacterial copper chaperone Atx1 and zinc homeostasis. *J. Biol. Inorg. Chem.* 15: 77-85.

D'Autreaux B., Pecqueur L., Gonzalez de Peredo A., Diederix R.E., Caux-Thang C., Tabet L., Bersch B., Forest E. & Michaud-Soret I. (2007) Reversible redox- and zinc-dependent dimerisation of the *Escherichia coli* fur protein. *Biochemistry.* 46: 1329-1342.

Davis B.M., Quinones M., Pratt J., Ding Y. & Waldor M.K. (2005) Characterization of the small untranslated RNA RyhB and its regulon in *Vibrio cholerae. J. Bacteriol.* 187: 4005-4014.

de Lorenzo V., Wee S., Herrero M. & Neilands J.B. (1987) Operator sequences of the aerobactin operon of plasmid ColV-K30 binding the ferric uptake regulation (fur) repressor. *J. Bacteriol.* 169: 2624-2630.

de Lorenzo V., Giovannini F., Herrero M. & Neilands J.B. (1988) Metal ion regulation of gene expression. Fur repressor-operator interaction at the promoter region of the aerobactin system of pColV-K30. *J. Mol. Biol.* 203: 875-874.

Delany I., Spohn G., Rappuoli R. & Scarlato V. (2001) The Fur repressor controls transcription of iron-activated and -repressed genes in *Helicobacter pylori. Mol. Microbiol.* 42: 1297-1309.

Delany I., Rappuoli R. & Scarlato V. (2004) Fur functions as an activator and as a repressor of putative virulence genes in *Neisseria meningitides. Mol. Microbiol.* 52: 1081-1090.

Díaz-Mireles E., Wexler M., Sawers G., Bellini D., Todd J.D. & Johnston A.W. (2004) The Fur-like protein Mur of *Rhizobium leguminosarum* is a Mn^{2+}-responsive transcriptional regulator. *Microbiology*. 150:1447-1456.

Díaz-Mireles E., Wexler M., Todd J.D., Bellini D., Johnston A.W. & Sawers R.G. (2005) The manganese-responsive repressor Mur of *Rhizobium leguminosarum* is a member of the Fur-superfamily that recognizes an unusual operator sequence. *Microbiology*. 151: 4071-4078.

Dietrich H., Maret W., Kozłowski H. & Zeppezauer M. (1981) Active site-specifically reconstituted nickel(II) horse liver alcohol dehydrogenase: optical spectra of binary and ternary complexes with coenzymes, coenzyme analogues, substrates, and inhibitors. *J. Inorg. Biochem.* 14: 297-311.

Ding H., Hidalgo E. & Demple B. (1996) The redox state of the [2Fe-2S] clusters in SoxR protein regulates its activity as a transcription factor. *J. Biol. Chem.* 271: 33173-33175.

Eicken C., Pennella M.A., Chen X., Koshlap K.M., VanZile M.L., Sacchettini J.C., Giedroc D.P. (2003) A metal-ligand-mediated intersubunit allosteric switch in related SmtB/ArsR zinc sensor proteins. *J. Mol. Biol.* 333: 683-695.

Endo G. & Silver S. (1995) CadC, the transcriptional regulatory protein of the cadmium resistance system of *Staphylococcus aureus* plasmid pI258. *J.Bacteriol.* 177: 4437-4441.

Erbe J.L., Taylor K.B. & Hall L.M. (1995) Metalloregulation of the cyanobacterial *smt* locus: identification of SmtB binding sites and direct interaction with metals. *Nucleic Acids Res.* 23: 2472-2478.

Ernst F.D., Homuth G., Stoof J., Mäder U., Waidner B., Kuipers E.J., Kist M., Kusters J.G., Bereswill S. & van Vliet A.H. (2005) Iron-responsive regulation of the *Helicobacter pylori* iron-cofactored superoxide dismutase SodB is mediated by Fur. *J. Bacteriol.* 187: 3687-3692.

Frausto da Silva J. & Williams R.J.P. (2002) *The Biological Chemistry of the Elements: The inorganic Chemistry of Life*. 2nd ed. USA: Oxford University Press.

Fuangthong M., Herbig A.F., Bsat N. & Helmann J.D. (2002) Regulation of the *Bacillus subtilis fur* and *perR* genes by PerR: not all members of the PerR regulon are peroxide inducible. *J. Bacteriol.* 184: 3276-3286.

Furukawa Y., Torres A.S. & O'Halloran T.V. (2004) Oxygen-induced maturation of SOD1: a key role for disulfide formation by the copper chaperone CCS. *EMBO J.* 23: 2872-2881.

Gaballa A. & Helmann J.D. (1998) Identification of a zinc-specific metalloregulatory protein, Zur, controlling zinc transport operons in *Bacillus subtilis*. *J. Bacteriol.* 180: 5815-5821.

Gaballa A & Helmann J.D (2002) A peroxide-induced zinc uptake system plays an important role in protection against oxidative stress in *Bacillus subtilis*. *Mol. Microbiol.* 45: 997-1005.

Gaballa A., Wang T., Ye R.W. & Helmann J.D. (2002) Functional analysis of the *Bacillus subtilis* Zur regulon. *J. Bacteriol.* 184: 6508-6514.

Gaballa A., Antelmann H., Aguilar C., Khakh S.K., Song K.B., Smaldone G.T. & Helmann J.D. (2008) The *Bacillus subtilis* iron-sparing response is mediated by a Fur-regulated small RNA and three small, basic proteins *Proc. Natl. Acad. Sci. USA*. 105: 11927-11932.

Gabriel S.E., Miyagi F., Gaballa, A. & Helmann, J.D. (2008) Regulation of the Bacillus subtilis *yciC* gene and insights into the DNA-binding specificity of the zinc-sensing metalloregulator Zur. *J. Bacteriol.* 190: 3482-3488.

Gabriel S.E. & Helmann J.D. (2009) Contributions of Zur-controlled ribosomal proteins to growth under zinc starvation conditions. *J. Bacteriol.* 191: 6116-6122.

García-Domínguez M., Lopez-Maury L., Florencio F.J. & Reyes J.C. (2000) A gene cluster involved in metal homeostasis in the cyanobacterium *Synechocystis* sp. strain PCC 6803. *J. Bacteriol.* 182: 1507-1514.

Gaudu P. & Weiss B. (1996) SoxR, a [2Fe-2S] transcription factor, is active only in its oxidized form. *Proc. Natl. Acad. Sci. USA*. 93: 10094-10098.

Gauntlett J.C., Gebhard S., Keis S., Manson J.M., Pos K.M. & Cook G.M. (2008) Molecular analysis of BcrR, a membrane-bound bacitracin sensor and DNA-binding protein from *Enterococcus faecalis*. *J. Biol. Chem.* 283: 8591-8600.

Gebhard S., Gaballa A., Helmann J.D. & Cook G.M. (2009) Direct stimulus perception and transcription activation by a membrane-bound DNA binding protein. *Mol. Microbiol.* 73: 482-491.

Ghassemian M. & Straus N.A. (1996) Fur regulates the expression of iron-stress genes in the cyanobacterium *Synechococcus* sp. strain PCC 7942. *Microbiology.* 142: 1469–1476.

Giedroc D.P. (2009) Hydrogen peroxide sensing in *Bacillus subtilis*: it is all about the (metallo) regulator. *Mol. Microbiol*. 73: 1-4.

Gladysheva T.B, Oden K.L & Rosen B.P. (1994) Properties of the arsenate reductase of plasmid R773. *Biochemistry.* 33: 7288-7293.

Glasfeld A, Guedon E, Helmann J.D. & Brennan R.G. (2003) Structure of the manganese-bound manganese transport regulator of *Bacillus subtilis. Nat. Struct. Biol.* 10: 652-657.

Golynskiy M.V, Gunderson W.A, Hendrich M.P. & Cohen S.M. (2006) Metal binding studies and EPR spectroscopy of the manganese transport regulator MntR. *Biochemistry.* 45: 15359-15372.

Good M. & Vasák M. (1986) Spectroscopic properties of the cobalt(II)-substituted alpha-fragment of rabbit liver metallothionein. *Biochemistry.* 25: 3328-3334.

Gostimskaya I.S., Cecchini G. & Vinogradov A.D. (2006) Topography and chemical reactivity of the active-inactive transition-sensitive SH-group in the mitochondrial NADH:ubiquinone oxidoreductase (Complex I). *Biochim. Biophys. Acta.* 1757: 1155-1161.

Graham A.I., Hunt S., Stokes S.L., Bramall N., Bunch J., Cox A.G., McLeod C.W. & Poole R.K. (2009) Severe zinc depletion of *Escherichia coli*: roles for high affinity zinc binding by ZinT, zinc transport and zinc-independent proteins. *J. Biol. Chem.* 284: 18377-18389.

Griggs D.W. & Konisky J. (1989) Mechanism for iron-regulated transcription of the *Escherichia coli* cir gene: metal-dependent binding of fur protein to the promoters *J. Bacteriology.* 171: 1048-1054.

Grunden A.M., Ray R.M., Rosentel J.K., Healy F.G. & Shanmugam K.T. (1996) Repression of the *Escherichia coli modABCD* (molybdate transport) operon by ModE. *J. Bacteriol.* 178: 735-744.

Grynkiewicz G., Poenie M. & Tsien R.Y. (1985) A new generation of Ca^{2+} indicators with greatly improved fluorescence properties. *J. Biol. Chem.* 260: 3440-3450.

Guo H.B., Johs A., Parks J.M., Olliff L., Miller S.M., Summers A.O., Liang L. & Smith J.C. (2010) Structure and conformational dynamics of the metalloregulator MerR upon binding of Hg(II). *J. Mol. Biol.* 398: 555-568.

Hall H.K. & Foster J.W. (1996) The role of fur in the acid tolerance response of *Salmonella typhimurium* is physiologically and genetically separable from its role in iron acquisition. *J.Bacteriol.* 178: 5683-5691.

Hamza I., Chauhan S., Hassett R. & O'Brian M.R. (1998) The bacterial Irr protein is required for coordination of heme biosynthesis with iron availability. *J. Biol. Chem.* 273: 21669-21674.

Hantke K. (1981) Regulation of ferric iron transport in *Escherichia coli* K12: isolation of a constitutive mutant. *Mol. Gen. Genet.* 182: 288-292.

Hantke K. (1984) Cloning of the repressor protein gene of iron-regulated systems in *Escherichia coli* K12. *Mol. Gen. Genet.* 197: 337-341.

Hantke K. (1987) Selection procedure for deregulated iron transport mutants (fur) in *Escherichia coli* K 12: fur not only affects iron metabolism. *Mol Gen Genet*. 210:135-139.

Harley C.B. & Reynolds R.P. (1987) Analysis of *E. coli* promoter sequences. *Nucleic Acids Res.* 15: 2343-2361.

Harrison S.C. & Aggarwal A.K. (1990) DNA recognition by proteins with the helix-turn-helix motif. *Annu. Rev. Biochem.* 59: 933-969.

Harvie D. R., Andreini C., Cavallaro G., Meng W., Connolly B. A., Yoshida, K., Fujita Y., Harwood C. R., Radford D. S., Tottey S., Cavet J. S. & Robinson N. J. (2006) Predicting metals sensed by ArsR-SmtB repressors: allosteric interference by a non-effector metal. *Mol. Microbiol.* 59: 1341-1356.

Heldt D., Lawrence A.D., Lindenmeyer M., Deery E., Heathcote P., Rigby S.E. & Warren M.J. (2005) Aerobic synthesis of vitamin B_{12}: ring contraction and cobalt chelation *Biochem. Soc. Trans*. 33: 815-819.

Heldwein E.E. & Brennan R.G. (2001) Crystal structure of the transcription activator BmrR bound to DNA and a drug. *Nature*. 409: 378-382.

Helmann J.D., Ballard B.T. & Walsh C.T. (1990) The MerR metalloregulatory protein binds mercuric ion as a tricoordinate, metal-bridged dimer. *Science.* 247: 946-948.

Helmann J.D., Wu M.F., Gaballa A., Kobel P.A., Morshedi M.M., Fawcett P. & Paddon C (2003) The global transcriptional response of *Bacillus subtilis* to peroxide stress is coordinated by three transcription factors. *J. Bacteriol.* 185: 243-253.

Heltzel A., Lee I.W., Totis P.A. & Summers A.O. (1990) Activator-dependent pre-induction binding of sigma-70 RNA polymerase at the metal-regulated *mer* promoter. *Biochemistry.* 29: 9572-9584.

Henehan C.J., Pountney D.L., Zerbe O. & Vasák M. (1993) Identification of cysteine ligands in metalloproteins using optical and NMR spectroscopy: cadmium-substituted rubredoxin as a model $[Cd(CysS)_4]^{2-}$ center. *Protein Sci.* 2: 1756-1764.

Herbig A.F. & Helmann J.D. (2001) Roles of metal ions and hydrogen peroxide in modulating the interaction of the *Bacillus subtilis* PerR peroxide regulon repressor with operator DNA. *Mol. Microbiol.* 41: 849-859.

Hirokawa T, Boon-Chieng S, Mitaku S. (1998) SOSUI: classification and secondary structure prediction system for membrane proteins. *Bioinformatics*. 14:378-379.

Hitomi Y, Outten C.E. & O'Halloran T.V. (2001) Extreme zinc-binding thermodynamics of the metal sensor/regulator protein, ZntR. *J. Am. Chem. Soc.* 123: 8614-8615.

Hobman J.L., Wilkie J. & Brown N.L. (2005) A design for life: prokaryotic metal-binding MerR family regulators. *Biometals.* 18: 429-436.

Hobman J.L. (2007) MerR family transcription activators: similar designs, different specificities. *Mol. Microbiol.* 63: 1275-1278.

Huckle J.W., Morby A.P., Turner J.S. & Robinson N.J. (1993) Isolation of a prokaryotic metallothionein locus and analysis of transcriptional control by trace metal ions. *Mol. Microbiol.* 7: 177-187.

Hunt J.B., Neece S.H. & Ginsburg A. (1985) The use of 4-(2-pyridylazo)resorcinol in studies of zinc release from *Escherichia coli* aspartate transcarbamoylase. *Anal. Biochem.* 146: 150-157.

Hynninen A., Touzé T., Pitkänen L., Mengin-Lecreulx D. & Virta M. (2009) An efflux transporter PbrA and a phosphatase PbrB cooperate in a lead-resistance mechanism in bacteria. *Mol. Microbiol.* 74: 384-394.

Irving H. & Williams R.J.P. (1948) Order of stability of metal complexes. *Nature.* 162: 746-747.

Iwig J.S., Leitch S., Herbst R.W., Maroney M.J. & Chivers P.T. (2008) Ni(II) and Co(II) sensing by *Escherichia coli* RcnR. *J. Am. Chem. Soc.* 130: 7592-7606.

Jacquamet L., Aberdam D., Adrait A., Hazemann J.L., Latour J.M. & Michaud-Soret I. (1998) X-ray absorption spectroscopy of a new zinc site in the fur protein from *Escherichia coli*. *Biochemistry.* 37: 2564-2571.

Jacquamet L., Traoré D.A., Ferrer J.L., Proux O., Testemale D., Hazemann J.L., Nazarenko E., El Ghazouani A., Caux-Thang C., Duarte V. & Latour J.M. (2009) Structural characterization of the active form of PerR: insights into the metal-induced activation of PerR and Fur proteins for DNA binding. *Mol. Microbiol.* 73: 20-31.

Jefferson J.R., Hunt J.B. & Ginsburg A. (1990) Characterization of indo-1 and quin-2 as spectroscopic probes for Zn^{2+}-protein interactions. *Anal. Biochem.* 187: 328-336.

Johnson D.A. & Nelson P.J. (1995) Factors Determining the Ligand Field Stabilization Energies of the Hexaaqua 2+ Complexes of the First Transition Series and the Irving-Williams Order. *Inorg. Chem.* 34: 5666-5671.

Kandegedara A., Thiyagarajan S., Kondapalli K.C., Stemmler T.L. & Rosen B.P. (2009) Role of bound Zn(II) in the CadC Cd(II)/Pb(II)/Zn(II)-responsive repressor. *J. Biol. Chem.* 284: 14958-14965.

Katoh H., Hagino N., Grossman A.R. & Ogawa T. (2001) Genes essential to iron transport in the cyanobacterium *Synechocystis* sp. strain PCC 6803. *J Bacteriol*. 183: 2779-2784.

Kelley R.L. & Yanofsky C. (1982) Trp aporepressor production is controlled by autogenous regulation and inefficient translation. *Proc. Natl. Acad. Sci. USA*. 79: 3120-3124.

Keren N., Aurora R. & Pakrasi H.B. (2004) Critical roles of bacterioferritins in iron storage and proliferation of cyanobacteria. *Plant Physiol*. 135: 1666-1673.

Khan S., Brocklehurst K.R., Jones G.W. & Morby A.P. (2002) The functional analysis of directed amino-acid alterations in ZntR from *Escherichia coli. Biochem. Biophys. Res.* 299: 438-445.

Kim J.S, Kang S.O & Lee J.K. (2003) The protein complex composed of nickel-binding SrnQ and DNA binding motif-bearing SrnR of *Streptomyces griseus* represses *sodF* transcription in the presence of nickel. *J Biol. Chem*. 278: 18455-18463.

Kliegman J.I., Griner S.L., Helmann J.D., Brennan R.G. & Glasfeld A (2006) Structural basis for the metal-selective activation of the manganese transport regulator of *Bacillus subtilis*. *Biochemistry.* 45: 3493-3505.

Kobayashi M., Ishizuka T., Katayama M., Kanehisa M., Bhattacharyya-Pakrasi M., Pakrasi H.B. & Ikeuchi M. (2004) Response to oxidative stress involves a novel peroxiredoxin gene in the unicellular cyanobacterium *Synechocystis* sp. PCC 6803. *Plant Cell Physiol.* 45: 290-299.

Krogh A., Larsson B., von Heijne G. & Sonnhammer E.L. (2001) Predicting transmembrane protein topology with a hidden Markov model: application to complete genomes. *J. Mol. Biol*. 305: 567-580.

Kulkarni R.D. & Summers A.O. (1999) MerR cross-links to the alpha, beta, and sigma 70 subunits of RNA polymerase in the pre-initiation complex at the *merTPCAD* promoter. *Biochemistry.* 38: 3362-3368.

Kunert A., Vinnemeier J., Erdmann N. & Hagemann M. (2003) Repression by Fur is not the main mechanism controlling the iron-inducible *isiAB* operon in the cyanobacterium *Synechocystis* sp. PCC 6803. *FEMS Microbiol. Lett.* 227: 255-262.

Kuroda M., Hayashi H. & Ohta T. (1999) Chromosome-determined zinc-responsible operon *czr* in *Staphylococcus aureus* strain 912. *Microbiol. Immunol.* 43: 115-125.

Kuzmic P. (1996) Program DYNAFIT for the analysis of enzyme kinetic data: application to HIV proteinase. *Anal. Biochem.* 237: 260-273.

Kwan C.Y & Putney J.W. (1990) Uptake and intracellular sequestration of divalent cations in resting and methacholine-stimulated mouse lacrimal acinar cells. Dissociation by Sr^{2+} and Ba^{2+} of agonist-stimulated divalent cation entry from the refilling of the agonist-sensitive intracellular pool. *J. Biol. Chem.* 265: 678-684.

Lam M.S., Litwin C.M., Carroll P.A. & Calderwood S.B. (1994) *Vibrio cholerae* fur mutations associated with loss of repressor activity: implications for the structural-functional relationships of fur. *J. Bacteriol.* 176: 5108-5115.

Lane T.W., Saito M.A., George G.N., Pickering I.J., Prince R.C. & Morel F.M. (2005) A cadmium enzyme from a marine diatom. *Nature.* 435: 42.

Lawrence A.D., Deery E., McLean K.J., Munro A.W., Pickersgill R.W, Rigby S.E. & Warren M.J. (2008) Identification, characterization, and structure/function analysis of a corrin reductase involved in adenosylcobalamin biosynthesis. *J. Biol. Chem.* 283: 10813-10821.

Leech H.K., Raux E., McLean K.J., Munro A.W., Robinson N.J., Borrelly G.P., Malten M., Jahn D., Rigby S.E., Heathcote P. & Warren M.J. (2003) Characterization of the cobaltochelatase $CbiX^{L}$: evidence for a 4Fe-4S center housed within an MXCXXC motif. *J. Biol. Chem*. 278: 41900-41907.

Le Cam E., Frechon D., Barray M., Fourcade A. & Delain E. (1994) Observation of binding and polymerisation of Fur repressor onto operator-containing DNA with electron and atomic force microscopes. *Proc. Natl. Acad. Sci. USA*. 91: 11816-11820.

Lee J.W. & Helmann J.D. (2006a) The PerR transcription factor senses H_2O_2 by metal-catalysed histidine oxidation. *Nature*. 440: 363-367.

Lee J.W. & Helmann J.D. (2006b) Biochemical characterization of the structural Zn^{2+} site in the *Bacillus subtilis* peroxide sensor PerR. *J. Biol. Chem.* 281: 23567-23578.

Lee J.W. & Helmann J.D. (2007) Functional specialisation within the Fur family of metalloregulators. *Biometals.* 20: 485-499.

Lee S., Arunkumar A.I., Chen X. & Giedroc D.P. (2006) Structural insights into homo- and heterotropic allosteric coupling in the zinc sensor *S. aureus* CzrA from covalently fused dimers. *J. Am. Chem. Soc.* 128: 1937-1947.

Leitch S., Bradley M.J., Rowe J.L., Chivers P.T. & Maroney M.J. (2007) Nickel-specific response in the transcriptional regulator, *Escherichia coli* NikR. *J. Am. Chem. Soc.* 129: 5085-5095.

Lewin A.C., Doughty P.A., Flegg L., Moore G.R. & Spiro S. (2002) The ferric uptake regulator of *Pseudomonas aeruginosa* has no essential cysteine residues and does not contain a structural zinc ion. *Microbiology.* 148: 2449-2456.

Li H., Singh A.K., McIntyre L.M. & Sherman L.A. (2004) Differential gene expression in response to hydrogen peroxide and the putative PerR regulon of the *Synechocystis* sp. strain PCC 6803. *J. Bacteriol.* 186: 3331-3345.

Li Y., Qiu Y., Gao H., Guo Z., Han Y., Song Y., Du Z., Wang X., Zhou D. & Yang R. (2009) Characterization of Zur-dependent genes and direct Zur targets in *Yersinia pestis. BMC Microbiol.* 25: 128.

Li Z. & Demple B. (1994) SoxS, an activator of superoxide stress genes in *Escherichia coli.* Purification and interaction with DNA. *J. Biol. Chem.* 269: 18371-18377.

Liberton M., Howard Berg R., Heuser J., Roth R. & Pakrasi H.B. (2006) Ultrastructure of the membrane systems in the unicellular cyanobacterium *Synechocystis* sp. strain PCC 6803. *Protoplasma.* 227: 129-138.

Lieser S.A., Davis T.C., Helmann J.D. & Cohen S.M. (2003) DNA-binding and oligomerization studies of the manganese(II) metalloregulatory protein MntR from *Bacillus subtilis. Biochemistry.* 42: 12634-12642.

Lin Y.F., Walmsley A.R. & Rosen B.P. (2006) An arsenic metallochaperone for an arsenic detoxification pump. *Proc. Natl. Acad. Sci. USA.* 103: 15617-15622.

Liu T., Nakashima S., Hirose K., Uemura Y., Shibasaka M., Katsuhara M. & Kasamo K. (2003) A metallothionein and CPx-ATPase handle heavy-metal tolerance in the filamentous cyanobacterium *Oscillatoria brevis. FEBS Lett.* 542: 159-163.

Liu T., Nakashima S., Hirose K., Shibasaka M., Katsuhara M., Ezaki B., Giedroc D.P, & Kasamo K. (2004) A novel cyanobacterial SmtB/ArsR family repressor regulates the expression of a CPx-ATPase and a metallothionein in response to both Cu(I)/Ag(I) and Zn(II)/Cd(II). *J. Biol. Chem.* 279: 17810-17818.

Liu T., Golden J.W. & Giedroc D.P. (2005) A Zinc(II)/Lead(II)/Cadmium(II)-Inducible operon from the cyanobacterium *Anabeana* is regulated by AztR, an α3N ArsR-SmtB Metalloregulator. *Biochemistry.* 44: 8673-8683.

Liu T., Ramesh A., Ma Z., Ward S.K., Zhang L., George G.N., Talaat A.M., Sacchettini J.C. & Giedroc D.P. (2007) CsoR is a novel *Mycobacterium tuberculosis* copper-sensing transcriptional regulator. *Nat. Chem. Biol.* 3: 60-68.

Liu T., Chen X., Ma Z., Shokes J., Hemmingsen L., Scott R.A. & Giedroc D.P. (2008) A Cu^{I}-Sensing ArsR Family Metal Sensor Protein with a Relaxed Metal Selectivity Profile. *Biochemistry* 47: 10564-75.

López-Maury L., García-Domínguez M., Florencio F.J. & Reyes J.C. (2002) A two-component signal transduction system involved in nickel sensing in the cyanobacterium *Synechocystis* sp. PCC 6803. *Mol. Microbiol.* 43: 247-256.

López-Maury L., Florencio FJ. & Reyes J.C. (2003) Arsenic sensing and resistance system in the cyanobacterium *Synechocystis* sp. strain PCC 6803. *J. Bacteriol*. 185:5363-5371.

Lucarelli D., Russo S., Garman E., Milano A., Meyer-Klaucke W. & Pohl, E. (2007) Crystal structure and function of the Zinc Uptake Regulator FurB from *Mycobacterium tuberculosis. J. Biol. Chem*. 282: 9914-9922.

Lucarelli D., Vasil M.L., Meyer-Klaucke W. & Pohl E. (2008) The Metal dependent regulators FurA and FurB from *Mycobacterium Tuberculosis. Int. J. Mol. Sci.* 9: 1548-1560.

Ma Z., Cowart D.M., Scott R.A. & Giedroc D.P. (2009a) Molecular insights into the metal selectivity of the copper(I)-sensing repressor CsoR from *Bacillus subtilis*. *Biochemistry.* 48: 3325-3334.

Ma Z., Cowart D.M., Ward B.P., Arnold R.J., DiMarchi R.D., Zhang L., George G.N., Scott R.A. & Giedroc DP. (2009b) Unnatural amino acid substitution as a probe of the

allosteric coupling pathway in a mycobacterial Cu(I) sensor. *J. Am. Chem. Soc.* 131: 18044-18045.

Macomber L. & Imlay J.A. (2009) The iron-sulfur clusters of dehydratases are primary intracellular targets of copper toxicity. *Proc. Natl. Acad. Sci. USA.* 106: 8344-8349.

Maggio-Hall L.A., Claas K.R. & Escalante-Semerena J.C. (2004) The last step in coenzyme B_{12} synthesis is localized to the cell membrane in bacteria and archaea. *Microbiology.* 150: 1385-1395.

Magnani D. & Solioz M. (2007) How Bacteria Handle Copper. In: D.H. Nies & S. Silver, ed. 2007. *Molecular Microbiology of Heavy Metals*. Springer, pp. 260-280.

Mandal S., Chatterjee S., Dam B., Roy P. & Das Gupta S.K (2007) The dimeric repressor SoxR binds cooperatively to the promoter(s) regulating expression of the sulfur oxidation (sox) operon of *Pseudaminobacter salicylatoxidans* KCT001. *Microbiology.* 153: 80-91.

Manson J.M., Keis S., Smith J.M. & Cook G.M. (2004) Acquired bacitracin resistance in *Enterococcus faecalis* is mediated by an ABC transporter and a novel regulatory protein, BcrR. *Antimicrob. Agents Chemother.* 48: 3743-3748.

Massé E. & Gottesman S. (2002) A small RNA regulates the expression of genes involved in iron metabolism in *Escherichia coli. Proc. Natl. Acad. Sci. USA.* 99: 4620-4625.

Mata-Cabana A., Florencio F.J. & Lindahl M. (2007) Membrane proteins from the cyanobacterium *Synechocystis* sp. PCC 6803 interacting with thioredoxin. *Proteomics* **7**: 3953-3963.

McGoldrick H.M., Roessner C.A., Raux E., Lawrence A.D., McLean K.J., Munro A.W., Santabarbara S., Rigby S.E., Heathcote P., Scott A.I. & Warren M.J. (2005) Identification and characterization of a novel vitamin B_{12} (cobalamin) biosynthetic

enzyme (CobZ) from *Rhodobacter capsulatus*, containing flavin, heme, and Fe-S cofactors. *J. Biol. Chem.* 280: 1086-1094.

McHugh J.P. Rodríguez-Quinoñes F., Abdul-Tehrani H., Svistunenko D.A., Poole R.K., Cooper C.E. & Andrews S.C. (2003) Global iron-dependent gene regulation in *Escherichia coli*. A new mechanism for iron homeostasis. *J. Biol. Chem.* 278: 29478-29486.

Metruccio M.M., Fantappiè L., Serruto D., Muzzi A., Roncarati D., Donati C., Scarlato V. & Delany I. (2009) The Hfq-dependent small noncoding RNA NrrF directly mediates Fur-dependent positive regulation of succinate dehydrogenase in *Neisseria meningitides*. *J. Bacteriol.* 191: 1330-1342.

Michaud-Soret I., Adrait A., Jaquinod M., Forest E., Touati D. & Latour J.M. (1997) Electrospray ionisation mass spectrometry analysis of the apo- and metal-substituted forms of the Fur protein. *FEBS Lett.* 413: 473-476.

Miller V.L. & Mekalanos J.J. (1984) Synthesis of cholera toxin is positively regulated at the transcriptional level by *toxR*. *Proc. Natl. Acad. Sci. U.S.A.* 81: 3471-3475.

Miller V.L. Taylor R.K. & Mekalanos J.J. (1987) Cholera toxin transcriptional activator ToxR is a transmembrane DNA binding protein. *Cell.* 48: 271-279.

Mills S.A. & Marletta M.A. (2005) Metal binding characteristics and role of iron oxidation in the ferric uptake regulator from *Escherichia coli*. *Biochemistry.* 44: 13553-13559.

Morby A.P., Turner J.S., Huckle J.W. & Robinson N.J. (1993) SmtB is a metal-dependent repressor of the cyanobacterial metallothionein gene *smtA*: identification of a Zn inhibited DNA-protein complex. *Nucleic Acids Res.* 21: 921-925.

Munson G.P., Lam D.L., Outten F.W. & O'Halloran T.V. (2000) Identification of a copper-responsive two-component system on the chromosome of *Escherichia coli* K-12. *J. Bacteriol.* 182: 5864-5871.

Nanamiya H., Akanuma G., Natori Y., Murayama R., Kosono S., Kudo T., Kobayashi K., Ogasawara N., Park S.M., Ochi K. & Kawamura F. (2004) Zinc is a key factor in controlling alternation of two types of L31 protein in the *Bacillus subtilis* ribosome. *Mol. Microbiol.* 52: 273-283.

Nandal A., Huggins C.C., Woodhall M.R., McHugh J., Rodríguez-Quiñones F., Quail M.A., Guest J.R. & Andrews SC. (2010) Induction of the ferritin gene (*ftnA*) of *Escherichia coli* by Fe^{2+}-Fur is mediated by reversal of H-NS silencing and is RyhB independent. *Mol. Microbiol*. 75: 637-657.

Nara T., Kouyama T., Kurata Y., Kikukawa T., Miyauchi S. & Kamo N. (2007) Anti-parallel membrane topology of a homo-dimeric multidrug transporter, EmrE. *J. Biochem.* 142: 621-625.

Natori Y., Nanamiya H., Akanuma G., Kosono S., Kudo T., Ochi K. & Kawamura F. (2007) A fail-safe system for the ribosome under zinc-limiting conditions in *Bacillus subtilis. Mol. Microbiol.* 63: 294-307.

Nevo R., Charuvi D., Shimoni E., Schwarz R., Kaplan A., Ohad I. & Reich Z. (2007) Thylakoid membrane perforations and connectivity enable intracellular traffic in cyanobacteria. *EMBO J.* 26: 1467-1473.

Newberry K.J. & Brennan R.G. (2004) The structural mechanism for transcription activation by MerR family member multidrug transporter activation, N terminus. *J. Biol. Chem.* 279: 20356-20362.

Nierzwicki-Bauer S.A. & Balkwill D.L. & Stevens S.E. (1983) Three-dimensional ultrastructure of a unicellular cyanobacterium. *J. Cell Biol.* 97: 713-722.

Nittis T., George G.N. & Winge D.R. (2001) Yeast Sco1, a protein essential for cytochrome c oxidase function is a Cu(I)-binding protein. *J. Biol. Chem.* 276: 42520-42526.

Nucifora G., Chu L., Misra T.K. & Silver S. (1989) Cadmium resistance from *Staphylococcus aureus* plasmid pI258 *cadA* gene results from a cadmium-efflux ATPase. *Proc. Natl. Acad. Sci. USA*. 86: 3544-3548.

Nunoshiba T., Hidalgo E., Amábile Cuevas C.F. & Demple B. (1992) Two-stage control of an oxidative stress regulon: the *Escherichia coli* SoxR protein triggers redox-inducible expression of the *soxS* regulatory gene. *J. Bacteriol.* 174: 6054-6060.

Nunoshiba T., deRojas-Walker T., Wishnok J.S., Tannenbaum S.R. & Demple B. (1993) Activation by nitric oxide of an oxidative-stress response that defends *Escherichia coli* against activated macrophages. *Proc. Natl. Acad. Sci. USA*. 90: 9993-9997.

Ogawa T., Bao D.H., Katoh H., Shibata M., Pakrasi H.B., & Bhattacharyya-Pakrasi M. (2002) A two-component signal transduction pathway regulates manganese homeostasis in *Synechocystis* 6803, a photosynthetic organism. *J. Biol. Chem.* 277: 28981-28986.

O'Halloran T. & Walsh C. (1987) Metalloregulatory DNA-binding protein encoded by the *merR* gene: isolation and characterization. *Science.* 235: 211-214.

O'Halloran T.V., Frantz B., Shin M.K., Ralston D.M. & Wright J.G. (1989) The MerR heavy metal receptor mediates positive activation in a topologically novel transcription complex. *Cell.* 56: 119-129.

Osman D. & Cavet J.S. (2010) Bacterial metal-sensing proteins exemplified by ArsR-SmtB family repressors. *Nat. Prod. Rep*. 27:668-680.

Outten C.E & O'Halloran T.V. (2001) Femtomolar sensitivity of metalloregulatory proteins controlling zinc homeostasis. *Science.* 292: 2488-2492.

Outten C.E., Tobin D. A., Penner-Hahn J.E. & O'Halloran T.V. (2001) Characterisation of the metal receptor sites in *Escherichia coli* Zur, an ultrasensitive Zn (II) metalloregulatory protein. *Biochemistry.* 40: 10417-10423.

Pakrasi H.B., Ogawa T. & Bhattacharyya-Pakrasi M. (2001) Transport of metals: a key process in oxygenic photosynthesis. In: E-M Aro & B. A. Anderson, eds.). *Regulatory Aspects of Photosynthesis*: Dordrecht: Kluer Academic, pp 253-264.

Pan Y. & Konermann L. (2010) Membrane protein structural insights from chemical labeling and mass spectrometry. *Analyst.* 135: 1191-1200.

Panina E.M., Mironov A.A. & Gelfand M.S. (2003) Comparative genomics of bacterial zinc regulons: enhanced ion transport, pathogenesis, and rearrangement of ribosomal proteins. *Proc. Natl. Acad. Sci. USA.* 100: 9912-9917.

Park S.J., Wireman J. & Summers A.O. (1992) Genetic analysis of the Tn*21 mer* operator-promoter. *J. Bacteriol.* 174: 2160-2171.

Parkhill J. & Brown N.L. (1990) Site-specific insertion and deletion mutants in the *mer* promoter-operator region of Tn*501*; the nineteen base-pair spacer is essential for normal induction of the promoter by MerR. *Nucleic Acids Res.* 18: 5157-5162.

Parkhill J., Ansari A.Z., Wright J.G, Brown N.L, O'Halloran T.V. (1993) Construction and characterization of a mercury-independent MerR activator (MerRAC): transcriptional activation in the absence of Hg(II) is accompanied by DNA distortion. *EMBO J.* 12: 413-421.

Patzer S.I. & Hantke K. (1998) The ZnuABC high-affinity zinc uptake system and its regulator Zur in *Escherichia coli*. *Mol. Microbiol.* 28: 1199-1210.

Patzer S.I. & Hantke K. (2000) The Zinc-responsive Regulator Zur and Its Control of the *znu* Gene Cluster Encoding the ZnuABC Zinc Uptake System in *Escherichia coli. J. Biol. Chem.* 275: 24321-24332.

Pennella M.A., Shokes J.E., Cosper N.J., Scott R.A. & Giedroc D.P. (2003) Structural elements of metal selectivity in metal sensor proteins. *Proc. Natl. Acad. Sci. USA.* 100: 3713-3718.

Petersen C. & Møller LB. (2000) Control of copper homeostasis in *Escherichia coli* by a P-type ATPase, CopA, and a MerR-like transcriptional activator, CopR. *Gene*. 261: 289-298.

Picot D., Loll P.J. & Garavito R.M. (1994) The X-ray crystal structure of the membrane protein prostaglandin H2 synthase-1. *Nature.* 367: 243-249.

Pisareva T., Shumskaya M., Maddalo G., Ilag L. & Norling B. (2007) Proteomics of *Synechocystis* sp. PCC 6803. Identification of novel integral plasma membrane proteins. *FEBS J.* 274: 791-804.

Pohl E., Haller J.C., Mijovilovich A., Meyer-Klauke W., Garmin E. & Vasil M.L. (2003) Architecture of a protein central to iron homeostasis: crystal structure and spectroscopic analysis of the ferric uptake regulator. *Mol. Microbiol.* 47: 903-915.

Pontel L.B., Audero M.E., Espariz M., Checa S.K., Soncini F.C. (2007) GolS controls the response to gold by the hierarchical induction of *Salmonella*-specific genes that include a CBA efflux-coding operon. *Mol. Microbiol*. 66: 814-825.

Portmann R., Magnani D., Stoyanov J.V., Schmechel A., Multhaup G. & Solioz M. (2004) Interaction kinetics of the copper-responsive CopY repressor with the *cop* promoter of *Enterococcus hirae. J. Biol. Inorg. Chem.* 9: 396-402.

Pountney D. L., Schauwecker I., Zarn J., & Vasak M. (1994) Formation of mammalian Cu8-metallothionein *in vitro*: evidence for the existence of two Cu(I)4 thiolate clusters. *Biochemistry.* 33: 9699-9705.

Qi Z., Hamza I. & O'Brian M.R. (1999) Heme is an effector molecule for iron-dependent degradation of the bacterial iron response regulator (Irr) protein. *Proc. Natl. Acad. Sci. USA*. 96: 13056-13061.

Qi Z. & O'Brian M.R. (2002) Interaction between the bacterial iron response regulator and ferrochelatase mediates genetic control of heme biosynthesis. *Mol. Cell.* 9: 155-162.

Que Q. & Helmann JD (2000) Manganese homeostasis in *Bacillus subtilis* is regulated by MntR, a bifunctional regulator related to the diphtheria toxin repressor family of proteins. *Mol. Microbiol.* 35: 1454-1468.

Rae T.D., Schmidt P.J., Pufahl R.A., Culotta V.C. & O'Halloran T.V. (1999) Undetectable intracellular free copper: the requirement of a copper chaperone for superoxide dismutase. *Science.* 284: 805-808.

Ranquet C., Ollagnier-de-Choudens S., Loiseau L., Barras F., Fontecave M. (2007) Cobalt stress in *Escherichia coli*. The effect on the iron-sulfur proteins. *J. Biol. Chem.* 282: 30442-30451.

Raux E., Lanois A., Levillayer F., Warren M.J., Brody E., Rambach A. & Thermes C. (1996) *Salmonella typhimurium* cobalamin (vitamin B_{12}) biosynthetic genes: functional studies in *S. typhimurium* and *Escherichia coli. J. Bacteriol.* 178: 753-767.

Rensing C., Mitra B. & Rosen B.P. (1997) The *zntA* gene of Escherichia coli encodes a Zn(II)-translocating P-type ATPase. *Proc. Natl. Acad. Sci. USA.* 94: 14326-14331.

Rensing C., Sun Y., Mitra B. & Rosen B.P. (1998) Pb(II)-translocating P-type ATPases. *J. Biol. Chem.* 179: 2769-2771.

Riddles P.W., Blakeley R.L. & Zerner B. (1979) Ellman's reagent: 5,5'-dithiobis(2-nitrobenzoic acid)-a re-examination. *Anal. Biochem.* 94: 75-81.

Rodionov D.A., Gelfand M.S., Todd J.D., Curson A.R. & Johnston A.W. (2006) Computational reconstruction of iron- and manganese-responsive transcriptional networks in alpha-proteobacteria. *PLoS Comput. Biol.* 2: e163.

Rosen B.P., Weigel U., Karkaria C. & Gangola P. (1988) Molecular characterization of an anion pump. The *arsA* gene product is an arsenite(antimonate)-stimulated ATPase *J. Biol. Chem.* 263: 3067-3070.

Rousselot-Pailley P., Sénèque O., Lebrun C., Crouzy S., Boturyn D., Dumy P., Ferrand M. & Delangle P. (2006) Model peptides based on the binding loop of the copper metallochaperone Atx1: selectivity of the consensus sequence MxCxxC for metal ions Hg(II), Cu(I), Cd(II), Pb(II), and Zn(II). *Inorg. Chem.* 45: 5510-5520.

Rulísek L. & Vondrásek J. (1998) Coordination geometries of selected transition metal ions (Co^{2+}, Ni^{2+}, Cu^{2+}, Zn^{2+}, Cd^{2+}, and Hg^{2+}) in metalloproteins. *J. Inorg. Biochem.* 71: 115-127.

Rutherford J.C., Cavet J.S. & Robinson N.J. (1999) Cobalt-dependent transcriptional switching by a dual-effector MerR-like protein regulates a cobalt-exporting variant CPx-type ATPase. *J. Biol. Chem.* 274: 25827-25832.

Saito M., Sigman D., & Morel F. (2003) The bioinorganic chemstry of the ancient ocean: the co-evolution of cyanobacterial metal requirements and the biogeochemical cycles at the Archean-Proterozoic Boundary. *Inorganica Chim. Acta.* 356: 308-318.

Saito T. & Williams R.J. (1991) The binding of the ferric uptake regulation protein to a DNA fragment *Eur. J. Biochem.* 197: 43-47.

Sambrook J. & Russell D. (2001) *Molecular Cloning: A laboratory Manual*. 3rd ed. Cold Spring Harbour Press, USA.

Sazinsky M.H., LeMoine B., Orofino M., Davydov R., Bencze K.Z., Stemmler T.L., Hoffman B.M., Argüello J.M. & Rosenzweig A.C. (2007) Characterization and structure of a Zn^{2+} and [2Fe-2S]-containing copper chaperone from *Archaeoglobus fulgidus*. *J. Biol. Chem.* 282: 25950-25959.

Schneider D., Fuhrmann E., Scholz I., Hess W.R. & Graumann P.L. (2007) Fluorescence staining of live cyanobacterial cells suggest non-stringent chromosome segregation and absence of a connection between cytoplasmic and thylakoid membranes. *BMC Cell Biol.* 8: 39.

Schröder J., Jochmann N., Rodionov D.A. & Tauch A (2010) The Zur regulon of *Corynebacterium glutamicum* ATCC 13032. *BMC Genomics.* 11: 12.

Schroeder S., Lawrence A.D., Biedendieck R., Rose R.S., Deery E., Graham R.M., McLean K.J., Munro A.W., Rigby S.E. & Warren M.J. (2009) Demonstration that CobG, the monooxygenase associated with the ring contraction process of the aerobic cobalamin (vitamin B_{12}) biosynthetic pathway, contains an Fe-S center and a mononuclear non-heme iron center. *J. Biol. Chem.* 284: 4796-4805.

Schwartz C.J., Giel J.L., Patschkowski T., Luther C., Ruzicka F.J., Beinert H. & Kiley P.J. (2001) IscR, an Fe-S cluster-containing transcription factor, represses expression of *Escherichia coli* genes encoding Fe-S cluster assembly proteins. *Proc. Natl. Acad. Sci. USA*. 98: 14895-14900.

Schwarz G., Mendel R.R. & Ribbe M.W. (2009) Molybdenum cofactors, enzymes and pathways. *Nature.* 460: 839-847.

Sen K.I., Sienkiewicz A., Love J.F., vanderSpek J.C., Fajer P.G. & Logan T.M. (2006) Mn(II) binding by the anthracis repressor from *Bacillus anthracis. Biochemistry.* 45: 4295-4303.

Sheikh M.A. & Taylor G.L. (2009) Crystal structure of the *Vibrio cholerae* ferric uptake regulator (Fur) reveals insights into metal co-ordination. *Mol. Microbiol.* 72: 1208-1220.

Shewchuk L.M., Helmann J.D., Ross W., Park S.J., Summers A.O. & Walsh C.T. (1989a) Transcriptional switching by the MerR protein: activation and repression mutants implicate distinct DNA and mercury(II) binding domains. *Biochemistry.* 28: 2340-2344.

Shewchuk L.M., Verdine G.L., Nash H. & Walsh C.T. (1989b) Mutagenesis of the cysteines in the metalloregulatory protein MerR indicates that a metal-bridged dimer activates transcription. *Biochemistry.* 28: 6140-6145.

Shi W., Dong J., Scott R.A., Ksenzenko M.Y. & Rosen B.P. (1996) The role of arsenic-thiol interactions in metalloregulation of the *ars* operon. *J. Biol. Chem.* 271: 9291-9297.

Shi J., Lindsay W.P., Huckle J.W., Morby A.P. & Robinson NJ. (1992) Cyanobacterial metallothionein gene expressed in *Escherichia coli*. Metal-binding properties of the expressed protein. *FEBS Lett*. 303:159-163.

Shin J.H., Oh S.Y., Kim S.J. & Roe J.H. (2007) The zinc-responsive regulator Zur controls a zinc uptake system and some ribosomal proteins in *Streptomyces coelicolor* A3(2). *J. Bacteriol.* 189: 4070-4077.

Singh V.K., Xiong A., Usgaard T.R., Chakrabarti S., Deora R., Misra T.K. & Jayaswal R.K. (1999) ZntR is an autoregulatory protein and negatively regulates the chromosomal zinc resistance operon *znt* of *Staphylococcus aureus. Mol. Microbiol.* 33: 200-207.

Sokołowska M. & Bal W. (2005) Cu(II) complexation by "non-coordinating" N-2-hydroxyethylpiperazine-N'-2-ethanesulfonic acid (HEPES buffer). *J. Inorg. Biochem.* 99: 1653-60.

Song L., Caguiat J., Li Z., Shokes J., Scott R.A., Olliff L. & Summers A.O. (2004) Engineered single-chain, antiparallel, coiled coil mimics the MerR metal binding site. *J. Bacteriol.* 186: 1861-1868.

Song L., Teng Q., Phillips R.S., Brewer J.M. & Summers A.O. (2007) ^{19}F-NMR reveals metal and operator-induced allostery in MerR. *J. Mol. Biol.* 371: 79-92.

Spiering M.M., Ringe D., Murphy J.R. & Marletta M.A. (2003) Metal stoichiometry and functional studies of the diphtheria toxin repressor. *Proc. Natl. Acad. Sci. USA*. 100: 3808-3813.

Storz G. & Imlay J.A. (1999) Oxidative stress. *Curr. Opin. Microbiol.* 2: 188-194.

Stoyanov J.V., Hobman J.L. & Brown N.L. (2001) CueR (YBBI) of *Escherichia coli* is a MerR family regulator controlling expression of the copper exporter CopA. *Mol. Microbiol.* 39: 502–511.

Stoyanov J.V. & Brown N.L. (2003) The *Escherichia coli* copper-responsive *copA* promoter is activated by gold. *J. Biol. Chem.* 278: 1407-1410.

Strop P. & Brunger A.T. (2005) Refractive index-based determination of detergent concentration and its application to the study of membrane proteins *Protein Sci.* 14: 2207-2211.

Summers A. O. (1992) Untwist and shout: a heavy metal-responsive transcriptional regulator. *J. Bacteriol.* 174: 3097-3101.

Sun Y., Wong M.D. & Rosen B.P (2002) Both metal binding sites in the homodimer are required for metalloregulation by the CadC repressor. *Mol. Microbiol.* 44: 1323-1329.

Taanman J.W. & Capaldi R.A. (1992) Purification of yeast cytochrome c oxidase with a subunit composition resembling the mammalian enzyme. *J. Biol. Chem.* 267: 22481-22485.

Tamagnini P., Axelsson R., Lindberg P., Oxelfelt F., Wünschiers R. & Lindblad P. (2002) Hydrogenases and hydrogen metabolism of cyanobacteria. *Microbiol. Mol. Biol. Rev*. 66: 1-20.

Tao X. & Murphy J.R. (1992) Binding of the metalloregulatory protein DtxR to the diphtheria *tox* operator requires a divalent heavy metal ion and protects the palindromic sequence from DNase I digestion. *J. Biol. Chem.* 267: 21761-21764.

Tetsch L., Koller C., Haneburger I. & Jung K. (2008) The membrane-integrated transcriptional activator CadC of *Escherichia coli* senses lysine indirectly via the interaction with the lysine permease LysP. *Mol. Microbiol.* 67: 570-583.

Thelwell C., Robinson N.J. & Cavet J.S. (1998) An SmtB-like repressor from *Synechocystis* PCC 6803 regulates a zinc exporter. *Proc. Natl. Acad. Sci. USA*. 95: 10728–10733.

Thibaut D., Couder M., Famechon A., Debussche L., Cameron B., Crouzet J. & Blanche F. (1992) The final step in the biosynthesis of hydrogenobyrinic acid is catalyzed by the *cobH* gene product with precorrin-8x as the substrate. *J. Bacteriol.* 174: 1043-1049.

Tisa L.S. & Rosen B.P. (1990) Molecular characterization of an anion pump. The ArsB protein is the membrane anchor for the ArsA protein. *J. Biol. Chem.* 265: 190-194.

Tong L., Nakashima S., Shibasaka M., Katsuhara M. & Kasamo K. (2002) A novel histidine-rich CPx-ATPase from the filamentous cyanobacterium *Oscillatoria brevis* related to multiple-heavy-metal cotolerance. *J. Bacteriol.* 184: 5027-5035.

Tottey S., Rich P.R., Rondet S.A. & Robinson N.J. (2001) Two Menkes-type ATPases supply copper for photosynthesis in *Synechocystis* PCC 6803. *J. Biol. Chem.* 276: 19999-20004.

Tottey S., Rondet S.A., Borrelly G.P., Robinson P.J., Rich P.R. & Robinson N.J. (2002) A copper metallochaperone for photosynthesis and respiration reveals metal-specific targets, interaction with an importer, and alternative sites for copper acquisition. *J. Biol. Chem.* 277: 5490-5497.

Tottey S., Harvie D.R. & Robinson N.J. (2007) Understanding How Cells Allocate Metals. In: D.H. Nies & S. Silver, ed. 2007. *Molecular Microbiology of Heavy Metals*. Springer, pp 3-35.

Tottey S., Waldron K.J., Firbank S.J., Reale B., Bessant C., Sato K., Cheek T.R., Gray J., Banfield M.J., Dennison C. & Robinson N.J. (2008) Protein-folding location can regulate manganese-binding versus copper- or zinc-binding. *Nature.* 455: 1138-1142.

Traoré D.A., El Ghazouani A., Ilango S., Dupuy J., Jacquamet L., Ferrer J.L., Caux-Thang C., Duarte V. & Latour J.M (2006) Crystal structure of the apo-PerR-Zn protein from *Bacillus subtilis. Mol. Biol.* 61: 1211-1219.

Traoré D.A., El Ghazouani A., Jacquamet L., Borel F., Ferrer J.L., Lascoux D., Ravanat J.L., Jaquinod M., Blondin G., Caux-Thang C., Duarte V. & Latour JM. (2009) Structural and functional characterization of 2-oxo-histidine in oxidized PerR protein. *Nat. Chem. Biol.* 5: 53-59.

Tsien R.Y. (1980) New calcium indicators and buffers with high selectivity against magnesium and protons: design, synthesis, and properties of prototype structures. *Biochemistry. 19*: 2396-2404.

Turner J.S., Morby A.P., Whitton B.A., Gupta A. & Robinson NJ. (1993) Construction of Zn^{2+}/Cd^{2+} hypersensitive cyanobacterial mutants lacking a functional metallothionein locus. *J. Biol Chem*. 268: 4494-4498.

Turner J.S., Robinson N.J. & Gupta A. (1995) Construction of Zn^{2+}/Cd^{2+}-tolerant cyanobacteria with a modified metallothionein divergon: further analysis of the function and regulation of smt. *J. Ind. Microbiol*. 14: 259-264.

Turner J.S., Glands P.D., Samson A.C. & Robinson N.J. (1996) Zn^{2+}-sensing by the cyanobacterial metallothionein repressor SmtB: different motifs mediate metal-induced protein-DNA dissociation. *Nucleic Acids Res*. 24: 3714-3721.

Ulrich L.E., Koonin E.V. & Zhulin I.B. (2005) One-component systems dominate signal transduction in prokaryotes. *Trends Microbiol.* 13: 52-56.

VanAken T., Foxall-VanAken S., Castleman S. & Ferguson-Miller S. (1986) Alkyl glycoside detergents: synthesis and applications to the study of membrane proteins *Methods Enzymol.* 125: 27-35.

VanZile M.L., Cosper N.J., Scott R.A. & Giedroc D.P. (2000) The zinc metalloregulatory protein *Synechococcus* PCC7942 SmtB binds a single zinc ion per

monomer with high affinity in a tetrahedral coordination geometry. *Biochemistry.* 39: 11818-11829.

VanZile M.L, Chen X. & Giedroc D.P. (2002a) Structural characterization of distinct α3N and α5 metal sites in the cyanobacterial zinc sensor SmtB. *Biochemistry* 31: 9765-9775.

VanZile M., Chen X. & Giedroc D.P. (2002b) Allosteric Negative Regulation of *smt* O/P Binding of the Zinc sensor SmtB by Metal Ions: A Coupled Equilibrium Analysis. *Biochemistry.* 41: 9776-9786.

Vasák M., Kägi J.H., Holmquist B. & Vallee B.L. (1981) Spectral studies of cobalt (II)- and Nickel (II)-metallothionein. *Biochemistry.* 20: 6659-6664.

Vasák M. & Kägi J.H. (1981) Metal thiolate clusters in cobalt(II)-metallothionein. *Proc. Natl. Acad. Sci. USA*. 78: 6709-6713.

Vitale S., Fauquant C., Lascoux D., Schauer K., Saint-Pierre C. & Michaud-Soret I. (2009) A ZnS_4 structural zinc site in the *Helicobacter pylori* ferric uptake regulator. *Biochemistry.* 48: 5582-5591.

Waldron K.J. & Robinson N.J. (2009) How do bacterial cells ensure that metalloproteins get the correct metal? *Nat. Rev. Microbiol.* 7: 25-35.

Waldron K.J., Rutherford J.C., Ford D. & Robinson N.J. (2009) Metalloproteins and metal sensing. *Nature.* 460: 823-830.

Waldron K.J., Firbank S.J., Dainty S.J., Perez-Rama M., Tottey S. & Robinson N.J. (2010) Structure and metal-loading of a soluble periplasm cupro-protein. *J. Biol. Chem.* (in press).

Wang S.C., Dias A.V., Bloom S.L. & Zamble D.B. (2004) Selectivity of metal binding and metal-induced stability of *Escherichia coli* NikR. *Biochemistry*. 43: 10018-28.

Wang Y., Hemmingsen L. & Giedroc D.P. (2005) Structural and functional characterisation of *Mycobacterium tuberculosis* CmtR, a Pb^{II}/Cd^{II}-Sensing SmtB/ArsR metalloregulatory repressor. *Biochemistry.* 44: 8976-8988.

Wang Y., Kendall J., Cavet J.S. & Giedroc D.P. (2010) Elucidation of the Functional Metal Binding Profile of a CdII/PbII sensor CmtRSc from *Streptomyces coelicolor. Biochemistry.* (Epub ahead of print).

Watnick P.I. Eto T., Takahashi H. & Calderwood S.B. (1997) Purification of *Vibrio cholerae* fur and estimation of its intracellular abundance by antibody sandwich enzyme-linked immunosorbent assay. *J Bacteriol.* 179: 243-247.

Wexler M., Todd J.D., Kolade O., Bellini D., Hemmings A.M., Sawers G. & Johnston A.W. (2003) Fur is not the global regulator of iron uptake genes in *Rhizobium leguminosarum. Microbiology.* 149: 1357-1365.

White A., Ding X., vanderSpek J.C., Murphy J.R. & Ringe D. (1998) Structure of the metal-ion-activated diphtheria toxin repressor/*tox* operator complex. *Nature.* 394: 502-506.

Wilderman P.J., Sowa N.A., FitzGerald D.J., FitzGerald P.C., Gottesman S., Ochsner U.A. & Vasil M.L. (2004) Identification of tandem duplicate regulatory small RNAs in *Pseudomonas aeruginosa* involved in iron homeostasis. *Proc. Natl. Acad. Sci. USA.* 101: 9792-9797.

Williams J.G.K. (1988) Construction of specific mutations in photosystem II reaction centre by genetic engineering methods in *Synechocystis* PCC 6803. *Methods Enzymol*.167: 766-778.

Williams S.G. & Manning P.A. (1991) Transcription of the *Vibrio cholerae* haemolysin gene, *hlyA*, and cloning of a positive regulatory locus, *hlyU. Mol. Microbiol.* 5: 2031-2038.

Williams S.G., Attridge S.R. & Manning P.A. (1993) The transcriptional activator HlyU of *Vibrio cholerae*: nucleotide sequence and role in virulence gene expression. *Mol. Microbiol.* 9: 751-760.

Williams R., & Da Silva F. (2003) Evolution was chemically constrained. *J. Theor. Biol.* 220: 323-343.

Wu C.C., MacCoss M.J., Howell K.E. & Yates J.R. 3rd. (2003) A method for the comprehensive proteomic analysis of membrane proteins. *Nat. Biotechnol.* 21: 532-538.

Wu J. & Rosen B.P. (1991) The ArsR protein is a trans-acting regulatory protein. *Mol. Microbiol.* 5: 1331-1336.

Wu J. & Rosen B.P. (1993) Metalloregulated expression of the *ars* operon. *J. Biol. Chem.* 268: 52-58.

Wu J. & Weiss B. (1991) Two divergently transcribed genes, *soxR* and *soxS*, control a superoxide response regulon of *Escherichia coli. J. Bacteriol.* 173: 2864-2871.

Xiao Z., Loughlin F., George G.N., Howlett G.J. & Wedd A.G. (2004) C-terminal domain of the membrane copper transporter Ctr1 from *Saccharomyces cerevisiae* binds four Cu(I) ions as a cuprous-thiolate polynuclear cluster: sub-femtomolar Cu(I) affinity of three proteins involved in copper trafficking. *J. Am. Chem. Soc.* 126: 3081-3090.

Xu C., Shi W. & Rosen BP. (1996) The chromosomal *arsR* gene of *Escherichia coli* encodes a trans-acting metalloregulatory protein. *J. Biol. Chem.* 271: 2427-2432.

Xu Y., Feng L., Jeffrey P.D., Shi Y. & Morel F.M. (2008) Structure and metal exchange in the cadmium carbonic anhydrase of marine diatoms. *Nature.* 452: 56-61.

Yang J., Ishimori K. & O'Brian M.R. (2005) Two heme binding sites are involved in the regulated degradation of the bacterial iron response regulator (Irr) protein. *J. Biol. Chem.* 280: 7671-7676.

Ye J., Kandegedara A., Martin P. & Rosen B.P. (2005) Crystal structure of the *Staphylococcus aureus* pI258 CadC Cd(II)/Pb(II)/Zn(II)-responsive repressor. *J. Bacteriol.* 187: 4214-4221.

Yoon K.P., Misra T.K. & Silver S. (1991a) Regulation of the *cadA* cadmium resistance determinant of *Staphylococcus aureus* plasmid pI258. *J. Bacteriol.* 173: 7643-7649.

Yoon K.P. & Silver S. (1991b) A second gene in the *Staphylococcus aureus cadA* cadmium resistance determinant of plasmid pI258. *J. Bacteriology.* 173: 7636-7642.

Zappa S., Li K. & Bauer C.E. (2010) The tetrapyrrole biosynthetic pathway and its regulation in *Rhodobacter capsulatus*. *Adv. Exp. Med. Biol.* 675: 229-250.

Zayas C.L., Claas K. & Escalante-Semerena J.C. (2007) The CbiB protein of *Salmonella enterica* is an integral membrane protein involved in the last step of the de novo corrin ring biosynthetic pathway. *J. Bacteriol.* 189: 7697-7708.

Zheng M., Doan B., Schneider T.D. & Storz G. (1999) OxyR and SoxRS regulation of fur. *J. Bacteriol.* 181: 4639-4643.

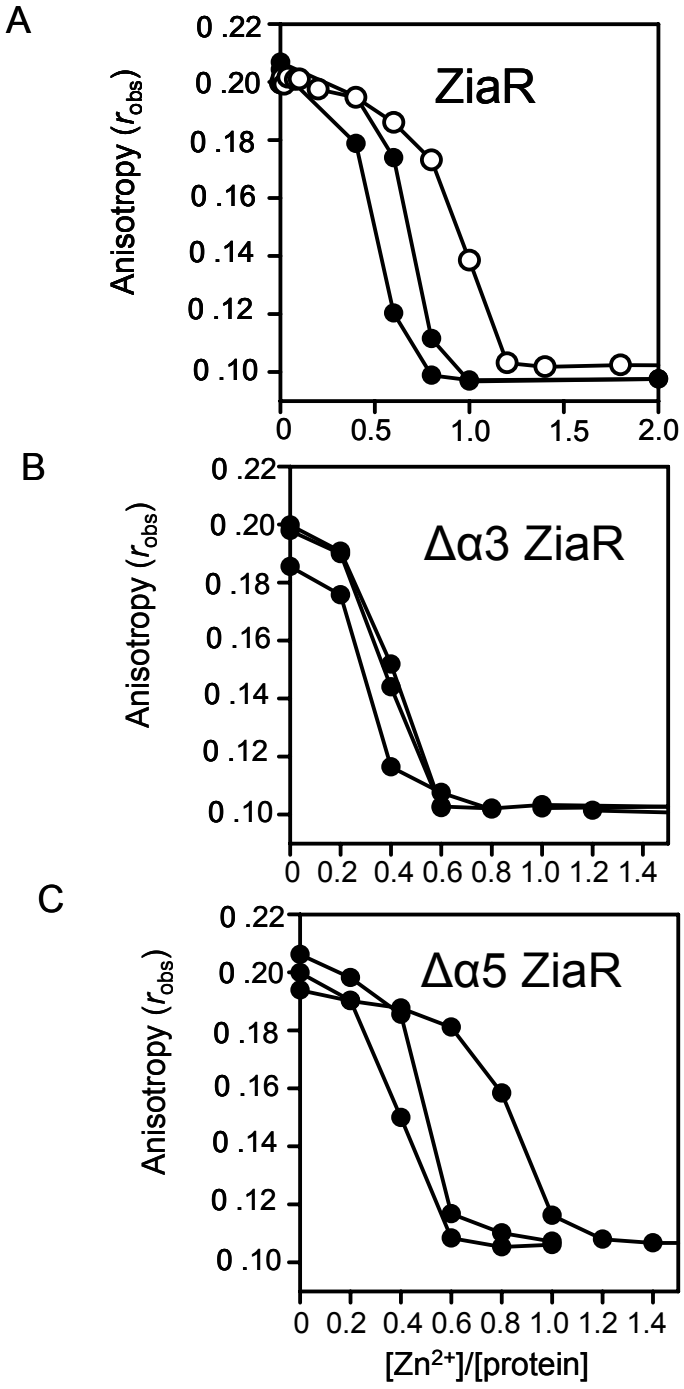

Figure 1. Effects of Zn^{2+} on wild-type and mutant ZiaR-DNA complexes monitored by fluorescence anisotropy. In each instance, 1 μM of protein was incubated with 10 nM of *zia* oligonucelotide and then the resultant complex titrated with Zn^{2+} under anaerobic conditions. The three datasets for each protein include one of the replicates presented in Figure 18a. The other replicates are not presented in the main thesis text. Note: for ZiaR data points shown as open circles are from an experiment performed aerobically in the presence of 1 mM DTT. This titration saturated at ~1.2 equivalents Zn^{2+} and so the x-axis scale has been expanded relative to those on panels B and C to show no further changes in anisotropy beyond this point.

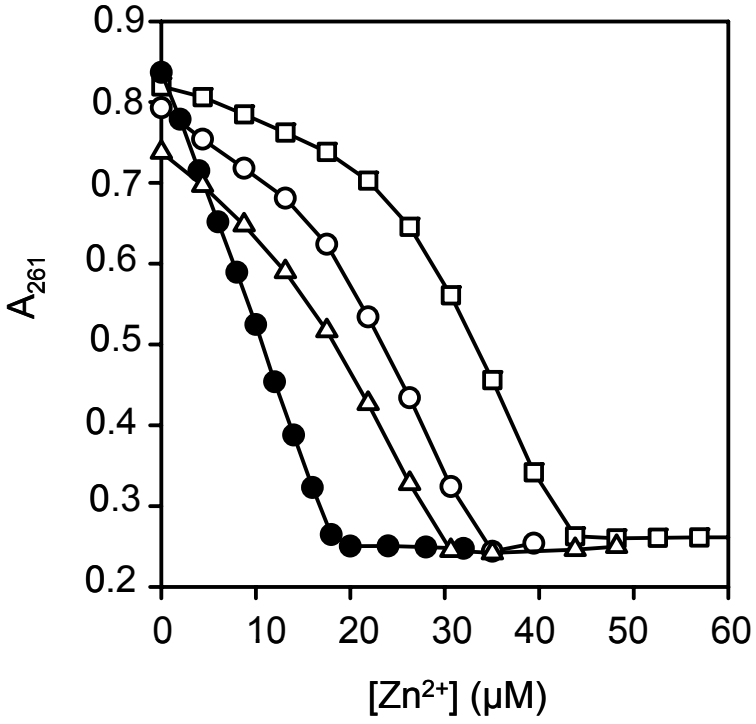

Figure 2. Titration of ZiaR, Δα5 ZiaR and Δα3 ZiaR with Zn^{2+} in the presence of Quin-2. The data from Figure 19a (ZiaR) (open squares), Figure 20a (Δα5 ZiaR) (open circles) and Figure 21b (Δα3 ZiaR) (open triangles) are shown without least squares regression analysis line fits. An example control titration (22 μM Quin-2) performed in the absence of protein (that was performed in association with the ZiaR replicate using the same Zn^{2+} and Quin-2 stocks) is also shown, with saturation occurring at approximately one equivalent of Zn^{2+}.

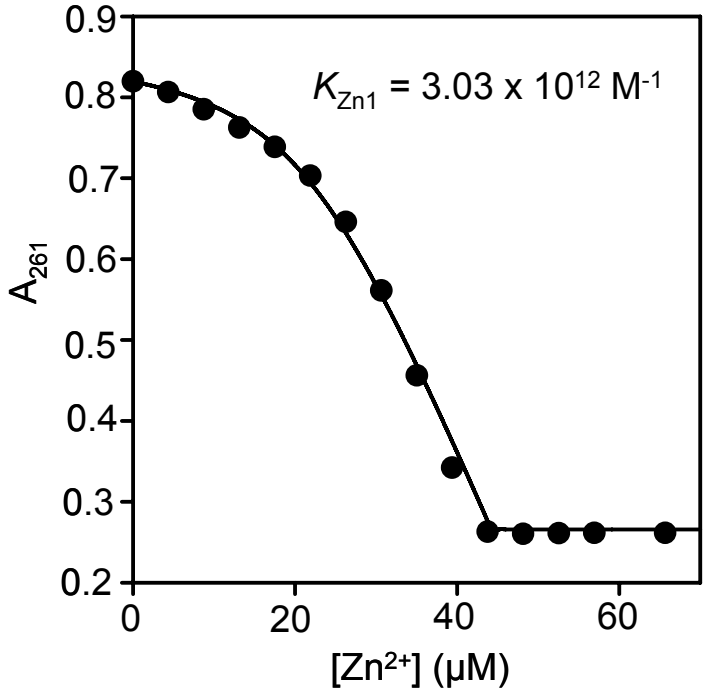

Figure 3. Two-site monomer fit from a titration of ZiaR with Zn^{2+} in the presence of Quin-2. Data from Figure 19a were fitted to a two-site monomer model by least squares linear regression analysis. The Zn^{2+} association constant for the first binding site is lower than when fitted to a two site dimer model.

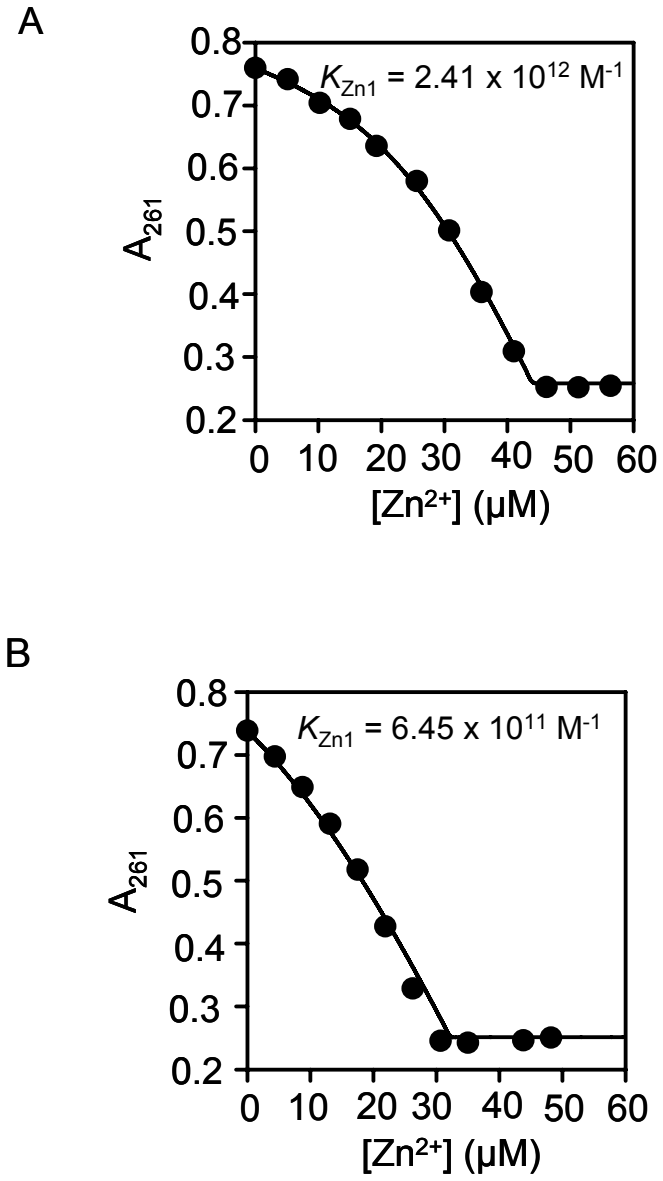

Figure 4. Zn^{2+} titration data for mutant ZiaR proteins and Quin-2. Data for Δα3 ZiaR (A) and Δα5ZiaR (B) from Figure 21a and Figure 20a respectively were fit to a two site dimer model and produced fits and binding constant values almost identical to those produced by a four site dimer model.

Appendix B

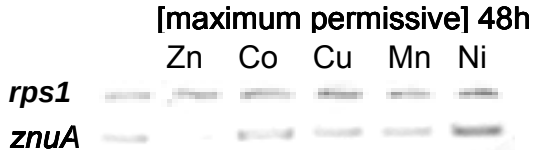

Figure 1. Example RT-PCR analyses showing changes in *znuA* gene expression following treatment with a range of metals. Cells were grown in the presence of maximum permissive concentrations of each metal for 48 hours prior to RNA isolation. These data were collected by Samantha Dainty.

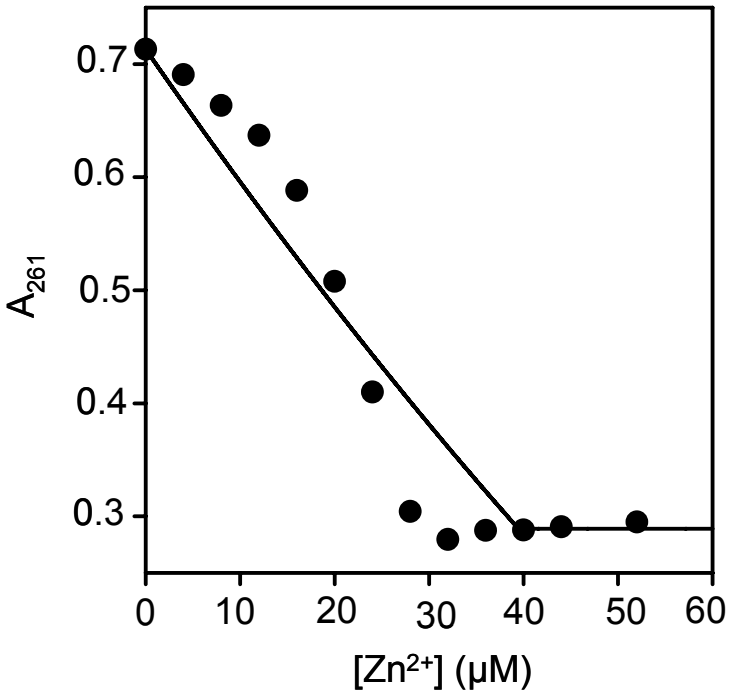

Figure 2. Measurement of the Zn^{2+} affinity of $Zn1Zur_{SS}$ by titration with Zn^{2+} in the presence of Quin-2 Data from Figure 32a is shown fitted by least squares linear regression analysis to a single-site monomer model; this model does not accurately describe the data.

Appendix C

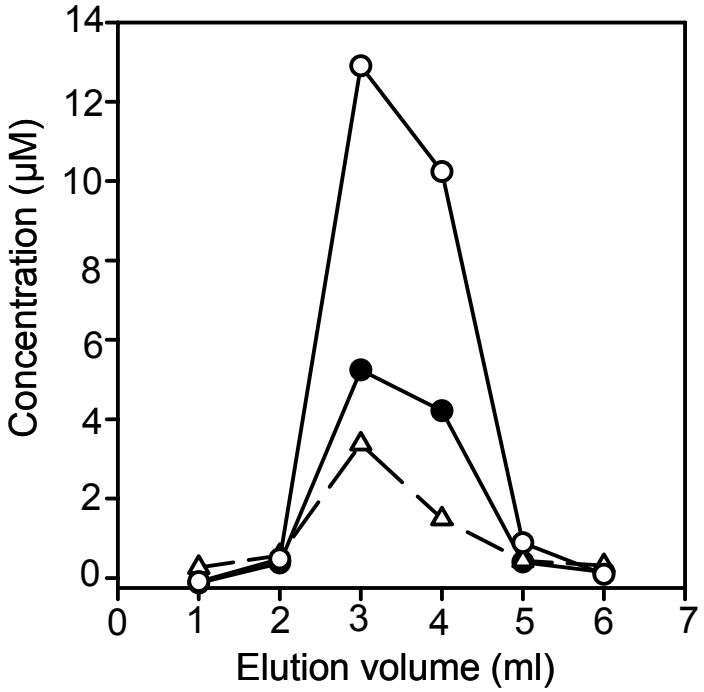

Figure 1. Size-exclusion fractionation of metal bound ZiaR. ZiaR was incubated anaerobically with four equivalents Cu^{+} and bound and free metal ions separated using Sephadex G-25 matrix (closed symbols; proten, open triangles; Zn^{2+}, open circles Cu^{+}). Approximately 2.45 equivalents of Cu^{+} and 0.52 equivalents of Zn^{2+} are associated with the protein in the two peak protein fractions. Note: only fractions immediately after the column void were analysed. Conditions: 400 mM KCl, 100 mM NaCl, 10 mM Hepes pH 7.8.

Figure 2. Analysis of the effect of Cu^{+} on the DNA binding properties of Zn^{2+}-bound ZiaR monitored by fluorescence anisotropy. These analyses were performed in buffer of higher salt concentration (400 mM KCl, 100 mM NaCl, 10 mM Hepes (pH 7.8)) than used in analyses shown in Figure 47. To confirm protein binding to DNA under these conditions, ZiaR was titrated with 10 nM *zia* O/P oligonucleotide following incubation in 1 mM EDTA (A). A lower maximal Δr_{obs} and weaker K_{DNA} are evident in these data; the higher concentrations of KCl and NaCl may have disrupted charge-dependent protein-protein interactions (which may underpin the formation of higher-order complexes observed under conditions of lower salt concentration) and protein-DNA interactions, which may be stronger under conditions of higher salt concentration producing tighter K_{DNA} values under these conditions. B. Based on the DNA binding isotherm shown in A, 5 μM ZiaR was sufficient to produce saturation of DNA. ZiaR-DNA complexes were pre-formed (5 μM ZiaR, 10 nM DNA) and titrated with an equimolar solution of Cu^{+} and Zn^{2+} under anaerobic conditions. Data points are also shown from experiments in which two equivalents Zn^{2+} (black circle) and two equivalents Cu^{+} (red circle) were added to ZiaR-DNA solutions prepared as described above. The mean anisotropy value (n=3) for a sample of this DNA preparation is shown (open triangle). The anisotropy value at 6 μM ZiaR from the titration shown in A is also shown (open square).

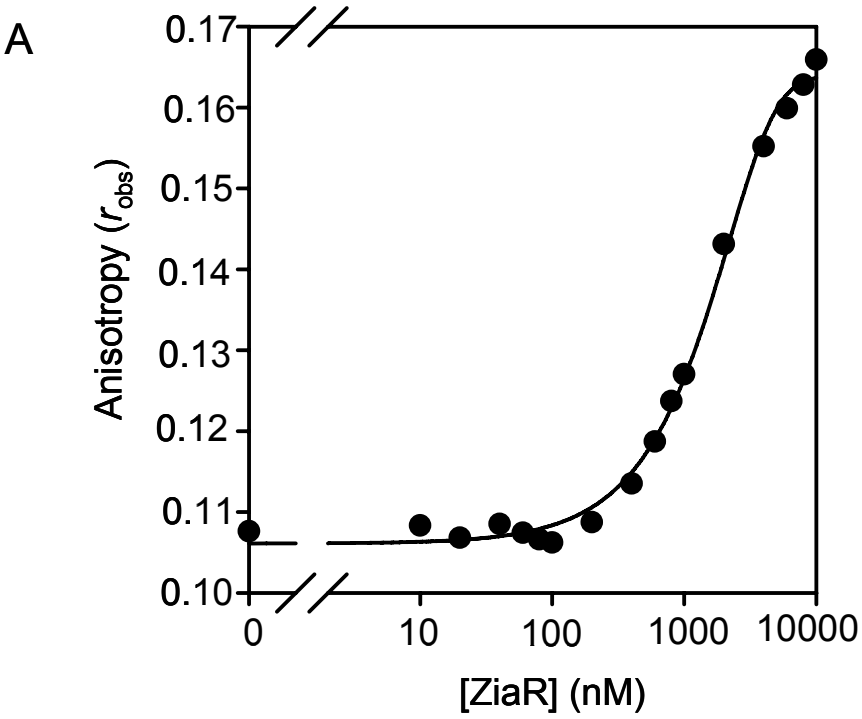
A
0.17
0.16
0.15
0.14
0.13
0.12
0.11
0.10
Anisotropy (r_{obs})
0
10
100
1000
10000
[ZiaR] (nM)

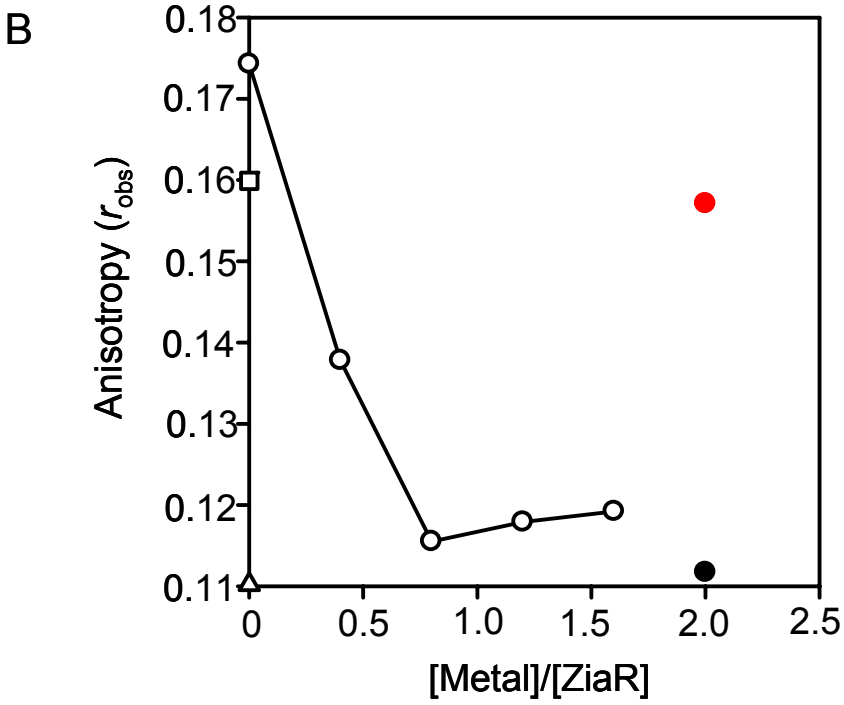
B
0.18
0.17
0.16
0.15
0.14
0.13
0.12
0.11
Anisotropy (r_{obs})
0
0.5
1.0
1.5
2.0
2.5
[Metal]/[ZiaR]

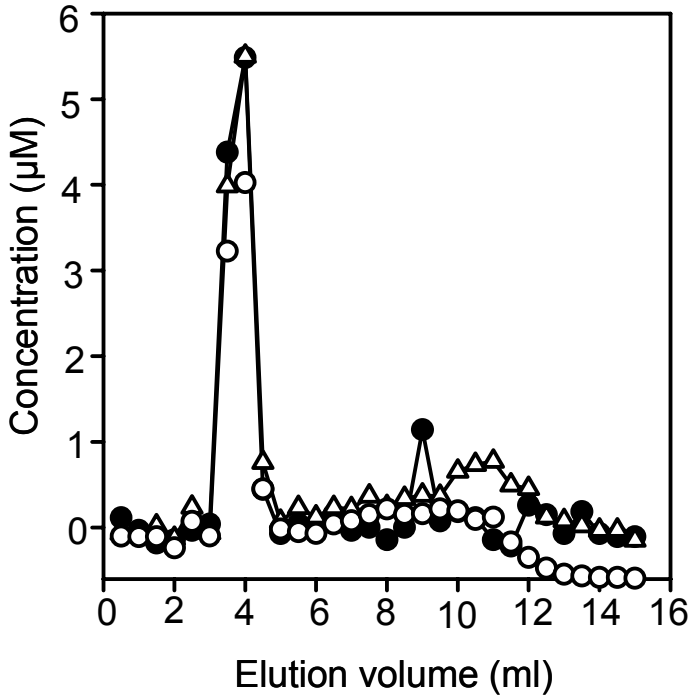

Figure 3. Analysis of Cu^{+}/Zn^{2+} binding to Zur_{SS} by size-exclusion fractionation of bound and free metal ions. This experiment was performed under conditions identical to those in Figure 49. Zn_1Zur_{SS} was prepared anaerobically and incubated with approximately one equivalent of Cu^{+} and one equivalent of Zn^{2+}. Bound and free species were resolved on Sephadex G-25 matrix and protein concentrations (closed symbols) determined by Coomassie assay and concentrations of Zn^{2+} (open triangles) and Cu^{+} (open circles) were determined by ICP-MS. The free metal peak for Zn^{2+} in this analysis (~6 μM) is lower than in the replicate shown in Figure 49. However, the total concentration of Zn^{2+} present in the binding reaction was confirmed as being ~36 μM (~20 μM was predicted) prior to sample fractionation, by ICP-MS analysis of an aliquot of the reaction mixture. This implies more Zn^{2+} was added to the reaction than anticipated in this analysis however, the Zn^{2+} (1.0:1) and Cu^{+} (0.75:1) binding stoichiometries are still consistent with preferential binding of Cu^{+} to the allosteric site with retention of binding of approximately one equivalent of structural Zn^{2+} (ICP-MS analyses of this protein preparation showed 0.9 equivalents Zn^{2+} prior to use in this experiment).

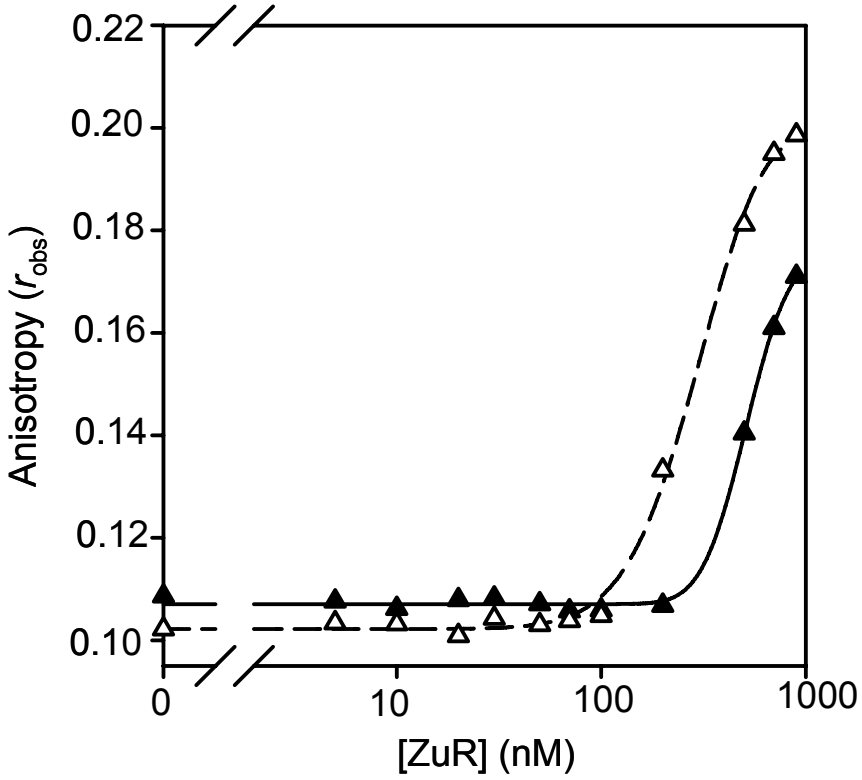

Figure 4. The effects of Cu^{+} on Zur_{SS} binding to DNA monitored by fluorescence anisotropy. These experiments were performed in an identical fashion to those shown in Figure 50. Zn_1Zur_{SS} protein was pre-incubated under anaerobic conditions in either 1.5 equivalents of Cu^{+} (closed symbols) or 1.5 equivalents each of Cu^{+} and Zn^{2+} (open symbols) and titrated with 10 nM DNA in the presence of approximately 3 μM Cu^{+}.

Appendix D

Figure 1. Optimised curve fitting for Fura-2 titration data. Least squares linear regression analyses of data from Co^{2+} titrations of ZiaR in the presence of Fura-2 modelled using a two-site monomer model. Fitted curves produced using this model consistently underestimated the affinity of the first binding site for Co^{2+}. A. Fitting of the first six datapoints only for data shown in Figure 51 (section 6.1.1) producing a K_d for the tightest Co^{2+} binding site of 2.92 x 10^{-9} M. B. Example data from replicate titration of ZiaR (1.5 μM) and Fura-2 (1.5 μM) with Co^{2+} producing a K_d of 4.09 x 10^{-9} M. Inset: fitting of the first six datapoints from these data producing a K_d for the tightest Co^{2+} binding site of 3.2 x 10^{-9} M. The average affinity values for these fitted curves are summarised in Table 10 in section 6.3.9.

A

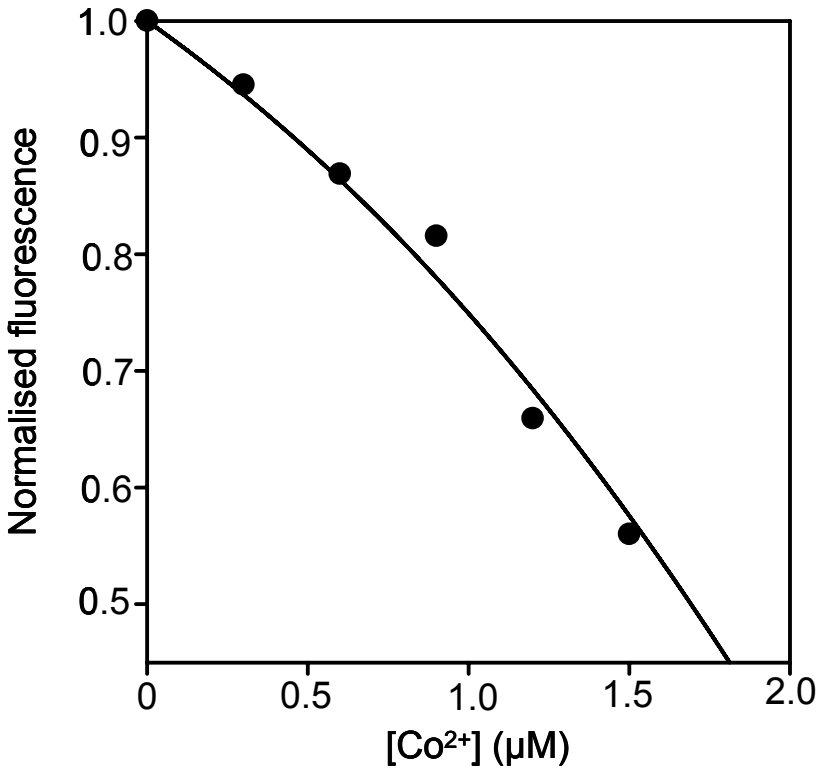
1.0
0.9
0.8
0.7
0.6
0.5
Normalised fluorescence
0
0.5
1.0
1.5
2.0
[Co2+] (μM)

B

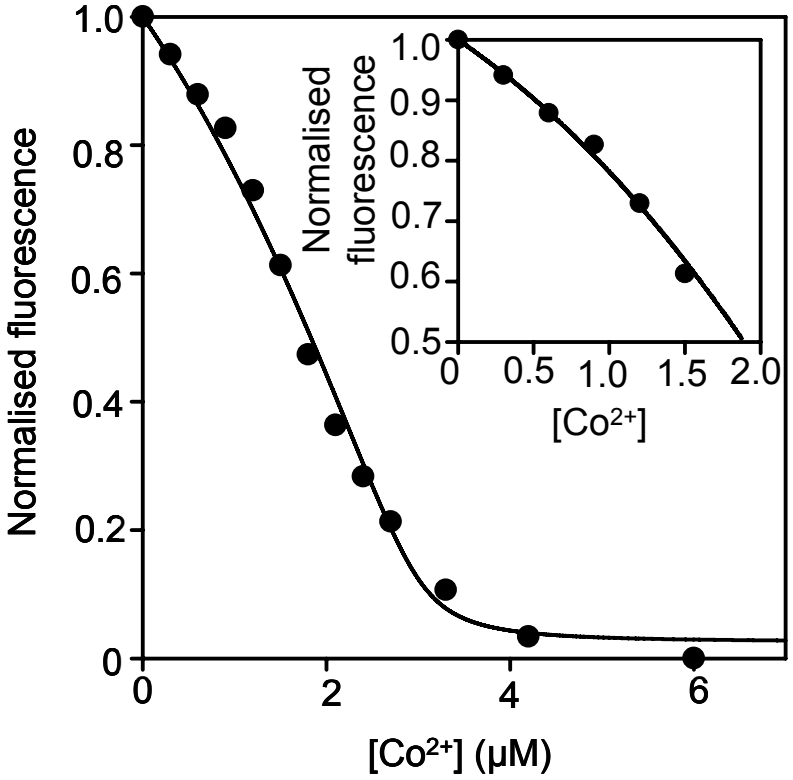
1.0
0.8
0.6
0.4
0.2
0
Normalised fluorescence
0
2
4
6
[Co2+] (μM)
Normalised fluorescence
1.0
0.9
0.8
0.7
0.6
0.5
0
0.5
1.0
1.5
2.0
[Co2+]

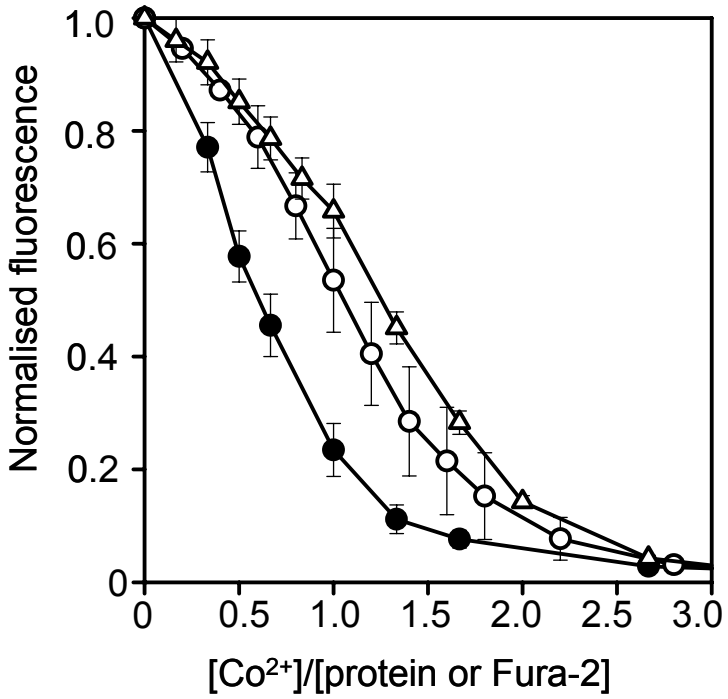

Figure 2. Anaerobic titration of ZiaR, Zur_{SS} with Co^{2+} in the presence of Fura-2. Mean (n=3) normalised changes in fluorescence are shown plotted as function equivalents of Co^{2+} added. Open circles represent ZiaR, open triangles are data for Zur and closed symbols represent mean values from three control experiments (Fura-2 titrated with Co^{2+} in the absence of protein).

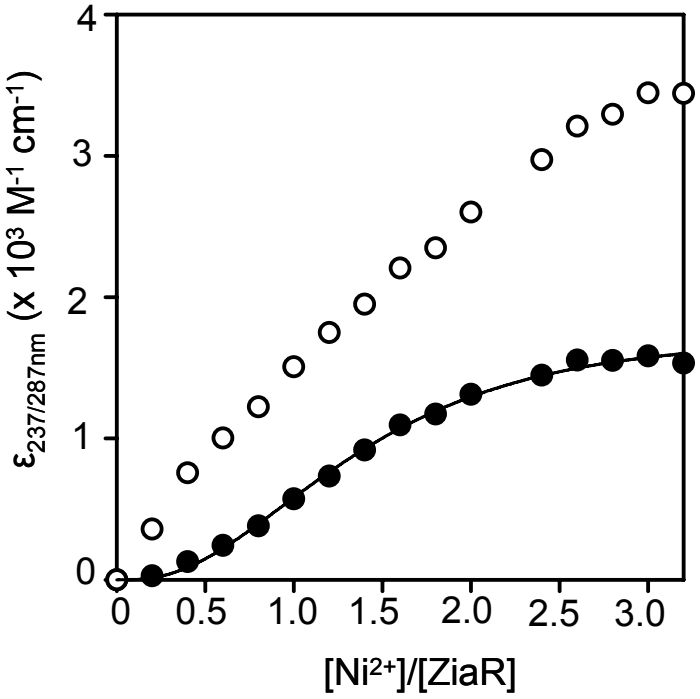

Figure 3. Increase in intensity of LMCT features at 237 nm and 287 nm on titration of ZiaR with Ni^{2+}. These data are from the experiment shown in Figure 53 (section 6.1.2). ZiaR was prepared anaerobically and approximately 40 μM protein titrated with Ni^{2+}. 237 nm data are shown as open symbols, 287 nm data as closed symbols.

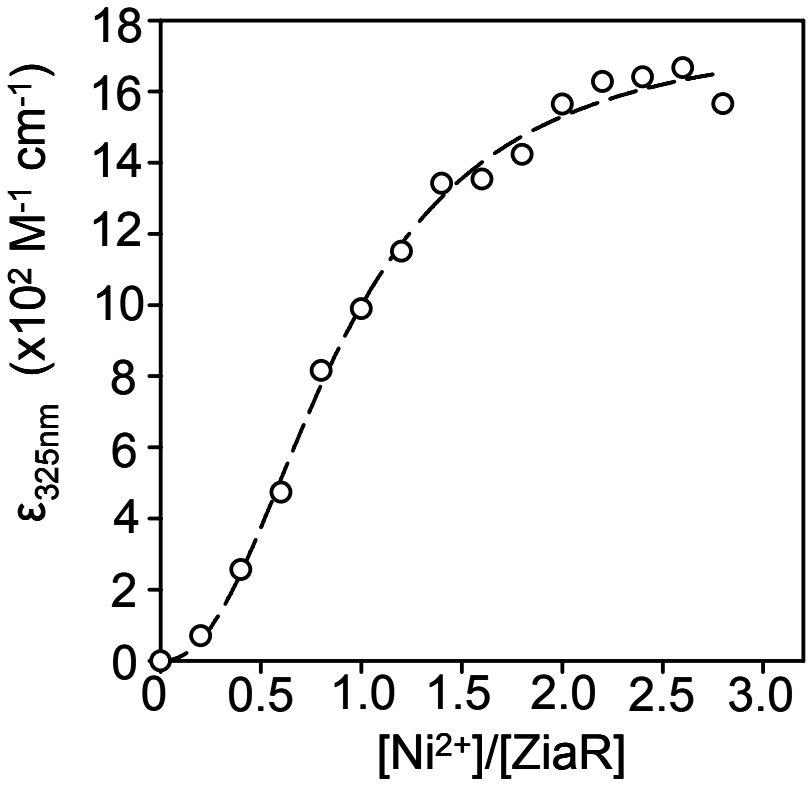

Figure 4. Anaerobic UV-Visible titration of ZiaR with Ni^{2+}. Apo-subtracted molar extinction coefficient values are shown for a titration of ZiaR (30 μM) with Ni^{2+}, performed under conditions identical to those shown for the titration at 40 μM ZiaR shown in Figure 53 (section 6.1.2).

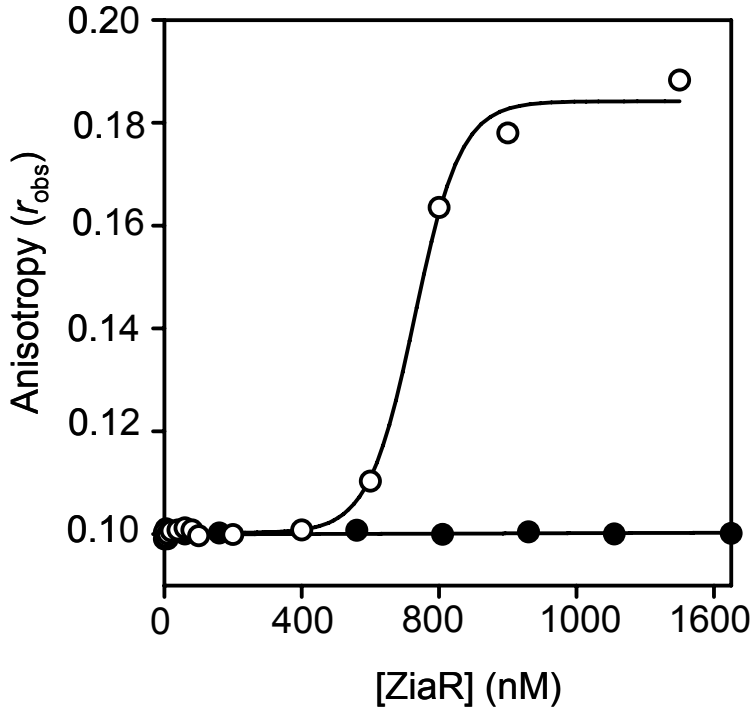

Figure 5. Titration of *zia* O/P oligonucleotide with ZiaR in the presence of Cd^{2+}. ZiaR was prepared anaerobically and titrated with 10 nM DNA in the presence (closed symbols) of a saturating excess of Cd^{2+} (4 μM) or in the absence of metal (open symbols). Data are plotted on a linear scale to more effectively show binding of apo-protein.

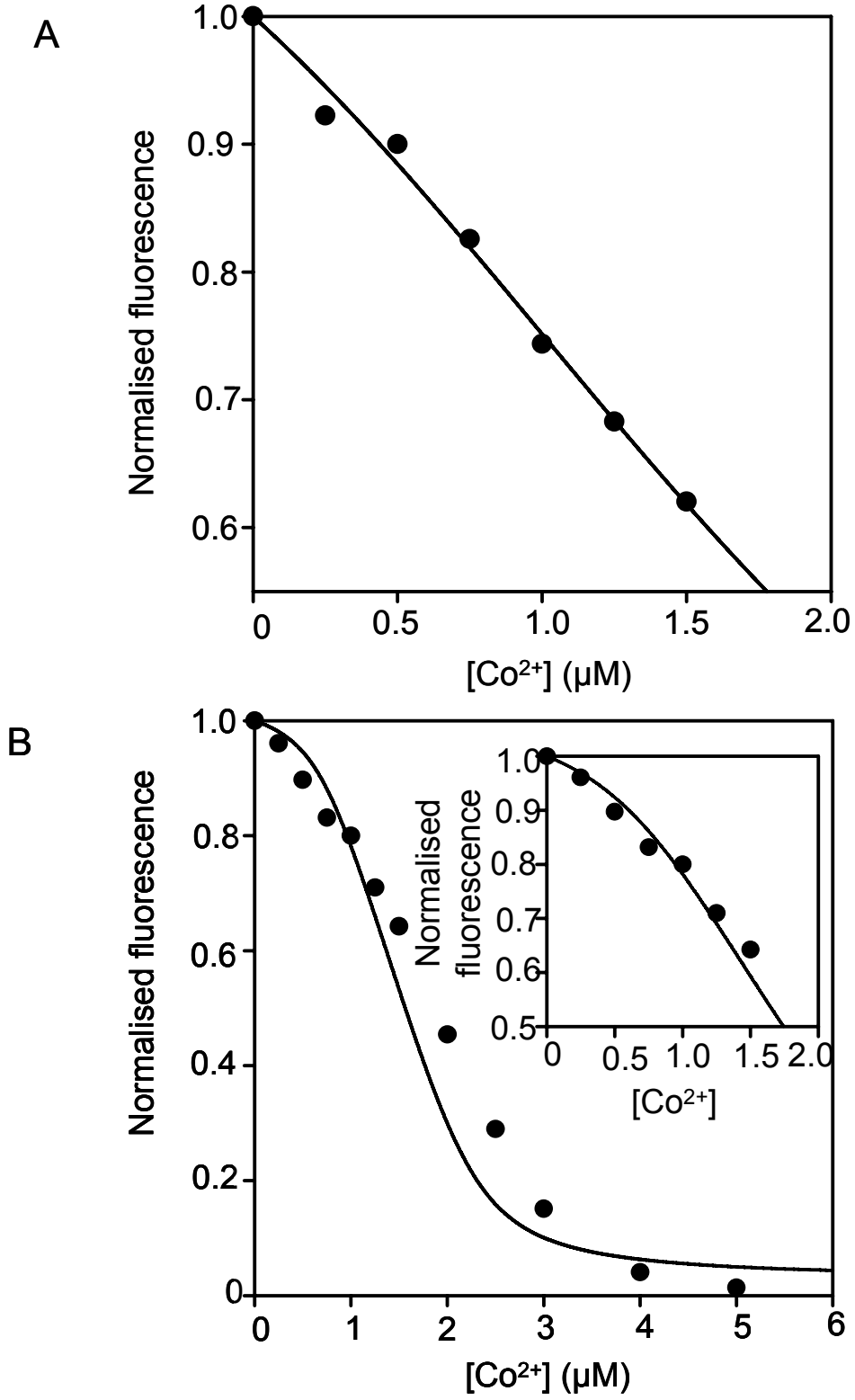

Figure 6. Optimised curve fitting for Fura-2 titration data. Least squares linear regression analyses of data from Co^{2+} titrations of Zur_{SS} in the presence of Fura-2 modelled using a two-site dimer model. Curves produced using this model did not accurately describe the data. A. Example fitting of the first six datapoints only from the replicate shown in Figure 56 section 6.2.1; this value produced a K_d of 2.32 x 10^{-9} M. B. Example data from a replicate titration of Zur_{SS} (1.5 μM) with Fura-2 (1.5 μM) with Co^{2+} fitted using a two-site dimer model producing a K_d of 4.42 x 10^{-10} M. *Inset*: fitting of the first six datapoints from these data producing a K_d of 1.01 x 10^{-9} M. The average affinity values for these fits are summarised in Table 10 in section 6.3.9.

Figure 7. Analysis of Ni^{2+} binding to Zur_{SS} by UV-Visible spectroscopy. Recombinant Zn_1Zur_{SS} (30 μM) was prepared anaerobically and titrated with Ni^{2+}. A. Apo-subtracted difference spectra are shown for an example titration. B. The LMCT features at 290 nm (closed symbols) and 350 nm (open symbols) were plotted as a function of the number of equivalents of added Ni^{2+}. Stoichiometric Ni^{2+} binding implies a $K_{Ni} \leq 15 \times 10^{-6}$ M with the actual value likely to be substantially tighter. This would be in accord with studies of Ni^{2+} binding centres in other Ni^{2+} sensing metalloregulators which have estimated K_{Ni} values in the 10^{-12}-10^{-13} M range for NikR (Chivers & Sauer 2002; Wang *et al.* 2004) and tighter than ~25×10^{-9} M for RcnR (Iwig *et al.* 2008). Interpretation of the electronic features in the longer wavelength region is complicated by the substantial rise in baseline absorbance observed during the course of the titration which was likely to be due to protein precipitation at higher metal and protein concentrations. Additionally, the LMCTs in the short wavelength range came to dominate the spectra at longer wavelengths later on in the titration. Nevertheless, following each addition of Ni^{2+} the spectra remained relatively flat with no discernable peaks or shoulders that would be indicative of square-planar or tetrahedral geometry, suggesting adoption of a high coordinate (6) geometry.

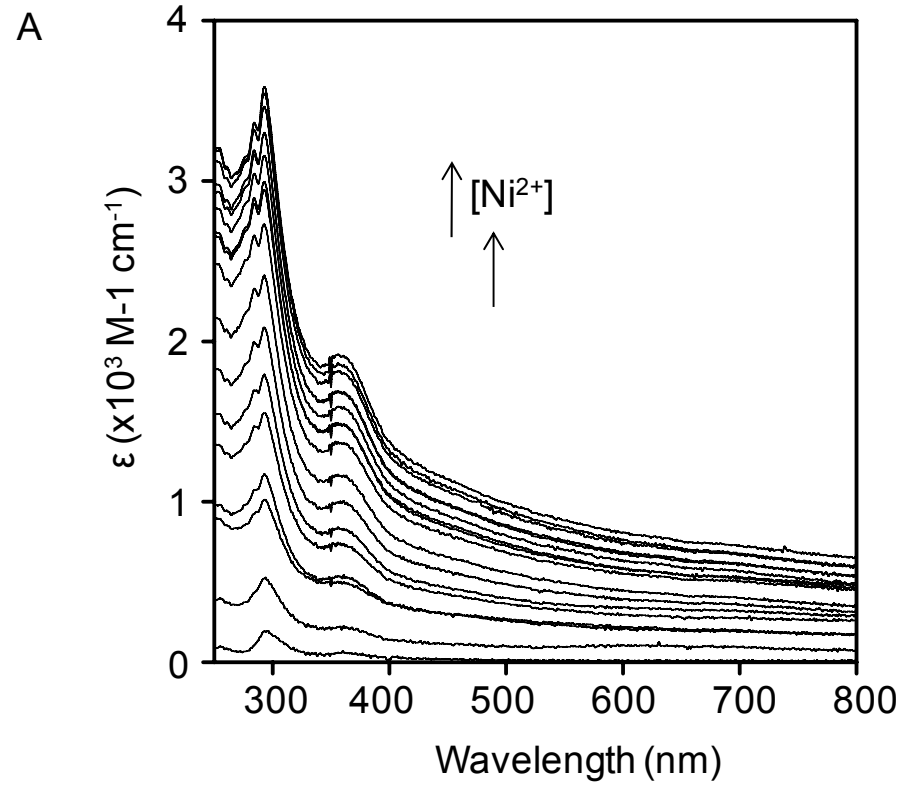
A
4
3
2
1
0
ε (x10³ M-1 cm⁻¹)
[Ni²⁺]
300
400
500
600
700
800
Wavelength (nm)

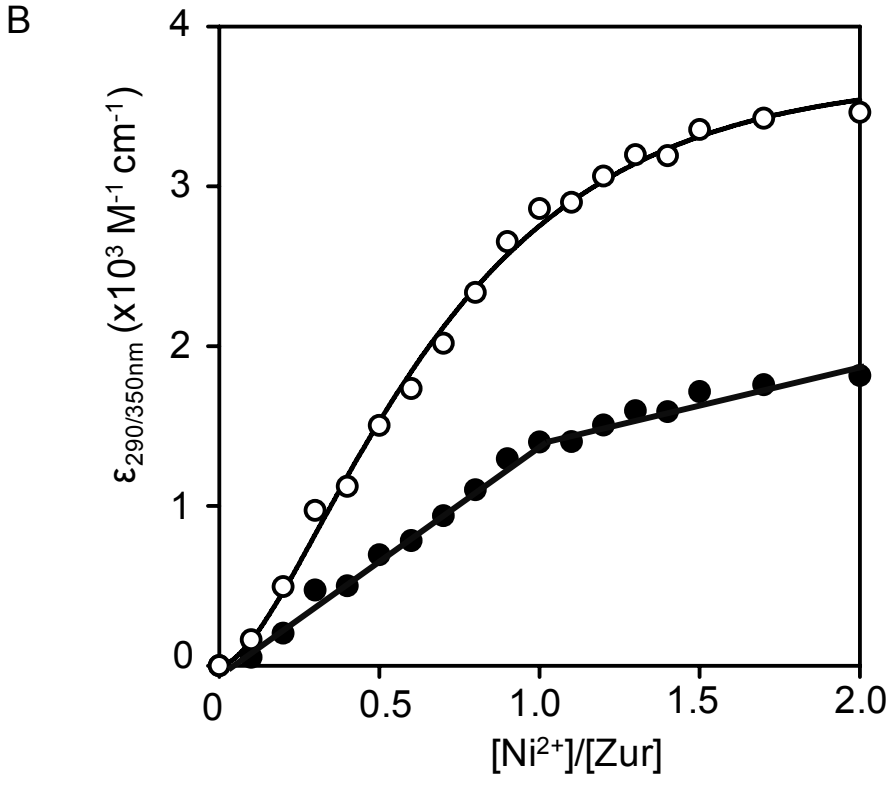
B
4
3
2
1
0
ε290/350nm (x10³ M⁻¹ cm⁻¹)
0
0.5
1.0
1.5
2.0
[Ni²⁺]/[Zur]

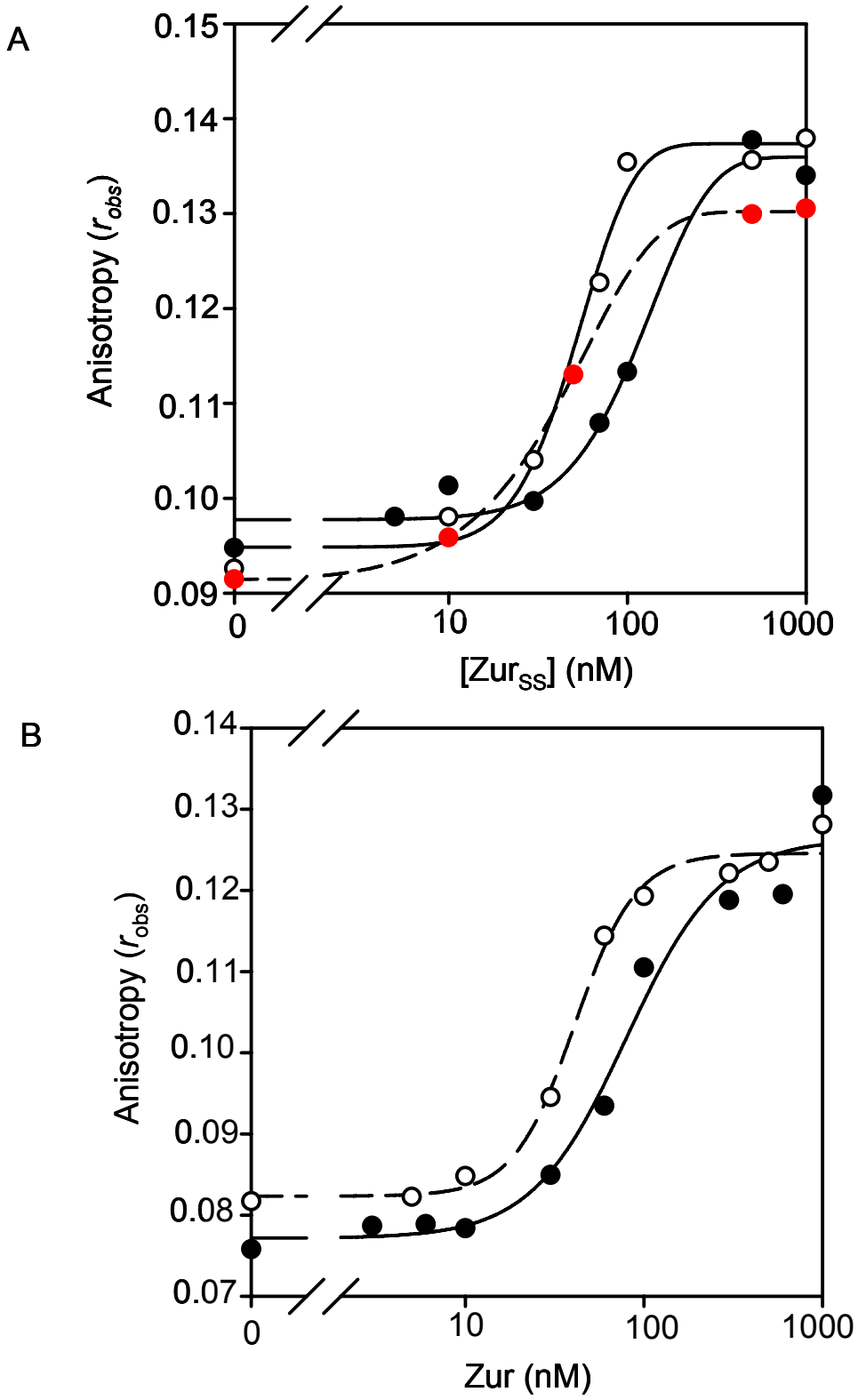

Figure 8. Measurement of the effects of Co^{2+}, Ni^{2+} and Mn^{2+} on the DNA binding affinity of Zur$_{SS}$. A. Example anaerobic titrations of recombinant Zur$_{SS}$ protein with *znu* O/P oligonucleotide following incubation of between 1.25 and 10 μM protein in either no metal (red symbols), 1 mM Mn^{2+} (black symbols) or 60 Ni^{2+} (open symbols) (metals present at the same concentration in the DNA binding reaction). B. Titration of Zur$_{SS}$ pre-incubated in Co^{2+} (1-10 μM protein with 30 μM Co^{2+} in the incubation and DNA binding reaction) (open symbols). An example Zn^{2+} titration is shown for comparison (0.6-6 μM Zur$_{SS}$ was pre-incubated with two equivalents Zn^{2+}) (closed symbols). The protein used in B was verified by ICP-MS to be Zn_1Zur$_{SS}$ (~0.9 equivalents Zn^{2+} present) prior to these experiments.

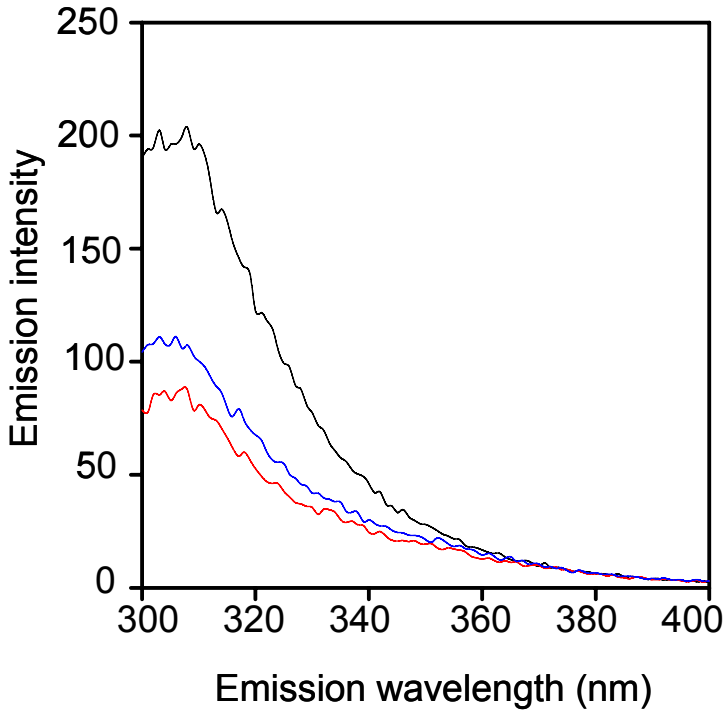

Figure 9. Quenching of intrinsic Zur_{SS} tyrosine fluorescence by Co^{2+} and Zn^{2+}. An anaerobic sample of Zn_1Zur_{SS} (5 μM) was excited at a wavelength of 280 nm and the emission spectrum recorded. One equivalent of Co^{2+} (red line) followed by one equivalent of Zn^{2+} (blue line) were then added and the spectra re-recorded.

A

```
CoaR            MKTNHLTIKELTDAVGGGVTPRMVRHYHTLGLLPPVQRSEGNYRLYTQQDVQRLQRVIAL 60
ZntR            ----MYRIGELAKMA--EVTPDTIRYYEKQQMMEHEVRTEGGFRLYTESDLQRLKFIRHA 54

CoaR            KQQGFQLSHIRQLLDSHSEESLDPTLMVQLQQQYQAVIQQITRLRQTASALEGLLGRDQS 120
ZntR            RQLGFSLESIRELLSIR----IDP-------------------------------EHHT 78

CoaR            CQITQAEALAQLKQLDVDVQEGLGKLDQLWTNLDAETTTHPEAFQESLKHLLPDLSAYSE 180
ZntR            CQESKGIVQERLQEVEARIAE------------------LQSMQRSLQRLN-------- 111

CoaR            ITIHLLHQLVLACGDVSLVNAVRLSQGAIASARDALKAGCPVVTDVPVVAAALDQTRLAH 240
ZntR            ----------DACCGTAHSSVYCSILEALEQGASGVKSGC-------------------- 141

CoaR            LGCTVKTLIDDPHITGLREAEQAFWHHDHWQQRLQQIPQGCVLAIGYAPSVLLTACKLIE 300
ZntR            ------------------------------------------------------------

CoaR            QQHIQPALVIGMPIGFSHAPGAKRRLMTSPIPHITIQGSLGGGLLAAVTLNALVETLIAK 360
ZntR            ------------------------------------------------------------

CoaR            PDCHCYLTCL 370
ZntR            ----------
```

B

```
CoaR            MKTNHLTIKELTDAVGGGVTPRMVRHYHTLGLLPPVQRSEGNYRLYTQQDVQRLQRVIAL 60
CueR            -----MNISDVAKITG--LTSKAIRFYEEKGLVTPPMRSENGYRTYTQQHLNELTLLRQA 53

CoaR            KQQGFQLSHIRQLLDSHSEESLDPTLMVQLQQQYQAVIQQITRLRQTASALEGLLGRDQS 120
CueR            RQVGFNLEESGELVNLFND----------PQRHSADVKRRT----------------- 84

CoaR            CQITQAEALAQLKQLDVDVQEGLGKLDQLWTNLDAETTTHPEAFQESLKHLLPDLSAYSE 180
CueR            --------LEKVAEIERHIEELQSMRDQLLALANACPGDD------------------- 116

CoaR            ITIHLLHQLVLACGDVSLVNAVRLSQGAIASARDALKAGCPVVTDVPVVAAALDQTRLAH 240
CueR            ----------------------------------SADCPIIENLSGCCHHRAG----- 135

CoaR            LGCTVKTLIDDPHITGLREAEQAFWHHDHWQQRLQQIPQGCVLAIGYAPSVLLTACKLIE 300
CueR            ------------------------------------------------------------

CoaR            QQHIQPALVIGMPIGFSHAPGAKRRLMTSPIPHITIQGSLGGGLLAAVTLNALVETLIAK 360
CueR            ------------------------------------------------------------

CoaR            PDCHCYLTCL 370
CueR            ----------
```

Figure 10. Alignment of sequences of CoaR, ZntR and CueR. The sequence of CoaR from *Synechocystis* was aligned with the sequence of ZntR (A) and CueR (B) from *E.coli*. The cysteines shown to be required for metal binding in ZntR and CueR and which align with cysteine residues in CoaR are highlighted in red. The other residues validated as Zn^{2+}/Cu^{+} ligands in ZntR/CueR (which are not conserved in CoaR) are shown in blue.

Appendix E

Structures of representative metal-sensing transcriptional regulators

Figure 1. Example structures for members of the ArsR-SmtB, Fur and MerR families of metal sensing transcriptional regulators. A. X-Ray crystal structure of the Zn^{2+}-bound form of SmtB from *Synechococcus* PCC 7942 (PDB:1R23) The symmetry-related regulatory α5 sites are circled and the Zn^{2+}-liganding residues are indicated. B. X-ray crystal structure of the Cu^{+}-bound form of the *E.coli* MerR-like Cu^{+} sensor CueR (PDB: 1Q05). Each Cu^{+} ion is ligated by two cysteine residues (note: some loop segments are not visible in the structure). The right hand image shows CueR from a different angle showing Cu^{+}-liganding cysteine residues. C. X-ray crystal structure of the Zn^{2+} sensing Fur homologue FurB from *M. tuberculosis* (PDB: 2O03), shown in monomer form. Structural metal ion ligands are shown in green and allosteric site ligands in orange.

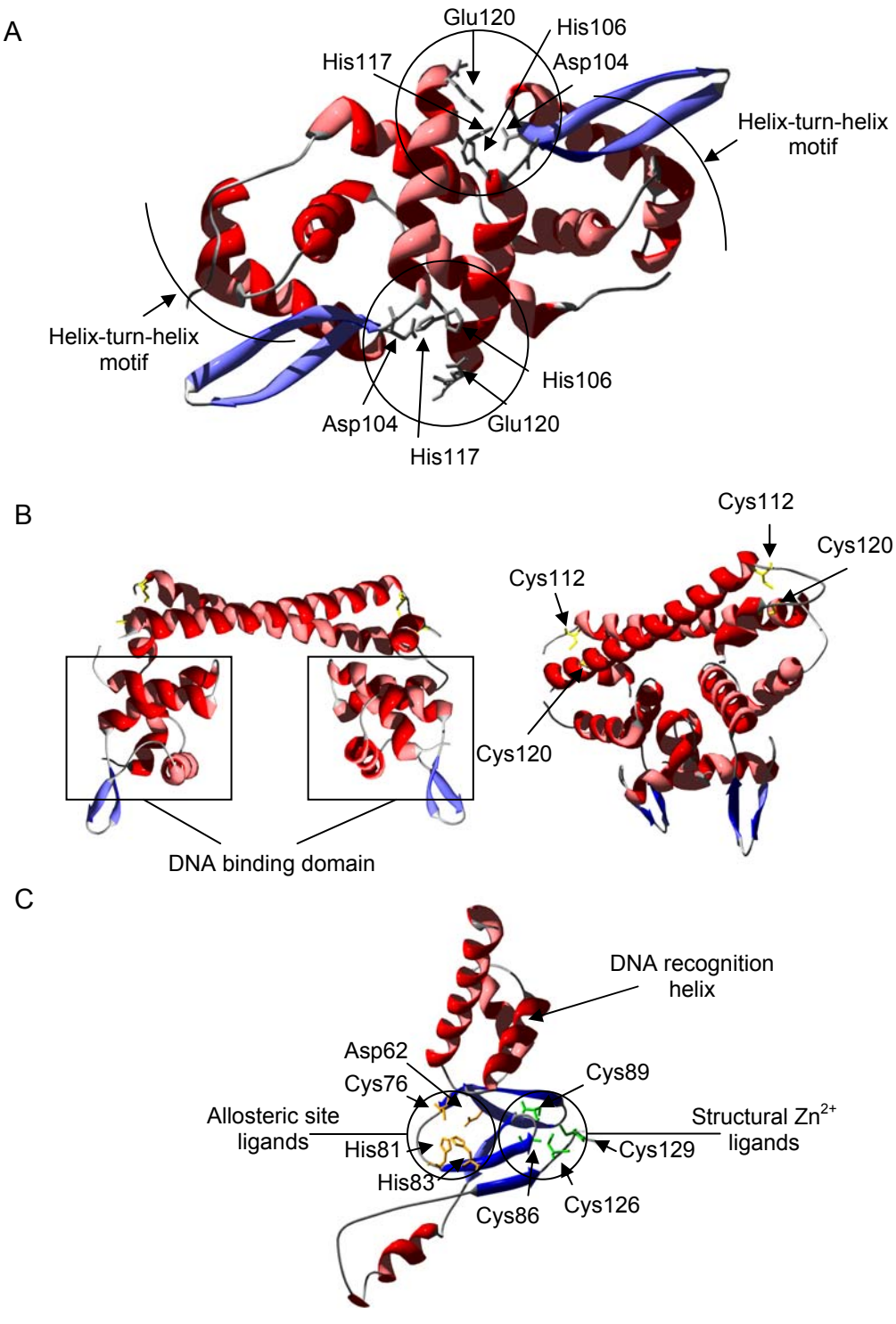
A
Glu120
His106
His117
Asp104
Helix-turn-helix motif
Helix-turn-helix motif
His106
Asp104
Glu120
His117
B
Cys112
Cys120
Cys112
Cys120
DNA binding domain
C
DNA recognition helix
Asp62
Cys76
Cys89
Allosteric site ligands
Structural Zn2+ ligands
His81
Cys129
His83
Cys86
Cys126

Appendix F

Dainty S.J., Patterson C.J., Waldron K.J. & Robinson N.J. (2010) Interaction between cyanobacterial copper chaperone Atx1 and zinc homeostasis. *J. Biol. Inorg. Chem.* 15: 77-85.